1.25
5/24/79

3054

MASTER

ORNL-5549
Dist. Category UC-20

Contract No. W-7405-eng-26

FUSION ENERGY DIVISION
ANNUAL PROGRESS REPORT

Period Ending December 31, 1978

AUGUST 1979

NOTICE

This report was prepared as an account of work sponsored by the United States Government. Neither the United States nor the United States Department of Energy, nor any of their employees, nor any of their contractors, subcontractors, or their employees, makes any warranty, express or implied, or assumes any legal liability or responsibility for the accuracy, completeness or usefulness of any information, apparatus, product or process disclosed, or represents that its use would not infringe privately owned rights.

Prepared by the
OAK RIDGE NATIONAL LABORATORY
Oak Ridge, Tennessee 37830
operated by
UNION CARBIDE CORPORATION
for the
DEPARTMENT OF ENERGY

Reports previously issued in this series are as follows:

ORNL-2693	Period Ending January 30, 1959
ORNL-2802	Period Ending July 31, 1959
ORNL-2926	Period Ending January 31, 1960
ORNL-3011	Period Ending July 31, 1960
ORNL-3104	Period Ending January 31, 1961
ORNL-3239	Period Ending October 31, 1961
ORNL-3315	Period Ending April 30, 1962
ORNL-3392	Period Ending October 31, 1962
ORNL-3472	Period Ending April 30, 1963
ORNL-3564	Period Ending October 31, 1963
ORNL-3652	Period Ending April 30, 1964
ORNL-3760	Period Ending October 31, 1964
ORNL-3836	Period Ending April 30, 1965
ORNL-3908	Period Ending October 31, 1965
ORNL-3989	Period Ending April 30, 1966
ORNL-4063	Period Ending October 31, 1966
ORNL-4150	Period Ending April 30, 1967
ORNL-4236	Period Ending October 31, 1967
ORNL-4401	Period Ending December 31, 1968
ORNL-4545	Period Ending December 31, 1969
ORNL-4688	Period Ending December 31, 1970
ORNL-4793	Period Ending December 31, 1971
ORNL-4896	Period Ending December 31, 1972
ORNL-4982	Period Ending December 31, 1973
ORNL-5053	Period Ending December 31, 1974
ORNL-5154	Period Ending December 31, 1975
ORNL-5275	Period Ending December 31, 1976
ORNL-5405	Period Ending December 31, 1977

CONTENTS

INTRODUCTION ... ix

1. EXPERIMENTAL CONFINEMENT ... 1

1.1 INTRODUCTION ... 2

1.2 EBT RESEARCH ... 3

1.2.1 Soft X-Ray Measurements ... 3

1.2.2 Charge Exchange Measurements ... 3

1.2.3 Thomson Scattering ... 5

1.2.4 Heavy Ion Beam Probe ... 5

1.2.5 Toroidal Plasma Impurities from vuv Emissions ... 6

1.2.6 Toroidal Current and Global Field Compensation ... 6

1.2.7 Absorption of the Ordinary Wave in Finite Temperature EBT Plasma ... 8

1.2.8 EBT-II ... 9

1.2.9 The 28-GHz, 200-kW cw Electron Cyclotron Heating System for EBT-S ... 11

1.2.10 28-GHz Oversized Waveguide Development ... 12

1.2.11 Wall Effects on the Absorption of Electron Cyclotron Waves in an EBT Plasma ... 13

1.3 TOKAMAK RESEARCH ... 13

1.3.1 The ISX-A Tokamak ... 13

1.3.2 The ISX-B Tokamak ... 19

1.3.3 Impurity Study Program ... 32

1.3.4 Long Pulse Technology Tokamak ... 34

REFERENCES ... 37

2. DIAGNOSTIC DEVELOPMENT ... 41

2.1 THE MEASUREMENT OF PLASMA ION TEMPERATURE BY THOMSON SCATTERING ... 41

2.2 MEASUREMENT OF TOKAMAK CURRENT PROFILES BY SUBMILLIMETER FARADAY ROTATION ... 42

2.3 ABSOLUTE CALIBRATION OF A H ATOM SECONDARY EMISSION DETECTOR ... 42

2.4 PLASMA ION TEMPERATURE MEASURED BY NEUTRON TRANSMISSION THROUGH LIQUID OXYGEN ... 43

3. PLASMA THEORY ... 45

3.1 EBT THEORY ... 46

3.1.1 ELMO Bumpy Torus ... 47

3.1.2 A Preliminary Investigation of Trapped Particle Instabilities in EBT ... 47

3.1.3 Macroscopic Stability and β Limits in the ELMO Bumpy Torus ... 48

3.1.4 Kinetic Transport Properties of a Bumpy Torus with Finite Radial Ambipolar Field ... 48

3.1.5 Radial Transport in the ELMO Bumpy Torus in Collisional Regimes ... 48

3.2 MHD THEORY ... 48

3.2.1 Analytic Model for the Nonlinear Interaction of Tearing Modes of Different Pitch in Cylindrical Geometry ... 49

3.2.2 Poloidal Magnetic Field Fluctuations in Tokamaks ... 49

3.2.3 Non-Linear Numerical Algorithms for Studying Tearing Modes 50
3.2.4 Comments on "Simulation of Large Magnetic Islands: Possible Mechanism for a Major Tokamak Disruption" 50
3.2.5 Mechanism for Major Disruptions in Tokamaks 51
3.2.6 Nonlinear Interaction of Tearing Modes in Highly Resistive Tokamaks 51
3.2.7 Magnetic "Islandography" in Tokamaks 51
3.2.8 Tearing Mode Activity for Hollow Current Profiles 52
3.2.9 Stabilization of Tearing Modes to Suppress Major Disruptions in Tokamaks 52
3.2.10 Tearing Mode Analyses of MHD Activity in ISX-A 53
3.2.11 Effects on the Nonlinear Interaction of Tearing Modes due to Temperature Evolution 53
3.2.12 Evolution of Flux Conserving Tokamak Equilibria with Preprogrammed Cross Sections 53
3.2.13 Intense Neutral Beam Heating in the Adiabatic Approximation 54
3.2.14 Continuous Tokamaks 54
3.2.15 Very Small Aspect Ratio Tokamaks 55
3.2.16 Low Density Ignition Scenarios Using Injection Heating 55
3.2.17 Resistive-Ballooning-Mode Equation 57
3.2.18 Necessary Stability Criterion for Plasma Equilibria with Tensor Pressure 59
3.2.19 Stability of Tokamaks with Elongated Cross Section 59

3.3 THEORY 59
3.3.1 Anomalous Transport 60
3.3.2 Neoclassical Transport and Analytic Finite Beta Equilibrium 63
3.3.3 Energetic Particle Orbits and Neutral Beam Injection 65
3.3.4 Numerical Simulation of Collisional Transport and Drift Waves 70

3.4 TRANSPORT SIMULATION 77
3.4.1 Simulation of Multispecies Impurity Transport in Tokamaks 77
3.4.2 Charge-Transfer Excitation of Impurity Ions in Tokamaks 78
3.4.3 Impurity Behavior during Neutral Beam Injection and Gas Puffing into ORMAK 78
3.4.4 Numerical Modeling of Impurity Effects 78
3.4.5 MHD/Transport Interactions in Tokamaks 79
3.4.6 On Measuring the Electron Heat Diffusion Coefficient in a Tokamak from Sawtooth Oscillation Observations 80
3.4.7 Heat Transport in Tokamaks as Observed from Sawtooth Oscillation Characteristics 80
3.4.8 Analysis of Heat Transport in ALCATOR from Sawtooth Observations 80
3.4.9 High-β Tokamak Modeling Studies 80
3.4.10 High Beta Tokamaks 81
3.4.11 Tokamaks Heated to High Beta 81

3.5 PLASMA ENGINEERING 82
3.5.1 Plasma Systems Analysis 82
3.5.2 Poloidal Field Studies 85
3.5.3 Advanced Fuels 86
3.5.4 Plasma Engineering Support of Advanced Systems 87

3.6 COMPUTING SUPPORT 91
- 3.6.1 User Service Center 91
- 3.6.2 Experimental Data Handling 91

REFERENCES 92

4. ATOMIC, MOLECULAR, AND NUCLEAR PHYSICS 97
- 4.1 EXCITED-STATE CONTRIBUTION TO THE ELECTRON LOSS COLLISIONS OF A FAST H^0 BEAM ON N^{3+} IONS 97
- 4.2 ELECTRON IMPACT IONIZATION OF MULTICHARGED IONS 98
- 4.3 ELECTRON IMPACT EXCITATION OF N^{4+} 100
- 4.4 LOW ENERGY MEASUREMENTS OF ELECTRON TRANSFER FROM HYDROGEN ATOMS AND MOLECULES TO MULTICHARGED IONS 100
- 4.5 LASER ION SOURCE 101
- 4.6 CONTROLLED FUSION ATOMIC DATA CENTER 101

REFERENCES 102

5. PLASMA HEATING AND FUELING 105
- 5.1 PELLET FUELING 106
- 5.2 NEUTRAL BEAM DEVELOPMENT 107
  - 5.2.1 Ion Source Development 107
  - 5.2.2 Ion Optics Theory 109
  - 5.2.3 Neutral Beam Line Development 110
  - 5.2.4 Energy Recovery Experiment 111
  - 5.2.5 Neutral Beam Systems 112
  - 5.2.6 Diagnostics 113
  - 5.2.7 Electrical Technology Development 114
- 5.3 VACUUM COMPONENTS DEVELOPMENT 115
  - 5.3.1 Beam Line Cryosorption Pump 115
  - 5.3.2 Energetic Particle Pumping 115
  - 5.3.3 Vacuum Engineering Data Studies 115
  - 5.3.4 Monte Carlo Simulation of Neutral Particle Transport in a System Containing Cryogenic Pumping Surfaces 115

REFERENCES 117

6. SUPERCONDUCTING MAGNET DEVELOPMENT 119
- 6.1 INTRODUCTION 120
- 6.2 LARGE COIL PROGRAM 120
  - 6.2.1 Program Management 120
  - 6.2.2 Test Coils 122
  - 6.2.3 Large Coil Test Facility 124
  - 6.2.4 Research and Development Activities (RDAC) 125

6.3 ADVANCED CONDUCTOR DEVELOPMENT 133
  6.3.1 Conductor Development Contracts 133
  6.3.2 Conductor Purchase 134
  6.3.3 Test Facilities 134
  6.3.4 Coil Winding and Test Experiment 134
  6.3.5 Analytic Solution for the Propagation Velocity in Superconducting Composites 134
  6.3.6 Transient Heat Transfer to Liquid Helium from Bare Copper Surfaces 135
  6.3.7 The Toroidal Energy Storage Experiment (TESPE) Project 135
6.4 12-T COIL DEVELOPMENT PROGRAM 135
6.5 MAGNET DESIGN FOR SPECIFIC MACHINES 136
  6.5.1 Superconducting Magnets for Heavy Ion Cyclotrons 136
  6.5.2 Coal Separation 136
  6.5.3 EBT-II 137

REFERENCES 137

7. ADVANCED SYSTEMS 139
7.1 THE NEXT STEP PROGRAM 141
7.2 ENGINEERING TEST FACILITY (ETF) DESIGN CENTER 145
  7.2.1 ETF Design Center Charter, Goals, and Objectives 146
  7.2.2 ETF Mission Statement 146
  7.2.3 ETF Design Center Staffing 147
7.3 ORNL FUSION POWER DEMONSTRATION STUDY 148
  7.3.1 The Emphasis on Reliability in Design Approach 148
  7.3.2 Development of a New Design 149
  7.3.3 Conclusions of Study 150
7.4 COMMITTED SITE EVALUATION 152
  7.4.1 Economic Impact 152
  7.4.2 Schedule Impact 153
7.5 TOKAMAK INSTRUMENTATION AND CONTROLS 153
7.6 LARGE ASPECT RATIO TOKAMAK STUDY 155

REFERENCES 156

8. MATERIALS 157
8.1 ALLOY DEVELOPMENT FOR IRRADIATION PERFORMANCE 157
  8.1.1 The Behavior of Type 316 Stainless Steel under Simulated Fusion Reactor Irradiation 157
  8.1.2 Tensile Properties of Type 316 Stainless Steel Irradiated in a Simulated Fusion Reactor Environment 158
  8.1.3 Precipitation Response of Austenitic Stainless Steel to Simulated Fusion Irradiation 159
  8.1.4 Estimates of Time-Dependent Fatigue Behavior of Type 316 Stainless Steel Subject to Irradiation Damage in Fast Breeder and Fusion Power Reactor Systems 159

8.1.5 **The Response of Inconel 600 to Simulated Fusion Reactor Irradiation** 160
8.1.6 **Plastic Instability in Neutron Irradiated Niobium** 160
8.1.7 **The Ductility in Bending of Molybdenum Alloys Irradiated between 425 and 1000°C** 160
8.1.8 **Neutron Irradiation Damage in Molybdenum at High Temperatures** 161
8.1.9 **The Tensile Properties of High Oxide SAP Containing Helium and Tritium** 161
8.1.10 **Recovery of Tritium from Solid Lithium-Sintered Aluminum Product (SAP) and Lithium-Aluminum Alloys** 162
8.1.11 **Current Irradiation Experiments in the MFE Materials Program** 162
8.1.12 **Future MFE Materials Irradiation Experiments** 162
8.1.13 **Design of Materials Irradiation Experiments Utilizing Spectral Tailoring** 164
8.1.14 **Thermal-Gradient Mass Transfer in Lithium-Stainless Steel Systems** 166
8.1.15 **Effects of Nitrogen and Nitrogen Getters in Static Lithium on the Corrosion of Type 316 Stainless Steel** 166
8.1.16 **Corrosion Tests of Austenitic Stainless Steels in Static Lithium** 167
8.1.17 **Corrosion of Long-Range-Ordered (Co-V-Fe) Alloy in Static Lithium** 167
8.1.18 **Compatibility of Molten Salts with Type 316 Stainless Steel** 167
8.1.19 **Procurement of Materials for the MFE Alloy Development for Irradiation Performance in Fusion Reactor Programs** 168

8.2 DAMAGE ANALYSIS 169
8.2.1 *Range Calculations Using Multigroup Transport Methods* 169
8.2.2 *Study of the Low Energy Responses of the BCA Code MARLOWE* 169

8.3 RADIATION EFFECTS ON ORGANIC INSULATORS FOR SUPERCONDUCTING MAGNETS 170

REFERENCES 171

9. NEUTRON TRANSPORT 173

9.1 ANALYSIS OF MAGNETIC FUSION ENERGY INTEGRAL EXPERIMENTS 173

9.2 MACROSCOPIC CROSS SECTION SENSITIVITY STUDY FOR FUSION REACTOR SHIELDING EXPERIMENTS 174

9.3 COMPARISON OF ONE- AND TWO-DIMENSIONAL CROSS SECTION SENSITIVITY CALCULATIONS FOR A FUSION REACTOR SHIELDING EXPERIMENT 175

9.4 CROSS SECTION SENSITIVITY ANALYSIS OF A PROPOSED NEUTRON STREAMING EXPERIMENT WITH A TWO-DIMENSIONAL MODEL 175

9.5 TWO- AND THREE-DIMENSIONAL NEUTRONICS CALCULATIONS FOR THE TFTR NEUTRAL BEAM INJECTORS 175

9.6 SHIELDING CALCULATIONS FOR THE TFTR NEUTRAL BEAM INJECTORS 175

9.7 DOSE RATES FROM INDUCED ACTIVITY IN THE TFTR TEST CELL 177

9.8 DESIGN CALCULATIONS FOR A 14-MeV NEUTRON COLLIMATOR 178

9.9 NUCLEAR PERFORMANCE OF MOLTEN SALT FUSION-FISSION SYMBIOTIC SYSTEMS FOR CATALYZED DD AND DT REACTORS 179

9.10 RADIATION SHEILDING INFORMATION CENTER 180

REFERENCES 180

10. MANAGEMENT SERVICES 183

10.1 INTRODUCTION 183

10.2 FINANCE OFFICE 183

10.3 OFFICE OF THE ADMINISTRATOR 185

10.3.1 Visitors 185

10.3.2 Personnel Functions 185

10.3.3 Subcontracts 186

10.3.4 FED Communications Center 186

10.4 MANAGEMENT INFORMATION SYSTEM 186

10.5 ENGINEERING SERVICES, QUALITY ASSURANCE, SAFETY AND EMERGENCY PLANNING, AND PROCUREMENT EXPEDITING 187

10.5.1 Engineering Services 187

10.5.2 Procurement Expediting 187

10.5.3 Safety and Emergency Planning 187

10.5.4 Quality Assurance 188

10.6 FED LIBRARY 188

LIST OF ABBREVIATIONS 189

PUBLICATIONS, PAPERS, AND REPORTS 191

INTRODUCTION

This has been another period in which the combined strengths of the Oak Ridge National Laboratory (ORNL) Fusion Energy Program in theoretical and experimental plasma confinement and fusion technology have resulted in a broad spectrum of significant accomplishments. The breadth and significance of these accomplishments are illustrated in the unique physics accomplishments of the Impurity Study Experiments (ISX-A and ISX-B) and the Elmo Bumpy Torus (EBT); the technology advances in neutral injection, pellet fueling, superconducting magnets, and materials; the integration of all these program strengths into the EBT-P and Long Pulse Technology Tokamak (LPTT) designs; and the recognition of our advanced design capability by the location of the national Engineering Test Facility (ETF) Design Center at ORNL. These accomplishments were possible because of the effective integration of our broad program and the contributions of a large number of organizations that include other ORNL divisions, UCC-ND Engineering, private industries, and other laboratories. We believe this breadth and multiorganizational involvement are the most effective role for the ORNL Fusion Energy Division, and we are striving to continue this theme with EBT-P, LPTT, advanced technologies, and the ETF design.

The highlights given in this introduction illustrate both the breadth and significance of the ORNL program. These major achievements give us confidence that we are making progress towards our goal of developing a viable fusion energy source for the future of mankind. While completing the projects and programs highlighted in this year's report, we have continued to plan programs and develop components essential for future contributions.

Conversion of the EBT-I experiment to EBT-S was completed in the first half of 1978 concurrently with the development of 28-GHz, high power, cw gyrotrons by Varian. During 1978 Varian demonstrated cw power output greater than 100 kW, and experimental gyrotrons resulting from this effort were utilized in the primary ECH system for operation of EBT-S. Operation with these first 28-GHz sources was, however, very limited and was restricted to a power of about 50 kW. As predicted from theoretical scaling considerations, a rise in toroidal plasma density of approximately 50% was observed in EBT-S operation. However, the electron and ion temperatures remained roughly constant, also as expected, because toroidal plasma temperatures scale with total microwave power, which so far has been the same as in the EBT-I mode. The simple theoretical stability criteria previously used for EBT have been substantiated through more detailed analysis of kinetic effects, and most of the primary experimental observations have been explained theoretically on the basis of neoclassical transport. These phenomena include the ambipolar potential, the level and scaling of thermal losses, the formation of a nonthermal ion distribution, and the tendency to operate at a very low degree of impurity contamination.

Studies of ohmically heated plasmas were made in ISX-A under a wide variety of conditions. Optimum confinement parameters were τ_E = 30 msec and Z_{eff} = 1.5. The initially linear increase of τ_E reached a limit as a function of plasma density, apparently as a result of transition from electron-dominated to ion-dominated loss regimes. In joint work with the General Atomic Company (GA), the inward transport of a neon test impurity was significantly reduced by poloidally asymmetric injection of hydrogen gas into the discharge, a result consistent with the impurity flow reversal effect as predicted by neoclassical transport theory. Operation of ISX-A was completed in March, and conversion began to the upgraded ISX-B tokamak. The new facility is equipped with neutral beam injectors and provisions for noncircular plasma cross sections, and its primary goal is study of the limits on plasma beta. With up to 0.7-MW neutral beam power, the results already obtained include an average toroidal beta of 1.4% and a central toroidal beta of 7%. Theoretical work on high beta tokamaks that was pioneered and made credible at ORNL has culminated in the demonstration of (1) stable equilibria at beta values as high as 10% for aspect ratio 4, (2) longevity of high beta cases in the presence of resistive skin diffusion, and (3) benign reaction to the full range of transport phenomena. As a result, the type of operation required for high energy-density, long-lived discharges in the LPTT device appears credible. Early testing of high beta theory has been made possible through our design of a very flexible plasma control field system for the second phase of the ISX-B device.

Significant advances have continued in the development of pellet injectors and neutral beam injectors. The pneumatic-type pellet injector was upgraded from a pellet velocity of 330 m/sec to 1000 m/sec with 1-mm-diam pellets. *Injection experiments on* ISX-B showed that for 600-700-eV central plasma temperatures, the pellets can penetrate the entire plasma discharge and impact on the inner wall. When accompanied by neutral beam injection, the plasma remains quiescent even with a factor of 2-3 density increase, and the pellet penetrates 20-30 cm into the discharge. A prototype centrifugal mechanical injector has been operated with 0.8-mm-diam pellets at a feed rate of 150 pellets/sec and has achieved pellet velocities of 290 m/sec. In the neutral beam development program, two ISX-B injectors similar to those developed for the Princeton Large Torus (PLT) but with shaped extraction apertures were tested on the Medium Energy Test Facility (METF). At extraction parameters of 42 kV and 61 A, the improved optics delivered 900 kW of H^0 power. The last of the four PLT beam lines was delivered to Princeton Plasma Physics Laboratory (PPPL), and the four injectors raised the PLT ion temperature to 6.5 keV. A 30-cm-grid-diam PDX (Poloidal Divertor Experiment) ion source has, in preliminary testing, produced 110-A beams at 41 kV for 100-msec pulses. An energy recovery experiment based on the ORNL concept of transverse magnetic field electron blocking yielded preliminary recovery efficiencies of 60 ± 20%. This is a very significant advancement in the development of high energy, steady-state injectors for future experiments because it simultaneously improves the system efficiency and drastically simplifies the beam target cooling problems. This continued advancement in both of these critical fueling and heating technologies is crucial to the future of advanced fusion devices.

The program to develop large toroidal superconducting magnets is now well established. Three major U.S. equipment manufacturers, under subcontracts to design and build one test coil each, spent the year in detailed design and in supporting verification tests. Japan and Switzerland joined EURATOM and the U.S. in an international agreement that will culminate in tests of a six-coil toroidal array at ORNL. The design of the U.S. coils has benefited significantly from the research and development support of the Magnetics and Superconductivity Section of the Fusion Energy Division. Several facilities have been constructed for verification testing of superconductors. The development, instrumentation, diagnostics, and protection systems have also made up a large part of the research and development. Another area of work involving considerable interaction with the subcontractors is coil fabrication technology. Construction of the Large Coil Test Facility (LCTF) began with preparing the site, pouring the concrete base for the vacuum tank in Building 9204-1, and forming the tank sections.

In September 1978 the Department of Energy (DOE) introduced a new policy statement for fusion energy. One key element of the strategy outlined in this policy was the decision to have an Engineering Test Facility built to serve as the vehicle by which the fusion program would move from the scientific phase into the engineering test phase. The ETF would provide a testbed for reactor components in a fusion environment. Following the review of recommendations from GA, ORNL, and PPPL, DOE selected ORNL to host an ETF Design Center with the responsibility of developing a detailed mission statement for an ETF that could begin operation in the late 1980's, a reference design for a facility with this mission, and recommendations on what program elements are necessary to ensure the technical success of the facility. The ETF Design Center team has been established with significant supporting responsibility being accepted by the major fusion centers of GA, PPPL, and the Massachusetts Institute of Technology.

1. EXPERIMENTAL CONFINEMENT

J. Sheffield, Section Head
J. L. Dunlap, Associate Head for Tokamak
G. R. Haste, Associate Head for EBT
H. O. Eason, Microwave Development

T. Amano[1]
J. L. Anderson[2]
B. R. Appleton[3]
F. W. Baity
D. D. Bates[2]
S. C. Bates
M. C. Becker[2]
W. R. Becraft[4]
L. A. Berry[5]
F. M. Bieniosek[6]
P. [illegible] Brown
T. G. Brown[2]
E. H. Bryant[8]
N. B. Bryson
P. B. Burn[6]
K. H. Burrell[9]
R. D. Burris[10]
[illegible] E. Bush
[illegible] B. Cain[8]
[illegible] D. Callen[1]
[illegible] L. Campen[8]
[illegible] H. Carpenter[10]
[illegible] Cecchi[11]
[illegible] K. Charlton[10]
[illegible] R. Clarkson[7]
[illegible] E. Clausing[12]
[illegible] A. Cobble
R. J. Colchin
K. A. Connor
V. Corso[11]
E. C. Crume, Jr.[1]
J. S. Culver
R. A. Dandl[13]
J. C. DeBoo[9]
S. K. DeCamp
R. A. Dory[1]
G. R. Dyer
R. B. Easter[8]
P. H. Edmonds
O. C. Eldridge*
L. C. Emerson[12]
A. C. England
E. S. Ensberg[9]
C. A. Foster[14]
R. H. Fowler[10]
J. E. Francis[1]
P. Gelpi[7]
J. C. Glowienka
Y. Gomay[9]
D. H. Gray[8]
A. D. Guttery
S. L. Halsted[12]
H. H. Haselton[14]
P. N. Haubenreich[15]
L. Heatherly[12]
M. E. Hesse[16]
R. L. Hickok[6]
K. W. Hill[17]
R. E. Hill[5]
S. Hiroe[18]
J. T. Hogan[1]
W. A. Houlberg[1]
H. C. Howe[1]
H. Ikegami[18]
R. C. Isler
T. C. Jernigan
R. L. Johnson[8]
G. G. Kelley[19]
A. R. Kemp[8]
H. E. Ketterer
H. J. Kim[14]
P. W. King
M. H. Kunselman[8]
S. P. Kuo[6]
R. A. Langley
N. H. Lazar[20]
E. A. Lazarus
R. L. Livesey
C. M. Loring
D. C. Lousteau[8]
M. S. Lubell[21]
R. V. Lunsford, Jr.[6]
J. F. Lyon
L. A. Massengill
C. S. Mayes
D. H. McCullough[13]
H. C. McCurdy
R. W. McGaffey[10]
M. W. McGuffin
D. H. McNeill[17]
V. J. Meece
M. M. Menon[14]
A. T. Mense[1]
L. San Miguel[22]
J. T. Mihalczo[7]
S. L. Milora[14]
P. Mioduszewski[23]
R. V. Miskell[8]
E. C. Moore
O. B. Morgan[24]
M. Murakami
C. W. Murphy[8]
W. Namkung[25]
A. P. Navarro[26]
R. V. Neidigh†
G. H. Neilson
B. E. Nelson[8]
D. B. Nelson[1]
M. Nishi[11]
I. U. Ojalvo[7]
J. A. O'Toole[7]
D. R. Overbey[1]
V. K. Paré[2]
J. W. Pearce
Y-K. M. Peng[1]
G. F. Pierce[6]
N. S. Ponte[14]
B. L. Pope
R. Prater[9]
J. A. Pusateri[7]
C. C. Queen[8]
B. H. Quon[26]
J. A. Ray[27]
P. L. Ray
T. F. Rayburn
W. J. Redmond
J. W. Reynolds[2]
J. B. Roberto[3]
J. A. Rome[1]
M. J. Saltmarsh
H. C. Sanderson
M. J. Schaffer[9]
D. E. Schechter[14]
S. D. Scott[28]
R. J. Sentell[29]
T. E. Shannon[8]
J. E. Simpkins
T. E. Smith[5]
[illegible] Steiner[30]
K. A. Stewart[1]
W. L. Stirling[14]
W. C. T. Stoddart[8]
J. D. Stout[8]
D. W. Swain
C. E. Thomas[28]
P. B. Thompson[8]
C. C. Tsai[14]
N. A. Uckan[1]
T. Uckan
R. D. Wall[8]
C. C. Weaver
T. L. White
P. W. Whitfield[8]
R. M. Wieland[10]
J. B. Wilgen
W. R. Wing
R. E. Wintenberg[2]
G. W. Wiseman[7]
S. P. Withrow[3]
S. K. Wong[9]
J. W. Wooten[10]
R. E. Worsham
W. L. Wright[8]
R. B. Wysor[8]
T. Yang[31]
O. C. Yonts[1]
R. A. Zuhr[3]
B. Zurro[26]

---

*Part-time
†Retired
1. Plasma Theory Section.
2. Instrumentation and Controls Division.
3. Solid State Division.
4. General Electric Company, Schenectady, New York.
5. Director, Fusion Program.
6. Consultant, Rensselaer Polytechnic Institute, Troy, New York.
7. Grumman Aerospace Corporation, Bethpage, New York.
8. UCC-ND Engineering.
9. General Atomic Company, San Diego, California.
10. Computer Sciences Division.
11. Princeton Plasma Physics Laboratory, Princeton, New Jersey.
12. Metals and Ceramics Division.
13. Retired, formerly Section Head, High Beta Plasma Section.
14. Plasma Technology Section.
15. Manager, Large Coil Program.
16. On Leave from Centre d'Études Nucléaires de Grenoble, Grenoble, France.
17. Present address: Princeton Plasma Physics Laboratory, Princeton, New Jersey.
18. Consultant, Institute of Plasma Physics, Nagoya University, Nagoya, Japan.
19. Retired, formerly Head, Special Projects.
20. Present address: TRW, Incorporated, Redondo Beach, California.
21. Magnetics and Superconductivity Section.
22. Participant in Great Lakes Colleges Association/Associated Colleges of the Midwest, Oak Ridge Science Semester Program.
23. Visiting scientist, Institut für Plasmaphysik, K.F.A., Jülich, F.R.G.
24. Director, Fusion Energy Division.
25. Present address: University of Maryland, College Park, Maryland.
26. Visiting scientist, Spanish Nuclear Energy Commission.
27. Physics Division.
28. Graduate student, Nuclear Engineering Department, Massachusetts Institute of Technology, Cambridge, Massachusetts.
29. Tennecomp Systems, Incorporated, Oak Ridge, Tennessee.
30. Manager, Advanced Systems Program.
31. Westinghouse Electric Corporation, Pittsburgh, Pennsylvania.

BLANK PAGE

Abstract. Conversion of the ELMO Bumpy Torus (EBT-I) experiment to EBT-Scale (EBT-S) continued in the first half of 1978 simultaneously with the Varian program under Oak Ridge National Laboratory (ORNL) subcontract for development of 28-GHz, superpower, continuous wave (cw) gyrotrons. During 1978 Varian demonstrated cw power output greater than 100 kW, and experimental gyrotrons resulting from this effort were utilized in the primary electron cyclotron heating (ECH) system for operation of EBT-S. Operation with 28-GHz power was, however, very limited and was restricted to a power of about 50 kW. As predicted from theoretical scaling considerations, a rise in toroidal plasma density of approximately 50% was observed in EBT-S operation. However, the electron and ion temperatures remained roughly constant, also as expected, because toroidal plasma temperatures scale with total microwave power, which was the same as in the EBT-I mode.

Additional work was directed towards refining diagnostic techniques and coordinating diagnostic measurements. A new Thomson scattering system and a charge exchange analyzer that measures ions from the mirror throat were installed near the end of the year during the overhaul of two of the motor-generators that provide magnetic field power for EBT.

Studies of ohmically heated plasmas were made in the Impurity Study Experiment (ISX-A) tokamak under a wide variety of conditions. Optimum confinement parameters were τ_E = 30 msec and Z_{eff} = 1.5. The initially linear increase of τ_E reached a limit as a function of plasma density, apparently as a result of transition from electron-dominated to ion-dominated loss regimes. The inward transport of a neon test impurity was significantly reduced by poloidally asymmetric injection of hydrogen gas into the discharge, a result consistent with the impurity flow reversal effect as predicted by neoclassical transport theory. Operation of ISX-A ceased in March for conversion to the upgraded ISX-B tokamak. The latter facility is equipped with neutral beam injectors and provisions for noncircular plasma cross sections. The primary goal is a study of the limits on plasma beta. With up to 0.7-MW neutral beam power, the results already obtained include an average toroidal beta of 1.4% and a central toroidal beta of 7%. Solid-hydrogen-pellet injection into ISX-B discharges has produced factors of 2-3 density increase. Details of a number of plasma measurements, the neutral beam system, and progress towards an upgrade of these systems are included. The results of the Impurity Study Program and the status of the Long Pulse Technology Tokamak (LPTT) are reviewed.

1.1 INTRODUCTION

The Experimental Confinement Section was formed by a merging of the two separate sections previously involved in this work: the Experimental Tokamak Section under J. Sheffield and the High Beta Plasma Section under R. A. Dandl, now retired. The work reported here was done mostly under the earlier administrative arrangement. The programmatic organization of the section is shown in Fig. 1.1, which also serves as an aid in identifying the principals involved in the different areas. The Atomic Physics and Diagnostic Development Group in the Physics Division, whose affiliation with the section is indicated in the figure, summarizes its work in Sects. 2 and 4 of this report.

The EBT experiment is described in Sect. 1.2. In Sects. 1.2.1-1.2.5 the principal diagnostic development programs are described. The effects of field errors on EBT plasma confinement are examined in Sect. 1.2.6, and a study of the absorption of the ordinary wave in a finite temperature EBT plasma is discussed in Sect. 1.2.7. In Sect. 1.2.8 the EBT-II developments are given. Sections 1.2.9-1.2.11 describe the microwave technology developments for 1978, and Sect. 1.2.9 is a description of the EBT-S ECH system.

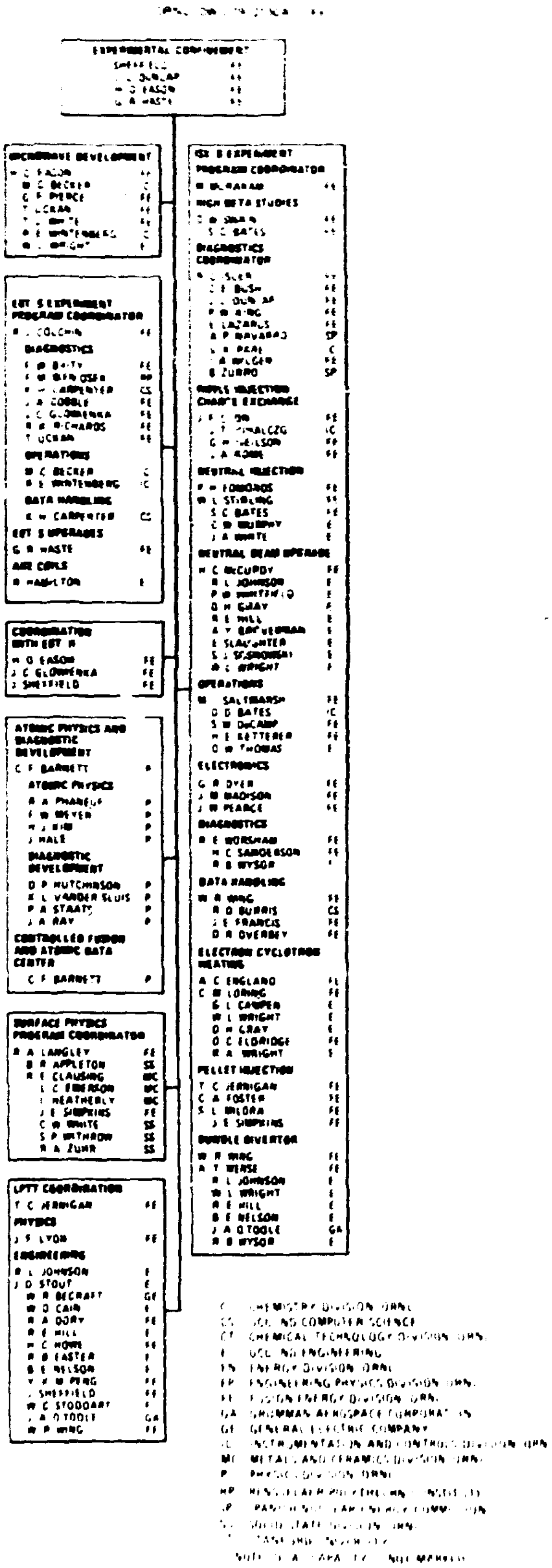
EXPERIMENTAL CONFINEMENT
EBT-S EXPERIMENT PROGRAM COORDINATOR
DIAGNOSTICS
OPERATIONS
DATA HANDLING
EBT-S UPGRADES
AIR COILS
COORDINATION WITH EBT-P
ISX-B EXPERIMENT PROGRAM COORDINATOR
HIGH BETA STUDIES
DIAGNOSTICS COORDINATOR
NEUTRAL INJECTION
NEUTRAL BEAM UPGRADE
OPERATIONS
ELECTRONICS
DIAGNOSTICS
DATA HANDLING
ELECTRON CYCLOTRON HEATING
PELLET INJECTION
BUNDLE DIVERTOR
ATOMIC PHYSICS AND DIAGNOSTIC DEVELOPMENT
ATOMIC PHYSICS
DIAGNOSTIC DEVELOPMENT
CONTROLLED FUSION AND ATOMIC DATA CENTER
SURFACE PHYSICS PROGRAM COORDINATOR
EPTT COORDINATION
PHYSICS
ENGINEERING

Fig. 1.1. Experimental Confinement Section programmatic organization.

Tokamak research is described in Sect. 1.3, starting with a review of ISX-A data in 1.3.1. Our initial results with the ISX-B are given in Sect. 1.3.2, along with reports of progress towards the ECH and neutral beam systems. Section 1.3.3 deals with the Impurity Study Program and 1.3.4 with the design studies for the EPTT.

1.2 EBT RESEARCH

1.2.1 Soft X-Ray Measurements

G. R. Haste S. Hiroe

The soft x-ray data reported in previous years have been taken with a single detector that views the plasma along the diameter. In the course of the past year, an array of such detectors has been added. This array, shown in Fig. 1.2, consists of five detectors collimated to view the plasma along five parallel lines. The experience with the single-channel detector has proven very valuable in the design and operation of the five-channel system. For example, the collimation, the shielding from visible light, and the vacuum control techniques are directly applied. The same in situ calibration method is also used.

The purpose of this new array is to provide profile information. The results of some of the first measurements are shown in Fig. 1.3, with only four of the five channels represented. These preliminary data seem to indicate that the temperature profile is flat and that the density profile is peaked with a center a little above the machine midplane.

1.2.2 Charge Exchange Measurements

F. W. Baity J. C. Glowienka
B. H. Quon

There were two types of charge exchange analyzers used on EBT during 1978, one employing a conventional nitrogen stripping cell for converting the escaping energetic neutral atoms to positive ions and the other

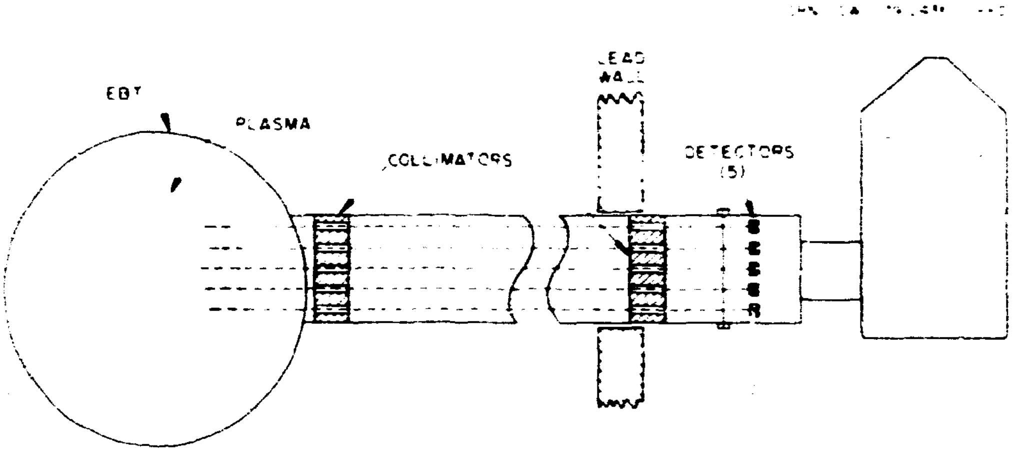

Fig. 1.2. Geometry of the five-channel soft x-ray detector.

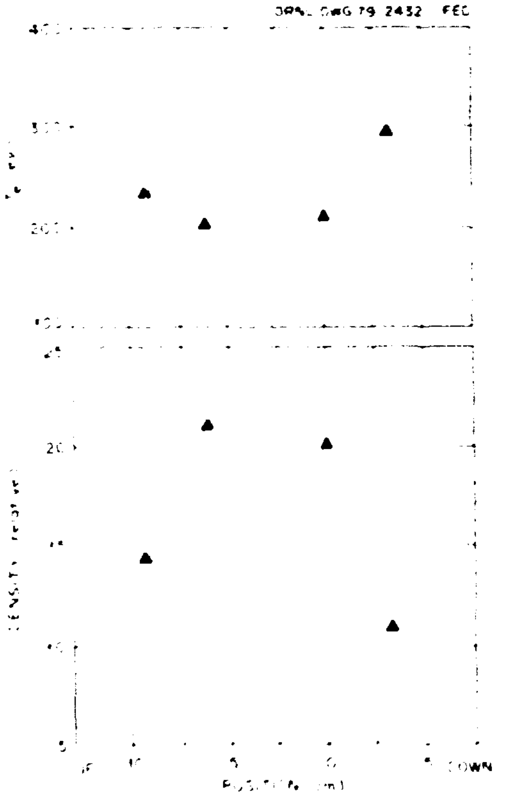

Fig. 1.3. Preliminary electron temperature and density profiles taken with the five-channel soft x-ray detector under typical T-mode conditions.

employing a cesium charge exchange cell for converting the neutrals to negative ions. The cesium cell analyzer, a new development specifically for application on EBT, has been previously described.[2]

The calibration for both spectrometers was carried out in the laboratory using a small diameter, monoenergetic neutral beam of low intensity. The intensity of the neutral beam was inferred by intersecting the beam with a Faraday cup and measuring the current due to secondary emission from the copper plate in the cup. The Faraday cup, in turn, was calibrated by an ion beam of the same energy, and the assumption was made that the secondary emission coefficients were the same for both ions and neutral particles. To test the validity of this assumption, a more sophisticated direct measurement was made of the secondary emission coefficient of neutral hydrogen atoms on copper.[3] It was discovered that, at energies greater than 100 eV, the secondary emission coefficients for ions and neutrals agree within 10% but that below 100 eV there is a large disparity in the two values, with the difference increasing rapidly as the energy decreases. These new secondary emission data were used to correct the calibration curves for both analyzers; also used was a new analysis that fits the charge exchange spectrum by adding several (usually three) Maxwellian distributions of different temperature. Simultaneous measurements were made with both analyzers and then compared.[4] Because of unresolved uncertainties, the toroidal plasma ion temperature determined by the cesium analyzer was higher by 10-20%, but the ion-neutral density product was lower by more than an order of magnitude. Work is now under way to determine the source of the error in the cesium analyzer results so that the improved low energy capability and increased count rate of this promising technique might be exploited.

During the period of downtime at the end of the year, a new charge exchange analyzer was installed that detects neutrals emitted in the mirror throat region of EBT. This analyzer should give information concerning the distribution of ion pitch angles in EBT.

1.2.3 Thomson Scattering

J. A. Cobble R. A. Dandl
M. C. Becker M. F. Hesse

Because of the low electron density, the high plasma light level, and the harsh x-ray environment, earlier laser scattering experiments on EBT have not generally been useful. This year installation of an improved Thomson scattering system was begun, and preliminary results indicate that plasma electron temperature and density will be measurable with the diagnostic. Initial experiments used new analog processing instrumentation to accumulate data from up to ten 500-MW laser shots per monochrometer setting. Signal-to-noise ratios of five have been recorded 100 Å from the ruby wavelength.

These first efforts showed the importance of a good viewing dump to suppress stray light and of shutters to protect vacuum windows from deposition of sputtered material. Also noted was the necessity of better radiation shielding for detectors and of more frequent system calibration.

Delivery is expected soon on a five-channel polychrometer that will decrease data acquisition time and the number of laser shots required. In addition, work has begun on a mirror rotation technique for obtaining spatial information.

1.2.4 Heavy Ion Beam Probe

S. P. Kuo F. M. Sieniosek

Measurements with the ion beam probe have been continued under EBT-I conditions. Areas of investigation have been the effect on the space potential of microwave heating and field errors and the continuity of potential along field lines.

The result of a study of the scaling with pressure and power for a number of space potential scans is illustrated in Fig. 1.4. Of interest is the evident smoothing of the potential well when 10.6-GHz profile heating is introduced.

Also, the continuity of the space potential along toroidal magnetic field lines has been investigated by eliminating the microwave power from the cavity in which the beam probe operates and from adjacent cavities. No appreciable change in the potential profile has been observed. It can be inferred from these measurements that the potential drop along field lines is negligible when compared to radial variations.

ORNL/DWG/FED 78 508

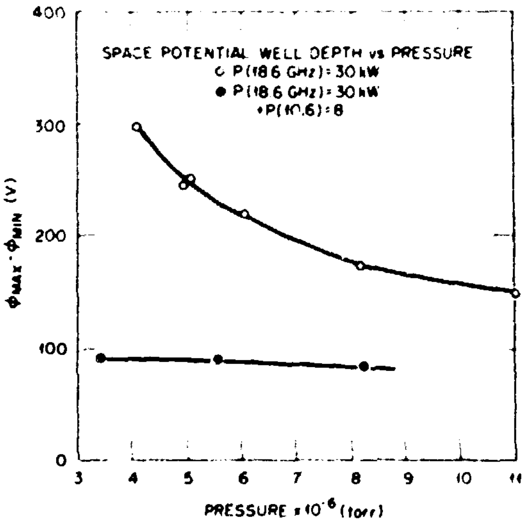

Fig. 1.4. Potential well depth vs ambient pressure for the cases with and without profile heating at 10.6 GHz.

The operating range of the heavy ion beam probe has been expanded to handle the increased voltage requirements, which are necessary because of the higher magnetic field of EBT-S. The entire beam line has been upgraded from 40 kV to 60 kV.

Further, the stability and accuracy of the high voltage detection circuit have been improved. This circuit must have temperature and voltage stability of one part in $10^{[illegible]}$-$10^{[illegible]}$. The ion gun structure has been modified to accommodate a commercial alkali emitter. The improved purity of this source allows measurement over a broader region of the plasma cross section.

1.2.5 Toroidal Plasma Impurities from vuv Emissions

N. H. Lazar   K. H. Carpenter

Analysis of data from spatial scans of vacuum ultraviolet (vuv) emissions of aluminum and carbon impurities was continued in EBT-I using a modified algebraic reconstruction technique. Earlier estimates of low impurity densities in the toroidal plasma were confirmed. Summarized in Table 1.1 are impurity ion densities at the center of the midplane.

Table 1.1. Impurity ion densities in the region of the toroidally confined plasma, assuming an electron density of 2.0×10^{12} cm^{-3}

Ion charge state	Density (cm^{-3}) at $r = 0$
H I	$8.2 \times 10^{[illegible]}$
C II	$5.9 \times 10^{[illegible]}$
C III	$3.9 \times 10^{[illegible]}$
C IV	$1.0 \times 10^{[illegible]}$
C V	$<1.4 \times 10^{[illegible]}$
Al II	$4.7 \times 10^{[illegible]}$
Al III	$1.3 \times 10^{[illegible]}$

1.2.6 Toroidal Current and Global Field Compensation

B. H. Quon   F. M. Bieniosek
S. P. Kuo

The global field compensation in EBT is used to reduce or enhance the system global field error, thus permitting studies of plasma stability and confinement with field error as a parameter.

In order to show the effect of field error on the structure of the potential profile, the potential profile was measured for a number of field error conditions with fixed pressure and power [see Figs. 1.5(a) and 1.5(b)]. Figure 1.5(a) shows the measured toroidal current as a function of applied horizontal correction field; at five points on this curve, potential profiles were measured along a canted vertical path defined by the heavy ion beam through the bottom half of the plasma [see Fig. 1.5(b)]. These figures are related as follows. In the region of minimum net toroidal current (between cases 3 and 4), the potential profiles remain nearly the same and are consistent with the typical two-dimensional (2-D) profile that exhibits a deep potential well. Outside this region, in both direction , the potential well is found to decrease as both field errors and the net toroidal current increase. Cases 1 and 5 show similar potential profiles at opposite extremes of toroidal current. In both directions the potential well is found to decrease as net toroidal current increases. The potential asymmetry that develops at these extremes appears to be related to the vertical drift of electrons whose drift surfaces intersect the system wall.

The feature of minimum net toroidal current, as observed in Fig. 1.5(a), suggests that an essentially current-free configuration is maintained when field errors are cancelled

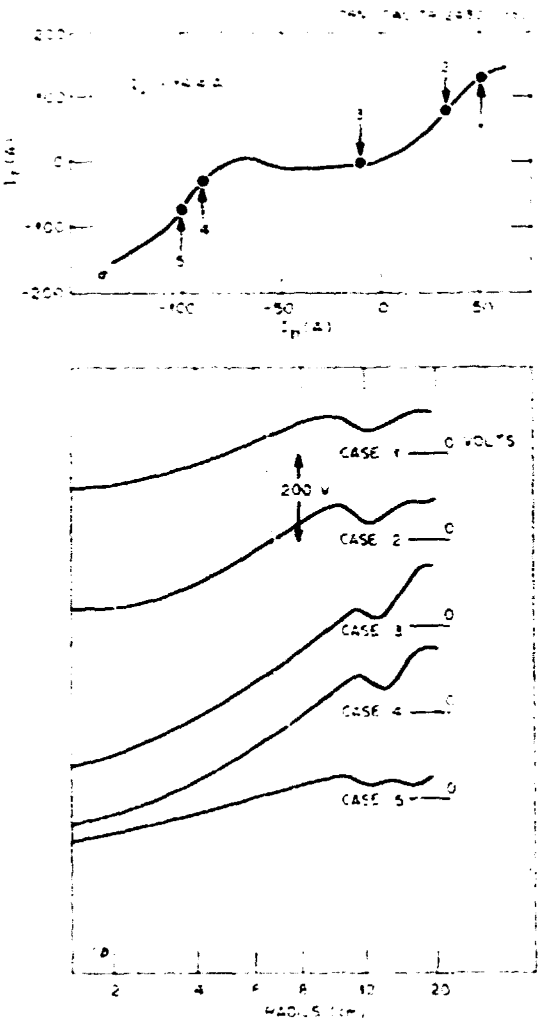

Fig. 1.5. (a) Toroidal current as a function of horizontal correction current; (b) radial potential profiles for the cases indicated in (a) under the plasma conditions of total applied microwave power, 43 kW, all at 18 GHz, and an ambient pressure of 6.1×10^{-6} Torr.

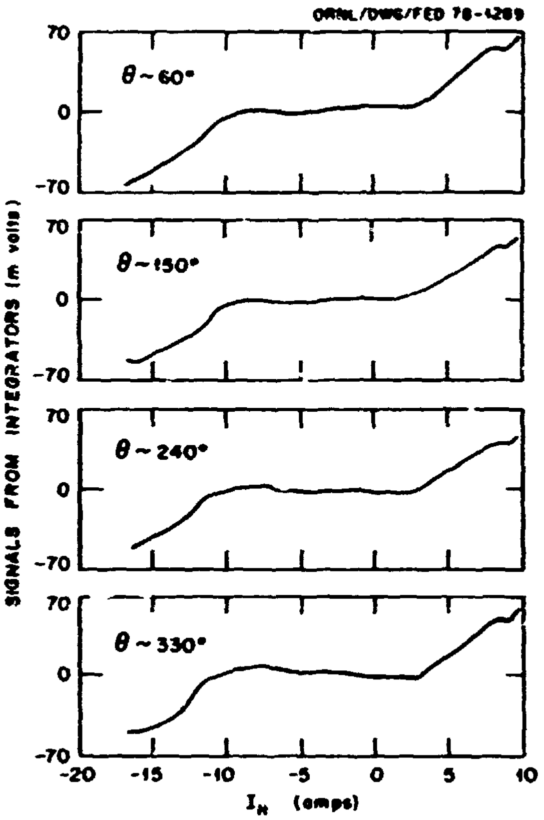

Fig. 1.6. Detailed current variation detected by four extra current pickup loops located at 60°, 150°, 240°, and 330° poloidal angle. The zero lines are provided for comparison.

out. In order to confirm this conjecture, four independent current pickup loops located on the outer surface at four different poloidal angles (θ = 60°, 150°, 240°, and 330°) have been used. The signals obtained from each of these pickup coils are plotted in Fig. 1.6. It is found from these measurements that, for error fields larger than the critical value $\delta B/B > (\delta B/B)_{cr}$, all four toroidal current signals are of the same sign and increase simultaneously to large amplitudes. In the region of small net toroidal current, the amplitudes of all signals reduce to small values, as expected. However, there is some detailed structure on the small residue current in this range of field errors. Each of these signals seems to vary sinusoidally and to cross zero once as the horizontal field error sweeps through this range. The sinusoidal behavior of each signal appears to be consistent with that expected from a diffusion-driven current $J_\parallel = (2\nabla \times \tilde{B})_\parallel/n\eta_\parallel = 2\nabla_r \delta B_\theta/n\eta_\parallel$.

1.2.7 Absorption of the Ordinary Wave in Finite Temperature EBT Plasma

T. Uckan

In EBT the coupling of the microwaves to the plasma is made through the electric field at the cavity port openings. Some portion of the wave energy is deposited in the region where the propagation frequency is near the electron cyclotron frequency. The electrons are heated as a result of this resonant interaction with the wave. The power absorption of the wave at the electron cyclotron frequency can be estimated from the injected wave, considering the finite electron temperature effects because cold plasma theory does not predict any absorption for the ordinary wave.

In the cavity the ordinary wave is propagating perpendicular to the magnetic field B with the frequency ω, which is higher than the plasma frequency ω_p. The microwave electric field, $E = E_0 e^{i(\omega t - kx)}$, must satisfy the following wave equation.

$$\frac{d^2E}{dx^2} + \left(\frac{\omega}{c}\right)^2 \epsilon_{zz}E = 0 . \qquad (1.1)$$

Here ϵ_{zz} is the dielectric constant; for Maxwellian electrons with the first order Larmor radius ρ corrections, it takes the form

$$\epsilon_{zz} = 1 - \left(\frac{\omega_p}{\omega}\right)^2 \left(1 + \frac{\mu}{4}\,\frac{\omega}{\Omega - \omega}\right) , \qquad (1.2)$$

where $\mu = k^2\rho^2/2 = T_e/m_ec^2$ and $\Omega = |e|B/m_ec$ is the cyclotron frequency. Further assume that the inhomogeneous magnetic field at the resonance region may be given as

$$B = B_\mu(1 - \alpha x) ,$$

$$\frac{|e|B_\mu}{m_ec} = \omega ,$$

which leads to

$$\Omega(x) = \omega(1 - \alpha x) . \qquad (1.3)$$

Using Eqs. (1.2) and (1.3) in Eq. (1.1), we get

$$\frac{d^2E}{dx^2} + \left(\frac{\omega}{c}\right)^2 \left(g_1^2 + \frac{g_2^2}{x + i\epsilon}\right) E = 0 , \qquad (1.4)$$

where

$$g_1^2 = [1 - (\omega_p/\omega)^2] , \qquad (1.5)$$

$$g_2^2 = \left(\frac{\omega_p}{\omega}\right)^2 \frac{\mu}{4\alpha} , \qquad (1.6)$$

and $\epsilon \ll 1$, which accounts for the other wave-damping mechanisms.

The solution of Eq. (1.4) can be expressed in terms of the Whittaker functions,[9] $W_{\mu,\nu=\pm1/2}(x)$. Using the large argument expansion of $W_{\mu,\nu}(x)$ for $x > 0$ and $x < 0$, the moduli of the reflection and transmission coefficients are[9] (as $\epsilon \to 0$)

$$|R| = 1 - \exp(-\pi\eta) ,$$

$$|T| = \exp(-\pi\eta/2) . \qquad (1.7)$$

Here $\eta = \left(\frac{\omega}{c}\right) g_2^2/g_1$. Hence, the fraction of the absorbed power A becomes

$$A = \exp(-\pi\eta)[1 - \exp(-\pi\eta)] . \qquad (1.8)$$

The characteristic magnetic field scale length α^{-1} may be expressed in terms of the mirror ratio M and the plasma radius a in the form

$$\alpha^{-1} = \left(\frac{2\sqrt{M}}{2 - \sqrt{M}}\right) a .$$

For the present EBT, $N = 2$; thus,

$$\alpha^{-1} = 5a \; . \tag{1.9}$$

Using Eqs. (1.5), (1.6), and (1.9) in Eq. (1.7), we get

$$\eta = \frac{\frac{5a}{4}\left(\frac{\omega}{c}\right)\left(\frac{\omega_p}{\omega}\right)^2\left(\frac{T_e}{m_e c^2}\right)}{\left|1-\left(\frac{\omega_p}{\omega}\right)^2\right|^{1/2}} \; . \tag{1.10}$$

The fraction of the power that is absorbed at the electron cyclotron resonance (ECR) region in EBT-S can now be estimated by the toroidal plasma with the following typical plasma parameters: $\omega_p/\omega = 0.7$, $\omega/2\pi = 28$ GHz, $T_e = 600$ eV, and $a = 12$ cm. From Eqs. (1.8) and (1.10), it is found that almost 16% of the incident microwave power is absorbed.

1.2.8 EBT-II

J. C. Glowienka

An engineering scoping study of the next generation EBT device (EBT-II) has been completed.[7] Except for an already funded, millimeter wavelength, very high power microwave source development program, the study stressed design compatibility with existing technology so as to permit establishing a baseline cost for the machine.

The EBT-II device represents a dramatic advance for EBT physics and technology and is based on two critical assumptions.

(1) Electron and ion transport in EBT-II will be neoclassical, as in the present EBT experiment.
(2) The requisite microwave and superconducting technology will be available if sufficient lead time is allowed for development.

The EBT-II machine will be able to test aggressively the validity of neoclassical scaling because of the increases in basic device parameters of microwave frequency ω_μ, magnetic field B, and mechanical aspect ratio.

The first stage of the experiment will concentrate on examining the scaling made possible with the device improvements. The higher ω_μ and B should allow operation at higher density where, as an added benefit, plasma diagnostics are more reliable. In addition, the larger aspect ratio should improve the neoclassical confinement time, which scales as the aspect ratio squared, by an order of magnitude. An additional feature designed into the device is the ability to control flexibly and to increase the effective aspect ratio with supplementary toroidal aspect ratio enhancement (ARE) coils, thereby pushing the scaling test even further. The current design calls for an ARE factor of about 2, which should increase the neoclassically calculated lifetime about a factor of 4. Under optimum conditions this phase of operation may yield confinement times of ~0.2 sec, temperatures of ~3 keV, and $n\tau$ of ~10^{13} sec/cm^3.

The second phase will center on the addition of auxiliary heating, most probably neutral beam heating. With the added heat and particle source allowing control of the electric field, we estimate an increase by a factor of 2 in energy lifetime at increased plasma density. It is possible to demonstrate reactor-like conditions in hydrogen with $\beta \sim 10\%$.

The parameters of the EBT-II scoping study are given in Table 1.2 and are compared with those of EBT-I and EBT-S. Design studies are continuing and are aimed at establishing a more cohesive overall EBT program that embraces (1) EBT-S, (2) the required development activities for EBT-II that can be addressed both on and independently of EBT-S, and (3) EBT-II.

Table 1.2. Machine and plasma parameters for EBT-I, EBT-S, and EBT-II

	Past EBT-I experiments concluded November 1977 (measured)	Present EBT-S experiments started summer 1978	Future EBT-II reference design (anticipated)
Machine			
Magnetic field (midplane, mirror)	0.45 T, 0.9 T	0.65 T, 1.3 T	3.0 T, 6.0 T
Magnetic field power			
Toroidal field coils	7.5 MW	10 MW	1.3 kW (refrigeration)
ARE coils	None		15 MW
Torus volume	1350 liters	1350 liters	5500 liters
Major radius	150 cm	150 cm	520 cm
Coil mean radius	18.8 cm	18.8 cm	28 cm
Aspect ratio	8:1	8:1	≈20:1
Microwave power, continuous wave (cw)			
Bulk heating	60 kW, 18 GHz	200 kW, 28 GHz	1.6 MW, 120 GHz
Profile heating	30 kW, 10.6 GHz	60 kW, 18 GHz	800 kW, 70-90 GHz
Neutral beam heating (cw)	None	None	1 MW at 20 kV
Hot electron annulus			
n_e	2-5 x 10^{11} cm^{-3}	2-5 x 10^{11} cm^{-3}	1-6 x 10^{12} cm^{-3}
T_e	≈100 keV	≈100 keV	500-2000 keV
$\beta_{annulus}$	10-40%	10-40%	10-50%

Toroidal plasma		Measured	Anticipated at full power	Anticipated at outset	With auxiliary heating
n_e	1-2 x 10^{12} cm^{-3}	EBT-I temperatures at higher densities (preliminary results)	2-6 x 10^{12} cm^{-3}	∼5 x 10^{13} cm^{-3}	
T_e	150-600 eV		300-800 eV	3 keV	8 keV
T_i	70-150 eV		100-200 eV	3 keV	8 keV
β_{max}	0.2-0.6%		∼0.5%	$\gtrsim$ 1%	10%
Midplane minor radius	10 cm		10 cm	≤17 cm	
Effective aspect ratio	8:1		8:1	≈40:1	
Volume	400 liters		400 liters	≤2000 liters	
$n\tau$	5 x 10^{10} sec cm^{-3}		∼10^{11} sec cm^{-3}	∼10^{13} sec cm^{-3}	

1.2.9 The 28-GHz, 200-kW cw Electron Cyclotron Heating System for EBT-S

H. J. Eason T. L. White
G. F. Pierce R. E. Wintenberg

Experiments in the EBT-I facility, a 24-sector, bumpy toroidal, dc magnetic trap heated at 18 GHz, have shown that plasma currents produced by microwave-heated, hot electron annuli can provide macroscopically stable plasma confinement in a steady-state bumpy torus. The EBT concept is attractive for extension to a fusion reactor and has been selected by the Department of Energy (DOE) as the leading alternative to the tokamak and mirror approaches to controlled fusion. Crucial to this extension is the development of high efficiency, multimegawatt, cw ECH systems operating at millimeter wavelength. Initial scaling experiments are being conducted at a heating frequency of 28 GHz in the EBT-S facility, a modification of EBT-I permitting operation at higher magnetic field strength.

Primary ECH power at 28 GHz for EBT-S is provided by a type VGA-8000 cw gyrotron oscillator developed by Varian Associates[1] under ORNL subcontract and designed for operation at a power output of up to 200 kW cw. The basic principle of its operation involves cyclotron resonance interaction of a hollow electron beam having large transverse energy with a cylindrical resonator operating in the TE_{021} mode. The basic elements of the gyrotron include the electron gun, the microwave interaction circuit, the electron beam collector, the microwave output coupling system, and the magnetic system, which is essential for focusing the electron beam and for the cyclotron resonance interaction.

The EBT-S 28-GHz gyrotron ECH system, which utilizes a power supply system constructed by Universal Voltronics, Mount Kisco, New York, to ORNL performance specification, includes an adjustable, negative 100-kV, dc, 10-A beam supply isolated from ground for monitoring of beam interception. It also includes a heater supply and an adjustable, well-regulated, low current, 40-kV positive supply referenced to the negative high voltage terminal for operation of the magnetron injection electron gun. Both the beam supply and the electron gun supply are equipped with fast crowbars to divert stored energy in the event of a fault. Typical VGA-8000 operating parameters are as follows: beam voltage of 80 kV, beam current of 8 A, and electron gun accelerating voltage of 27 kV. The required magnetic field of ≈11 kG is provided by a water-cooled copper magnet energized by a bank of four well-regulated, high current, low voltage supplies. Microwave power output is controlled over a dynamic range of 18 dB by variation of the transverse energy component of the electron beam. Transverse energy control is accomplished by a combination of small magnetic trim coils surrounding the electron gun and by variation of the extraction voltage. The gyrotron is constructed with a large, water-cooled, copper collector capable of dissipating the full 640-kW power of the electron beam. System cooling requirements are met by a closed loop heat exchange system using demineralized water. The collector flow requirement is 300 gpm at a pressure drop of 150 psi.

The output waveguide of the VGA-8000 has a 6.35-cm-diam circular cross section, and the output power propagates primarily in the TE_{02} mode, one of the family of circular electric modes that have very low-loss transmission characteristics. The output waveguide window of the gyrotron consists of two transverse disks of BeO ceramic separated by $\approx\lambda_g/2$ and cooled by circulation of a low-loss fluorocarbon liquid through the space between. The output waveguide is capable of supporting almost 100 propagating modes at 28 GHz, and extreme care is exercised to maintain constant cross section and minimize discontinuities in the transmission system, the objective being to minimize conversion of power between modes and to avoid trapped-mode resonances in the system. Miter bends of 90° are used to accomplish changes in waveguide direction. A "cross guide" directional coupler, developed for monitoring gyrotron output power and power reflected from EBT-S, is comprised of intersecting, circular waveguides with a 45° metallic septum perforated with an array of circular holes. Integral power measurements are obtained by calorimetric loads of low thermal capacity connected to the coupled ports of the directional coupler. Additional fast response monitoring of power and frequency is accomplished through use of samplers that respond primarily to TE°_{0n} modes. Waveguide material is copper except for short lengths of stainless steel waveguide inserted into each straight run for the purpose of introducing preferential loss for higher order modes. This results in damping of trapped-mode resonances. Waveguide arc protection is accomplished by a photoelectric detector that views the output window and activates the power supply crowbar. Waveguide and components are water cooled for environmental compatibility with associated equipment. The waveguide vacuum window used for entry into EBT-S is similar in design to that used on the gyrotron. The waveguide transmission system is operated at a slight positive pressure of dry nitrogen to minimize corrosion and to prevent the entry of moisture or foreign matter. The 28-GHz microwave power is fed into a large, copper-plated, water-cooled, stainless steel toroidal manifold (major diameter = 200 cm; minor diameter = 20 cm) that also serves as a vacuum pumping manifold for EBT-S. Radio frequency (rf) isolation of the vacuum pumps is provided by copper plates perforated with an array of below-cutoff circular holes. Power at 28 GHz is distributed to each of the 24 sectors of EBT-S through additional perforated copper plates, each having a centrally located, circular coupling aperture several wavelengths in diameter. Thus, the rf distribution manifold functions as a very low-Q reflecting chamber in which the loading is provided by strong coupling to the cyclotron-resonant magnetic field regions of EBT-S. Power distribution is adjusted empirically by changing aperture diameters. Measured plasma parameters, which are strongly dependent upon applied ECH power (viz., balance of the stored energy in the high beta, hot electron rings in all of the 24 sectors of EBT-S) are used as criteria for adjustment of power distribution. Initial operation of EBT-S at power levels exceeding 50 kW cw was attained during September 1978.

1.2.10 28-GHz Oversized Waveguide Development

T. L. White

Work during the past year has concentrated on improving our measurement techniques in an oversized waveguide at 28 GHz. In particular, a miter bend detector was developed to measure r variations in the E_z field in a 6.35-cm-diam oversized waveguide, and a rotary detector was built to measure ϕ and z variations in the H_z field at the wall of the waveguide. These measurements greatly increase our understanding of the effects on mode purity of miter bends, tapers, and other components in oversized systems.

Also, methods of measuring low level (≲1 mW) microwave power independent of mode content are being investigated so that oversized waveguide components can be characterized by their quasi-optical transmission properties rather than by a complete mode-by-mode description.

In addition, the electronic measurement techniques have been improved by the use of lock-in amplifiers and other signal processing techniques to improve signal-to-noise ratios.

A TE[illegible] to TE[illegible] mode transducer was developed to test a new output coupling system applicable to gyrotrons. This transducer has excellent mode purity, and similar techniques can be used to excite any TE_{0n} mode. The transducer consists of a TE[illegible] resonant ring, that is, an integer number of guide wavelengths in mean circumference, wrapped around a cylindrical cavity. Coupling to the cavity is achieved by using the same integer number of coupling holes (all in phase) that preferentially excite the TE_{0n} modes in the cavity. The cavity has large irises at each end to resonate the desired TE_{0n} mode with a high Q while allowing lower order, circular electric modes to radiate out at very low levels. The TE_{0n} mode is loaded by coupling out of the cavity through one of the irises into a circular waveguide, thus producing a TE_{0n} mode of high purity suitable for testing oversized waveguide components.

1.2.11 Wall Effects on the Absorption of Electron Cyclotron Waves in an EBT Plasma

T. Uckan

The absorption of electron cyclotron waves propagating along an externally applied magnetic field in a uniform plasma surrounded by a cylindrical, metallic cavity wall was studied. In the model the cavity wall, the vacuum-plasma interface, and the effects of finite electron temperature were considered, and the dispersion relation for the wave propagation was derived. The results were then applied to the EBT-I plasma and the propagation characteristics computed. The wave absorption in the ordinary mode was found to be a result of the wall effects, which cannot be predicted with the infinite plasma theory. The loaded quality factor Q_L was also estimated from the model to be about 12, which is in good agreement with the experimentally observed value.

1.3 TOKAMAK RESEARCH

1.3.1 The ISX-A Tokamak

Plasma Confinement and Impurity Flow Reversal Experiments in the ISX-A Tokamak[16]

M. Murakami
K. H. Burrell
T. C. Jernigan
T. Amano
S. C. Bates
C. E. Bush
R. E. Clausing
R. J. Colchin
E. C. Crume, Jr.
J. C. DeBoo
J. L. Dunlap
G. R. Dyer
P. H. Edmonds
L. C. Emerson
A. C. England
E. S. Ensberg
C. A Foster
Y. Gomay
K. W. Hill
H. C. Howe
R. C. Isler
H. E. Ketterer
P. W. King
R. A. Langley
J. F. Lyon
D. H. McNeill
J. T. Mihalczo
S. L. Milora
W. Namkung
A. P. Navarro
R. V. Neidigh
G. H. Neilson
V. K. Paré
R. Prater
M. J. Saltmarsh
M. J. Schaffer
J. E. Simpkins
D. W. Swain
J. B. Wilgen
W. R. Wing
S. K. Wong
B. Zurro

This paper describes experimental studies in ISX-A, a tokamak with circular cross section, moderate size, and relatively low toroidal field, B_T [illegible] 15 [illegible] The confinement studies investigated plasma behavior (especially effects of impurities on plasma confinement) under a wide range of discharge conditions, wall cleanliness (discharge cleaning vs titanium gettering), limiter materials (stainless steel, carbon, and molybdenum), plasma fueling methods (gas puffing and pellet injection), and working gases (hydrogen and deuterium). Optimum confinement parameters (τ_E = 30 msec, Z_{eff} = 1.5) resulted with a stainless steel limiter and titanium gettering. The initially linear increase of gross energy confinement time τ_E

saturated at high density, apparently because [illegible] approximately neoclassical for most [illegible] conduction loss, relatively large because of [illegible] and increased electron-ion coupling, [illegible] which overcame a continuing improvement of electron energy confinement with [illegible] density. The optimal values of τ_E and [illegible] central toroidal beta, 2.2%) achieved are significantly higher than those obtained in other tokamaks of similar scales. The good confinement was mainly the result of reduction of radiation losses, especially those from high-Z impurities. This conclusion was supported by deliberate injection of tungsten into the discharge. Studies of impurity behavior were highlighted by the impurity flow reversal experiment. A poloidally asymmetric source of protons substantially altered the transport of an injected neon test impurity, and the changes observed were consistent with expectations based on simple neoclassical transport models.

Experimental Observation of the Impurity-Flow-Reversal Effect in a Tokamak Plasma

K. H. Burrell
J. C. DeBoo
E. S. Ensberg
R. Prater
S. K. Wong
C. E. Bush
R. J. Colchin
P. H. Edmonds
K. W. Hill
R. C. Isler
T. C. Jernigan
M. Murakami
G. H. Neilson

The inward transport of a neon test impurity injected into the plasma in the ISX tokamak has been significantly reduced by poloidally asymmetric injection of hydrogen gas into the discharge. The result is consistent with the impurity flow reversal effect as predicted by neoclassical transport theory.

Plasma Confinement Studies in the ISX-A Tokamak

M. Murakami
G. H. Neilson
H. C. Howe
T. C. Jernigan
S. C. Bates
C. E. Bush
R. J. Colchin
J. L. Dunlap
P. H. Edmonds
K. W. Hill
R. C. Isler
H. E. Ketterer
P. W. King
D. H. McNeill
J. T. Mihalczo
R. V. Neidigh
V. K. Paré
M. J. Saltmarsh
J. B. Wilgen
B. Zurro

Gross energy confinement times τ_E in the ISX-A tokamak exceeded predictions of the usual empirical scaling relations. We attribute this performance to reductions of impurity radiation and magnetohydrodynamically driven loss channels. The value of τ_E reached a limit as a function of plasma density. We suggest that this limit is due to a transition from electron-dominated to ion-dominated loss regimes. Maximum attainable values of τ_E increased with discharge current, in agreement with this interpretation.

Spectroscopic studies

R. C. Isler

One aspect of the confinement studies in ISX-A concerned correlation of the total power losses at the walls of the device with spectrally resolved intensity measurements in order to assess the radiative losses from various impurity ions. This program was pursued over a wide variety of experimental conditions and, in particular, over a range of values of Z_{eff} from 1-6.

Two spectrometers were used to investigate the vuv region where most of the radiative losses occur. A McPherson model 225 normal-incidence instrument was employed for the spectral region between 360 Å and 1250 Å. and a McPherson model 247 grazing-incidence spectrometer was used for photographic studies between 15 Å and 650 Å. The efficiency of the normal-incidence spectrometer and of the detectors used with it was determined separately in order to obtain an absolute calibration of the system. Power losses from specific ions were obtained during each sequence of shots from time-dependent measurements of the intensities of several spectral lines together with the use of photographic spectra that enabled us to estimate the relative intensities of lines above and below 360 Å.

The results for three sequences of shots are shown in Tables 1.3-1.5. The agreement between the radiometer data (which measures the total power appearing at the wall) and the spectroscopic estimates is within 30% for most of the cases studied. A notable exception is the result at 50 msec after breakdown presented in Table 1.3; here the two measurements differ by a factor of more than 2.5. Figures 1.7 and 1.8 show the evolution of the electron concentration, the radiometer signal, and several spectral lines during the discharges from which Table 1.3 was constructed. A strong hydrogen gas puff is introduced into the plasma at 80 msec after breakdown. The electron concentration increases by a factor of almost 4, but the radiometer signal goes up only by a factor of 2. In contrast, the impurity line radiation rises by factors of 3-7 between 80 and 100 msec. Those results indicate that as much as 20-30 kW of the radiometer signal in the low density part of the discharge may be due to energetic neutral particles that escape from the plasma. This conclusion is substantiated by other experiments in which large, rapid changes of the electron concentration were employed. It appeared that at concentrations of $\bar{n}_e \leq$ 1.0×10^{13}, 20-40 kW of the radiometer signal could be attributed to neutral particles.

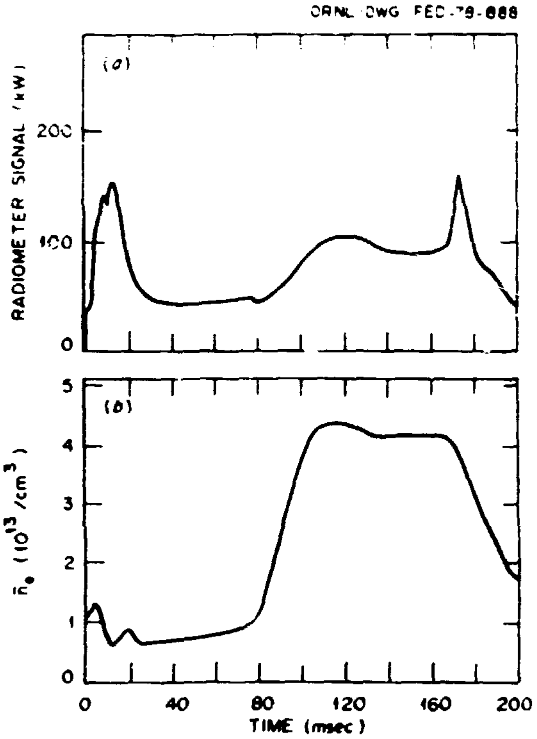

Fig. 1.7. Time dependences of (a) radiometer signal and (b) n_e for a shot from ISX-A during which a rapid, strong puff of hydrogen is introduced at 75 msec.

One other striking feature of the discharges analyzed in Tables 1.3-1.5 is that the hydrogen radiation not only accounts for a larger fraction of the power loss as Z_{eff} becomes lower but that the absolute intensities also increase.

Energy flux measurements on ISX-A

C. E. Bush G. R. Dyer
R. E. Worsham

Time and spatially resolved energy flux measurements on ISX-A were carried out using single uncollimated detectors and an array of six collimated detectors. Uncollimated detectors give the total power loss to the walls, and the array allows determination of the spatial origin of these losses. Initial results were documented in the last report.[14]

Table 1.3. Analysis of plasmas with $\langle Z_{eff} \rangle \approx 2$

	Time after breakdown (msec)					
	50		100		150	
Emission rate/power	(gR)[a]	(kW)	(gR)	(kW)	(gR)	(kW)
HI: 1s-2p	44.0	3.1	101.2	7.2	39.7	2.8
OVI: 2s-2p	7.1	0.6	52.9	4.4	50.8	4.2
NV: 2s-2p	2.6	0.2	26.0	1.8	19.4	1.4
CIII: $2s^2$-2s2p	1.3	0.1	4.5	0.4	2.1	0.2
FeXVI: 3s-3p	4.4	0.7	4.4	0.7	10.3	1.5
Estimated power	(kW)		(kW)		(kW)	
Hydrogen	3.9		9.1		3.5	
Oxygen	4.5		35.8		30.7	
Nitrogen	1.3		12.9		9.5	
Carbon	2.0		6.6		3.1	
Metals	8.0		8.0		17.1	
Total	19.7		72.4		63.9	
Radiometer signal	54 kW		101 kW		111 kW	
P_{OH}	252 kW		226 kW		212 kW	
$\langle Z_{eff} \rangle$					2.2	
$\bar{n}_e$	$0.9 \times 10^{13}/cm^3$		$3.5 \times 10^{13}/cm^3$		$4.5 \times 10^{13}/cm^3$	

[a] gR = giga RAYLEIGH = 10^{15} photons cm^{-2} sec^{-1}.

Table 1.4. Analysis of plasmas with $\langle Z_{eff} \rangle < 2$

	Hydrogen puff into hydrogen plasma		Deuterium puff into hydrogen plasma	
Emission rate/power	(gR)	(kW)	(gR)	(kW)
HI: 1s-2p	292.3	22.4	88.2	6.8
OVI: 2s-2p	13.2	1.1	22.4	1.8
NV: 2s-2p	13.2	1.0	14.7	1.1
CIII: $2s^2$-2s2p	1.6	0.1	1.3	0.1
FeXVI: 3s-3p	0.8	0.1	4.4	0.7
Estimated power	(kW)		(kW)	
Hydrogen	28.6		8.7	
Oxygen	8.3		13.5	
Nitrogen	7.0		7.7	
Carbon	1.8		1.8	
Metals	3.0		16.0	
Total	48.7		47.7	
Radiometer signal	35 kW		55 kW	
P_{OH}	225 kW		210 kW	
$\langle Z_{eff} \rangle$	1.07		1.68	
$\bar{n}_e$	$3.8 \times 10^{13}/cm^3$		$4.7 \times 10^{13}/cm^3$	

Table 1.5. Analysis of plasmas with $\langle Z_{eff} \rangle \approx 5.6$

	Time after breakdown (msec)					
	100		120		140	
Emission rate/power	(gR)	(kW)	(gR)	(kW)	(gR)	(kW)
HI: 1s-2p	30.8	2.4	30.8	2.4	48.3	3.7
OVI: 2s-2p	83.0	6.7	74.0	6.7	74.0	5.5
NV: 2s-2p	18.5	1.3	26.4	1.9	22.9	1.7
CIII: $2s^2$-2s2p	31.2	2.8	33.2	2.8	33.2	2.9
FeXVI: 3s-3p	22.0	3.3	24.3	3.6	26.5	4.0
Estimated power	(kW)		(kW)		(kW)	
Hydrogen	3.1		3.5		4.7	
Oxygen	50.3		50.3		41.3	
Nitrogen	9.1		13.3		11.9	
Carbon	48.5		51.6		51.6	
Metals	37.6		41.0		45.6	
Total	149.0		160.0		155.0	
Radiometer signal	130 kW		140 kW		130 kW	
P_{OH}	223 kW		234 kW		219 kW	
$\langle Z_{eff} \rangle$	5.6		5.8		4.7	
$\bar{n}_e$	$2.0 \times 10^{13}/cm^3$		$2.0 \times 10^{13}/cm^3$		$1.95 \times 10^{13}/cm^3$	

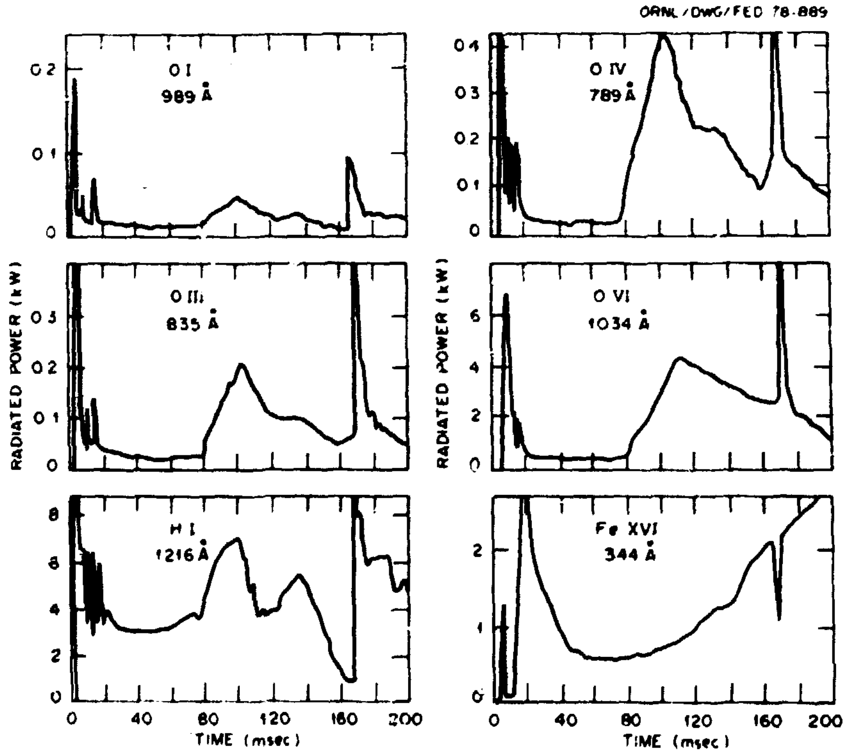

Fig. 1.8. Power emitted by several spectral lines when n_e evolves as shown in Fig. 1.7.

The data analysis is now fairly complete, and the qualitative conclusions presented there have been verified. For example, Fig. 1.9 shows the scaling of losses to the wall P_W with input ohmic power P_{OH}. For a wide variety of discharges, the fraction $P_W/P_{OH} \sim 30\%$. This is about half that observed for the Oak Ridge Tokamak (ORMAK), which had a tungsten limiter rather than the stainless steel limiter on ISX. The low radiative losses found on ISX-A (and more recently on ISX-B) apparently resulted from the absence of high-Z contamination. This conclusion was supported by the tungsten blowoff experiment for which uncollimated and chordal intensity (from the six-detector array) data were presented in the earlier report. The data point △ at $P_W/P_{OH} \sim 70\%$ is for the tungsten blowoff experiment. This is slightly greater than double that without tungsten.

The graphite limiter experiment on ISX-A gave additional support to the high-Z argument. In that experiment a graphite limiter was inserted beyond the stainless steel limiter. Vacuum ultraviolet spectroscopic data showed a resulting reduction in the intensity of line radiation due to oxygen and other impurities to about half that observed with the stainless steel limiter (graphite limiter withdrawn). Some of the spectroscopic data are summarized in Table 1.6. Figure 1.10 shows the uncollimated radiometer signal, with and without the graphite limiter inserted, along with other parameters. The radiometer shows the radiative losses to the wall to be reduced by ~50% with the graphite limiter; this is in good agreement with vuv data.

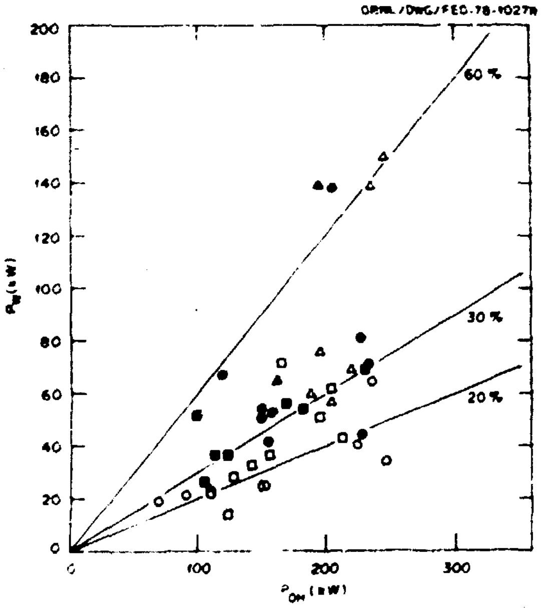

Fig. 1.9. The fraction of power lost to the wall in ISX-A was ~30% on the average. This is ~0.5 that found on ORMAK. The data point △ above the 60% line (at ~70%) resulted from the tungsten injection experiment.

Table 1.6. Comparison of plasma parameters

	Stainless steel	Graphite
I (kA)	120.0	120.0
V (volts)	2.0	1.6
$\bar{n}_e$ (10^{13} cm^{-3})	2.15	1.25
$\langle Z_{eff} \rangle$	5.6	5.1
Emission rate/$\bar{n}_e$ (gR/10^{13} cm^{-3})		
1034 A – OVI	47.0	28.3
629 A – OV	9.4	5.8
977 A – CIII	14.5	4.5
1216 A – HI	14.1	5.8
P_W/P_{OH}	0.55	0.25

Soft x-ray enhancement factors

A. P. Navarro J. L. Dunlap
E. C. Crume, Jr. V. K. Paré

Analysis of the soft x-ray data included a systematic study of the enhancement factor ζ, the ratio by which the measured signal exceeds that expected for a pure hydrogen plasma. The detector viewed a minor diameter and was operated with a low energy cutoff of ~1500 eV. Expected signal levels were calculated using $n_e(r)$ and $T_e(r)$ from Thomson scattering. When operation was with only stainless steel limiters in the machine and

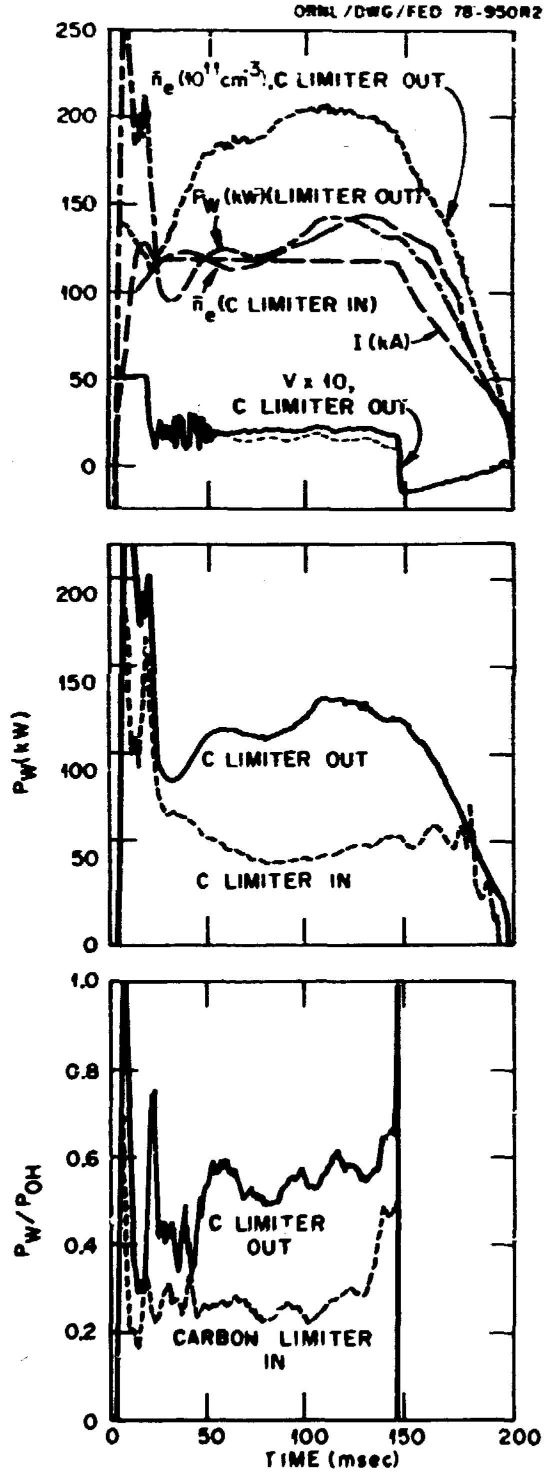

Fig. 1.10. Time history of (a) plasma parameters $\bar{n}_e$, I, and V; (b) P_W; and (c) P_W/P_{OH} with and without graphite limiter inserted. Energy flux to the wall with graphite limiter was less than half that with the stainless steel limiter. This agrees with the spectroscopic data given in Table 1.6.

without deliberate introduction of impurities. [illegible] was in the range 5-25 without gettering, 2-6 with light titanium gettering, and ~1 with heavy gettering. Values of Z_{eff} were 1.6-4.4 without gettering and 1-2 with gettering. In most of the cases, the observed signal level was consistent with that calculated, including carbon and oxygen impurities in the amounts determined spectroscopically.

Charge exchange excitation of impurity ions in tokamaks

R. C. Isler E. C. Crume, Jr.

Although electron collisions usually dominate atomic processes in tokamak-produced plasmas, charge transfer from hydrogen atoms should theoretically constitute an important recombination process for certain impurity ions. The charge transfer takes place into excited states, and in some circumstances excitation via this mechanism should dominate excitation by electrons. Charge transfer had previously been observed through the sudden increase of radiation from the $n = 3 \rightarrow n = 2$ transition of O^{7+} when 10-30-keV hydrogen beams are injected into a tokamak,[14] but detection of this process had not been reported for the more typical, noninjected discharges where the temperature of hydrogen atoms is <1 keV and their ambient current densities $n_H\langle v\rangle$ are one to two orders of magnitude smaller than the current densities of the beams. In the ISX-A tokamak we observed certain spectral lines of O^{5+} and O^{6+} that appeared to be too anomalously intense to have been excited solely by electrons. However, these anomalies are consistent with theoretical considerations of excitation through charge transfer.[15]

1.3.2 The ISX-B Tokamak

Description and program

In early 1977 a proposal was made to broaden the scope of the original ISX experimental program to include the study of the stability and confinement of high beta plasmas with noncircular cross section subjected to massive external heating (many times the ohmic heating (OH) power). This required replacing the ISX vacuum vessel and poloidal coils with new ones to make and control noncircular plasmas and strengthening the torque structure. In addition, the heating required the installation of two neutral beam injectors that were originally intended for the ORMAK Upgrade and were already under construction. This proposal was approved in June 1977, and work started immediately on the construction of the necessary components. The estimated cost of the project was $2.36 million, with a completion date of June 1, 1978. A description of the tokamak and neutral beam parameters, as well as predicted plasma parameters for ISX-B, are in last year's annual report.[16]

In January 1978 another experiment was added to the ISX-B experimental program: a ripple injection experiment to be done in collaboration with Princeton Plasma Physics Laboratory (PPPL). This experiment is designed to test the concept of the injection of neutral beams into a localized ripple in the toroidal field, a technique that may allow the use of much lower energy beams for the heating of reactor-size tokamaks. The construction of additional equipment for this experiment (in particular, two ripple coils by PPPL) moved the scheduled completion date to August 31 and postponed the shutdown of ISX-A from February 1 to March 5.

The conversion from ISX-A to ISX-B was completed at estimated cost and on schedule. The first 100-kA tokamak discharge was obtained on June 24, and the neutral beam installation phase was completed on August 21. A floor plan of the new facility is given as Fig. 1.11.

The primary goal of the ISX-B facility is to study the limits on beta that can be achieved with neutral beam injection and electron cyclotron heating. Up to 1.8 MW of neutral beam injection will be available in 1979, with an upgrade of power to 3 MW planned (see below). ECH experiments in 1979 will use up to 200 kW at 28 GHz, and an upgrade to 1 MW is proposed.

The confinement, high beta, shaped plasma studies will constitute the major research program with ISX-B. However, we will also be conducting vigorous studies in the areas of surface physics and plasma edge effects, ripple injection, other ECH applications, impurity flow reversal, fueling by pellet injection, and advanced diagnostic development. As with ISX-A, collaboration with other research and technology groups is a significant feature of the program.

Confinement and heating studies

Introduction. In the short time since the startup of the ISX-B experiment, we have reproduced essentially all the major results of the ORMAK[17,18] and ISX-A[10,12] experiments and have produced relatively high beta circular plasmas. Successes in control of macroscopic instabilities and in control of impurities without the aid of titanium gettering have led to confinement times as favorable and an operational space as wide as those achieved in ISX-A under similar experimental conditions. Neutral beam injection of up to 0.7 MW (which is four to five times larger than the OH input power) into clean plasmas has demonstrated significant ion and electron heating and provided improved macroscopic stability. The combination of these favorable features has led to higher values of β_T [$\langle\beta_T\rangle$ up to 1.4% and $\beta_T(0)$ up to 7%] than those obtained in previous tokamaks. Pellet injection, started in ORMAK[19] and continued in ISX-A,[20] has been applied to ISX-B, where it has produced factors of 2-3 increases of plasma density. Initial results with combined pellet and neutral beam injection suggest that the combination will be very useful in attaining higher values of β_T.

Comparisons of ISX-B discharge characteristics with those of ISX-A. Considering

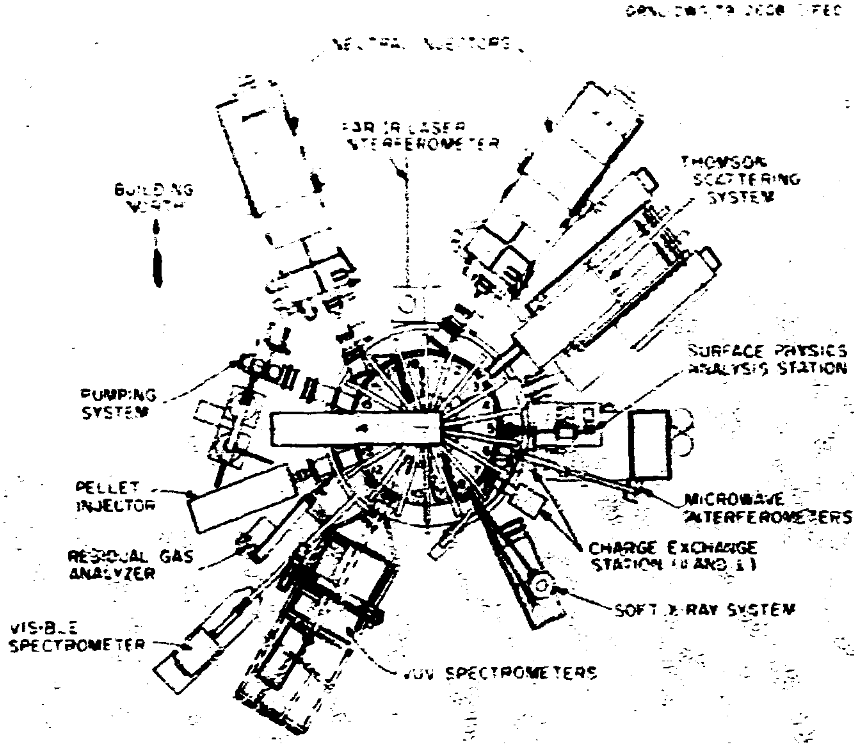
ORNL-DWG 78-2008 FED
NEUTRAL INJECTORS
FAR IR LASER INTERFEROMETER
BUILDING NORTH
THOMSON SCATTERING SYSTEM
SURFACE PHYSICS ANALYSIS STATION
PUMPING SYSTEM
PELLET INJECTOR
MICROWAVE INTERFEROMETERS
CHARGE EXCHANGE STATION (I AND II)
RESIDUAL GAS ANALYZER
SOFT X-RAY SYSTEM
VISIBLE SPECTROMETER
VUV SPECTROMETERS

Fig. 1.11. Floor plan of the ISX-B facility.

many features (particularly machine dimensions and the relatively low toroidal field) inherited from ISX-A and some significant changes as well (such as the poloidal field system and the discharge vessel), it was important to verify at an early stage of operation that the basic characteristics of plasma in ISX-B are similar to those in ISX-A.

The most fundamental contributor to the good performance of ISX-A was the cleanliness of the plasma. With the exception that no titanium gettering is employed, the ISX-B experiments utilize basically the same procedures for impurity control as those used in ISX-A and have obtained a degree of cleanliness similar to that of ISX-A. High-Z ($Z > 28$) materials were excluded in the initial machine configuration through the use of stainless steel limiters. In addition to H_2 (or D_2) discharge cleaning as employed in ISX-A, helium glow discharges are used to clean the discharge volume prior to a day's operation. Feedback control is used to keep the equilibrium plasma position close to the center of the vacuum vessel both horizontally and vertically. These efforts have led to clean plasmas. The Z_{eff} values from the resistivity measurements are between 1 and 2.5. The ratio of the radiative power to the OH power, as measured by a pyroelectric detector, is ~30%. Vacuum ultraviolet spectroscopy indicates that the power radiated from iron impurities is somewhat higher than that in ISX-A.

Cleanliness of the plasmas contributes to macroscopic magnetohydrodynamic (MHD) stability. The residual MHD activity often observed at the beginning of the regulated current phase is controlled by the technique developed in ISX-A:[10] a moderate level of gas puffing with appropriate timing. This procedure results in the majority of discharges being characterized by low levels of Mirnov oscillations and clear internal disruptions. The maximum values of $\bar{n}_e$ achieved without disruptive instabilities have been 9×10^{13} cm^{-3} at B_T = 11.5 kG. This value is about seven times larger than that resulting from the usual B_T/R_0 scaling and is higher than that attained in ISX-A (7×10^{13} cm^{-3}).

Low impurity content and suppression of MHD oscillations have led to good energy confinement times τ_E in ISX-B, where τ_E values significantly exceed predictions of the usual scaling laws. Figure 1.12 shows, superimposed upon the data from ISX-A,[10,12] values of τ_E as a function of line-averaged electron density in ISX-B under uniform experimental conditions ($I \simeq 120$ kA, B_T = 11.5 kG, $D_2 \to D^+$). The values of τ_E in ISX-B are about equal to those in ISX-A at the same densities with similar field and current, especially considering the fact that the τ_E determination for ISX-B does not include the slight noncircularity ($b/a \simeq 1.2$). The ISX-B data also exhibit the limitation of τ_E as a function of plasma density that was interpreted in ISX-A as a transition from electron-dominated to (essentially neoclassical) ion-dominated loss regimes.[12,22] A calculation of the detailed energy balance from these data is now in progress.

Plasma heating with neutral beam injection. Up to 700 kW of 45-keV hydrogen beam power has been injected into ISX-B through a single beam line (the West Beam Line). The majority of the data has been taken with deuterium plasmas. The response of the ion temperature with 660-kW injection is shown in Fig. 1.13. At densities of ~3×10^{13} cm^{-3}, the heating coefficient observed ($\simeq 3 \times 10^{13}$ eV cm^{-3}/kW) is like that in ORMAK[17] and the Princeton Large Torus (PLT).[23] However, it shows an unexpectedly large density dependence; the details are under investigation.

Figure 1.14 shows the $T_e(r)$ and $n_e(r)$ profiles with ~630-kW H^0 injection into a high density deuterium discharge. For comparison, a typical discharge at a similar density but with ohmic heating only is also shown. The density-averaged electron temperature approximately doubles, and the temperature profile is broadened by injection. The increases are nearly independent of electron density, essentially confirming the scaling $\tau_{Ee} \propto \bar{n}_e$. Significant decreases in loop voltage accompany injection. The values of

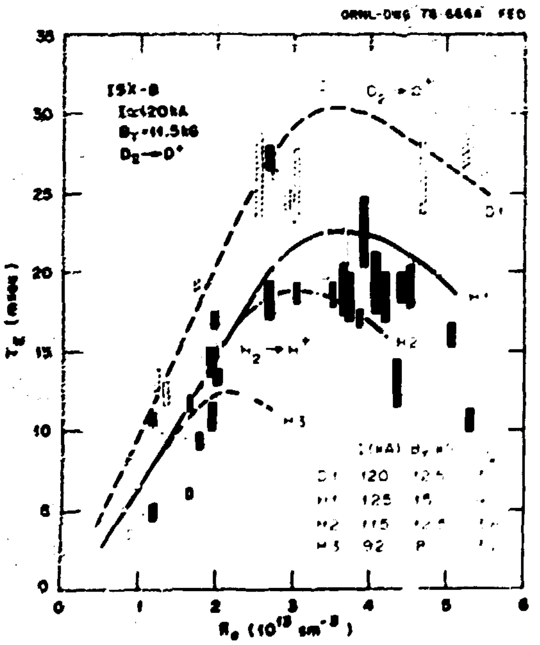

Fig. 1.12. Comparison of gross energy confinement times in ISX-A and ISX-B.

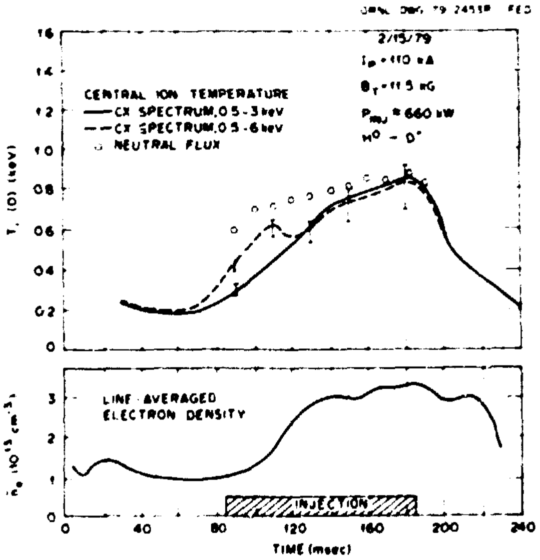

Fig. 1.13. Peak ion temperature vs time with neutral beam injection into a plasma of moderate density.

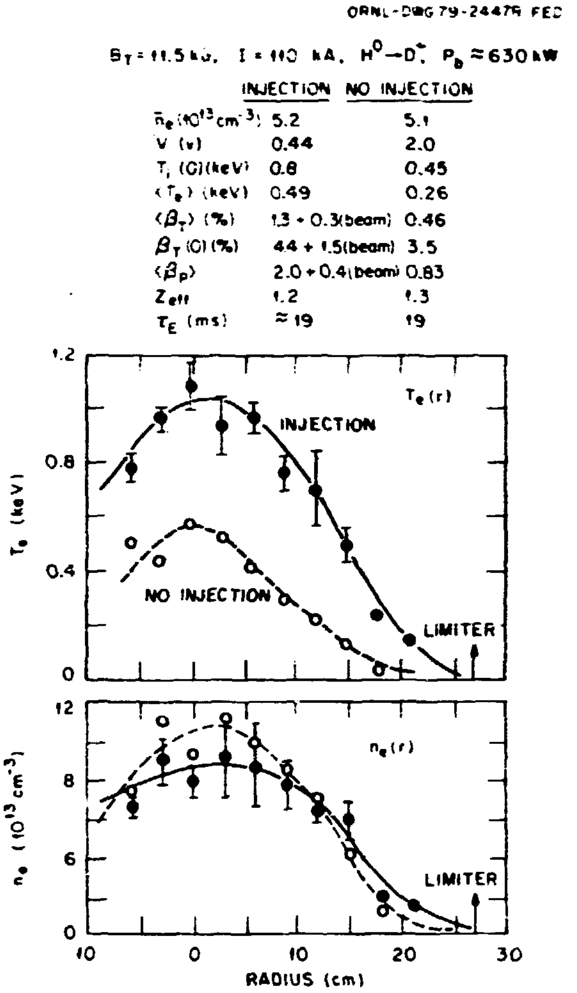

	INJECTION	NO INJECTION
$\bar{n}_e$ (10^{13} cm^{-3})	5.2	5.1
V (v)	0.44	2.0
T_i (0)(keV)	0.8	0.45
$\langle T_e \rangle$ (keV)	0.49	0.26
$\langle \beta_T \rangle$ (%)	1.3 + 0.3(beam)	0.46
β_T (0) (%)	4.4 + 1.5(beam)	3.5
$\langle \beta_p \rangle$	2.0 + 0.4(beam)	0.83
Z_{eff}	1.2	1.3
τ_E (ms)	≈ 19	19

Fig. 1.14. Radial profiles of T_e and n_e with and without neutral beam injection.

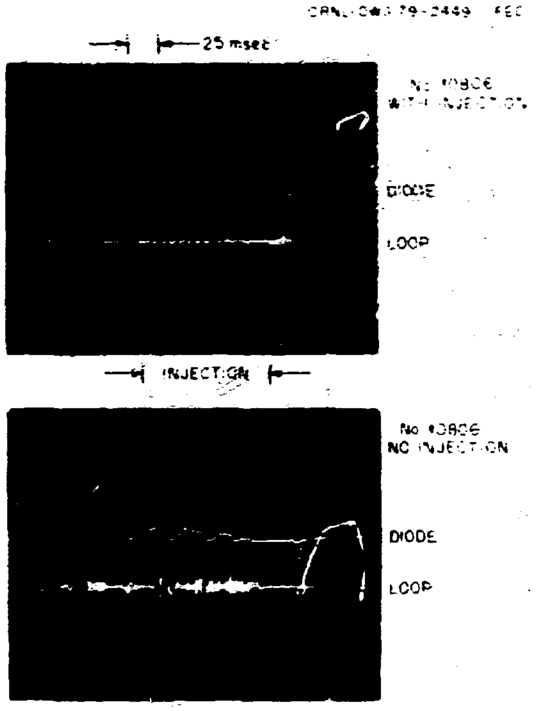

Fig. 1.15. Soft x-ray and magnetic loop signals with and without neutral beam injection. Gas input rates were the same.

Z_{eff} estimated from the resistivity usually remain the same (≈1.3) before and after injection. The wall energy flux measurement with a simple pyroelectric detector indicates that the ratio of the wall flux to the total input power is <30% and frequently decreases with injection.

Cleanliness and possibly profile broadening appear to improve macroscopic stability. This effect leads to a wider parameter regime for operation. Figure 1.15 depicts the central chord soft x-ray emission detected by a PIN diode for discharges with and without injection. The discharges with injection exhibit sawtooth oscillations with a long relaxation period, indicative of a relatively stable, well-confined discharge, whereas the discharge without injection shows repeated minor external disruptions for gas puffing of an equal throughput. This illustrates the tendency of increasing attainable maximum density with injection power. However, systematic studies of the maximum density and the minimum q_ℓ attainable with injection are yet to be done.

Attainment of high beta. In ohmically heated discharges, volume-averaged poloidal beta $\langle \beta_p \rangle$ is commonly observed to scale with $\bar{n}_e/I$. This scaling can be translated to $\langle \beta_T \rangle \sim \bar{n}_e/B_T q_\ell$. Neutral beam injection should be effective in achieving higher β_T by increasing the input power (without deteriorating confinement), increasing the maximum density achievable, and allowing operation at lower q_ℓ than with ohmic heating alone.

Figure 1.16 shows improvement of values of $\langle \beta_T \rangle$ for injected plasmas over those with

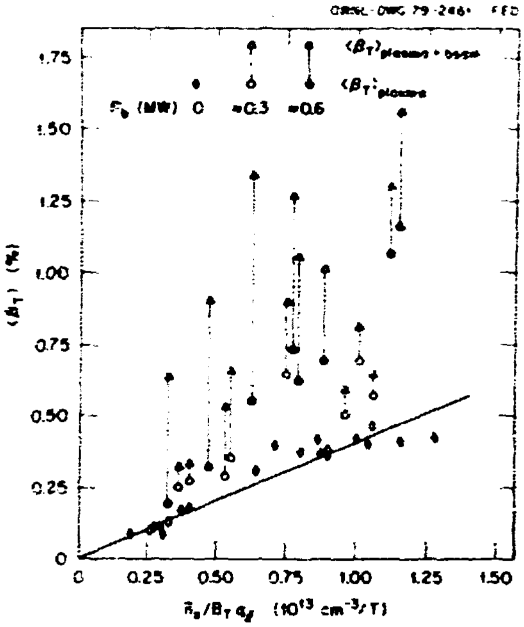

Fig. 1.16. Values for $\langle\beta_T\rangle$ with and without neutral beam injection.

ohmically heated plasmas as a function of $\bar{n}_e/B_T q_\ell$, and Fig. 1.17 shows improvement of values of $\beta_T(0)$. In each figure two different values of β_T are shown for each value of $\bar{n}_e/B_T q_\ell$; the lower points correspond to the β_T values of the bulk plasmas and the upper points to those including the contribution of slowing-down fast ions as calculated by the Fokker-Planck code. Values for $\langle\beta_T\rangle$ of 1.4 and for $\beta_T(0)$ of [illegible] have been obtained with [illegible]-kW injection power. These values are among the highest ever achieved in tokamaks. The corresponding volume-averaged β_p of 2.5 is also among the highest for quasi-steady, as opposed to transient, states. Because these measurements were at high densities where the beam contribution is relatively small, uncertainties in achieved β_T values due to fast ion losses unaccounted for by theory are relatively small. Significant beam heating is demonstrated by comparison with OH results, which follow closely the scaling of $\beta_T \sim \bar{n}_e/B_T q_\ell$. Variations of B_T and q_ℓ have been limited in the injection experiments so far; thus, the dependences of β_T values on these parameters are uncertain with injection. The main effect of increasing injection power, especially at high density, is broadening of the temperature profiles; significant increases (roughly linear) of $\langle\beta_T\rangle$ are observed with beam power at a fixed value of $\bar{n}_e/B_T q_\ell$, but only small increases of $\beta_T(0)$ are observed.

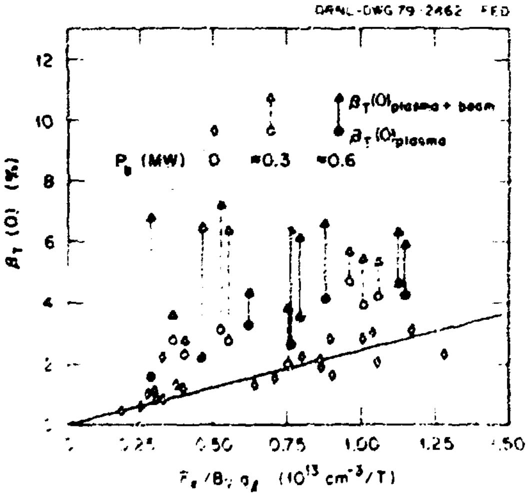

Fig. 1.17. Values for $\beta_T(0)$ with and without neutral beam injection.

The forthcoming increase in beam power (with the use of the second beam line) and optimization of plasma parameters (n_e, B_T, and q_ℓ) are expected to raise the β_T values substantially. However, MHD theory[2] predicts that ballooning modes are likely to limit the β_T values at $\langle\beta_T\rangle$ = 2-3% in circular plasmas. The theory also predicts an advantage for vertically elongated, D-shaped plasma cross sections, i.e., raising the threshold β_T values for the instabilities. In ISX-B, noncircular plasmas with an elongation ratio of 1.5 have been created, and the magnetics and control studies of such noncircular plasmas are under way.

Pellet injection. Solid-hydrogen-pellet injection into ISX-A demonstrated that the technique of plasma fueling could produce substantial density increases (of up to 30% or more) without apparent deleterious effects on plasma stability and confinement.[3] In ISX-B the study has been extended to larger pellet size and higher injection speed and to operation with neutral beam injection.

The pellet injector is, as described in Sect. 5, an upgraded version of the injector used in ISX-A. Pellets approximately 1 mm in diameter (containing $4 \times 10^{[illegible]}$ hydrogen atoms) are injected with a speed of 850 m/sec. Because of the larger size and higher speed, pellets penetrate farther than those in ISX-A, as revealed in pictures taken tangentially by a high speed framing camera. The ablation rate of an injected pellet is monitored by a photodiode recording the H_α light emanating from the luminous cloud of neutral hydrogen around the pellet. The ablation rate and, thus, the response of the plasma are sensitive to the preinjection electron temperature. At low temperature the low ablation rate usually results in an unablated fraction of the pellet striking the inner wall of the vacuum chamber to cause a gas burst. At high temperature [$T_e(0)$ [illegible] 1 keV], however, pellets are completely absorbed before or upon reaching the center of the plasma.

Figure 1.18 shows $T_e(r)$ and $n_e(r)$ at 1 msec after pellet injection compared with those without pellet injection in an ohmically heated discharge. The line-averaged electron density (based on these profiles) increased from $1.2 \times 10^{[illegible]}$ to $4.9 \times 10^{[illegible]}$ cm^{-3}. The calculated increase in total electron density is $(2.8 \pm 0.4) \times 10^{[illegible]}$, which is in reasonable agreement with the total hydrogen atoms in the pellet less the unablated fraction. Therefore, simple particle balance is obtained. This result is in contrast to the density increase with gas puffing, in which only one-third to one-fourth of the injected gas is absorbed in the plasma. Although the addition of cold electrons (plus a small ionization loss) dramatically lowers the electron temperature, the total electron energy content remains roughly constant (1.2 ± 0.15 kJ before injection and 1.0 ± 0.3 kJ after it).

Figure 1.19 illustrates the time evolution of the central electron temperature and density with pellet injection under experimental conditions similar to the above, but with slightly lower central electron temperature. The pellet reaches the outer edge of the plasma at t = 0 and the center at 300 μsec. An additional 100 μsec is required for the central plasma viewed at the laser diagnostic port, almost 180° around the torus from the pellet, to respond. Therefore, the 500-μsec points essentially correspond to the initial conditions for evolution after pellet injection. A central density of $2 \times 10^{[illegible]}$ cm^{-3} was recorded at that time. The initial density distribution is sharply peaked at the center because of the higher temperature there before injection and the small volume of the central flux tubes. This distribution quickly relaxes to one of normal shape (Fig. 1.18) but elevated value. Pellet injection can

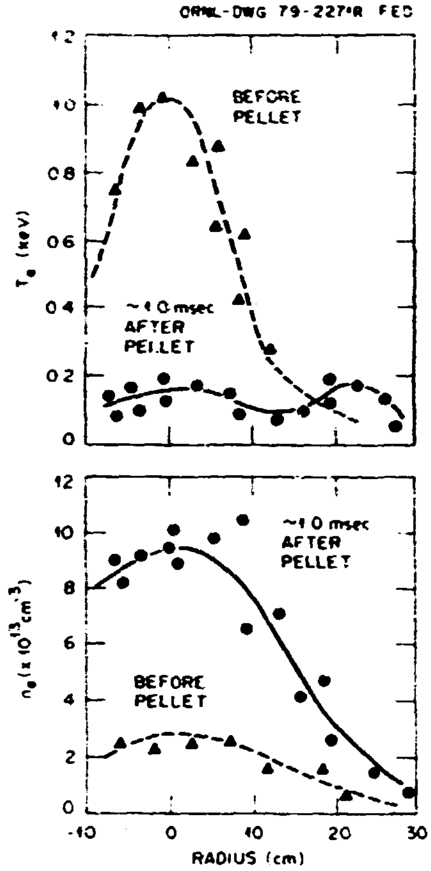

Fig. 1.18. Radial profiles of T_e and n_e with and without pellet injection.

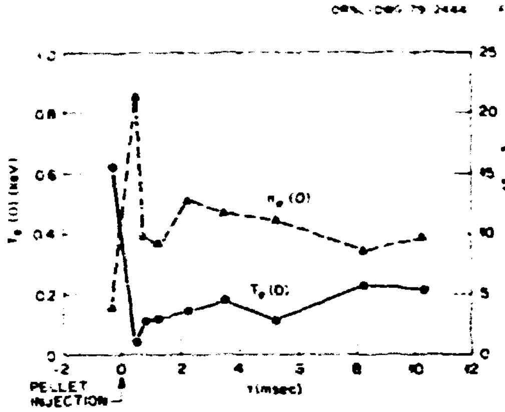

Fig. 1.19. Changes in $T_e(0)$ and $n_e(0)$ with pellet injection.

excite large Mirnov oscillations and subsequently repeated "soft" disruptions but rarely "hard" (or current) disruptions. Injection can also damp out Mirnov oscillations.

Beam-heated plasmas are less susceptible to MHD instability upon pellet injection than are those that are only ohmically heated. A particularly interesting aspect of injection into beam-heated plasmas is enhanced ablation of the pellet by the trapped fast ion component. The perpendicular charge exchange diagnostic indicates a very rapid slowing down of the fast ion population and heating of the pellet ions and only a small temporary cooling of the background ions. Electron cooling is less than with ohmic heating alone, and a low level of Mirnov oscillation is retained. These preliminary observations are encouraging for attaining higher beta in ISX-B.

Charge exchange measurements on ISX-B

G. H. Neilson D. R. Overbey
E. C. Moore J. T. Mihalczo
J. F. Lyon R. E. Worsham

Charge exchange neutral measurements are made on ISX-B using a mass-resolving neutral particle analyzer viewing along a fixed, quasi-perpendicular, midplane chord. This analyzer has been used on ISX-A and was described in the previous annual report.[26] Only minor modifications to the instrument itself have been made in the interim. However, the PDP-8-based data acquisition system has been upgraded, employing CAMAC instrumentation to provide greater operational flexibility and on-line analysis capability.

In 1979 the present analyzer will be reconfigured to view the plasma tangentially. A spatially scanning velocity filter/parallel plate analyzer will then be used on the perpendicular viewing port. The diagnostic capability will be further enhanced by the addition of a vertical diagnostic beam that will also be used for ripple injection studies.

In neutral-beam-heating studies done to date, up to 700 kW of hydrogen neutrals has been injected into deuterium plasmas. Central ion temperatures inferred from the thermal (deuterium) spectrum are plotted as a function of time for a typical case in Fig. 1.13. The solid and dashed curves were obtained by fitting the data out to 3 keV and 6 keV, respectively. The higher apparent temperature for the latter and those from neutron measurements reflect the existence of a non-Maxwellian tail on the ion distribution that appears immediately after beam turnon and disappears later in time, as shown in Fig. 1.20(a). The nature of this distortion and its disappearance are not fully explained at this time, although qualitatively similar phenomena have been observed in other experiments, for example, T-11.[27]

We have measured fast ion (hydrogen) spectra out to 40 keV, with results for the aforementioned case shown in Fig. 1.20(b). For a perpendicular spectrum, the early spectrum exhibits a remarkable degree of structure, evidently corresponding to the one-third, one-half, and full energy beam components. This structure gradually "washes out" and is no longer seen later in the discharge. Detailed analysis of these observations is now beginning.

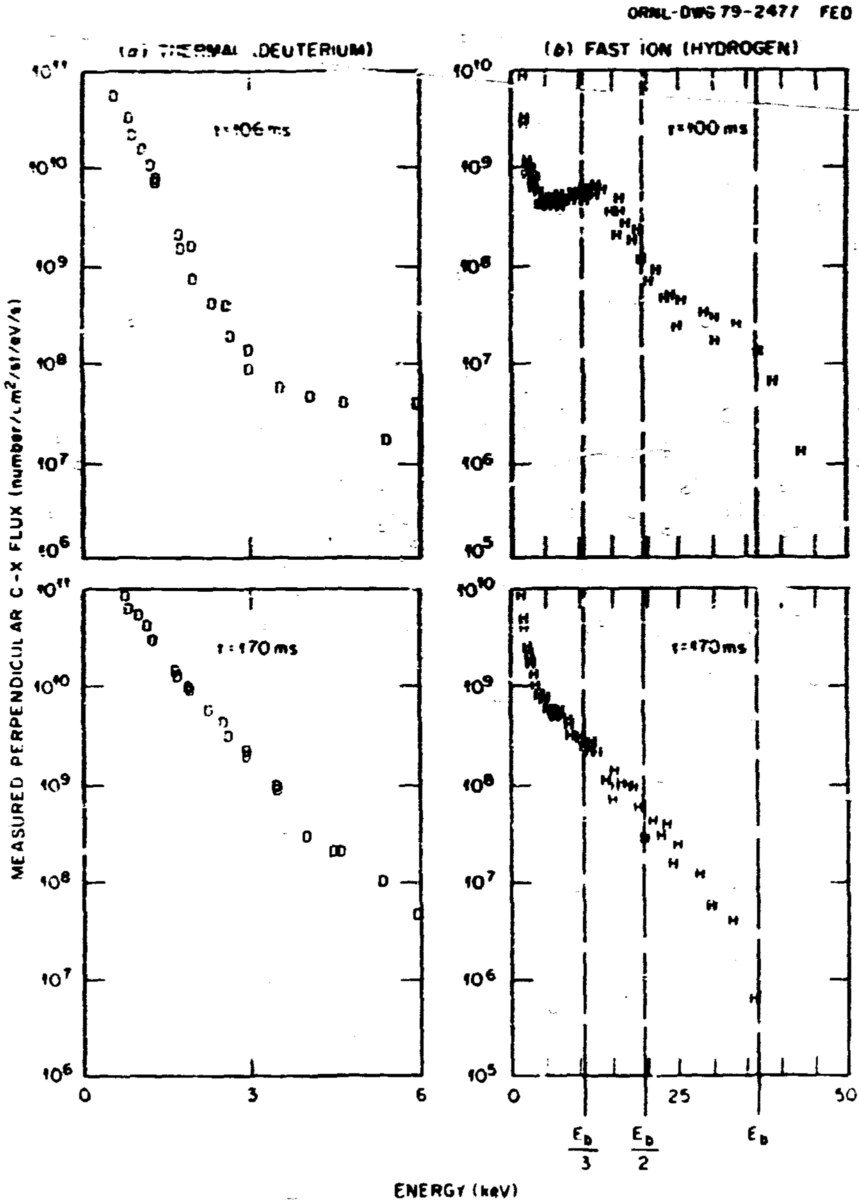

Fig. 1.20. (a) Thermal ion spectra for the case shown in Fig. 1.13. The non-Maxwellian tail at earlier times distorts the inferred temperature when included in the analysis. (b) Fast ion spectra. Beam-component-related structure appears after beam turn on; the spectrum smooths out with time.

Energy flux measurements on ISX-B

C. E. Bush R. C. Isler
G. R. Dyer R. E. Worsham

Energy flux measurements similar to those made on ISX-A have been made and are in progress on ISX-B. As on ISX-A, radiometry on ISX-B shows the average ratio P_W/P_{OH} to be ~30%. However, there are some differences in parametric dependence. For example, on ISX-A, with $\bar{n}_e$ and B_T held constant, P_W/P_{OH} appeared to decrease with increasing plasma current I_p whereas on ISX-B, a preliminary scan in I_p showed this fraction to increase significantly with increasing I_p, i.e., from

15% at 70 kA to 35% at 150 kA. (However, the losses in general are still quite low.) For this same scan, MHD activity was also seen to increase with increasing I_p; this may in some way account for the increase in P_w/P_{OH}. Power losses to the wall for both ISX-A and ISX-B appeared to be a slightly increasing function of n_e, approaching a plateau for n_e [illegible] 3×10^{13} cm^{-3}.

In addition to the usual confinement experiments, energy flux studies with neutral beam injection heating are also being made on ISX-B. On ORMAK the ratio P_w/P_{total}, where $P_{total} = P_{OH} + P_{inj}$, was approximately the same with and without injection. For injection on ISX-B, this constancy has not been observed, and a clear picture has yet to be formulated. Losses to the wall with injection on ISX-B can vary from 30% of P_{total} down to 10-15%, implying that in certain cases the increase of P_w is proportional to the input injection power and that in others ~~the~~ resulting increase is much less. For fixed injector parameters (40 kV, 600 kW) and B_T and I_p, the losses to the walls appear to decrease with increasing $\bar{n}_e$. In general, however, radiometry on ISX-B with injection appears to support results on ORMAK that showed little or no additional contamination of the plasma as a result of neutral beam injection.

The power not accounted for as energy flux to the walls, which can be greater than 85%, with and without injection is usually assumed to be deposited at the limiters. An AGA 680 infrared camera is now being used to monitor the temperature of, and, thus, the energy flux incident on, the limiters of ISX-B in order to determine whether or not this is the case. Preliminary data for a limited number of runs show no extreme net heatup of the outer limiter (beyond ~100 to 200°C) during a day of operation. The measurements were complicated somewhat by the glow discharge cleaning that precedes each day's operation. During glow discharge cleaning, the outer limiter is used as the electrode, and it heats linearly with time to [illegible]C. The bar then cools down during the day's operation, indicating that the accumulated energy of many shots deposited at the limiter is much less than that provided by 20 min of glow discharge cleaning. One of several such heating and cooling curves is reproduced in Fig. 1.21. Future machine operation will include several runs in which the glow discharge preconditioning is eliminated.

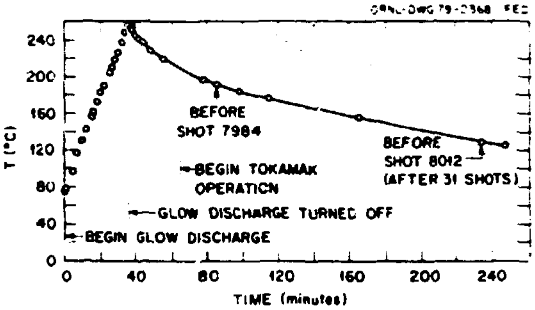

Fig. 1.21. Heating-cooling curve for the outer limiter obtained using the infrared camera. Heatup was due to glow discharge cleaning and was linear with time. The resulting temperature was high enough that the limiter cooled down during the series of tokamak discharges.

Single uncollimated radiometers for determining radiative and charge exchange losses associated with pellet injection are completed and awaiting installation, along with an array of 12 collimated detectors. The array is to be mounted on top of ISX on a rectangular port and will monitor emitted intensity along 12 wedge-shaped vertical chords. The chordal intensities are to be inverted in order to obtain spatially resolved emission profiles.

Neutron measurements on ISX-B

J. T. Mihalczo A. C. England

The ISX-B is equipped with ^{3}He proportional counters and ^{235}U fission chambers. An absolute calibration of these detectors has been performed with a ^{252}Cf neutron source located at [illegible] positions along the plasma axis to permit determination of ion temperature for ohmically heated deuterium plasmas or deuterium plasmas with hydrogen neutral beam injection. The multiplicity of detectors and their locations will allow measurements of deuterium-deuterium (D-D) reaction rates from [illegible] sec and verification of the independence of the reaction rate on toroidal angle. Ion temperatures from reaction rate measurements with ohmically heated plasmas or plasmas heated by neutral beam injection agree with those from charge exchange measurements except for certain low density plasmas soon after injection starts. In these the Maxwellian distribution is distorted by a high energy tail. Results of the measurements are shown in Fig. 1.13.

Perpendicular charge exchange analyzer for ISX-B

J. T. Mihalczo	J. F. Lyon
J. A. Ray	R. D. Wall
R. E. Worsham	G. H. Neilson

One prototype velocity filter/electrostatic analyzer module of a multimodule array for charge exchange analysis on ISX-B is under development. A commercially available velocity filter was obtained and incorporated into the system, and the combined system was tested both with ion and neutral particle beams. The analyzer is undergoing final modifications and calibration before installation on ISX-B. There it can be moved between plasma discharges so as to view various chords through the plasma and thus provide spatial ion temperature profiles.

ECH experiments on ISX-B

C. M. Loring	G. L. Campen
O. C. Eldridge	A. C. England

A 200-kW gyrotron from the EBT program will be used for ECH heating in ISX-B. This gyrotron is not suitable for cw operation but should be adequate for 100-msec pulsed operation.

The power supply consists of a 60-μfd capacitor bank charged to 100 kV by a Universal Voltronics Corporation (UVC) low current charging supply. The gyrotron will be located on the platform above the ISX-B control room adjacent to the diagnostic neutral beam supply. An oversize waveguide (2.5" ID) will run from the gyrotron over the ISX-B enclosure wall and then turn down to one of several ports on the ISX-B vacuum tank assigned to the ECH program.

Initially, several kinds of antennas will be used. A novel way to produce approximately linearly polarized radiation has been found. With this technique extraordinary waves will be launched from the high field side of the tokamak at the midplane. Antennas in other ports will launch unpolarized radiation. Ordinary polarized waves will be launched from the outside if a suitable port can be found.

The construction is under way, and initial operation of the gyrotron should begin in late spring with experiments expected to start in midsummer of 1979.

Neutral beam systems for ISX-B

R. E. Hill	[illegible] C. Queen
H. C. McCurdy	C. M. Loring
A. R. Kemp	W. L. Stirling
W. L. Wright	

Introduction. The purpose of this task was to design, procure, and construct neutral beam systems for the initial phase of ISX-B experimentation. Two neutral beam systems consisting of beam lines, electrical systems, and related instrumentation were completed; installation of these systems was performed under the ISX-B (Major Device Fabrication funding category) task. New accel power supplies are being purchased and installed under this task but were not scheduled for initial ISX-B operation; for an interim period ISX-B will time-share modules of the existing [illegible] power supply.

The ISX-B beam lines are basically the same design as previously provided for PLT except for modifications in the drift tube region. They use the 60-A, PLT-type ion source, but the electrical systems (except accel supplies) are designed with the capability for driving 100-A ion sources.

The two neutral beam systems have a target capability for a total of 1.8 MW of neutral beam power injected into the ISX-B plasma. A follow-on program (see below) will replace the 60-A, PLT-type ion source, with the 100-A source being developed for the Poloidal Divertor Experiment (PDX), and make other modifications to increase ISX-B injection capability to 3 MW.

Cryocondensing pump procurement. Each ISX-B beam line includes a cryocondensing pump that is identical to the Type A pump developed and supplied by Arnold Engineering Development Center (AEDC) for the PLT injection systems. Procurement of these cryopumps was identified as a potential schedule problem at the start of the ISX-B program.

Parallel procurement efforts were carried out in which three pumps were obtained from AEDC and two pumps of somewhat different design were obtained from United Technologies Research Center (UTRC). Two of the AEDC pumps were the first to become operational and were installed on ISX-B; the other three pumps are assigned to Plasma Technology programs. The two UTRC cryopumps have not been performance tested. A single attempt was made to test each UTRC pump, but in each case the test was terminated when the pump developed a vacuum leak upon being cooled down to cryogenic temperature. A further effort will be made to performance test these pumps when a test facility can be scheduled.

Accel power supplies. Two identical supplies are being procured and installed. Provisions are being made in the installation for accommodating two additional power supplies at a later date and for time sharing of the supplies by beam development facilities.

The capability of each supply is given in Table 1.7; the two supplies can also be used together in a series or parallel arrangement to double either voltage or current capability. A tap board is provided for convenient selection of the operating mode and for connecting the output to an alternate load.

Table 1.7. ISX-B neutral beam accel power supply specifications

Output rating	60-A or 100-A pulses at 9 kV to 60 kV
Duty	
60-A pulses	10 duty
100-A pulses	300 msec at 10-sec intervals
	30 sec at 1000-sec intervals
Secondary insulation	132 kV DC
Regulation	
No load to full-load	10 max
During pulse	1 max
Primary voltage controller	Tap changer
Crowbars	50/day
Short circuit current	6600 A max

All components of the power supplies except the step voltage regulators (tap changers) were received from the UVC supplier in October 1978. However, in August 1978 the step voltage regulator failed to pass the specified 6600-A short circuit test; these units are being redesigned and rebuilt by Siemens-Allis supplier to Universal Voltronics.

Posttest examination of the failed regulator revealed that the transformer coils were damaged beyond use by the short circuit forces because the construction did not provide adequate structural support for the conductor. Siemens-Allis redesigned the transformer coil and core assembly, including the structural bracing, and manufactured a single-phase prototype that was short circuit tested in December 1978 to prove the revised design. The prototype coil failed by open circuiting during the last of six shots required for the specified test; however, posttest examination showed that the coil was undamaged except near local voids and unbonded regions at lead connections and cooling channels. Siemens-Allis will fabricate and test a second single-phase prototype coil incorporating improvements in design details and fabrication procedure.

The new accel power supplies are expected to be completed in June 1979.

ISX-B neutral beam power increase

S. M. DeCamp	H. C. McCurdy
P. H. Edmonds	W. L. Stirling
R. L. Johnson	P. W. Whitfield

R. E. Worsham

A follow-on program was initiated in October 1978 to increase ISX-B neutral beam heating capability to 3 MW by modifying the existing systems to use the 100-A ion sources being developed under the Plasma Technology program for initial use on PDX. The modifications, which will cost an estimated $2.4 million including two new ion sources, are expected to be completed in March 1980; conversion will require a shutdown of ISX-B for approximately three months beginning in January 1980.

Baseline performance goals for the modified neutral beam systems are given in Table 1.8. For comparison, the performance goals for the present ISX-B and for PDX neutral beam systems are also shown. Other desirable goals for ISX-B are (1) capability for 500-msec pulse length and (2) ability to operate over the range of 30-50-kV injection energy. For these latter goals, however, we will accept whatever power level can be obtained from the system optimized for the baseline performance goals.

The basic plan is to fabricate new ion sources and front ends and to modify the existing beam lines on-site by swapping out components. Other beam line components will be modified or replaced to accommodate the larger 100-A ion source. The existing decel power supplies will be replaced.

Assembly and conditioning of the ion sources were identified as critical path schedule activities. Agreement was reached on a plan to leave the PDX prototype beam line at ORNL, thus assuring that a test facility will be available for conditioning the ISX-B ion sources. The completion schedule of March 1980 is consistent with the present schedule for PDX and with the ISX-B ion sources to be done immediately after the PDX sources.

Although we wish to take maximum advantage of the designs prepared for PDX, full use of PDX component designs would increase source-to-plasma distance on ISX-B from 4.1 m to 4.4 m and almost certainly preclude meeting the 3-MW performance objective. We chose to redesign several components and to move the existing vacuum enclosures towards the tokamak in order to reduce source-to-plasma distance and thereby increase neutral beam power reaching the plasma.

The new front end has provision for a Type C cryopump and incorporates an inertial calorimeter that is a shortened version of the PDX design. In view of the relatively short pulse length (200 msec) specified for ISX-B, it is not certain that the front end cryopump will be required; the shorter calorimeter is permissible because of the shorter pulse length.

The new front end design, together with a new electric break/isolation valve arrangement, will permit the existing vacuum enclosure to be moved ~0.5 m closer to the tokamak. Another 0.1-0.18-m reduction in beam line length will be achieved by modifying the PDX beam alignment assembly design. The total effect of the redesign effort will be to reduce the source-to-plasma distance to

Table 1.[illegible]. Performance goals for ISX-B neutral beam power increase

	Present ISX-B	PDX	Modified ISX-B
Injection energy, keV	40	50	40
Neutral power into tokamak, MW (per beam line)	0.9	1.5	1.5
Pulse length, msec	100	500	200
Total accel supply drain, A	60	100	100

[illegible] and to make 3 MW of neutral power a credible performance goal.

During 1979 a detailed design of the modifications will be performed, and components will be procured or fabricated.

1.3.3 Impurity Study Program

B. R. Appleton	R. A. Langley*
R. E. Clausing	P. Mioduszewski
R. J. Colchin	J. B. Roberto
L. C. Emerson	J. E. Simpkins
S. L. Halsted	S. P. Withrow
L. Heatherly	R. A. Zuhr

Introduction

The purpose of the Impurity Study Program is to identify the controlling impurity generation mechanisms and to minimize their effects. The approach of the ORNL program is a vigorous, interactive coalition of surface scientists and plasma physicists that focuses on in situ tokamak experiments. It has coordinated efforts in four main task areas: (1) in situ measurements, (2) development of new diagnostics, (3) plasma-materials simulation experiments, and (4) controlled laboratory investigations.

The program involves the study of hydrogen recycle, the study of impurity introduction mechanisms, the in situ testing of special materials such as limiters, beam dumps, armor plate, and divertor plates, the measurement of impurity charge state in the plasma scrape-off region and the study of cleanup techniques.

In order to pursue these tasks, in situ experiments were undertaken on ISX-A, T-12 (Kurchatov Institute), ISX-B, and Doublet III (General Atomic). These experiments were supported by controlled laboratory investigations. Detailed information may be found in references given at each subheading.

ISX-A[illegible]

ISX-A was designed to study plasma-wall interactions and the role of impurities in tokamak plasmas. It was constructed with vacuum cleanliness as a primary concern. Both a quadrupole mass analyzer and a surface analysis system coupled with a vacuum transfer system were installed before tokamak operation. The analysis provided data on typical wall material and a variety of other materials exposed at positions between the surface of the first wall and the limiter inner radius. Samples were introduced from air into the ultrahigh vacuum transport system without disturbing the vacuum in ISX-A or the analysis system. The samples were then prepared (by sputter cleaning or outgassing), analyzed before exposure to the plasma, and subsequently reanalyzed by Auger electron spectroscopy (AES) to determine what changes had occurred. The analysis station, together with the residual gas analyzer and plasma diagnostics, has provided information on the initial cleanup, changing wall conditions, and hydrogen [illegible] during the startup period as well as during the subsequent routine operation of ISX-A. During the startup period, substantial sulfur contamination was evident, but this was greatly reduced as hydrogen discharge cleaning proceeded. Samples of oxidized stainless steel were not cleaned to an oxygen-free status, but the surface was reduced to a thin substoichiometric oxide. Carbon was significantly removed but not entirely eliminated.

---

*Program Coordinator

Sample exposures designed to study heavy impurity transport and hydrogen isotope recycling in ISX-A were completed. Samples of single-crystal silicon and silicon with an amorphous near-surface region were exposed. Analysis by ion scattering and ion-induced nuclear reaction techniques was used to determine the quantity and depth distribution of impurities and hydrogen isotopes implanted into the exposed samples. Radiation damage analysis of silicon samples exposed in ISX-A indicates significant displacement damage to a depth of 170 Å. This correlates well with the observed depth distribution of deuterium in the samples as determined from the D(^{3}He,p)^{4}He reaction. The range and damage distribution are consistent with 300-eV deuterium bombardment of the wall. Spatial analysis of metallic impurity deposition shows a marked decrease as distance behind the limiter increases. Time-resolved studies of iron and titanium deposition during the discharge indicate increased deposition rates during MHD instabilities in the startup and decay of the plasma.

As part of the ISX surface physics program and the TFTR materials research program, ATJS graphite rail limiters were installed in the ISX tokamak in order to compare them with the existing stainless steel limiters and to investigate any deleterious effects arising from operation at elevated temperatures of the graphite. To facilitate the latter experiment, heaters were installed in the graphite limiters because the power deposition on the limiter in ISX was expected to be considerably less than for TFTR. No large systematic differences were observed in the electron temperature profiles, electron density profiles, or Z_{eff} between successive runs with the stainless steel limiters and graphite limiters. There was, however, a monotonic decrease in Z_{eff} for both cases from 5.6 in the first run following the installation of the graphite limiters to 2.8 after a two-week period when the experiment was terminated because of a scheduled shutdown. Normal-incidence ultraviolet spectroscopic measurements of carbon, nitrogen, oxygen, and hydrogen radiation showed a factor of 3-4 greater hydrogen light for the stainless steel case over the carbon case and systematic differences in the impurity radiation light. Arc tracks were observed on the graphite limiters upon removal, and scanning electron microscope (SEM) analysis was performed so that the amount of material removed could be estimated. In the hot graphite limiter experiment, the temperature of one of the graphite limiters was increased on successive shots. The hydrocarbons formed, as determined by residual gas analysis (RGA), increased monotonically with increasing limiter temperature; for example, mass 16 (presumed to be CH_4) increased about a factor of 2 as the temperature was raised from 150 to 500°C. The carbon impurity radiation was also observed to increase by a factor of 2 as the limiter temperature was raised from 150 to 500°C.

T-12 (Kurchatov Institute)[11]

The ORNL portable surface analysis station provided a valuable new insight into helium glow discharge cleaning as a result of a joint experiment on T-12 at the Kurchatov Institute. This experiment showed that helium glow discharge cleaning was very effective and provided faster and easier wall cleaning than hydrogen discharge cleaning.

The studies have been continued on ISX-B and in laboratory simulation experiments with excellent results.

ISX-B

The surface analysis facilities were used to follow changes in surface composition during tokamak cleanup and normal plasma operations. Cleanup techniques were optimized to reduce plasma impurities to acceptable levels in minimum times. A combination of glow discharge cleaning using a mixture of hydrogen and helium followed by a brief series of weak hydrogen or deuterium discharges has reduced the cleanup time to the point that long time penalties are no longer incurred by venting the machine to air for diagnostic changes or maintenance. This facilitates machine operations and saves considerable time and money. The mechanisms of cleanup are gradually being understood, but studies must be continued so that cleanup can be optimized and technology transferred to other tokamaks.

Arcing has been proposed as a major source of metal impurities in tokamak plasmas. Arc tracks have been observed in the ISX-B tokamak on the limiter, the inner wall surface, and the samples exposed to the plasma from the surface analysis station. Linear and fern-like arc tracks have been observed. From optical and SEM analysis of the tracks, it was estimated that about 10^{16}-10^{17} atoms were released per arc. To study the influence of arcing on the tokamak discharge, an experiment was set up to measure electrical and optical signals of arcing in situ. In well-controlled tokamak discharges, arcing was observed only during the initial breakdown of the plasma and during the quenching phase at the end of the discharge. In disrupted discharges each plasma disruption was accompanied by arcing. The pulse length of a single unipolar arc was measured to be ~ 50 µsec, and the current amplitude was typically ~ 20 A. Erosion rates were measured to be $\sim 10^{-7}$-10^{-8} kg/C.

Doublet III (General Atomic)[37]

After completion of the T-12 experiments, the ORNL portable surface analysis station was moved to Doublet III, where it was one of the first diagnostics used. It has been used for cleanup studies from the very start of machine operation. Its use has optimized machine cleanup, thereby reducing cleanup time. In addition to cleanup studies, the transport of limiter material (90% tantalum/10% tungsten) was measured. During early tokamak discharges when the plasma position was not well controlled, the wall became covered with limiter material. These results have provided a strong impetus to change the limiters to a material of lower atomic number.

1.3.4 Long Pulse Technology Tokamak

T. C. Jernigan J. Sheffield

In the recent publication *The Department of Energy Policy for Fusion Energy Research*,[38] John M. Deutsch, Director of Energy Research, enumerated nine critical technical issues upon which significant progress must be made in order to make and operate an economically satisfactory magnetic fusion power plant. Six of these nine issues pertain to generic fusion reactor problems or to tokamak fusion reactor problems specifically:[39]

(1) detailed understanding of particle and energy confinement in tokamaks and of scaling laws for such confinement; limitations on plasma and magnetic field density;

(2) limitations on the pulse length of tokamaks operating under burn conditions;

(3) impurity control in tokamaks;

(4) first wall conditions and lifetimes in both tokamak and mirror reactors;

⋮

(7) limiting powers and efficiencies of auxiliary heating techniques for both tokamaks and mirrors; and

(8) i.e., practical techniques of energy removal and utility at high efficiency from any magnetic confinement systems (including, in the applicable systems, direct conversion to electricity).

The Fusion Energy Division (FED) has been involved actively for the past ten years in the study and development of solutions to precisely these technological and physics questions. ORNL has played and continues to play a major role in the development of many reactor-relevant technologies (e.g., neutral-beam-heating systems, pellet fueling systems, superconducting coil systems, high beta tokamaks, high power microwave sources, and materials studies). Utilizing the experience from this technological background, a scoping study has developed the outline for a proposed new facility at ORNL, the Long Pulse Technology Tokamak (LPTT).

It is generally considered that economic power production by magnetic fusion will be achieved in devices that include certain features. Plasmas with the following minimum parameters are required:

$T = 5\text{-}10$ keV

$n\tau \geq 10^{14}$ cm^{-3} sec

$\beta = 5\text{-}10\%$

$P_W \sim 20\text{-}100$ W/cm^2 thermal

$Z_{eff} < 2$, with few high-Z impurities.

The device will almost certainly require superconducting coils, a plasma duration considerably in excess of 10 sec, a high duty factor, and components that are reliable, long lived, and practical to maintain because the reactor must operate and be serviced in a hostile radiation environment.

In the U.S. program as presently conceived, all of these features will come together for the first time in an Engineering Test Facility (ETF). One perspective of a tokamak version is that it will have a pulse length of at least 20 sec and perhaps as much as 300 sec with 0.25-0.5 duty factor. At longer pulse length it will be necessary to remove helium ash produced by the deuterium-tritium (D-T) burn. The LPTT program is proposed to support and speed up the realization of an ETF by

(1) addressing the challenge of demonstrating production and sustenance of a high beta ($\gtrsim 5\%$) plasma with $Z_{eff} \sim 1$ at reactor level thermal power fluxes ($\gtrsim 40$ W/cm^2) for at least some tens of seconds (issues #1, #2, and #4 above);

(2) developing an ETF-relevant, long pulse impurity control scheme for which a superconducting bundle divertor is proposed for the first part of the program (issues #3 and #8 above);

(3) developing superconducting coils systems integration experience in a tokamak environment;

(4) capitalizing upon the new physics currently being developed (plasma cross-section optimization, pellet fueling, etc.) so as to maintain the momentum of the fusion program; and

(5) establishing a program to develop reliable, long pulse, high duty factor, ETF-relevant components, such as first walls, divertor targets, pumps, heating, and fueling systems (issue #7 above).

Thus, the LPTT program is intended to form a complementary part of the U.S.-DOE magnetic fusion program by tackling, in collaboration with industry and other laboratories, areas not being pursued and by reinforcing other areas that receive inadequate attention in the present program.

After various iterations the LPTT design scoping study has arrived at the following parameters for the tokamak:

9 superconducting NbTi TF coils

1-3 superconducting bundle divertors

$$\left.\begin{array}{r} R = 1.6 \text{ m} \\ a = 0.45 \text{ m} \\ b/a \leq 1.6 \end{array}\right\} \quad \begin{array}{c}\text{minimum plasma dimensions} \\ \text{at low ripple}\end{array}$$

$$\delta = \frac{B_{max} - B_{min}}{B_{max} + B_{min}} = \begin{array}{l} 0.25\% \text{ at } R = 1.6 \text{ m ,} \\ \quad 1.7\% \text{ at } R = 2.05 \text{ m} \end{array}$$

ORNL-DWG 79-2211 FED

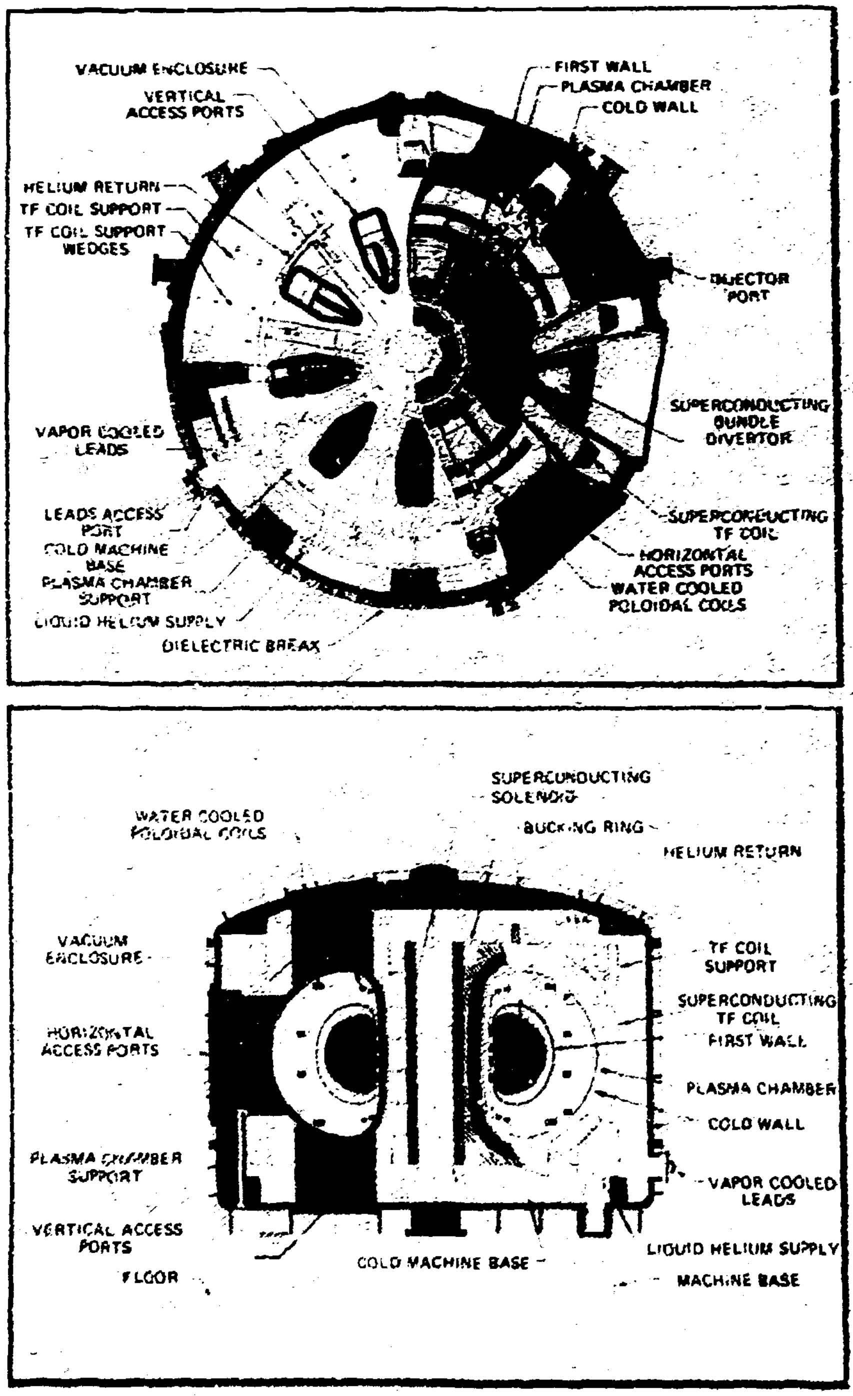
VACUUM ENCLOSURE
VERTICAL ACCESS PORTS
HELIUM RETURN
TF COIL SUPPORT
TF COIL SUPPORT WEDGES
VAPOR COOLED LEADS
LEADS ACCESS PORT
COLD MACHINE BASE
PLASMA CHAMBER SUPPORT
LIQUID HELIUM SUPPLY
DIELECTRIC BREAKS
FIRST WALL
PLASMA CHAMBER
COLD WALL
INJECTOR PORT
SUPERCONDUCTING BUNDLE DIVERTOR
SUPERCONDUCTING TF COIL
HORIZONTAL ACCESS PORTS
WATER COOLED POLOIDAL COILS
SUPERCONDUCTING SOLENOID
WATER COOLED POLOIDAL COILS
BUCKING RING
HELIUM RETURN
VACUUM ENCLOSURE
HORIZONTAL ACCESS PORTS
PLASMA CHAMBER SUPPORT
VERTICAL ACCESS PORTS
FLOOR
COLD MACHINE BASE
TF COIL SUPPORT
SUPERCONDUCTING TF COIL
FIRST WALL
PLASMA CHAMBER
COLD WALL
VAPOR COOLED LEADS
LIQUID HELIUM SUPPLY
MACHINE BASE

Fig. 1.22. LPTT elevation.

$B = 15$ kG } nominal operating conditions
$I = 0.4$ MA

B_{max} 35-kG maximum toroidal field at $R = 1.6$ m

≥ 5 volt-seconds

20-sec pulse length

5-12-MW neutral injection at 40-60-keV H^0 (80 keV max)

5 radial ports ∼1.9 m vertical x 1.6 m horizontal.

An overriding requirement for LPTT is that it have very good access to permit relatively easy modifications to such components as the first wall, poloidal system, and edge control systems. In other words, it must have considerable experimental flexibility. The designers were well aware of the pitfall of being so ambitious in a desire to maximize one parameter, the toroidal field, for example, that simplicity, accessibility, and subsequent usefulness were lost. They appreciated equally the argument that a device should be capable of operating above the nominal level in case that level turned out to be too low.

A cross-sectional view of LPTT is shown in Fig. 1.22. It is estimated that LPTT would be operational four years after authorization at a cost of $40-60 million. The scoping study is now concentrating on developing specific engineering and physics solutions to the points that have been raised in the design work so far.

REFERENCES

1. Varian Associates, Palo Alto Microwave Tube Division, Palo Alto, California.
2. *Fusion Energy Division Annual Progress Report for the Period Ending December 31, 1977*, Oak Ridge National Laboratory Report ORNL-5405, pp. 6-8, Oak Ridge, Tennessee (1978).
3. C. F. Barnett, J. A. Ray, and B. van Zyl, "Absolute Measurement of Low Energy H^0 Fluxes by a Secondary Emission Detector," submitted to J. Appl. Phys.
4. R. A. Dandl et al., *Summary of EBT-I Experimental Results*, Oak Ridge National Laboratory Report ORNL/TM-6457, Oak Ridge, Tennessee (1978).
5. *Fusion Energy Division Annual Progress Report for the Period Ending December 31, 1977*, Oak Ridge National Laboratory Report ORNL-5405, p. 13, Oak Ridge, Tennessee (1978).
6. K. H. Carpenter and [illegible] Lazar, *NCHARF: Algorithms and Computer Codes for a Modified Algebraic Spatial Reconstruction of Spectroscopic Emissivities in EBT Bumpy Torus*, Oak Ridge National Laboratory Report ORNL/TM-6500, Oak Ridge, Tennessee (1978).
7. B. H. Quon, R. A. Dandl, P. L. Colestock, and H. Ikegami, *Effects of Global Field Errors on ELMO Bumpy Torus*, Oak Ridge National Laboratory Report ORNL/TM-6075, Oak Ridge, Tennessee (1977).
8. B. H. Quon, R. A. Dandl, P. L. Colestock, F. M. Bieniosek, and H. Ikegami, *Influence of Global Magnetic Perturbations on Plasma Behavior in ELMO Bumpy Torus*, Oak Ridge National Laboratory Report ORNL/TM-6704, Oak Ridge, Tennessee (1979).
9. K. G. Budden, *Radio Waves in the Ionosphere*, p. 436, Cambridge University Press, Cambridge, 1961.
10. M. Murakami et al., "Plasma Confinement and Impurity Flow Reversal Experiments in the ISX-A Tokamak," paper IAEA-CN-37-N-4 presented at the 7th Int. Conf. on Plasma Physics and Controlled Nuclear Fusion Research, Innsbruck, Austria, August 23-30, 1978; to be published in proceedings.
11. K. H. Burrell et al., Phys. Rev. Lett. 41, 1382 (1978).
12. M. Murakami et al., Phys. Rev. Lett. 42, 655 (1979).
13. *Fusion Energy Division Annual Progress Report for the Period Ending December 31, 1977*, Oak Ridge National Laboratory Report ORNL-5405, pp. 40-43, Oak Ridge, Tennessee (1978).

14. R. C. Isler, Phys. Rev. Lett. 38, 1359 (1977).
15. R. C. Isler and E. C. Crume, Phys. Rev. Lett. 41, 1296 (1978).
16. *Fusion Energy Division Annual Progress Report for the Period Ending December 31, 1977*, Oak Ridge National Laboratory Report ORNL-5405, pp. 59-63, Oak Ridge, Tennessee (1978).
17. L. A. Berry et al., *Proc. 6th Int. Conf. on Plasma Physics and Controlled Nuclear Fusion Research*, Vol. I, pp. 49-68 (1977).
18. M. Murakami et al., Phys. Rev. Lett. 39, 615 (1977).
19. C. A. Foster et al., Nucl. Fusion 17, 1967 (1977).
20. S. L. Milora, C. A. Foster, P. H. Edmonds, and G. L. Schmidt, Phys. Rev. Lett. 42, 97 (1979).
21. M. Murakami, J. D. Callen, and L. A. Berry Nucl. Fusion 16, 347 (1976).
22. R. E. Waltz and G. E. Guest, Phys. Rev. Lett. 42, 651 (1979).
23. H. Eubank et al., "PLT Neutral Beam Heating Results," paper IAEA-CN-37-C-3 presented at the 7th Int. Conf. on Plasma Physics and Controlled Nuclear Fusion Research, Innsbruck, Austria, August 23-30, 1978; to be published in proceedings.
24. The current Oak Ridge versions of that originally described in J. D. Callen et al., *Proc. 5th Int. Conf. on Plasma Physics and Controlled Nuclear Fusion Research*, Vol. I, pp. 645-658 (1975).
25. R. A. Dory et al., "High Beta Tokamaks," paper IAEA-CN-37-K-1 presented at the 7th Int. Conf. on Plasma Physics and Controlled Nuclear Fusion Research, Innsbruck, Austria, August 23-30, 1978; to be published in proceedings.
26. *Fusion Energy Division Annual Progress Report for the Period Ending December 31, 1977*, Oak Ridge National Laboratory Report ORNL-5405, pp. 51-56, Oak Ridge, Tennessee (1978).
27. V. S. Vlasenkov et al., *Proc. 6th Int. Conf. on Plasma Physics and Controlled Nuclear Fusion Research*, Vol. I, pp. 35-94 (1977).
28. *Fusion Energy Division Annual Progress Report for the Period Ending December 31, 1977*, Oak Ridge National Laboratory Report ORNL-5405, p. 62, Oak Ridge, Tennessee (1978).
29. L. C. Emerson, R. E. Clausing, and L. Heatherly, J. Nucl. Mater. 76, 472 (1978).
30. R. J. Colchin, C. E. Bush, P. H. Edmonds, A. C. England, K. W. Hill, R. C. Isler, T. C. Jernigan, P. W. King, R. A. Langley, D. H. McNeill, M. Murakami, R. V. Neidigh, G. H. Neilson, J. E. Simpkins, J. Wilgen, J. C. DeBoo, K. H. Burrell, and E. S. Ensberg, J. Nucl. Mater. 76 405 (1978).
31. R. E. Clausing, L. C. Emerson, and L. Heatherly, J. Nucl. Mater. 76, 267 (1978).
32. J. E. Simpkins and R. J. Colchin, "Time Dependence of Gases from Plasma-Wall Interactions in ISX-A," to be published in J. Nucl. Mater.
33. R. A. Zuhr, B. R. Appleton, R. E. Clausing, L. C. Emerson, and L. Heatherly, "Time-Resolved Measurements of Impurity Deposition in ISX," to be published in J. Nucl. Mater.
34. Y. Gomay, R. E. Clausing, R. J. Colchin, L. C. Emerson, L. Heatherly, W. Namkung, and J. E. Simpkins, "Wall Conditioning by Low Power Discharge in the ISX-A Tokamak," to be published in J. Vac. Sci. Technol.; also published as General Atomic Report GA-A 15072.
35. R. A. Langley, R. J. Colchin, R. C. Isler, M. Murakami, J. E. Simpkins, J. L. Cecchi, V. L. Corso, H. F. Dylla, R. A. Ellis, Jr., and M. Nishi, "The ISX-A Graphite Limiter Experiment," to be published in J. Nucl. Mater.
36. N. N. Brevnov and R. E. Clausing, "Study of a Tokamak Cleaning Method Utilizing Glow Discharge," to be submitted.
37. P. Mioduszewski, R. E. Clausing, and L. Heatherly, "Microarcing as an Impurity Source in Tokamak," to be published in IEEE Trans. Nucl. Sci.

38. A. F. Lietzke, S. Ejima, R. E. Clausing, L. C. Emerson, L. Heatherly, S. Halsted, and S. Seki, "Glow Discharge Cleaning During Initial Operation of Doublet III," to be submitted.
39. John M. Deutch, *The Department of Energy Policy for Fusion Energy*, DOE/ER-0018, 1978.

2. DIAGNOSTIC DEVELOPMENT

C. F. Barnett[1]
D. P. Hutchinson[1]
C. H. Ma[2]
J. A. Ray[1]
P. A. Staats[1]
P. H. Stelson[1]
K. L. Vander Sluis[1]
B. Van Zyl[3]

Abstract. Further investigations of the unstable resonator-oscillator spectral characteristics of the 1-MW D_2O ion Thomson scattering laser have indicated the presence of transverse mode structure. To eliminate these unwanted frequencies, the laser configuration was changed to a linear oscillator with mode-selecting optics. The formic acid submillimeter-laser, single-channel interferometer was operated successfully on the second phase of the Impurity Study Experiment (ISX-B) and was expanded to multichannels to include plasma current density measurements using Faraday rotation of the polarization vector. A fast H atom secondary emission detector was calibrated in the energy range of 30 eV-2.5 keV by photodetaching H^- to provide a known beam of H^0. Preliminary plasma ion temperature measurements were made in ISX-B using the method of neutron transmission through liquid oxygen.

2.1 THE MEASUREMENT OF PLASMA ION TEMPERATURE BY THOMSON SCATTERING

During the past year work has continued towards the development of a high power, narrow band, submillimeter laser for ion Thomson scattering. An unstable resonator-oscillator was coupled with a 3-m amplifier to produce power levels of 1 MW from D_2O at a wavelength of 385 μm. An injection-locked, narrow line CO_2 laser, which can produce up to 150-J pulses, was used to pump the submillimeter oscillator-amplifier configuration. Linewidth measurements of the pulsed submillimeter laser were made with a Fabry-Perot interferometer and a fast transient recorder. Previous measurements made with a transient recorder on a 200-kW oscillator-amplifier system indicated that the linewidth was less than the 50-MHz maximum linewidth required for the Thomson scattering experiment. However, as the system was scaled to the 1-MW level, additional frequencies were detected beyond the permissible linewidth limits. Using a Tektronix transient digitizer with the capability of fast Fourier transform analysis, we determined that some of the additional emission spectra are due to modes in the unstable optics oscillator caused by spurious reflections from smooth metal surfaces within the optical cavity and the vacuum enclosure. These oscillations were identified and partially removed with suitable baffling and minor modifications in the oscillator design. However, wideband structure remained in the laser output. This wideband emission has been attributed to two sources: (1) superradiant emission from the amplifier that has not been removed by the strong (~200-300-kW) oscillator output and (2) unwanted transverse mode structure in the oscillator itself. The unstable oscillator was originally selected for its two main advantages: (1) excellent transverse mode suppression and (2) large volume-to-length ratio to provide for good pump laser absorption. Apparently, in media with extremely large gain coefficients such as those in a submillimeter laser, the unstable resonator does not produce spectrally pure emissions. One of the ways to solve the emission problems is to replace the oscillator-amplifier configuration with a scaled-up, 1-MW oscillator having some type of mode-selecting optics to

---

1. Physics Division.
2. Participant from the University of Mississippi, University, Mississippi.
3. Participant from the University of Denver, Denver, Colorado.

BLANK PAGE

prevent wideband transverse structure. Because of the particular scheme of optical pumping, the unstable resonator does not lend itself to the addition of an intracavity mode selector. Therefore, a different high power oscillator employing an internal mode selector is being constructed.

The design of the receiver for the Thomson scattering experiment has been completed, and the receiver, essentially a double conversion, superheterodyne receiver, is currently under construction. The front end consists of a Schottky diode mixer with a submillimeter laser/local oscillator operating at a frequency 8.4 GHz above the frequency of the D_2O scattering laser. The Thomson-scattered signal, converted to sidebands impressed on an 8.4-GHz carrier by the first mixer, will be amplified by a low-noise GaAs FET amplifier with a bandwidth of 2 GHz and a noise temperature of ~100K. The amplified 8.4-GHz signal will be mixed in a second conventional X-band mixer with an 8.4-GHz oscillator to provide an output containing the scattered spectra from 0-1000 MHz. This information will be stored on a fast transient recorder for analysis by fast Fourier transform. The receiver noise is expected to be in the vicinity of 20,000K when completed.

The optical system necessary to implement the Thomson scattering experiment on the ISX-B tokamak during the next year is now under design.

2.2 MEASUREMENT OF TOKAMAK CURRENT PROFILES BY SUBMILLIMETER FARADAY ROTATION

Further progress has been made on a combined electron density interferometer/Faraday rotation polarimeter for the investigation of tokamak plasmas. This instrument, when extended to several channels or chords cutting across the plasma, will yield both the electron density and current density profiles of the plasma discharge.

A two-laser, heterodyne interferometer/polarimeter was installed on the Rensselaer Torus (RENTOR) tokamak at Rensselaer Polytechnic Institute to test the polarimeter apparatus in preparation for the design of a more sophisticated multichannel analyzer for the ISX-B tokamak. However, the electron density of this small tokamak was too low and the plasma too unstable to permit measurement of a Faraday rotation signal. A four-channel system has been placed on the ISX-B tokamak, and preliminary measurements of the electron density have been made in preparation for the Faraday rotation experiments. At moderate densities ($n_e \sim 1$-5×10^{13} cm^{-3}) where both the 2-mm microwave interferometer and the submillimeter interferometer are operational, the two systems agreed on measurements of the line-averaged electron density. The amount of Faraday rotation expected at these densities for typical plasma currents of ~100 kA is ~50 milliradians, well above the ~1-milliradian sensitivity of the polarimeter.

2.3 ABSOLUTE CALIBRATION OF A H ATOM SECONDARY EMISSION DETECTOR

Most neutral particle analyzers used to measure plasma ion temperatures by detecting low velocity H^+, H^0, and H^- have been calibrated under the assumption that secondary electron emission is the same for both ions and atoms. This assumption has remained untested because of the difficulty of determining the absolute flux of low energy atoms independent of secondary electron emission. An independent calibration of the H^0 flux was achieved by photodetaching a H^- beam passed through a neodymium laser cavity. The attenuation of the H^- beam provided a known absolute flux of H atoms. Over the energy range 30-2500 eV, the secondary emission by H was 15% greater than that by H^+, as shown in Fig. 2.1. In this energy range the secondary emission of H^- was consistently greater than that for H^+ or H^0, being a factor of 6

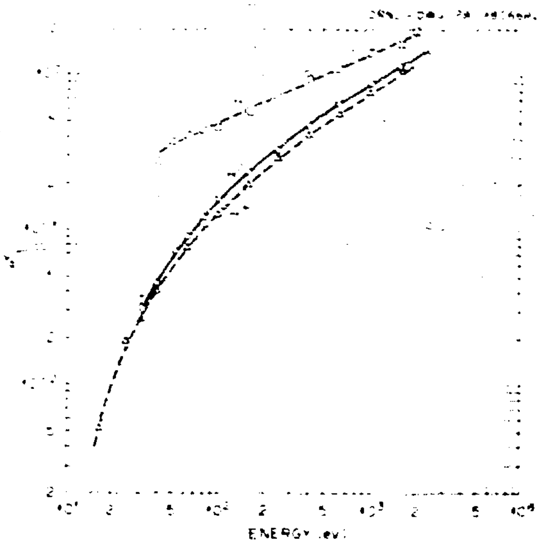

Fig. 2.1. Secondary emission coefficient for H^-, H^+, and H^0 impact on a gas-covered copper surface.

greater at 50 eV. For clean surfaces the secondary emission yield should be dominated by potential electron ejection below 200 eV and is characterized by the electron yield being independent of incident particle energy. At energies as low as 30 eV, there was no evidence of the potential electron ejection mechanism. Comparison of the data in Fig. 2.1 with cross sections for production of free electrons in O_2 and N_2 and with electron yields from clean surfaces gave indications that the secondary yield from surfaces normally found in vacuum systems is dominated by the gas contamination on the surface. The absolute measurements of neutral particles permit the use of both neutral particle analyzers and time-of-flight analyzers for low energy neutral particles coming from plasmas or reflected from surfaces.

2.4 PLASMA ION TEMPERATURE MEASURED BY NEUTRON TRANSMISSION THROUGH LIQUID OXYGEN

At a neutron energy of 2.35 MeV, the total neutron cross section σ_T of oxygen has an unusually deep minimum, down to 0.1 b, compared with values of over 1 b on the shoulders. The mean energy of the deuterium-deuterium (D-D) neutrons, 2.46 MeV, places these neutrons on the shoulder of the minimum in the σ_T for oxygen. However, the kinetic broadening in neutron energies from the plasma D-D reactions puts some of these neutrons into the minimum region. Because the fraction of neutrons in the minimum region is a strong function of ion temperature, one can use a simple transmission measurement to deduce the ion temperature. Calculations indicate that for a thick oxygen sample, a 5% accuracy in a transmission measurement results in a 10% accuracy in the temperature determination, which is independent of both the absolute D-D cross section and the ion density. Preliminary measurements on the ISX plasma were inconclusive because the ion temperature was approximately 0.3 keV. This method should be successful for determining ion temperatures from 1 to 10 keV.

3. PLASMA THEORY

J. D. Callen, Section Head

R. A. Dory, Assistant Section Head

T. Amano[1]
C. W. An[2]
D. E. Arnurius[2]
S. E. Attenberger[3]
M. Azumi[4]
D. B. Batchelor
R. G. Bateman, Jr.[5]
C. O. Beasley, Jr.
D. P. Berger
S. K. Borowski[6]
T. Breazeale[7]
I. Burnett, III
R. D. Burris[3]
B. Carreras[8]
P. J. Catto[9]
L. A. Charlton[3]
D. N. Clark[3]
W. A. Cooper[6]
E. C. Crume, Jr.
J. N. Davidson[10]
L. E. Deleanu
J. Denavit[11]
O. C. Eldridge[12]
G. A. Emmert[13]
R. H. Fowler[3]
J. E. Francis, Jr.
P. W. Gaffney[3]
R. C. Goldfinger[3]
H. Grad[14]
R. K. Gryder[15]
C. E. Hammons
C. L. Hedrick, Jr.
H. R. Hicks[3]
S. P. Hirshman[16]
L. M. Hively[17]
J. T. Hogan
J. A. Holmes[3]
W. A. Houlberg
H. C. Howe
M. A. Iskra[3]
E. F. Jaeger
C. O. Kemper[3]
A. H. Kritz[18]
D. K. Lee[3]
S. J. Lynch[3]
D. G. McAlees[19]
J. E. McCune[20]
J. R. McNally, Jr.
H. K. Meier
A. T. Mense
J. K. Munro, Jr.[3]
D. B. Nelson
A. Nicolai[21]
R. J. Onega[22]
D. R. Overbey
L. W. Owen[3]
C. E. Parker
Y-K. M. Peng
J. W. Reynolds[23]
J. A. Rome
K. E. Rothe[3]
D. J. Sigmar[24]
J. Smith[3,25]
M. Soler[8]
D. A. Spong
W. M. Stacey, Jr.[10]
C. R. Stewart, Jr.[3]
K. A. Stewart
D. J. Strickler[3]
J. S. Tolliver[3]
K. T. Tsang
T. C. Tucker[3]
N. A. Uckan
G. Vahala[26]
W. I. van Rij[3]
B. V. Waddell[27]
H. Weitzner[14]
J. C. Whitson[3]
R. M. Wieland[3]
O. C. Yonts

---

1. Osaka University, Osaka, Japan.
2. Student, University of Tennessee, Knoxville, Tennessee.
3. Computer Sciences Division.
4. Visitor from JAERI, Tokai, Japan.
5. On leave of absence to Georgia Institute of Technology, Atlanta, Georgia.
6. Student, University of Michigan, Ann Arbor, Michigan.
7. Y-12 Maintenance Division.
8. Visitor from Spanish Nuclear Energy Commission, Madrid, Spain.
9. SAI, Boulder, Colorado.
10. Consultant, Georgia Institute of Technology, Atlanta, Georgia.
11. Northwestern University, Evanston, Illinois.
12. Consultant, University of Tennessee, Knoxville; part-time with Experimental Confinement Section.
13. University of Wisconsin, Madison, Wisconsin.
14. New York University, New York, New York.
15. On leave of absence to IAEA, Vienna, Austria.
16. ORNL Wigner Fellow.
17. Student, University of Illinois, Champaign/Urbana, Illinois.
18. Hunter College, New York, New York.
19. Consultant, Exxon Nuclear Co., Inc., Richland, Washington.
20. Consultant, Massachusetts Institute of Technology, Cambridge, Massachusetts.
21. KFA/Jülich, Jülich, Germany.
22. Virginia Polytechnic Institute and State University, Blacksburg, Virginia.
23. Instrumentation and Controls Division.
24. Adjunct Professor of Nuclear Engineering, Massachusetts Institute of Technology, Cambridge, Massachusetts.
25. Consultant, University of Tennessee, Knoxville, Tennessee.
26. ORAU Faculty Research Participant, College of William and Mary, Williamsburg, Virginia.
27. Deceased (September 14, 1978).

BLANK PAGE

Abstract. Among the broad spectrum of advances made by the Theory Section in the understanding of tokamaks and the ELMO Bumpy Torus (EBT), the following stand out as items of special importance to the fusion program:

(1) The high beta tokamak approach pioneered and made credible at Oak Ridge National Laboratory (ORNL) has culminated in the demonstration of (1) stable equilibria at beta values as high as 10% for aspect ratio 4, (2) longevity of high beta cases in the presence of resistive skin diffusion, and (3) benign reaction to the full range of transport phenomena. As a result, the type of operation required for high energy-density, long-lived discharges in the Long Pulse Technology Tokamak (LPTT) device appears credible, and early testing of high beta theory has been made possible through our design of a very flexible plasma control field system for the second phase of the Impurity Study Experiment (ISX-B) device.

(2) The major experimental features of today's low beta, short pulse length devices have been explained adequately using the well-crafted models developed at ORNL of the resistive magnetohydrodynamic (MHD) instabilities and kinetic modes (drift, trapped particle, etc.). These, together with advanced knowledge of impurity and neutral injection physics, provide natural explanation for the observed energy confinement scaling, Mirnov and sawtooth oscillations, the relaxation of skin current distributions, major and minor plasma disruptions, and the poor performance that dominates devices that are insufficiently clean and magnetically well controlled.

(3) For the EBT device, the simplified stability criteria previously used have been substantiated through more detailed analysis of kinetic effects, and most of the primary experimental observations have been explained on the basis of neoclassical transport theory. These phenomena include the ambipolar potential, the level and scaling of thermal losses, the formation of a nonthermal ion distribution function, and the tendency to operate at a very low degree of impurity contamination. With the resulting understanding, we are able to identify two outstanding critical problems in the theoretical area: (1) the behavior of the hot electron rings (particularly energy loss mechanisms and scaling) and (2) the physics of the low collisionality regime. The latter ties the ring dynamics very closely to the behavior of the toroidal plasma (as is seen experimentally in the transition into the noisy M-mode and theoretically in thermal excursion phenomena). The need is clear for still further refinements in the treatment of gradients near the plasma edge and the rings.

The conclusions rest on a firm and broad base of contributory work that should be apparent from the many other topics discussed in the body of this section of the report.

3.1 EBT THEORY

D. B. Batchelor
R. C. Goldfinger
C. L. Hedrick, Jr.*
L. W. Owen
A. H. Kritz
L. E. Deleanu
D. B. Nelson
E. F. Jaeger
D. A. Spong
J. S. Tolliver
H. Weitzner

During this reporting period, the EBT Theory Section has

(1) codified a basic scaling law for EBT in conjunction with the EBT Experimental Group (see Sect. 3.1.1),
(2) participated in design studies of future EBT experiments,[1]
(3) developed stability criteria (see Sects. 3.1.2 and 3.1.3),
(4) developed new expressions for transport coefficients for EBT (see Sect. 3.1.4), and
(5) applied these transport coefficients through a radially resolved transport code (see Sect. 3.1.5).

---

*Group Leader

3.1.1 ELMO Bumpy Torus

L. A. Berry* C. L. Hedrick, Jr.
N. A. Uckan

The EBT program of experiment, theory, and reactor studies has been a remarkably successful one. In the five years since EBT-I began operating, work has progressed from a demonstration of macrostability to an increasingly detailed understanding of transport properties. Collisionless scaling (τ_E increases with temperature) has been observed, and the magnitude of the energy confinement time is consistent with neoclassical theory. Experiments on EBT-S (for scale) are now being conducted at the increased magnetic field levels and higher microwave power and frequency made possible by a 28-GHz gyrotron development program. Initial results confirm our assumptions of neoclassical scaling. In conjunction with the experimental advances, EBT theory now has a well-developed transport theory that models the physics we now think to be important: for example, it yields negative ambipolar electric fields that are consistent with those measured. Stability calculations continue to predict stable equilibrium with $\beta_{ring} \sim \beta_{core} \sim 20\text{-}40\%$.

Based on experiment and theory, projected reactor concepts are economically competitive with those of other geometries, and they offer flexibility to deal with the critical reactor questions of maintenance, accessibility, fueling, ash removal, impurity control, and power handling. Technological demands are relatively modest and, with the exception of microwave power sources, can be met within existing programs. Moreover, rapid progress is being made in microwave tube development.

When we examine the dimensionless plasma parameters required for an EBT reactor (EBTR), we find that, with the exception of beta, the EBT-I experiment is already operating in the correct regimes. Thus, it is possible to supply the necessary bridge to reactor levels with one major experiment. At the same time, this experiment should achieve, in Phase I, $n \sim 5 \times 10^{12}$ cm^{-3}, $T_e \sim 3$ keV, $T_i \sim 1$ keV, and $\beta \sim 2\%$. For Phase II, with neutral injection, we expect $n \sim 10^{14}$ cm^{-3}, $T_e \sim$ 5-10 keV, $T_i \sim$ 5-10 keV, and $\beta \sim$ 5-10%. Performance at this level would provide a critical test of equilibrium, stability, and transport properties of EBT's and of our ability to heat and fuel a larger, denser plasma.

The successful operation of EBT-II will provide the physics base for a reactor-scale extension of the concept.

Finally, it should be noted that the operation of a large, superconducting, microwave-heated, steady-state device would benefit the entire magnetic confinement fusion community.

3.1.2 A Preliminary Investigation of Trapped Particle Instabilities in EBT[1]

D. B. Batchelor C. L. Hedrick, Jr.

An investigation is presented of the role trapped particles might play in the drift wave stability of EBT. The model adopted consists of a bounce-averaged drift kinetic equation with a Krook collision operator. Care has been taken to model, at least in an elementary way, the features that distinguish the physics of EBT from that of tokamaks, namely the large magnitude and velocity space dependence of the poloidal drift frequency Ω, the relatively small collisionality ν/Ω, the enhancement of ν_{eff} for passing particles, and the closed nature of the field lines. Instabilities are found that have a somewhat dissipative character; however, the precessional drift is found to be a significant stabilizing influence. In most cases, the modes are completely stabilized when $\omega_*/\ell\Omega < 1$ for normal gradients. For reversed gradients ($\omega_*/\ell\Omega < 0$), stability is greatly enhanced.

---

*Director, ORNL Fusion Program

3.1.3 Macroscopic Stability and β Limits in the ELMO Bumpy Torus

D. B. Nelson   C. L. Hedrick, Jr.

Magnetohydrodynamic stability limits are determined for EBT. The relativistic hot electron annuli are considered to be rigid, modifying the magnetic field but not interacting with the instability. A modified energy principle is used, and the stability problem is reduced to determination of the eigenvalues of an ordinary differential equation along each field line. A threshold hot electron current is required for stability; its value agrees with experimental measurements. The calculations show that stable high beta equilibria are easily created.

3.1.4 Kinetic Transport Properties of a Bumpy Torus with Finite Radial Ambipolar Field

D. A. Spong   E. G. Harris*
C. L. Hedrick, Jr.

Neoclassical transport coefficients for a bumpy torus have been calculated by solving a bounce-averaged drift kinetic equation locally in radius. In contrast with previous work, where the ambipolar field was assumed to be large relative to the plasma thermal energy $(e_j\phi/kT_j \gg 1)$, finite electric fields are considered here $[e_j\phi/kT_j = O(1)]$. Both the Landau operator and the particle- and energy-conserving BGK model operator have been used, and a comparison of the two sets of results indicates reasonable agreement. The resulting transport coefficients exhibit a strong dependence on the ambipolar field and on plasma collisionality; in the large field limit, the present results correlate closely with earlier work.

3.1.5 Radial Transport in the ELMO Bumpy Torus in Collisional Regimes

E. F. Jaeger   C. L. Hedrick, Jr.

Neutral and charged particle densities and temperatures are calculated as functions of radius for the toroidal plasma in EBT. Energy-dependent ionization and charge exchange rates, ambipolar diffusion, and self-consistent radial electric field profiles are included. Variations in the magnetic field due to finite toroidal plasma pressure and transport due to drift waves and magnetic field errors are neglected. When the large electric field limit of the neoclassical transport coefficients is used, results are limited to relatively cool electrons $(kT_e \lesssim 100\text{-}200\ \mathrm{eV})$ and collisional scaling for radially inward pointing electric fields.

3.2 MHD THEORY

C. H. An
R. G. Bateman, Jr.
B. Carreras
L. A. Charlton
R. A. Dory
H. R. Hicks
J. A. Holmes
J. K. Munro, Jr.
D. B. Nelson*
Y-K. M. Peng
D. J. Strickler
G. Vahala
B. V. Waddell

In the past year the MHD group has continued to pursue its two main goals of understanding the equilibrium and stability behavior of present tokamaks and developing tokamak concepts with optimally high beta. (Beta is the ratio of plasma energy to magnetic energy.)

The MHD behavior of present tokamaks appears to be dominated by resistive tearing modes, which are responsible for the m = 1 sawtooth oscillations observed near the center of the discharge, the $m = 2$ Mirnov oscillations observed near the edge, and the major disruptive instability that engulfs the entire cross section. There is by now very good experimental and computational evidence that the major disruption is precipitated by the nonlinear interaction of the $m = 2$, $n = 1$ (2/1) and 3/2 modes (Sects. 3.2.1, 3.2.4, 3.2.5, 3.2.6, 3.2.7, 3.2.8, 3.2.10, 3.2.11). Fortunately, this realization has led to the discovery of a possible feedback system to suppress the interaction and avoid disruption (Sect. 3.2.9). If experiment proves the validity of this method, very large savings in cost and improvement in reliability of tokamak reactors could result. The Mirnov oscillations are almost certainly saturated $m = 2$ modes near the limiter, as shown by the agreement between theory and experiment (Sect. 3.2.2). Because they limit confinement in present tokamaks, extrapolation of their behavior to future experiments is important.

---

*University of Tennessee

*Group Leader

We have continued to study evolution to high beta using various approximations of plasma behavior (Sects. 3.2.12, 3.2.13). Extensive analyses of resulting stability limits on beta have been carried out (Sect. 3.2.15). The earlier predictions of stable beta for ideal MHD modes in the range 5-10% have been borne out by careful analysis. Inclusion of resistivity has shown that the actual stability may be somewhat lower but should be evidenced by gradual worsening of confinement rather than by sudden catastrophe (Sect. 3.2.16). Shaping can lead to improvement in beta, but too great an elongation is undesirable (Sect. 3.2.18).

In other directions recognition of the desirability of a higher duty cycle for tokamaks has led to a novel proposal for a continuous tokamak (Sect. 3.2.14). Also, we have continued our extension of MHD by inclusion of tensor pressure and other complicating phenomena (Sect. 3.2.17).

3.2.1 Analytic Model for the Nonlinear Interaction of Tearing Modes of Different Pitch in Cylindrical Geometry[7]

B. Carreras B. V. Waddell
H. R. Hicks

An analytic model has been developed for describing the nonlinear interaction of tearing modes of different pitch in cylindrical geometry for equilibria characterized by flat safety factor profiles. The analysis shows that the 2/1 tearing mode can destabilize odd m modes, particularly the 3/2 mode. The model compares well with our three-dimensional (3-D) code with respect to the time evolution of the 0/0, 1/1, 2/1, 3/2, and 5/3 modes. Scaling rules are obtained for the position and location in time of the maximum or peak in the 3/2 growth rate. The characteristic time of destabilization of the odd m modes predicted by the model correlates well with the observed time scale for the major disruption in tokamaks.

3.2.2 Poloidal Magnetic Field Fluctuations in Tokamaks[8]

B. Carreras B. V. Waddell
H. R. Hicks

Elementary nonlinear tearing mode theory in a 2-D cylindrical geometry is used to predict accurately the amplitude of the $m = 2$ poloidal magnetic field fluctuations (Mirnov oscillations) at the limiter of a tokamak. The input required is the electron temperature radial profile from which the safety factor profile can be inferred. The saturation amplitude of the $m = 2$ tearing mode is calculated from the safety factor profile using a nonlinear Δ' analysis. This gives an absolute result (no arbitrary factors) for the amplitude of the perturbation in the poloidal magnetic field everywhere, at the limiter in particular. An analysis of the

Oak Ridge Tokamak (ORMAK) and T-4 safety factor profiles (inferred from electron temperature profiles) gives results that are in agreement with the experimental data (see Fig. 3.1).

A study of a general profile shows that as a function of the safety factor at the limiter, a maximum occurs in the amplitude of the Mirnov oscillation. The magnitude of the maximum increases with a decrease in temperature near the limiter.

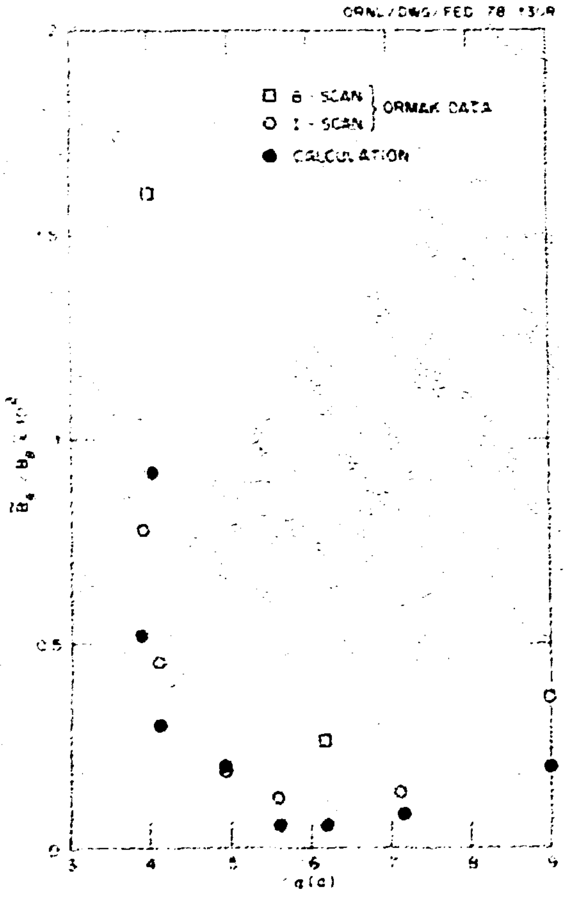

Fig. 3.1. Comparison of the experimental and theoretical values of B_θ/B_ϕ at the limiter as a function of q at the limiter for ORMAK.

3.2.3 Non-Linear Numerical Algorithms for Studying Tearing Modes[9]

B. V. Waddell* M. N. Rosenbluth*
D. A. Monticello† R. B. White†
B. Carreras

The numerical methods that have recently been developed to study the nonlinear evolution of tearing modes in tokamaks are summarized. The essential features of tearing modes can be described by the resistive MHD equations. The numerical algorithms described here are based on a reduced set of 2-D resistive MHD equations that are numerically tractable. Two distinct types of numerical methods are described in detail. In the first method, referred to as the MASSLESS algorithm, the inertia is neglected. On the other hand, in the second method, referred to as the MASS algorithm, the inertia is retained; consequently, the scheme is capable of handling a larger variety of problems. Codes based on these two algorithms give similar results for the nonlinear evolution of the $m = 2$ tearing mode.

3.2.4 Comments on "Simulation of Large Magnetic Islands: A Possible Mechanism for a Major Tokamak Disruption"[10]

B. Carreras H. R. Hicks
B. V. Waddell S. J. Lynch

In this Comment it is established that the numerical results for the nonlinear evolution of the $m = 2$ tearing mode are affected by the density of the poloidal grid.

---

*Institute for Advanced Study
†Princeton Plasma Physics Laboratory

A coarse grid gives results that are quantitatively and qualitatively incorrect. The important qualitative error is that with a coarse grid the growth of the width of the associated magnetic island is exponential rather than algebraic.

3.2.5 Mechanism for Major Disruptions in Tokamaks[11]

B. V. Waddell H. R. Hicks
B. Carreras J. A. Holmes
D. K. Lee

We propose a mechanism for the major disruption in tokamaks that involves the nonlinear destabilization of tearing modes by the 2/1 tearing mode, where m and n denote the poloidal and toroidal mode numbers, respectively. The magnetic islands generated can extend across the plasma cross section. For resistivities of the order of magnitude of these in TOSCA and LT-3, the time scale for their appearance is consistent with the time for the major disruption.

3.2.6 Nonlinear Interaction of Tearing Modes in Highly Resistive Tokamaks[12]

B. V. Waddell H. R. Hicks
B. Carreras J. A. Holmes

A mechanism for the major disruption in tokamaks is proposed involving the nonlinear destabilization of tearing modes by the 2/1 tearing mode, where m and n denote the poloidal and toroidal mode numbers, respectively. A 3-D cylindrical nonlinear code based on a set of equations valid in the limit of low beta and large ratio of the toroidal and poloidal magnetic fields has been constructed. The essential result is that for safety factor profiles flat in the plasma core (square profiles), the 2/1 mode significantly destabilizes other modes, particularly odd modes such as the 3/2 mode, before the 2/1 island in the single-pitch limit has expanded to its maximum width. Many magnetic islands of different pitch are produced, and the corresponding deformation of the toroidal current density is more severe than in the 2-D (single-pitch) case. The magnetic islands generated can extend across the plasma cross section; presumably, the corresponding ergodic magnetic fields can result in the escape of particles and heat from the plasma core. An analytic model in agreement with these results is also presented.

With respect to experiment, the 3/2 mode has been reported to be observed in the LT-3 tokamak. A poloidal asymmetry in the disruption has been observed in ALCATOR, the Princeton Large Torus (PLT), and T-4, but the mode numbers have not been determined. For resistivities that correspond to those in TOSCA and LT-3, the time scale for the appearance of the islands is consistent with the observed time for the major disruption. If the results are extrapolated to small resistivities using the analytic model, the time scale is consistent with PLT and a variety of other machines.

Figure 3.2 illustrates nonlinear coupling effects.

3.2.7 Magnetic "Islandography" in Tokamaks[13]

J. D. Callen J. A. Holmes
B. V. Waddell D. K. Lee
B. Carreras S. J. Lynch
M. Azumi J. Smith
P. J. Catto M. Soler
H. R. Hicks K. T. Tsang
J. C. Whitson

Tearing modes are shown to be responsible for most of the experimentally observed macroscopic behavior of tokamak discharges. The effects of these collective magnetic

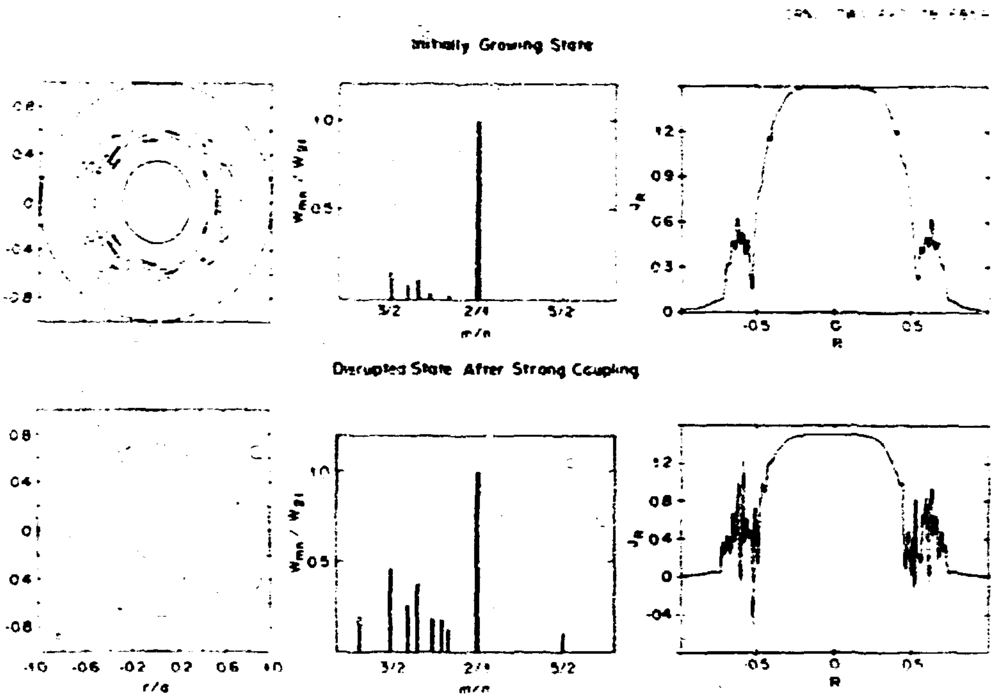

Fig. 3.2. Nonlinear coupling of unstable tearing modes of different helicity can lead to a disruptive instability.

perturbations on magnetic topology and plasma transport in tokamaks are shown to provide plausible explanations for internal disruptions (m/n = 1), Mirnov oscillations (m/n = 2,3,...), and major disruptions (coupling of 2/1-3/2 modes). The nonlinear evolution of the tearing modes is followed with fully 3-D computer codes. The effects on plasma confinement of the magnetic islands or stochastic field lines induced by the macroscopic tearing modes are discussed and compared with experiment. Finally, microscopic magnetic perturbations are shown to provide a natural model for the microscopic *anomalous transport processes in tokamaks.*

3.2.8 Tearing Mode Activity for Hollow Current Profiles[14]

B. Carreras H. R. Hicks
B. V. Waddell

We present the results of a study of the nonlinear stability of tearing modes for hollow current profiles in cylindrical geometry. We have studied their nonlinear evolution that, through magnetic island formation, leads either to saturation of the tearing mode (a new nonaxisymmetric equilibrium is reached) or to a redistribution of the flux and field line reconnection in Kadomtsev's sense (a new axisymmetric equilibrium is obtained). An empirical prediction for the accessibility of the reconnected state is given. In particular, we consider tearing modes with low poloidal mode number (m = 2, 3) to interpret some minor disruptions observed in tokamaks, namely, m = 3 minor disruptions in PLT. We have also considered tearing *modes with higher poloidal mode number.*

3.2.9 Stabilization of Tearing Modes to Suppress Major Disruptions in Tokamaks[15]

J. A. Holmes H. R. Hicks
B. Carreras S. J. Lynch
B. V. Waddell

We show, for q-profiles that lead to a disruption, that the control of the amplitude of the 2/1 tearing mode avoids the disruption. We have studied q-profiles measured in T-4 and PLT before a major disruption. Two methods of controlling the 2/1 mode amplitude have been considered: (1) Feedback stabilization with the feedback signal locked in phase with the 2/1 mode. The major disruption is suppressed if the feedback parameters (time delay and gain) are properly chosen. Otherwise, we observe only a delay in the disruption. (2) Heating slightly outside the $q = 2$ surface. Modifying the current density profile can decrease, and even eliminate, the 2/1-3/2 interaction. In this way the disruption is avoided.

In both cases it is only necessary to decrease the 2/1 mode amplitude to suppress the disruption. It is not always necessary to stabilize the unstable modes fully.

3.2.10 Tearing Mode Analyses of MHD Activity in ISX-A

B. Carreras　　J. L. Dunlap*
A. P. Navarro*　　H. R. Hicks
R. D. Burris　　M. Murakami*
V. K. Paré*

We have studied an ISX-A sequence of ISX-A discharges that became disruptive after tungsten was injected at $\sim$100 msec. These discharges can be classified into two groups from the point of view of MHD activity: type H discharges (hard disruption) and type S discharges (soft disruption). This different behavior has been compared with nonlinear tearing mode theory. The 3/2 mode is found to be stable for the current profiles associated with type S discharges and unstable for type H discharges. In cylindrical approximation this leads to identifying type S discharges as those dominated by a single 2/1 mode and type H discharges as those involving mixed helicities.

3.2.11 Effects on the Nonlinear Interaction of Tearing Modes due to Temperature Evolution

H. R. Hicks　　B. V. Waddell
B. Carreras　　D. K. Lee

Previously we presented numerical results of the nonlinear interactions of tearing modes as a mechanism for the major disruption. In the cases studied, instead of using a time-independent resistivity, we utilized Spitzer resistivity in conjunction with an electron temperature equation. The effect of evolving resistivity on the saturation of single-helicity tearing modes can, in principle, be large. However, as realistic values of resistivity and parallel electron thermal conductivity are approached, the effect becomes minimal. The effect on multihelicity cases is to speed up slightly the process by which a large region of stochastic field lines is formed.

3.2.12 Evolution of Flux Conserving Tokamak Equilibria with Preprogrammed Cross Sections[16]

J. A. Holmes　　Y-K. M. Peng
S. J. Lynch

The evolution of MHD equilibria towards high beta is modeled by magnetic flux conservation with a given $q(\psi)$ and by particle and energy balances that determine $p(\psi,t)$. One-dimensional single-fluid transport equations, written with the magnetic flux ψ as the independent variable, are coupled to the 2-D axisymmetric MHD equilibrium and flux conservation equations through ψ and $p(\psi,t)$. In moving boundary studies (plasma compression), the resulting system of equations is advanced in time from an initial state by a procedure that utilizes two nested predictor-corrector loops together with an implicit time-stepping technique. The inner predictor-corrector loop advances the transport equations subject to a given equilibrium configuration while the outer loop evolves the equilibrium using a fixed boundary flux-conserving code. For fixed plasma boundaries, this procedure is modified for greater computational speed. Our results show satisfactory quality in numerical convergence. The use of the fixed boundary equilibrium technique allows the evolution of the plasma cross section to be programmed. This method can be applied to the study of flux-conserving evolution of equilibria involving dramatic changes of plasma position, shape, and profiles while prescribing the evolution of the plasma boundary. As an example, the compressional scaling laws of Furth and Yoshikawa are modified for small aspect ratio.

---

*Experimental Confinement Section

3.2.13 Intense Neutral Beam Heating in the Adiabatic Approximation[17]

D. B. Nelson

The economic viability of tokamak fusion reactors improves significantly if beta can be raised above 5% to 10%. High-powered neutral particle injection makes possible the attainment of such beta values if the corresponding equilibria exist, are dynamically accessible, and can be maintained against instabilities and transport. Early analytic work seemed to indicate a restrictive equilibrium constraint, $\beta_{pol} < 1/\epsilon$ or $\beta < \epsilon/q^2$, with ϵ the inverse aspect ratio (typically 1/3 to 1/5) and q the safety factor at the wall (typically 3 to 5). The physical process that limits beta was the appearance of a poloidal field (PF) null (stagnation point) at the inside edge of the plasma. However, if energy is deposited on a time scale that is rapid compared with the resistive skin time, the magnetic flux remains frozen. The plasma then evolves as a flux-conserving tokamak (FCT), and a stagnation point cannot move into the plasma. Recent calculations have exploited the FCT concept to produce equilibria with beta exceeding 30%, considerably above the supposed limit. These calculations do not demonstrate the dynamic accessibility of high beta equilibria; in fact, the authors were able to calculate FCT equilibria only over a limited range of parameters. If this were due to nonexistence of equilibrium, the initial state and heat deposition profile would have to be carefully tailored to achieve success.

This paper exhibits a simple method for following the dynamic evolution of the plasma under neutral beam heating. While the method used is also being applied to more general transport calculations, for these results it is assumed that the heating is rapid compared with resistive diffusion or cross field heat conductivity. Thus, the plasma evolves adiabatically, i.e., according to the ideal MHD equations. It is found that high beta states can be attained with a wide variety of initial conditions and heating profiles.

3.2.14 Continuous Tokamaks[18]

Y-K. M. Peng

We propose a tokamak configuration that permits the rapid replacement of a plasma discharge in a burn chamber by another one in a time scale much shorter than the elementary thermal time constant of the chamber first wall. Thus, with respect to the chamber, the effective duty cycle factor can be made arbitrarily close to unity, minimizing the cyclic thermal stress in the first wall. At least one plasma discharge always exists in the new tokamak configuration, hence, we have a continuous tokamak. By incorporating adiabatic toroidal compression, configurations of continuous tokamak compressors are introduced. To operate continuous tokamaks, it is necessary to introduce the concept of mixed PF coils, which spatially groups all the PF coils into three sets, all contributing simultaneously to inducing the plasma current and maintaining the proper plasma shape and position. Preliminary numerical calculations of axisymmetric MHD equilibria in continuous tokamaks indicate the feasibility of their continued plasma operation (see Fig. 3.3 and Table 3.1). Advanced concepts of continuous tokamaks to reduce the topological complexity and to allow the burn plasma aspect ratio to decrease for increased beta are then suggested. Comparisons with conventional tokamaks are made in the light of reactor applications, indicating several potential advantages of some advanced continuous tokamaks that require comparable toroidal magnetic field energy to produce comparable fusion power.

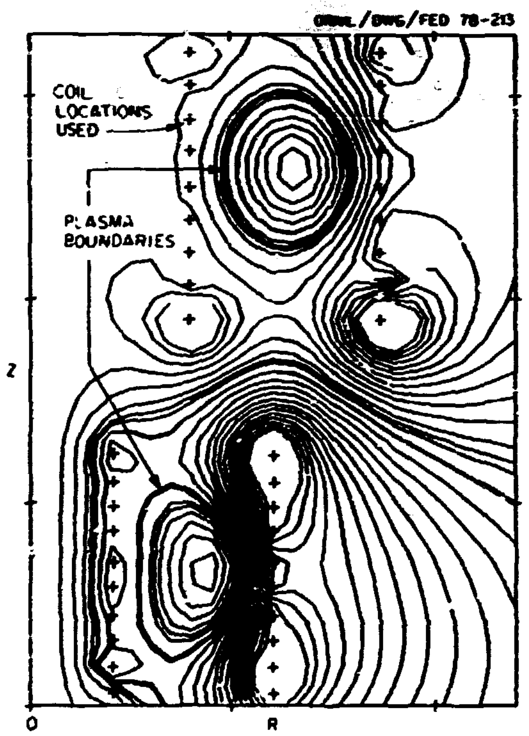

Fig. 3.3. Poloidal flux produced by all current sources in a continuous tokamak compressor with plasmas B and C of Table 3.1.

3.2.15 Very Small Aspect Ratio Tokamaks[19]

Y-K. M. Peng R. A. Dory

Magnetohydrodynamic (MHD) stability analyses are carried out for tokamak equilibria with $A = 2.0$ and 1.5, $q(\text{boundary})/q(\text{axis}) \geq 2$, and $\beta_p \simeq A/2$ (see Fig. 3.4). When a conducting wall is at a distance $0.2a$ from the plasma with $A = 1.5$, the critical $\bar{\beta}_T (= 8\pi p/B_{T0})$ values are found to be 0.47, 0.37, and 0.33 for toroidal mode numbers $N = 1$, 2, and 3, respectively (see Table 3.2). A linear extrapolation in $1/N \to 0$ results in a $\bar{\beta}_{Tc}$ of 0.28, which is consistent with the results based on analyses of large ballooning modes on each flux surface. For the case of $A = 2.0$, $\bar{\beta}_{Tc}$ values on plasma parameters are quantified together with suggested approaches to produce the plasma via adiabatic compression. For demonstrating high $\bar{\beta}_T$ with $A = 2$, $B_{T0} = 1.2$ T, and $R_0 = 16$ cm via a compression ratio of $C = 3$, a neutral beam power of ~1 MW, a resistive coil power of 2 MW, and a compression energy input of 3.3 kJ in 1.4 msec would be required. For demonstrating thermonuclear ignition with $A = 1.5$, $B_{T0} = 4.0$ T, and $R_0 = 60$ cm via a compression ratio of $C = 4$, a neutral beam power of ~5 MW, a resistive coil power of ~170 MW, and a compression input energy of ~6 MJ in 0.2 sec would be required. Based on reasonable scaling assumptions, the plasma would ignite with a total fusion power of ~100 MW. With a burn-time of 6 sec (which is one third of the L_p/R_p), the plasma energy gain per discharge is estimated to be ~50. Because of the reduced toroidal transit length for suprathermal ions and the increased beta and pressure gradient, it becomes relatively easy to drive large current via neutral beam injection or the bootstrap effect. Comparisons with other toroidal concepts show that, given the calculated high $\bar{\beta}_T$ values, very small aspect ratio tokamaks have relatively good confinement and efficient use of field energy.

3.2.16 Low Density Ignition Scenarios Using Injection Heating

J. A. Holmes Y-K. M. Peng
J. A. Rome S. J. Lynch

By taking advantage of central alpha heating, profile effects, and flux surface

Table 3.1. Currents in coils for plasmas B and C when they are alone and when they are coexisting in a continuous tokamak compressor corresponding to the equilibria shown in Fig. 3.4

	Plasma B ($\Sigma I_c = -3\ I_p$, $I_p = 16$)		Plasma C ($\Sigma I_c = -2\ I_p$, $I_p = -7.6$)	
Coil No.	$-I_i^0/I_p$	$-(I_i^0 + \Delta I_i^c)/I_p$	$-I_i^0/I_p$	$-(I_i^0 + \Delta I_i^c)/I_p$
1	0	-0.219	0	1.128
2	0.465	0.630	0.393	-0.571
3	0	-0.111	0	0.201
4	0.210	0.225	0.089	-0.027
5	0.210	0.167	0.089	0.054
6	0.210	0.211	0.089	0.012
7	0.210	0.139	0.089	0.071
8	0	0.131	0	-0.158
9	0.465	0.049	0.393	0.614
10	0	0.389	0	-0.445
11	0.205	0.426	0.143	-0.007
12	0.205	0.085	0.143	0.268
13	0	0.038	0	-0.046
14	0.205	0.206	0.143	0.159
15	0	0.006	0	-0.011
16	0	0.004	0	0.015
17	0.205	0.207	0.143	0.097
18	0	0.009	0	0.187
19	0.205	0.196	0.143	-0.492
20	0.205	0.211	0.143	0.952

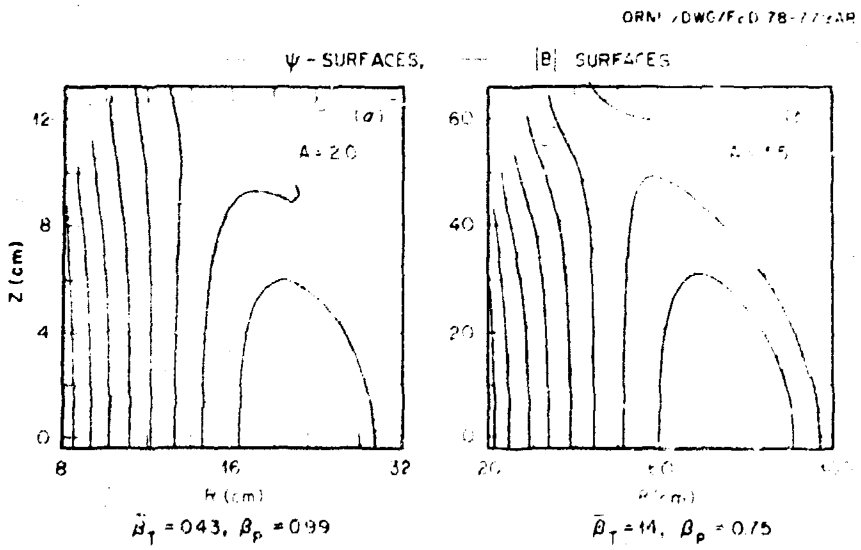

Fig. 3.4. Constant ψ and |B| surfaces for MHD equilibria with A = 2.0 and 1.5 and parameters shown in Table 3.1.

Table 3.2. Parameters of marginal stability based on the equilibria shown in Table 3.1 and Fig. 3.4

	Aspect ratio (A)	
	2.0	1.5
Major radius (R_o)	16	60
Minor radius (a)	8	40
Elongation (κ)	1.65	1.65
B_{To} ($R = R_o$)	1.20×10^4 G	4.0×10^4 G
Plasma current (I_p)	0.268×10^6 A	6.54×10^6 A
q_o	1.59	2.08
q_b	3.25	4.47
β_p	0.99	0.75
$\bar{\beta}$ ($\equiv 8\pi\bar{p}/\bar{B}^2$)	0.14	0.17
$\bar{\beta}_{Tc}$	0.18	0.28
β_{Tc} (peak)	0.40	0.57
B_T ($R = R_o - a$)	2.40×10^4 G	12.0×10^4 G
B_T ($R = R_o + a$)	0.80×10^4 G	2.4×10^4 G
B_p ($R = R_o - a$)	0.681×10^4 G	3.65×10^4 G
B_p ($R = R_o + a$)	0.597×10^4 G	2.58×10^4 G
V_p	2.91×10^4 cm^3	2.70×10^6 cm^3

shifts in elongated plasmas, it is possible to ignite a modeled, prototypical reactor plasma using 100-150 keV (D^+) neutral beams. To do this, the plasma is started at full bore but low density. The density is [illegible] increased by peripheral fueling so [illegible] central core begins to ignite at the [illegible] when the neutral beams no longer penetrate to this region. The fusion alpha particles take over the heating requirements in the core region.

Examples of our results are shown in Figs. 3.5 and 3.6. As seen in Fig. 3.5, ignition is achieved with 92 MW of neutral beam power despite pessimistic heat conduction coefficients of $\chi_e = 10^{18}/n_e$ cm^2/sec and $\chi_i = 2 \times \chi_{neoclassical}$. Comparable results are obtained with 50 MW of neutral beam power when $\chi_e = 5 \times 10^{17}/n_e$ cm^2/sec and $\chi_i = \chi_{neoclassical}$. As the density increases, the neutral beam heating is increasingly screened out of the plasma center, but the increased nuclear heating in the center takes over. Also, the plasma center shifts with increasing $\bar{\beta}_T$.

Because of the decreasing beam line efficiency with increasing energy, it is found that a nearly constant extracted power is needed for ignition in the range studied. There is, thus, little economic difference in this energy range. However, the higher energies $\gtrsim$150 keV imply fewer injectors and perhaps lower impurity production rates during heating to ignition.

3.2.17 Resistive-Ballooning-Mode Equation[20]

R. G. Bateman, Jr. D. B. Nelson

A second order ordinary differential equation on each flux surface is derived for the high-mode-number limit of resistive MHD ballooning modes in tokamaks with arbitrary cross section, aspect ratio, and shear. The equation is structurally similar to that used

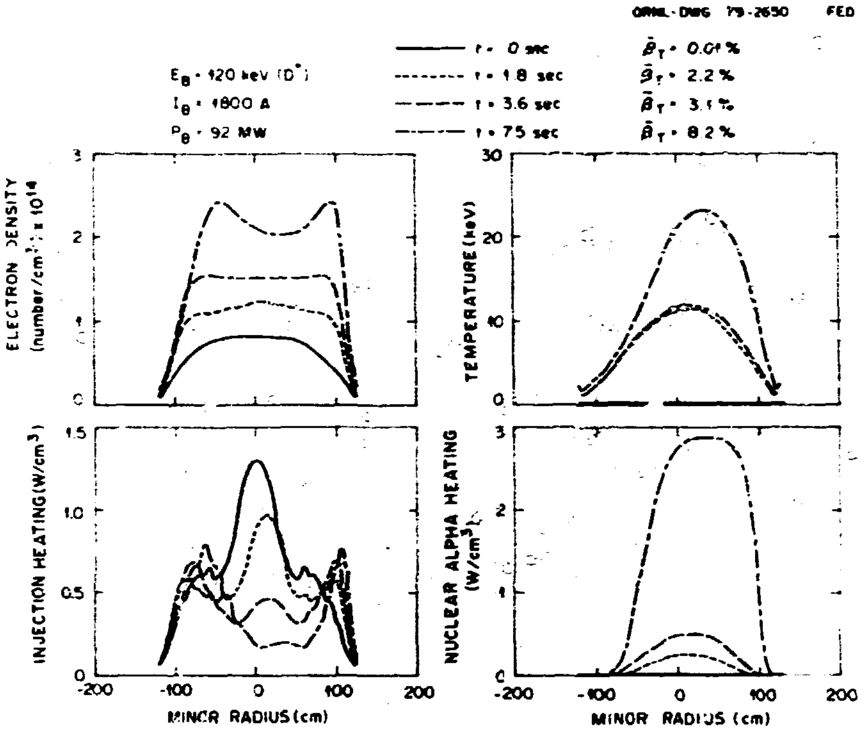

Fig. 3.5. Electron density, temperature, neutral beam heating, and alpha heating profiles are shown at several times for a 120-keV (D^+) run.

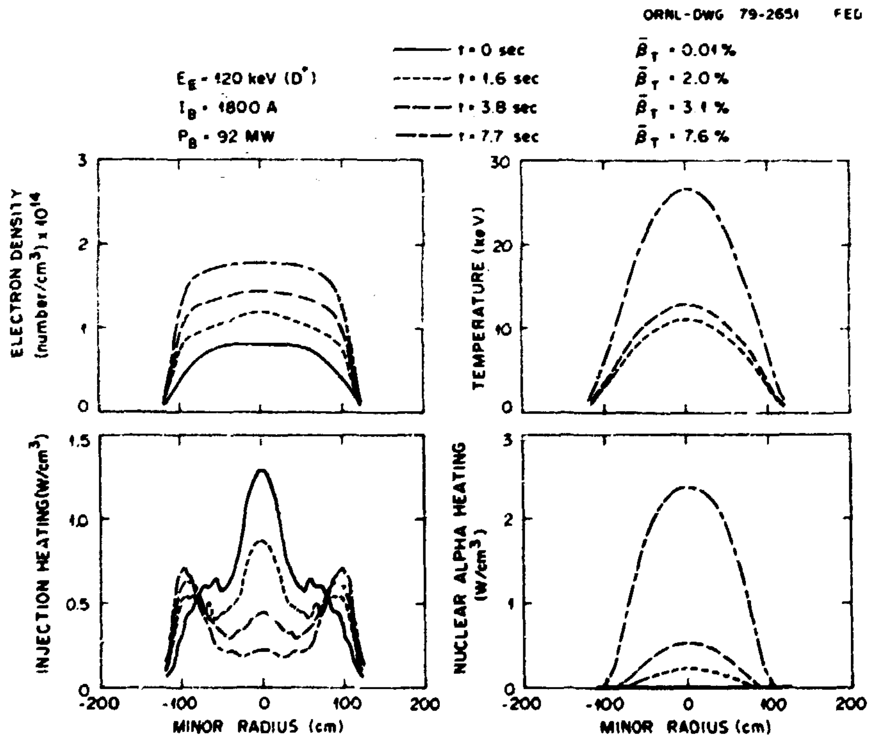

Fig. 3.6. This case is identical to that shown in Fig. 3.5 except that MHD equilibrium effects of the flux surface shifts and related compression were not included. The main difference in the results is seen in the overall magnitude and shape of the electron density profile.

to study ideal MHD ballooning modes computationally. The model used in this paper predicts linear instability in the high-mode-number limit, with growth rate proportional to resistivity when the pressure gradient is small compared with the critical value needed for ideal MHD stability.

3.2.18 Necessary Stability Criterion for Plasma Equilibria with Tensor Pressure[21]

D. B. Nelson G. O. Spies*
C. L. Hedrick, Jr.

A necessary stability criterion is derived that is valid within ideal MHD, one-fluid guiding center theory, and double-adiabatic theory. The equilibria considered are such that the magnetic field lines either are closed or intersect insulating end plates. Due to the inclusion of ballooning perturbations, the criterion is stronger than that for stability to line-preserving perturbations; unlike the latter, it is violated in the bulk of the plasma of EBT-like equilibria. This disagreement with observations suggests that kinetic effects must be included to explain the experiment.

3.2.19 Stability of Tokamaks with Elongated Cross Section[22]

C. H. An R. G. Bateman, Jr.

Fixed boundary $n = 1$ MHD instabilities are studied computationally as a function of diamagnetism (ε_{pol}) and current profile in elongated toroidal equilibria ($1 < b/a < 4$). It is found that even slightly diamagnetic plasmas with broad current profile and a highly elongated cross section are subject to a ballooning instability for q-values well above unity at the magnetic axis. A peaked current profile in a mildly diamagnetic plasma decreases the elongation of the inner flux surfaces and reduces the marginal q-value by suppressing ballooning modes. The maximum stable volume-averaged beta is achieved with a broad current profile and either a paramagnetic plasma (ε_{pol} [illegible] 1) with a highly elongated cross section ($b/a > 2$) or a diamagnetic plasma (ε_{pol} [illegible] 1) with only a mildly elongated cross section ($b/a < 2$).

3.3 KINETIC THEORY

C. O. Beasley, Jr.	H. K. Meier
J. D. Callen	J. A. Rome
P. J. Catto	D. J. Sigmar*
E. C. Crume, Jr.	J. Smith
J. Denavit	W. M. Stacey, Jr.
S. P. Hirshman	K. T. Tsang
L. M. Hively	G. Vahala
J. E. McCune	W. I. van Rij

J. C. Whitson

Kinetic Theory research will be broken down into the following categories: (1) anomalous transport (Sect. 3.3.1), (2) neoclassical transport and analytic finite beta equilibrium (Sect. 3.3.2), (3) energetic particle orbits and neutral beam injection (Sect. 3.3.3), and (4) numerical simulation of collisional transport and drift waves (Sect. 3.3.4). For each area a summary will be given, followed by short abstracts of individual work. Following are some overall highlights.

Foremost, there were major contributions to the linear and nonlinear theory of anomalous drift-like transport in tokamaks. Linearly, a new branch of finite beta shear Alfvén waves was discovered in sheared tokamak equilibria. Nonlinearly, the longstanding resonance broadening theory of drift waves was fundamentally extended to sheared magnetic fields and to include a self-consistent determination of the saturation amplitudes. Returning to linear theory, the low m and ℓ shear Alfvén radial eigenmodes in a tokamak reactor were shown to be strongly destabilized by a drift resonance due to the density gradient of the alpha particles, and a high frequency mode driven by the nonthermal velocity distribution of the alpha particles was found indicating anomalously rapid alpha slowing down.

---

*New York University

*Group Leader

3.3.1 Anomalous Transport

Besides the results just mentioned, there was systematic progress regarding the stability behavior of the drift Alfvén wave branch (at high-mode numbers). This area was reviewed at the American Physical Society (APS) meeting, and alpha particle dynamics were reviewed at the Gordon Conference. The more fundamental work on drift and drift shear Alfvén waves predominated over the previous emphasis on trapped-electron instabilities whose treatment, however, also advanced to include the 2-D eigenvalue problem. As an intermediate step between the historic resonance broadening theory in shearless geometry and the most recent self-consistent advance to sheared magnetic field geometry, a turbulence theory for the dissipative trapped electron instability appeared in *Physics of Fluids*.

Anomalous Alpha-Particle Transport in Thermonuclear Tokamak Plasma[23]

D. J. Sigmar H. C. Chan*

Because of the strong localization of the fusion-born alpha particles in velocity and configuration space and their coupling to Alfvén waves in the background plasma, the relaxation of alphas is anomalous. In a finite system, the enhanced electromagnetic fluctuations can produce rapid spatial losses of alpha population and energy. These losses prevent the alpha velocity distribution from attaining a stable collisional equilibrium, thus maintaining a steady-state turbulence level. A self-consistent numerical quasilinear calculation is performed for one of the most dominant low-frequency modes, showing the evolution of the alpha distribution and yielding the anomalous loss rates.

Adiabatic Modifications to Plasma Turbulence Theories[24]

P. J. Catto

Improved particle trajectories are employed to treat the adiabatic or Maxwell-Boltzmann response of a plasma in order to choose between contradictory prescriptions for obtaining the nonlinear dispersion relation from the linear one.

Turbulence Theory for the Dissipative Trapped Electron Instability[25]

K. T. Tsang J. D. Callen
G. Vahala

Drift orbit diffusion induced by turbulence acting on trapped electrons is shown to reduce and broaden the magnetic drift resonance and produce the dominant nonlinear saturation mechanism for the dissipative trapped electron instability. The fluctuation level obtained from such a theory is found to be consistent with present experimental observations.

Trapped Electron Instability in Tokamaks: Analytic Solution of the Two-Dimensional Eigenvalue Problem[26]

P. J. Catto K. T. Tsang

The 2-D eigenvalue equation for the trapped electron instability in tokamaks is solved analytically by both a perturbation technique and a more exact method of matched asymptotic expansions. The important physical effect is shown to be the radial localization of the trapped electron term caused by the difference between the pitch of the magnetic field and that of the mode. This localization results in a completely new form for the dispersion relation and does not impede magnetic shear stabilization. Coupling of neighboring rational surfaces is shown to result in an increase of only $\pi/2$ (at most) in the growth rate.

---

*Massachusetts Institute of Technology

Linearized Gyro-Kinetics[27]

P. J. Catto

Finite gyroradius effects are retained in a far simpler manner than previous treatments by transforming to the guiding center variables and gyroaveraging before introducing magnetic coordinates.

"Absolute Universal Instability" Is Not Universal[28]

K. T. Tsang	J. C. Whitson
P. J. Catto	J. Smith

The roots of an improved analytic eigenvalue equation for the absolute universal or collisionless drift instability in a sheared magnetic field are found numerically and compared with the eigenvalues obtained from a numerical solution of the exact differential equation. The startling result is that both techniques predict stability, no matter how weak the shear or how large the transverse wave number, in contradiction to all previous work. Stability is due primarily to the stabilizing influence of the nonresonant electrons.

Drift Alfvén Waves in Tokamaks[29]

K. T. Tsang	J. D. Callen
J. C. Whitson	P. J. Catto

J. Smith

A new branch of solutions of the finite beta, drift wave radial eigenmode equations has been found. The branch is heavily damped in the low beta regime and identified with the shear Alfvén wave. This branch and the usual electrostatic branch are damped in a collisionless plasma. Including trapped electron effects introduces an instability that is potentially harmful to plasma confinement.

Numerical Studies of Electromagnetic Drift Wave Stability in a Sheared Magnetic Field[30]

K. T. Tsang

For beta values of present-day tokamaks, $\beta > m_e/m_i$, the electrostatic approximation for drift waves begins to break down and finite beta effects become important. The radial eigenmode equations for electromagnetic drift waves in a sheared magnetic field consist of two coupled second order differential equations that, in the local approximation, depict the coupling between the drift wave and the shear Alfvén wave due to finite Larmor radius effects. In the nonlocal analytic calculation, only the drift eigenmode has been unambiguously recovered. We investigate this fourth order system numerically and discover two distinct eigenmode branches. One of them is the finite beta modified drift wave eigenmode that reduces to the electrostatic drift wave as beta decreases to zero. The other branch, whose eigenfrequency scales roughly like $\beta^{-1/2}$ for low beta, has no electrostatic limit. The drift branch is further stabilized by finite beta effects while the second branch, which we call the Alfvén branch, is destabilized by finite beta. In a collisionless plasma, both eigenmodes are absolutely stable. Including electron collisions by a number-conserving Krook collision term with energy-independent collision frequency, we find collisions have a stabilizing influence. Both modes can be destabilized by a parallel current, although the critical current is high. Inclusion of trapped electrons phenomenologically can also lead to instabilities. In these calculations we have retained the full ion plasma dispersion function. If the high phase velocity expansion $(\omega/k_{\parallel} v_i \gg 1)$ in the ion response is used, then a spurious unstable mode can be found. However, the eigenfrequency of this mode gradually goes to zero as we switch from the high phase velocity expansion to the ion Z function. For very small perpendicular wave number, eigenmodes with parity odd for the perturbed electrostatic potential and even for the perturbed radial magnetic field have infinite radial extent. When boundary conditions are changed to match the external MHD solution, kinetic tearing modes can be obtained. Only the shear Alfvén branch can be destabilized by a finite Δ'. We conclude from these studies that the shear Alfvén eigenmode is probably more relevant to present experiments than the drift wave eigenmode.

Numerical Study of Drift-Alfvén Waves in a Sheared Magnetic Field[31]

K. T. Tsang J. C. Whitson
J. Smith

In this study the coupled radial eigenmode equations for electromagnetic drift waves in a sheared magnetic field are solved numerically. In addition to the familiar drift eigenmodes, a different set of eigenmodes was found that is the analog of the sheared Alfvén waves of local theory in a sheared magnetic field. The drift mode is mainly electrostatic, and the shear Alfvén mode is mainly electromagnetic and closely related to the high order tearing modes.

Turbulent Destabilization and Saturation of the Universal Drift Mode in a Sheared Magnetic Field[32]

S. P. Hirshman K. Molvig*

In a sheared magnetic field, turbulent diffusion of electrons in the vicinity of a mode rational surface can eliminate the stabilizing influence of nonresonant electrons and lead to an absolute instability at small but finite wave amplitudes. As the turbulence grows, the inverse electron Landau resonance is broadened in both velocity and configuration space, and the convective shear damping due to ions is enhanced by turbulent spatial broadening of the mode until saturation occurs.

Anomalous Slowing Down of Alpha Particles in Toroidal Plasma[33]

K. Molvig D. J. Sigmar

A systematic search for alpha-driven high frequency instabilities with substantial anomalous transport consequences results in bands of modes in the frequency range $\omega_{ci} < \omega < \omega_{pi}$, with the fastest mode near ω_{pi} being mainly electrostatic. For the wave vector k such that $m = \ell = 0$, $k = k_r$, to lowest order, the lack of poloidal mode structure leads to spatial detuning of the destabilizing term and an essentially unmagnetized response function.

We calculate the linear growth rate and the alpha threshold density, solve the steady-state quasi-linear equations for $f_{1\alpha}$ and $D_{1\alpha}$, and determine the relaxation time of perpendicular alpha energy. (The resonance does not affect the parallel energy, to leading order.) This instability provides anomalous slowing down to near thermal energy at a rate much faster than collisional, as will be shown quantitatively.

Shear Alfvén Wave Destabilized by Alpha Particles in a Tokamak Reactor[34]

D. J. Sigmar S. P. Hirshman
J. C. Whitson

Recently, Tsang et al.[35] have demonstrated the existence of a shear Alfvén radial eigenmode in a sheared magnetic field geometry and found destabilization by trapped electrons. In a tokamak reactor this mode may be driven by the free energy of the alpha particle gradients[36] or by the positive slope of the thermonuclear alpha distribution.[37] In Ref. 36 a fourth order radial differential equation was derived and an approximate stability criterion inferred from a WKB condition (without obtaining the mode structure). We derive the integral equation for this mode from the gyrokinetic equation and investigate stability and mode structure for finite $\rho_t \partial/\partial r$. Differences between the integral and differential formulations are discussed.

---

*Massachusetts Institute of Technology

3.3.2 Neoclassical Transport and Analytic Finite Beta Equilibrium

Our longstanding effort in (1) the fundamental development of multispecies (impurity) transport, (2) its application to tokamaks, and (3) the numerical evaluation of (1) and (2) has led to a larger-than-average stream of publications in 1978. An extremely useful constitutive relation between the neoclassical parallel viscous force and the poloidal flow velocity, valid for all collisionality regimes and arbitrary tokamak equilibrium has enabled a complete fluid equation formulation of neoclassical theory. This in turn has facilitated the extension of this theory to include particle and momentum sources (a forthcoming need of our ISX-B program) following an earlier paper this year on the time evolution of the ambipolar potential in axisymmetric neoclassical plasmas. Numerically, our Collisional Plasma Model (CPM) code was used for precise studies of the transition from the plateau to the collisional regime. Numerous other important contributions are abstracted in this section.

Related to and necessary for collisional transport theory in this laboratory, orientation towards higher beta tokamaks has motivated us to analyze analytically as far as possible finite beta, noncircular cross-section MHD equilibria.

Equilibria of High Pressure Elliptic Flux-Conserving Tokamak[38]

T. Mizoguchi* T. Kammash*

D. J. Sigmar

An analytical calculation is carried out to determine the plasma current and poloidal beta for a toroidal plasma with an elliptic cross section under the constraint of flux conservation. It is shown that the pressure buildup during heating occurs in two stages: an outward shift in the magnetic axis and an elongation in the flux surfaces. The total plasma current increases with the pressure variable more rapidly for an elliptic cross section than it does for a circular cross section. This current rise produces a rather slow rise of the poloidal beta with pressure, particularly for large elongations. The ensuing class of flux-conserving equilibria is characterized by large beta but modest poloidal beta.

Analytic High β, Flux Conserving Equilibria for Cylindrical Tokamaks[39]

D. J. Sigmar G. Vahala

Using Grad's theory of generalized differential equations, the temporal evolution from low to high beta due to adiabatic and nonadiabatic (i.e., neutral beam injection) heating of a cylindrical tokamak plasma with circular cross section and peaked current profiles is calculated analytically. The influence of shaping the initial safety factor profile and the beam deposition profile and the effect of minor radius compression on the equilibrium are analyzed.

Fundamental Time Scales for Flux Conserving Tokamak Heating and Certain Global FCT Equilibrium Properties[40]

D. J. Sigmar

Because the existence of high beta, flux-conserving equilibria has been established, it becomes important to analyze the accessibility of these equilibria via auxiliary heating, to discuss the resistive decay of the safety factor profile, and to extend the virial theory to noncircular plasma cross sections.

---

*University of Michigan

Hot-Ion Distribution Function in ORMAK, the Oak Ridge Tokamak[41]

R. V. Neidigh*   D. J. Sigmar

A distortion of the Maxwellian ion-energy distribution function in tokamak-produced plasmas may be revealed in the spectral line radiation. We report experimental evidence that (1) a change in the value of Z_{eff}, (2) delayed gas injection, (3) neutral beam injection, and (4) liner-cleaning procedures can alter the profile of the Balmer-α (6563 Å) line of hydrogen. The distortion is analyzed in terms of an effective toroidal-drift velocity, ion-temperature relation.

Comments on the Effects of Gas Injection Upon Radial Particle Fluxes in the ISX-A Flow Reversal Experiment[42]

W. M. Stacey, Jr.   D. J. Sigmar

A recently formulated theory about the effects of sources upon particle transport in the collisional regime is applied to estimate the magnitude of effects that would be expected in the ISX-A flow reversal experiment.

The Response of a Tokamak Plasma to Particle and Momentum Sources[43]

W. M. Stacey, Jr.   D. J. Sigmar

The response of an axisymmetric toroidal tokamak plasma to first order particle and momentum sources is investigated. The momentum sources drive coupled poloidal and toroidal mass flows and electrostatic field evolution that relax to asymptotic values on a time scale that is characteristic of the dominant viscous or external drag mechanism. The asymptotic steady-state momentum balance provides the necessary condition to completely determine the particle fluxes and currents in the flux surfaces and, hence, to determine transport fluxes across flux surfaces. Transport fluxes are driven across flux surfaces both by interspecies collisional momentum exchange, the usual case, and by momentum exchange between the plasma and external sources and/or drags. A generalized Ohm's law is obtained and used to determine the manner in which particle and momentum sources can drive parallel currents and can alter the evolution of the q-profile. The theory is formulated for arbitrary plasma cross sections, beta, and collision regimes.

Collisionality Dependence of the Pfirsch-Schlüter Contribution to Neoclassical Diffusion[44]

S. P. Hirshman*   E. C. Crume, Jr.

The contribution to the neoclassical transport coefficients in an axisymmetric toroidal plasma that arises from the poloidal variation of the parallel friction forces is investigated in the transition between plateau and Pfirsch-Schlüter (PS) regimes. A coupled system of kinetic equations for the $\ell = 0, 1$ velocity harmonics of the distribution function is obtained. This system is solved using a generalized moment expansion whose closure is based on a mini-max variational procedure. Although the PS diffusion coefficients scale as $\alpha q^2 D_c$ in all collision frequency regimes, the magnitude of the numerical coefficient α undergoes a transition from a collisionless value[45] to a collisional value[46] when $\nu_s \nu_E \sim \omega_t^2$, i.e., $\epsilon^{3/2} \nu_* \sim (\nu_s/\nu_E)^{1/2} > 1$ (here, ν_s and ν_E are the momentum and energy exchange collision frequencies). In contrast to previous treatments utilizing a maximal variational principle[45] or a model collision operator,[47] the fluxes computed here are asymptotically equal to the exact collisional values.[46] The extremum principle[45] is found to overestimate the PS contribution. Comparing the total neoclassical flux (PS and anisotropy-driven portions) with Ref. 47, it is found that the model operator method underestimates the PS flux. Our results are fitted to simple formulas for numerical application.

---

*Experimental Confinement Section

*Research done at Princeton Plasma Physics Laboratory

Analytical High Beta Tokamak Equilibria[48]

H. K. Meier   D. J. Sigmar

In response to the experimental (e.g., ISX-B) and theoretical need for analytic, $\beta \lesssim a/R$, elongated, tight aspect ratio tokamak equilibria, we have investigated solutions to the Grad-Shafranov equation of the "inverse form," $R = \Sigma Rn(\psi) \cos n\theta$, $Z = \Sigma Zn(\psi) \sin n\theta$, where ψ is the poloidal flux variable and θ a suitable poloidal angle chosen to minimize the number of harmonics required. Given a Solov'ev solution $\psi(R,Z)$, it is possible to derive the inverse form purely analytically. For more general equilibria the Fourier amplitudes Rn and Zn can readily be determined numerically. The fundamental problem, namely to prescribe $p'(\psi)$, $FF'(\psi)$ and a boundary in order to determine the amplitudes Rn and Zn for high beta, leads to a highly nonlinear set of second order ordinary differential equations still under investigation.

Summary of Collisional Particle Fluxes in a Tokamak Plasma[49]

S. P. Hirshman

The neoclassical (long mean free path) and generalized PS contributions to the particle flux are summarized in a concise form readily amenable for comparison with experimental data.

3.3.3 Energetic Particle Orbits and Neutral Beam Injection

Influenced by our experimental program, the theoretical and computational needs for the description of injected ions and/or alpha particles are strongly increasing. We have advanced the pure theory via extensions of the higher order guiding center theory and the creation of a suitable constants-of-motion (COM) phase space and orbit description. Numerically, a Monte Carlo beam deposition code for arbitrary equilibria and a ripple bundle divertor code were brought on line; these are described in more detail as follows.

Effects of ripple coils on fast ions

J. A. Rome   J. F. Lyon*
R. H. Fowler

ISX-B will have two sources of strong external magnetic field ripple due to the bundle divertor coils and the ripple injector coils. The two bundle divertor coils are centered on the equatorial plane, and the two ripple injector coils are under the vacuum chamber. However, the two coil sets are similar in that each produces a large minimum in $|B|$ flanked on either side (toroidally) by a sharp maximum.

An undesirable effect of these coils is the loss of certain fast particles. This can be seen by the following argument. Because the ripple is localized, an ion orbit is the same as it is without the ripple; that is, the magnetic moment μ, energy ε, and toroidal canonical angular momentum P_ϕ are all conserved except near the ripple, where P_ϕ is no longer conserved. This change of P_ϕ is especially severe at banana tips, where $V_\parallel = 0$ and $P_\phi = -e\psi$. Thus, if the ripple causes the banana tips to occur early or late, the flux surface on which the tip occurs will change and P_ζ will change. This argument can be extended to show that the change of the maximum value of ψ along the orbit is given by

---

*Experimental Confinement Section

$$\Delta\psi_{max} \propto V(\delta B)^{1/2} .$$

Although this is a crude estimate, it agrees quite well with the behavior of calculated guiding center orbits if δB is not too large. Thus, orbits whose banana tips occur near the ripple can walk out of the machine, and there is, in effect, a new ripple-generated loss region. This loss region occurs when $\zeta(\equiv V_\parallel/V$ at $\psi = \psi_{max})$ is positive (≈ 0.2 for the divertor coils) in the COM (v, ζ, ψ_{max}) space.[50] This is unfortunate because the ordinary banana loss region[51] occurs when ζ is negative and is usually inaccessible for coinjected particles.

Accordingly, we estimated the loss of coinjected ions in ISX-B to the bundle divertor loss region by using the Fokker-Planck equation which included the effects of slowing down, pitch angle scattering, and charge exchange. To simplify the analysis we assumed that the loss region occurred at $\zeta = 0$. Figure 3.7 shows the integrated loss from the injection velocity downward for H^0 injected into a D^+ plasma in ISX-B with parameters of $T_e = 1.5$ keV, $Z_{eff} = 2$, and $\tau_s/\tau_{cx} = 0.5$. About 35% of the fast ion energy is lost to the ripple loss region. This amount will be significant but tolerable. If D^0 is injected into H^+, the loss is reduced to 26% because the pitch angle scattering parameter is proportional to m_i/m_b.

To see if bundle divertors are viable in a reactor due to possible ripple-induced alpha particle losses, we performed similar calculations for a prototypical reactor. Because the alpha particles primarily slow down without pitch angle scattering, the worst effect of the ripple is to cause those alpha particles born in the loss region to be lost. This effect amounts to 20-30% of the alpha energy.

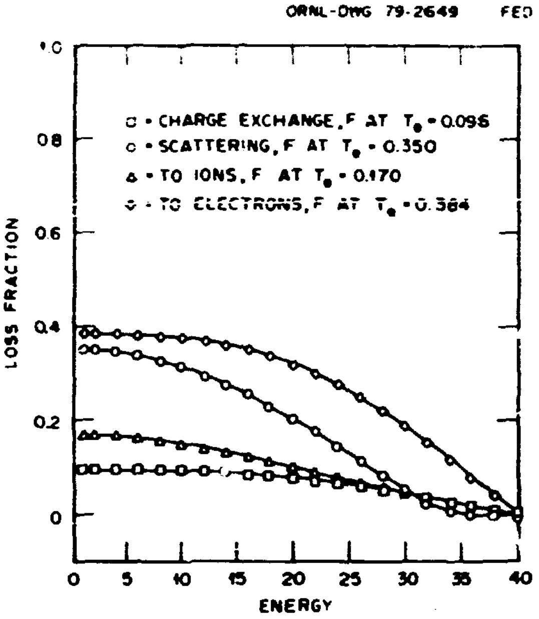

Fig. 3.7. Integrated energy loss. Parameters are: T_e(keV) = 1.50, Z_{eff} = 2.00, τ_s/τ_{cx} = 0.50, m_{beam} = 1.00, m_{ion} = 2.00, and ζ_c = 0.60.

Fokker-Planck calculations for energetic ions

L. M. Hively J. A. Rome

Fast ions have large banana-width guiding center orbits in noncircular tokamaks, causing the usual locally defined distribution functions to lose much of their usefulness. Accordingly, we are formulating the fast ion slowing-down problem in the 3-D COM space that characterizes axisymmetric tokamak orbits. Finding the fast ion distribution function in this space is equivalent to knowing all the bounce-averaged quantities for every particle in the machine.

In particular, we treat the alpha particle slowing-down problem by at first ignoring pitch-angle scattering and speed diffusion. This reduces the drift-kinetic equation to a first order, 3-D partial differential equation. Using multiple time scale analysis, bounce integrals average only the coefficients of the differential operators, and only particle flows on the slowing-down time scale remain. In contrast, bounce averages of the collision operator in local coordinates yield a 3-D integrodifferential equation that is intractable.

The slowing-down code at present determines the flux-surface-averaged alpha particle source rate $\dot{n}_\alpha(\psi)$ and the rate of increase of the net alpha current $\dot{I}_\alpha(\psi)$. This net current arises because some alpha birth orbits intersect the wall. We find the resulting alpha heating is peaked on axis but is somewhat lower and broader than the alpha birth distribution due to the large, banana-width orbits and losses to the wall. In a $\bar{\beta} = 0.8\%$ plasma, the total alpha current increase is $\sim 5\%$ of the plasma current in one slowing-down time. The effect of this current could be important in prolonged discharges because the associated momentum is continuously delivered to the plasma.

Extensions of Guiding Center Motion to Higher Order[52]

T. G. Northrop*   J. A. Rome

In a static magnetic field, some well-known guiding center equations maintain their form when extended to next order in gyroradius. In these cases it is only necessary to include the next order term in the magnetic moment series. The differential equation for guiding center motion that describes both the parallel and perpendicular velocities correctly through first order in gyroradius is given. The question of how to define the guiding center position through second order arises and is discussed, and second order drifts are derived for one usual definition. The toroidal canonical angular momentum P_ϕ of the guiding center in an axisymmetric field is shown to be conserved using the guiding center velocity correct through first order. When second order motion is included, P_ϕ is no longer a constant. The above extensions of guiding center theory help to resolve the different tokamak orbits obtained either by using the guiding center equations of motion or by using conservation of P_ϕ.

Fusion: Neutral Beam Technology[53]

J. A. Rome   W. A. Houlberg
Y-K. M. Peng

We strongly disagree with the statement by William D. Metz[54] that "it is generally acknowledged that the neutral beam technology used at Princeton (based on positive ions) cannot be extrapolated to a reactor-level plasma because the already modest efficiency plummets when the beam energy is raised." In fact, we believe it is likely that very high energy beams will not be needed for tokamak reactors. Early assessments[55] of neutral beam energy requirements indeed led to Metz's conclusion. However, these were typically made for circular, cross-section plasmas with neutral beams injected tangent to the inside edge of the plasma and with some combination of large plasma size, high density, or both. Conservative assumptions were also made about the required depth of penetration for the neutral beams. The resulting rules of thumb for injection requirements are not borne out in current conceptual designs for tokamak plasmas heated to ignition.

Because of increased understanding of tokamak plasmas, recent reassessments of beam energy requirements have led to a relaxation of some of the conservative assumptions. Smaller, elongated plasmas with nearly perpendicular injection will provide for a large decrease in beam energy requirements. These energy requirements are further reduced by low plasma density ($\bar{n}$) during the injection heating phase ($\bar{n} < 10^{14}$ ions per cubic centimeter), outward shift of the magnetic axis as the plasma pressure increases, heating of the core of the plasma by alpha particles produced in fusion reactions, and the possibility of expanding the plasma radius during the approach to ignition.

---

*Goddard Space Flight Center

These considerations have been incorporated into new assessments[56] of the required neutral beam energies for a noncircular tokamak reactor plasma with a minor radius of 1.25 m. Beam energies in the range of 100 to 150 keV (deuterium) are calculated to provide adequate penetration for heating to ignition. Lowering the beam energy requires increasing power input to the plasma, but the higher neutralization efficiency of lower energy positive ion beams leads to roughly constant power supply requirements over the range of energies considered (100 to 150 keV deuterium). Direct conversion of the unneutralized positive ion beams has already been demonstrated[57] and, when perfected, will make neutral beams based on positive ion sources an efficient heating mechanism.

If the presently estimated sizes for conceptual reactor plasmas prove to be correct, positive ion deuterium beams below 200 keV can be efficiently used to heat tokamaks to ignition, at least through the first demonstration reactor. The PLT results have certainly helped increase our confidence both in neutral beam heating and in scaling to reactor plasmas.

The Topology of Tokamak Orbits[58]

J. A. Rome Y-K. M. Peng

The topology of all contained tokamak guiding center orbits is displayed in a 3-D COM space. The treatment is perfectly general and holds for arbitrary axisymmetric MHD equilibria. We show that significant topological changes occur in the high beta ($\gtrsim 6\%$) cases that are associated with a region of absolute minimum B in the plasma.

The Topology of Tokamak Orbits[50]

J. A. Rome Y-K. M. Peng

Guiding center orbits in noncircular axisymmetric tokamak plasmas are studied in the COM space of (v, ζ, ψ_m). Here, v is the particle speed, ζ is the pitch angle with respect to the parallel equilibrium current $J_\parallel$, and ψ_m is the maximum value of the poloidal flux function (increasing from the magnetic axis) along the guiding center orbit. Two D-shaped equilibria in a flux-conserving tokamak having betas of 1.3% and 7.7% are used as examples. In this space each confined orbit corresponds to one and only one point, and different types of orbits (e.g., circulating, trapped, stagnation, and pinch orbits) are represented by separate regions or surfaces in the space. It is also shown that the existence of an absolute minimum B in the higher beta (7.7%) equilibrium results in a dramatically different orbit topology from that of the lower beta case. The differences indicate the confinement of additional high energy ($v \to c$, within the guiding center approximation) trapped, cocirculating, and countercirculating particles whose orbit ψ_m falls within the absolute B well.

The Topology of Large Banana-Width Tokamak Orbits[59]

J. A. Rome Y-K. M. Peng

To properly understand neutral injection or alpha particle heating in large banana-width systems, a detailed knowledge of guiding center orbits is required. Previous treatments of such orbit-related topics as beam deposition, loss regions, and wall loading have relied on large amounts of computational effort to account for the possible orbits, birth points in the plasma, pitch angles, and energies of interest. These approaches become increasingly more difficult when high beta, noncircular plasmas are involved. These problems can be systematically treated by proper categorization and description of the orbits.

In an axisymmetric tokamak, each guiding center orbit is completely described by a point in a 3-D COM space. In particular, we choose the speed (v), the maximum value of poloidal flux along the orbit (ψ_m), and the value of $v_\parallel/v$ at $\psi_m(\zeta)$. The various types of orbits (banana, circulating, stagnation, etc.) can be depicted by different regions and surfaces in this space. In this space each orbit is represented only once, and the loss regions are easily and fully represented. Beam deposition and the complete fast ion slowing-down problem may be more easily done in the COM space.

Some preliminary results of this detailed analysis are as follows: (1) for high enough energies, no particles are trapped, (2) particles with pitch angles of 90° are barely trapped, (3) particles can go from being "co" to being "counter" only by scattering through the orbit on which the points of the banana meet, and (4) all topological properties of the orbits depend only upon B(ψ), F(ψ), and their ψ derivatives on the equatorial plane.

The Role of Beam Induced Currents in High-β_T Experiments[60]

J. F. Lyon J. A. Rome
J. T. Hogan

The high power injection experiments planned for the Poloidal Divertor Experiment (PDX) and ISX-B may have strikingly different outcomes. While injection into PDX is planned to be predominantly perpendicular and balanced in direction, the ISX-B beams are parallel and unidirectional. Thus, with the beam currents in ISX-B (~40 A), beam-induced currents comparable with the plasma current (~200 kA) may be produced in contrast with PDX, where such currents should be minimal. Transport calculations predict such currents for ISX-B with $T_e(0) \sim 2\text{-}3$ keV, $\bar{n}_e \sim 2 \times 10^{13}$ cm^{-3}, and $Z_{eff} \sim 3$. MHD/transport calculations further show that these currents have a strong effect on the stability criteria both for ballooning modes and for nonlinearly saturated resistive tearing modes. In a typical 1.8-MW ISX-B case, beam-induced currents are responsible for a change of safety factor ratio $q_{boundary}/q_{axis}$ from 3.6 to 3.0 (for coinjection) and from 3.6 to 4.3 (for counterinjection). This shear variation in noncircular high β_T experiments can be enhanced with higher beam power and with H^0 and impurity injection techniques.

Effects of Finite Orbit Size on Interpretation of Charge-Exchange Flux in Non-Circular Tokamaks with Toroidal Field Ripple[61]

J. A. Rome R. H. Fowler
J. F. Lyon

At energies significantly above the thermal energy of the plasma, ions have large banana widths and may sample the plasma density and temperature on many different flux surfaces. To determine the localization of the measurements of the ion temperature and injected ion distribution function, a computer code follows the fast ions backwards in time from the point of charge exchange. For fast neutrals with velocity vectors in the equatorial plane, the ion orbits studied are more localized as the analyzer is moved closer to a direction perpendicular to $\vec{B}$. However, ripple due to the toroidal field coils causes trapping of the fast ions if the viewing angle is closer than 7° to the perpendicular in ISX. These calculations become even more important for analysis of ripple injection experiments.

FIFPC – A Fast Ion Fokker-Planck Code[62]

R. H. Fowler J. Smith
J. A. Rome

The distribution function of fast ions resulting from neutral beam injection into a tokamak plasma is calculated. The Fast Ion Fokker-Planck Code (FIFPC) also computes the momentum and power delivered to the electrons and ions in the background plasma, the power lost through charge exchange, the particle transport to the plasma, and other quantities of interest.

NFREYA — A Monte Carlo Beam Deposition Code for Non-Circular Tokamak Plasmas

R. H. Fowler   J. A. Rome

A computer code is described that calculates the initial fast ion deposition for neutral beam injection into noncircular tokamak plasmas. The beam deposition is calculated by Monte Carlo techniques as a function of the poloidal flux function. The flux function and plasma parameters are obtained from the numerical solution of the axisymmetric MHD equilibrium equation. Bounce averages are performed over the initial ion orbits, and the deposition is weighted by the fraction of time the ion spends in each interval of the ψ grid. The divergence, focusing, and shape of the neutral beam are modeled. The beam geometry part of this problem was solved by G. G. Lister, D. E. Post, and R. Goldston of the Princeton Plasma Physics Laboratory in a code called FREYA. The code described here is a modification of FREYA. Comparisons of the beam depositions calculated with bounce averaging are made with the ion birth depositions for the PDX and ISX-B tokamaks.

FLOC — Field Line and Orbit Code for the Study of Ripple Beam Injection into Tokamaks[64]

R. H. Fowler   D. K. Lee
P. W. Gaffney

The computer code described is used to study ripple beam injection into a tokamak plasma. The collisionless guiding center equations of motion are integrated to find the orbits of single particles in realistic magnetic fields for ripple injection. In order to determine if the ripple is detrimental to the plasma, the magnetic flux surfaces are constructed by integration of the field line equations. The numerical techniques are described, and use of the code is outlined. A program listing is provided, and the results of sample cases are presented.

3.3.4 Numerical Simulation of Collisional Transport and Drift Waves

C. O. Beasley   H. K. Meier
J. Denavit   K. E. Rothe
J. E. McCune   W. I. van Rij

Using the CPM,[65] studies of low frequency universal instabilities were done. However, a basic shortcoming of the modeling, i.e., the inability of the Laguerre spherical harmonic representation to properly model the Landau resonance in velocity space limited the studies to (1) stable modes, (2) unstable modes in which both electrons and ions were fluid-like, and (3) very high growth rate drift modes. In the last case, a finite Larmor radius (FLR) correction was added. In the course of these studies, a numerical check of the formulation of quasi-neutrality developed elsewhere[66] was done.

The handicap of not being able to include Landau damping properly led to a new computer model: TEDI (Time Evolution of Drift Instabilities). Codes using this model for studying the linear radial time evolution of drift modes are currently being developed.

Simulation of Stable Electrostatic Drift Modes in Cylindrical Geometry[67]

We use a nonlinear drift kinetic equation for a straight cylindrical plasma without collisions,

$$\frac{\partial f_s}{\partial t} + v_\parallel \frac{\partial f_s}{\partial z} + \vec{v}_E \cdot \nabla f_s + \frac{eZ_s}{m_s} E_\parallel \frac{\partial f_s}{\partial v_\parallel} = 0 \qquad \vec{v}_E = \frac{\vec{E} \times \vec{B}}{c} , \qquad (3.1)$$

and the statement of quasi-neutrality derived earlier,

$$E_{\parallel}^{(1)} = \frac{4\pi}{\omega_p^2}\frac{\partial}{\partial z}\, e \sum_s Z_s \int d^3v\, v_{\parallel} f_s \,, \tag{3.2}$$

within the electrostatic approximation

$$\vec{E} = -\nabla\phi \tag{3.3}$$

to find the solution of a stable drift wave, which was followed numerically using the CPM[65] code DKES. The plasma equilibrium taken was

$$f_{0_s} = \pi^{-3/2} N_{0_s}(r)\,\alpha_s^{-3}(r) \exp\left\{-\left[\frac{\vec{v} - \hat{z}v_s(r)}{\alpha_s(r)}\right]^2\right\}$$

$$\alpha_s(r) = \sqrt{\frac{2T_{0_s}(r)}{m_s}} \,. \tag{3.4}$$

The initial distribution function perturbation was taken as the fundamental mode solution of the dispersion relation resulting from linearizing Eq. (3.1) for ions and electrons. Parameters used were:

$$\frac{\omega}{\omega_*} = 1.00 \qquad \frac{\omega}{k_{\parallel}\alpha_e} = 0.213$$

$$\frac{\omega}{\omega_p} = \left(\frac{\omega}{\omega_{pe}}\right)\left(\frac{k}{k_{\parallel}}\right) = 3.33 \times 10^{-2}$$

$$\frac{V_e}{\alpha_e} = \frac{1}{\sqrt{2}} \times 10^{-5} \qquad \frac{V_i}{\alpha_i} = 0$$

$$T_e = T_i = 1\ \text{keV}$$

$$\frac{d}{dr}\ln N_0 = -0.08\ \text{cm}^{-1} \qquad \frac{d}{dr}\ln T_0 = 0$$

$$B_0 = 20\ \text{kG}$$

$$\frac{k_{\parallel}}{(\nu/r)} = 10^{-3}, \text{ where } (\nu/r) = k_y$$

The initial perturbation is proportional to ϕ; and, because it is an exact eigenmode of a drift wave, would not exhibit the high frequency effective plasma oscillation. However, the first harmonic ($\ell = 2$) does naturally appear with this plasma oscillation if one used Poisson's equation to calculate the electric field [see Fig. 3.8(b)].

By adding a 10% admixture of plasma oscillation to the fundamental [see Fig. 3.8(a)] and then using the quasi-neutral formalism, we are able to reproduce correctly the low frequency parts of the spectrum while filtering the modified plasma oscillations in both the fundamental [Fig. 3.8(c)] and the first harmonic [Fig. 3.8(d)].

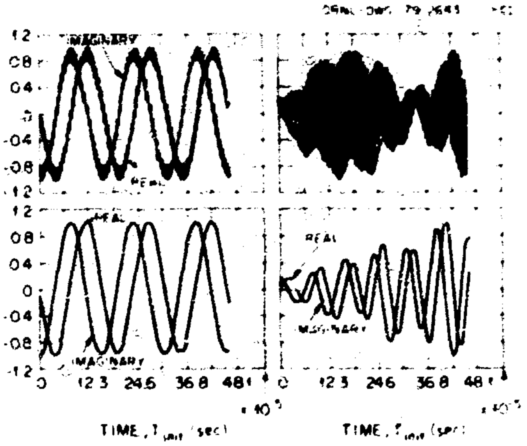

Fig. 3.8. Electric field (ϕ component) of a stable drift wave and its first harmonic as calculated by the CPM code DKES using Poisson's equation and quasi-neutrality.

These calculations show that (1) the CPM is able to correctly model a local stable drift wave and (2) the quasi-neutral formalism[64] does correctly permit the calculation of low frequency behavior independent of the presence of a high frequency plasma oscillation.

Simulation of an unstable quasi-drift mode using the CPM

For either unstable or damped modes, difficulty in properly representing the

Landau resonance by the CPM restricted studies to either very high growth rate modes (where the resonances are broadened) or to cases in which the resonances occurred on the tail of the distribution (i.e., the species was "cold"). This latter case corresponds to a study of the local behavior of a drift mode very close to a mode rational surface. This is seen in Fig. 3.9, where we show the local ($k_r = 0$) solution to a drift mode at fixed density with shear in the vicinity of a $k_\parallel = 0$ surface. (The case shown has $k_y \rho_i \neq 0$, but the behavior is the same for the 0 Larmor radius case.) Although $\omega < \omega_*$ for the case shown, which has a density gradient but no temperature gradient, we can also find cases in which $\omega > \omega_*$ when we have both a temperature gradient and an electron current. It is such a case that we study.

The drift kinetic equation is identical to Eq. (3.1) in the previous section. The parameters are as follows:

$$\frac{V_e}{v_e} = \frac{1}{\sqrt{2}} \times 10^{-} \qquad \frac{V_i}{v_i} = 0$$

$$T_e = T_i = 1 \text{ keV}$$

$$\frac{d \ln N_o}{dr} = \frac{d \ln T_o}{dr} = -0.5299 \text{ cm}^{-1}$$

$$B_o = 20 \text{ kG} \qquad N_o = 10^{9} \text{ cm}^{-3}$$

$$\frac{k_\parallel}{(\ell/r)} = 10^{-3} .$$

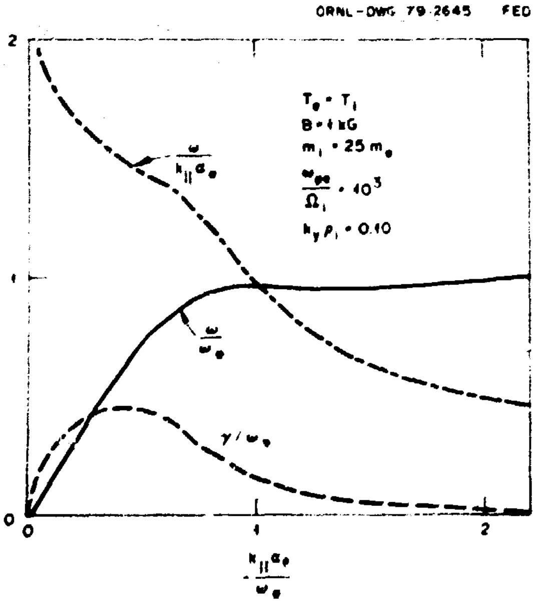

Fig. 3.9. Frequency, growth rate, and phase velocity of a local drift mode near a mode rational surface.

The fundamental is an unstable mode with low growth rate; the harmonics have higher growth rates:

	$\omega/k_\parallel v_e$	ω/ω_*	ω/ω_{pe}	γ/ω_r
Fundamental	4.46	3.16	0.695	0.033
1st harmonic	2.54	1.80	0.688	0.580
2nd harmonic	1.87	1.32	0.759	0.673
3rd harmonic	1.51	1.07	0.819	0.682

As seen from $\omega/\omega_{pe} \sim 1$, Poisson's equation must be used to determine ϕ rather than assuming quasi-neutrality.

In the time evolution of the fundamental and first two harmonics shown in Fig. 3.10, the frequencies and growth rates are very close to prediction. The harmonics are nonlinearly excited, and the first harmonic eventually grows to dominate the electric field.

Due to a combination of (1) the difficulty in representing the Landau resonance and (2) a gross distortion of the distribution from a Maxwellian resulting from the lack of

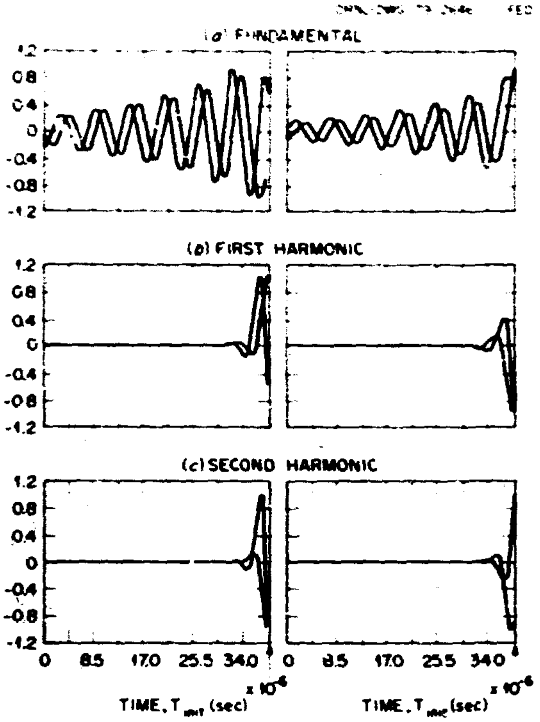

Fig. 3.10. The Fourier components of ϕ for an unstable drift mode.

a damping mechanism, the results well into the nonlinear regime are of limited value. However, we show a comparison of the electric distribution function at $t = 0$ (with the pure perturbation in the fundamental) and at onset of nonlinearity of the fundamental mode and its harmonics in Fig. 3.11. Figures 3.11(a) and 3.11(d) represent the $\mu = 0$ (spatially homogeneous) $\bar{f}_s$, showing in 3.11(a) the streaming electrons at $t = 0$, and in 3.11(d) the change in that distribution due to nonlinear effects. Similarly, 3.11(b), (c), (e), and (f) show these perturbations for the $\mu = 1$ component at $\theta = 0$ and $\theta = 180°$ at the two times. Finally, 3.11(g), (h), and (i) show the $\mu = 2$ and $\mu = 3$ components at the final time (at $t = 0$ these were 0). Note the scale factors at $t = 3.8 \times 10^{-5}$ sec; the first harmonic is the largest mode, but still $e\phi/T < 2\%$.

In summary, we have demonstrated that the CPM can calculate a nonlinear drift kinetic time evolution of a set of unstable waves locally, provided Landau damping is not too important. The limitations of lack of finite Larmor radius are dealt with elsewhere, but limitations to a local treatment and avoidance of cases with strong Landau damping present major obstacles to practical use of the CPM in studying interesting instabilities.

Inclusion of finite Larmor radius effects in the CPM

We note here a formalism that permits the addition of finite Larmor radius (FLR) effects to the CPM without a rewriting of the code to include a complete gyrokinetic equation. However, these FLR effects are presently only in the linear sense.

We begin by noting the similarity between the nonadiabatic part of the linear drift kinetic distribution function perturbation,

$$h_{DK} = \frac{e\phi}{T}\left(\frac{\omega + \omega_*}{\omega + k_\parallel v_\parallel}\right) f_0 , \qquad (3.5)$$

and the corresponding part of the distribution function, which is a solution of the Vlasov equation,

$$h = \frac{e\phi}{T} \sum_{m,n=-\infty}^{\infty} J_m\left(\frac{k_\perp v_\perp}{\Omega}\right) J_n\left(\frac{k_\perp v_\perp}{\Omega}\right)$$

$$\times \frac{\omega + \omega_*}{\omega + k_\parallel v_\parallel - n\Omega} e^{i(m-n)(\beta-\alpha)} f_0 . \qquad (3.6)$$

If we take the low frequency ($\omega \ll \Omega$) limit of Eq. (3.6) and average over gyroangle β,

$$\bar{h} = \frac{e\phi}{T} J_0^2\left(\frac{k_\perp v_\perp}{\Omega}\right) \frac{\omega + \omega_*}{\omega + k_\parallel v_\parallel} f_0 , \qquad (3.7)$$

and if we make the ansatz that the FLR correction to h_{DK} from Eq. (3.5) may be written

$$h' = h_{DK} e^{-b} I_0(b) , \qquad (3.8)$$

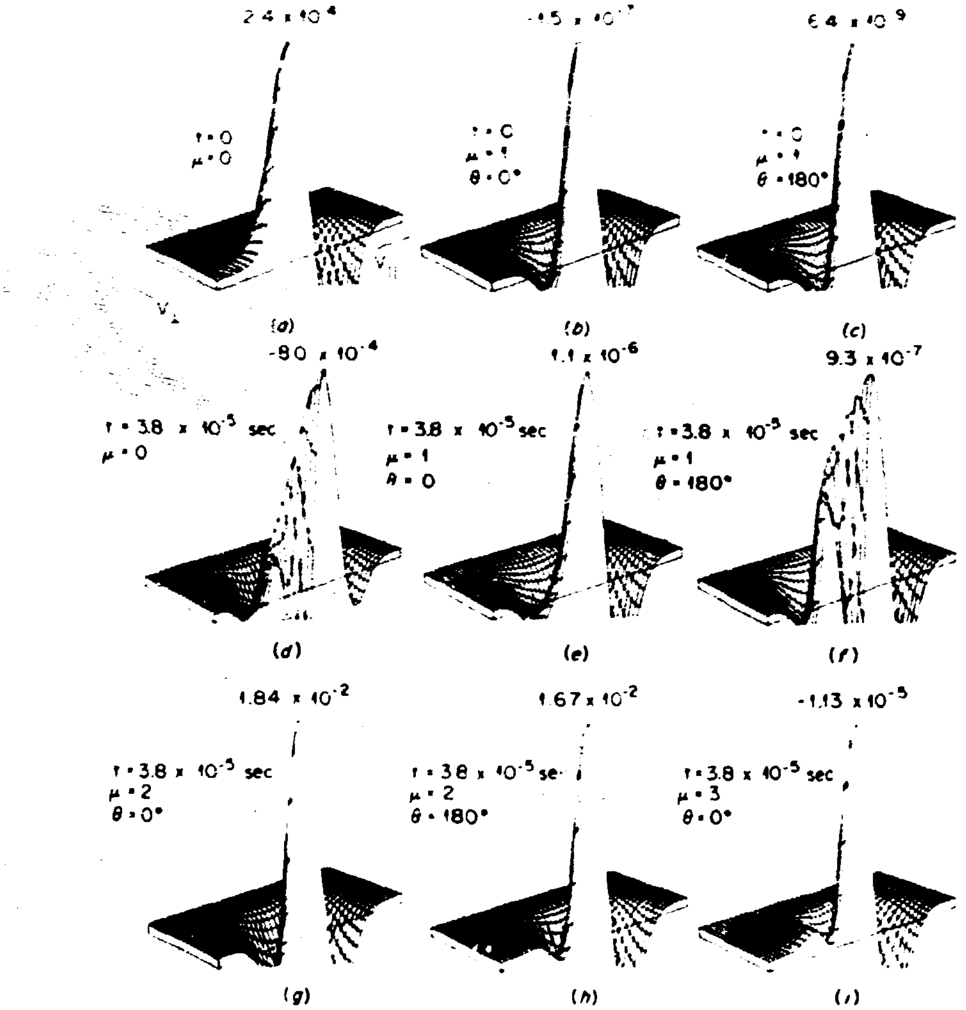

Fig. 3.11. Perturbation of $f(v_\parallel, v_\perp)$ from a Maxwellian at $t = 0$ and onset of nonlinearity.

where

$$b = \frac{k_\perp^2 \alpha^2}{2\Omega^2} ,$$

then we note that

$$\int_0^\infty v_\perp \, dv_\perp \bar{h}' = \int_0^\infty v_\perp \, dv_\perp \bar{h} \qquad (3.9)$$

or that we obtain the same density and parallel current perturbations using Eq. (3.8) as we do from Eq. (3.7). It was noted that the same ansatz [Eq. (3.8)] is not valid for calculating $J_\perp$, the perpendicular current.

Using Eq. (3.8), we may then write the drift kinetic distribution function with FLR effects

$$\bar{f}' = \left(\bar{f} + \frac{e\phi}{T} f_0\right) e^{-b} I_0(b) - \frac{e\phi}{T} f_0 \qquad (3.10)$$

and

$$\frac{\partial \bar{f}'}{\partial t} = \frac{\partial \bar{f}}{\partial t} e^{-b} I_0(b) - \frac{ef_0}{T} \left[1 - e^{-b} I_0(b)\right] \frac{\partial \phi}{\partial t} . \qquad (3.11)$$

using Poisson's equation to write [illegible] and integrating Eq. (3.11) to form [illegible], we find

$$\text{[illegible]}\, e^{-b} I_0(b) - \frac{\text{[illegible]}}{\text{[illegible]}} [1 - e^{-b} I_0(b)]$$

$$\times \left\{ \frac{\frac{n^i}{\text{[illegible]}} e^{-b} I_0(b) - \frac{n^e}{\text{[illegible]}}}{1 + \frac{\text{[illegible]} n_0 e}{\text{[illegible]}} [1 - e^{-b} I_0(b)]} \right\} . \qquad (3.12)$$

Thus, we can follow the drift kinetic distribution in time, including linear FLR effects from a knowledge of b and $k^2 = k_x^2 + k_y^2$ and the drift kinetic $\bar{f}$.

This model was checked numerically by following the time evolution of a high growth rate drift mode with the following parameters:

$k\rho_e = 0.63$ $\qquad$ $\omega_* = 0.315$

$T_e = 1$ keV $\qquad$ $T_i = 0.1$ keV

$B_0 = 51.7$ G $\qquad$ $b = 0.05$

$k\lambda_{De} = 0.1866$ $\qquad$ $\frac{k_\parallel}{k_\perp} = 0.0125$

$\frac{d \ln N_0}{dr} = -0.024$ $\qquad$ [illegible] $= 0.75$

In Fig. 3.12, we factor out the linear growth rate; in this case a pure oscillation should ensue. Although not readily apparent, small discrepancies exist; these may be attributed to difficulties of the CPM representation in handling the Landau resonance.

In summary, we have shown that we can include linear FLR effects in the nonlinear CPM.

TEDI: A numerical model for studying the time evolution of drift instabilities

We have begun work on a new model to study drift instabilities, including their radial eigenmode structure in sheared magnetic fields. Eventually the code should be able to provide a time evolution picture of a nonlinear, finite beta drift mode in a toroidal system (i.e., including trapped particle effects). However, our first calculation will be simpler, using slab geometry and following the linear time evolution of a low beta plasma (i.e., retaining the electrostatic approximation). We solve the appropriate drift or gyrokinetic equation on a grid in velocity space. The appropriate v-integral (to obtain the density or current) then trivially yields the correct Landau damping. This has already been verified in an earlier calculation.

Studies of nonlocal drift waves are not new. However, in studies to date, no simulation of the distribution function has been attempted; normally an eigenvalue problem is posed, with velocity integrals having been done analytically. Using a distribution function permits the analytically difficult trapping problems to be handled trivially. It also permits a maximum amount of information with a minimum number of approximations. Hence, this work may be labeled a simulation effort rather than a numerical solution to an analytically posed problem.

There are two options with regards to treating the linear problem. One approach, the eigenvalue approach, will be used by

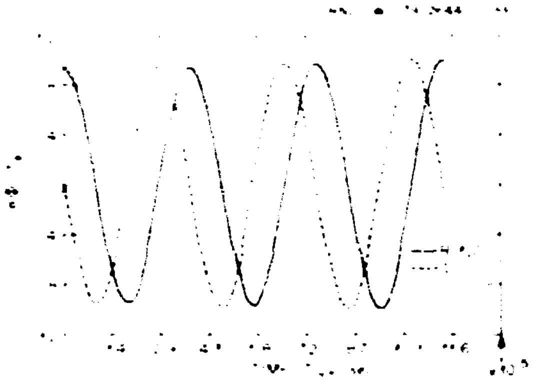

Fig. 3.12. Time evolution of a linear mode scaled by $e^{-\gamma t}$.

Denavit and Crystal at Northwestern, using shooting codes developed at ORNL and made available in a cooperative effort. The second, a time evolution problem, is the one pursued at ORNL. The former will probably be quicker and will be useful in large parameter scans of the properties of the time asymptotic state. On the other hand, the second method is useful in providing information of the time evolution and radial propagation properties of the unstable drift waves and assures one as well that the maximum growing mode will always be found.

The initial model is based on the $v_\perp$-integral of Catto's linear gyrokinetic equation for the nonadiabatic part of the distribution function for ions,

$$\frac{\partial g^i}{\partial t} + i\gamma k_y v_\parallel g^i = -i\,\frac{ZeF_m^i}{T_i}\,\Gamma_0\left\{\left[1+\left(1-\frac{I_1}{I_0}\right)\right.\right.$$

$$\left.\times\,\frac{\eta_i}{1+\eta_i}\right]\left[\omega_{*i} + i\,\frac{\partial}{\partial t} + \eta\omega_{*}\left(\frac{v^2}{\alpha_i^2}-\frac{3}{2}\right)\right]\phi(x,t)$$

$$-\,i\,\frac{ZeF_m^i}{T_i}\,\omega_{*i}\,\Gamma_0\left\{1-b+b\,\frac{I_1}{I_0}\right.$$

$$\left.+\left[1-b+\left(b-\frac{1}{2}\right)\frac{I_1}{I_0}\right]\eta_i\right\}\rho_i^2\,\frac{\partial^2}{\partial x^2}\,\phi(x,t)\ ,$$

(3.13)

and on the drift kinetic equation for electrons,

$$\frac{\partial g^e}{\partial t} + i\gamma k_y v_\parallel g^e = i\,\frac{eF_m^e}{T_e}\left\{\omega_{*e} + i\,\frac{\partial}{\partial t}\right.$$

$$\left. +\ \eta\omega_{*}\left(\frac{v_\parallel^2}{\alpha_e^2}-\frac{1}{2}\right)\right\}\phi(x,t)\ , \qquad (3.14)$$

where $\gamma = x/L_s$, L_s is the shear length, $\Gamma_0 = I_0(b_y)$, I_1 = modified Bessel function, $b = k_y\alpha/\Omega$, and $\alpha = \sqrt{2T/m}$. By integrating Eq. (3.13) and Eq. (3.14) over $v_\parallel$, one may obtain n_i and n_e, which may be coupled by quasi-neutrality (for $k_\perp$ large enough) or Poisson's equation (for $k_\perp \to 0$).

Proper boundary conditions must be included in order to prevent nonphysical end effect phenomena such as reflection. Because we are concerned with modes in the region of a mode rational surface (where $k_\parallel = 0$), we may impose symmetry conditions at this point ($x = 0$). For large x we have a choice of methods of applying boundary conditions. These are currently being tested.

In summary, we have developed a model for studying the time evolution of nonlocal drift waves. The model is extendable in a straightforward manner to include toroidal trapping, finite beta, and nonlinear effects. We are currently testing the model.

Precision Calculation of Neoclassical Electron Transport Coefficients Using the CFM

W. I. van Rij E. C. Crume, Jr.
W. F. Rothe

The potential precision of the DKES computer program that implements the CFM[65] is great enough that DKES results could be used as standards of comparison for analytic treatments of neoclassical transport problems. To gain confidence in such comparisons, DKES results require calibration against known analytic results. We have calculated electron particle and heat transport coefficients in an electron-ion plasma over the whole range of electron collisionality and compared them with more recent analytic results[70,44] than were used in an earlier comparison.[71] Generally, we find agreement to within ~10%. However, we find larger discrepancies when we compare DKES-calculated fluxes with fluxes calculated using the analytically defined transport coefficients when those fluxes depend on differences between these coefficients.

3.4 TRANSPORT SIMULATION

T. Amano J. T. Hogan*
D. E. Arnurius H. C. Howe
E. C. Crume, Jr. M. Soler

Tokamak transport modeling has seen a long-standing model for ion confinement convincingly affirmed in recent high power neutral beam heating experiments. This success, however, reemphasizes that the central problems opposing the operation of a clean, high beta tokamak for economically useful pulse lengths are that the scaling of transport losses in the high pressure regime is unknown at present, that plasma-wall interaction physics is in a primitive state of understanding, and that even the fundamental predictions of neoclassical theory for the movement (and eventual accumulation) of impurities are uncertain because of the computational complexity of this multispecies problem.

In order to prepare the way for an understanding of high pressure transport scaling, an improvement has been sought in our models for such low pressure phenomena as sawtooth instabilities, saturated resistive tearing modes, and relaxation due to nonmonotone current density profiles. With criteria developed by Waddell, Carreras, Hicks, and coworkers, we have been able to obtain agreement between transport models and basic experimental trends due to these processes, so they should not confuse our interpretation of high beta scaling changes.[72] Work on incorporating stability criteria for high beta directly into the 1 1/2-D transport code has been completed (see Sect. 3.4.9).

Ion confinement has been studied in detail in conjunction with ISX-A experimental work. The neoclassical model has been shown to be valid within a factor of 2 for these moderate collisionality experiments.[73] ISX-A has also provided meaningful tests of impurity rate and transport theory. Comparative modeling of the injection of tungsten into ISX-A and argon into the T-4 device at the Kurchatov Institute in Moscow has provided a useful test of neoclassical impurity ion theory.[74-76] The (now absent) charge exchange data for hydrogen-impurity interactions at low energy have been shown to be critical both for detailed spectroscopic studies and for estimating impurity sputtering rates (see Sect. 3.4.2). The impurity flow reversal experiment on ISX-A has been studied in detail with codes developed earlier.[77] Pellet fueling of contemporary experiments has been modeled in detail both to assess pellet ablation models and to study the plasma particle balance.[78]

With the role of stability clarified by future high pressure injection experiments, the identification of the specific mechanism for impurity production at high power loading will become critical. With a valid high pressure energy loss model and improvements in our particle and impurity transport models, this question should be answered by long pulse neutral injection experiments.

3.4.1 Simulation of Multispecies Impurity Transport in Tokamaks[79]

T. Amano E. C. Crume, Jr.

To simulate multispecies impurity transport in tokamaks, a set of coupled continuity equations including source and sink terms from atomic processes (rate terms) was solved numerically. The diffusion and rate terms are integrated separately in time using a fractional step-splitting technique that is accurate to second order in the time step. The rate terms are integrated using an eigenvalue method that allows such a large time step that diffusion constrains the step size. For the diffusion coefficients, approximate forms of the PS coefficients calculated by Hirshman were generally used (to save computer time), but the exact forms were used for certain comparisons. Anomalous diffusion was treated using a pseudoclassical diffusion coefficient. Calculations were performed treating individually all the ionization stages of oxygen and iron impurities in a hydrogen plasma. Calculated O VI and O VII relative density profiles agree qualitatively with profiles measured in the Adiabatic Toroidal Compressor (ATC) tokamak when purely neoclassical diffusion coefficients are used. Because the calculated profiles are also very sensitive to the magnitude of the neutral oxygen influx and atomic process rate coefficients, it is difficult to separate the diffusion and the atomic physics problems. The calculated Fe XV relative density profile is much less sensitive to the neutral iron influx although it also is sensitive to the rate coefficients. A model in which pseudoclassical diffusion coexists with neoclassical gives nearly as good agreement with experiment as one with only neoclassical. Better resolution of this problem requires coordinated measurements of absolute intensities of impurity spectra and radial profiles, along with other plasma parameters such as the electron density and temperature profiles and the ion temperature profile. Additionally, measurements of impurity source parameters such as the neutral energy or energy distribution are needed.

---

*Group Leader

3.4.2 Charge-Transfer Excitation of Impurity Ions in Tokamaks[80]

R. C. Isler* E. C. Crume, Jr.

Detailed studies of spectra from the ISX-A tokamak at ORNL have shown that certain oxygen-ion lines appear too anomalously intense to have been excited solely by electron collisions. These results are interpreted as being due to charge transfer and suggest the necessity of incorporating this mechanism into analyses of tokamak plasmas.

3.4.3 Impurity Behavior during Neutral Beam Injection and Gas Puffing into ORMAK[81]

R. C. Isler E. C. Crume, Jr.
H. C. Howe

Variations of the intensities of spectral lines are utilized to determine the extent to which the impurity concentrations of ORMAK-produced plasmas are altered by neutral beam injection and, in some cases, by the simultaneous introduction of a puff of hydrogen. Concurrent variations of oxygen emissions resulting from alterations in the profiles of electron temperatures and concentrations are taken into account through solving the coupled continuity equations of the several ionic species of this element. Ad hoc transport velocities are utilized, and a complete recycling model is assumed.

3.4.4 Numerical Modeling of Impurity Effects[82]

J. T. Hogan A. T. Mense

Atomic collisions – H^0 with multicharged ions

The presence of iron, molybdenum, tungsten, oxygen, and/or titanium in tokamak experiments has led to well-documented effects on the overall energy balance. There are two areas in which modeling can suggest the need for additional data.

Neutral injection. A possible beam deposition instability, caused by the trapping of injected neutral beams by impurity ions of charge Z, was proposed earlier. Detailed calculations, to be presented elsewhere, show that with the scaling of the total electron loss cross section that is now understood (Z^α, $\alpha \leq 1.4$), the beam deposition instability is not a factor in the performance of devices such as the Tokamak Fusion Test Reactor (TFTR) with minor radius $\lesssim$1 m and injection energy $\lesssim$60 keV/AMU. Larger devices with higher injection energy and longer pulse length may still be affected, pending further atomic physics information.

---

*Experimental Confinement Section

Recycling. The electron loss cross section for the interaction of neutral atoms and multicharged ions at lower (1 eV < E < 2 keV) energy is unknown and may affect the interpretation of two issues in present confinement experiments.

(1) Confinement scaling: Ion confinement scaling is described either by the "extended plateau" or the neoclassical plateau-banana model. The interpretation depends, in some cases, on estimates of the $T_i(r)$ profile, which is inferred, in turn, from a model for the radial profile of neutral density.

(2) Gas puffing: Injection of low energy (∿5 eV) neutrals is used to fuel present tokamak devices. A significant amount of oxygen can enter with this gas even though the resulting $Z_{eff} \sim 1.3$. The electron loss reaction provides a new ionization loss for electrons and a mechanism for depressing the charge state of oxygen. This reaction may, thus, play a role in resolving the present anomaly concerning the fast relaxation of $n_e(r)$ to a monotonic shape.

Compression and heavy metals

The radiative power loss from heavy metals has been estimated recently, and the power density scales as $n_e n_z f(T_e)$, where n_z is the impurity density. A promising technique for enhancing neutron output is to compress the plasma in major radius. All densities scale as C^2 before and after this compression ($C \equiv R_{initial}/R_{final}$; R = major radius). Thus, the power density increases as C^4. Calculations with a self-consistent compression model (1-D transport coupled with a 2-D MHD code) disclose significant differences from the usual instantaneous compression model in this case in that compression actually decreases the neutron output if heavy metal impurities such as tungsten are present.

Divertor calculations

Radial (1-D) modeling of the PDX and ASDEX tokamaks using a self-consistent particle and energy loss model for the divertor zone shows that fueling by gas puffing may be feasible. For ohmically heated discharges with average densities in the range 3–8 × 10^{13}/cm^3, calculations have been made for an assumed separatrix-wall spacing of 5 cm. Under a variety of assumptions about transport coefficients, the resulting shielding efficiencies are 40-75% for 20-eV iron atoms. Fueling rates of 10^{22} atoms/sec are needed to sustain the plasma enclosed by the separatrix.

3.4.5 MHD/Transport Interactions in Tokamaks[e3]

J. T. Hogan B. Carreras
W. A. Houlberg

Tokamak transport simulation codes are intended to model the evolution of a discharge on a "diffusive" time scale. However, the usual theoretical separation into diffusive and Alfvén time scales, with fast motions ignored in the former, breaks down when resistive MHD instabilities play a role in the energy balance or when fast time scale instabilities saturate at a finite amplitude. Models that describe the intermediate time scale evolution are inherently 3-D and are computationally expensive. Although they are essential for a description of the stability problem, the transport calculation requires a faithful approximation that can be checked against the 3-D model but that provides a time- and flux-surface-averaged description of the enhanced transport across axisymmetric flux surfaces (1-D).

We have developed such models for three different MHD/transport problems: (1) the finite amplitude saturated helical modes m = 2 → 6, and n = 1, 2; (2) the internal minidisruption (sawtooth); and (3) the ballooning instability due to high beta tokamak operation. Each of these cases requires a study of the fast time scale behavior to determine the appropriate time-averaged result for the fast process and a prescription for incorporating this effect in the usual diffusive transport model.

3.4.6 On Measuring the Electron Heat Diffusion Coefficient in a Tokamak from Sawtooth Oscillation Observations[84]

M. Soler J. D. Callen

A number of new methods are discussed for determining the electron heat conduction coefficient χ_e in a tokamak from the experimental observation of the space-time evolution of the temperature perturbations induced by internal disruptions. In ORMAK the various average values of χ_e and the radial dependence of χ_e are found to be consistent with and more precise than the $\chi_e(r)$ determined by conventionally analyzing the electron power balance equation. The net result of these measurements is to prove conclusively that the dominant radial electron heat transport mechanism in tokamaks is a microscopic, diffusive process.

3.4.7 Heat Transport in Tokamaks as Observed from Sawtooth Oscillation Characteristics[85]

M. Soler J. D. Callen

We illustrate recently derived methods[86] (also see Sect. 3.4.6) of measuring heat transport by analyzing some high density ALCATOR discharges. The analysis is shown to provide very accurate results for $\chi(r) = 1/2[\chi_e(r) + \chi_i(r)]$. The importance is stressed of τ_{ie}, the electron-ion temperature equilibration time in deciding which is the effective (electron or ion) transport mechanism. Examples are shown where transport is dominated by electrons, by ions, and initially by electrons and then by ions. A survey is presented of heat transport in tokamaks using these methods.

3.4.8 Analysis of Heat Transport in ALCATOR from Sawtooth Observations[87]

M. Soler R. Granetz[*]
J. D. Callen F. Sequin[†]
A. P. Navarro R. Petrasso[†]

Heat transport coefficients χ_e and χ_i at very high density ($2.5 \times 10^{14} \leq \bar{n} \leq 7.4 \times 10^{14}$ cm^{-3}) ALCATOR regimes are determined from soft x-ray observations of $m = 1$ sawtooth disruptions. At $r = 0$ a simple analytic model is proposed for the coupled electron and ion transport. The model assumes flattening of both T_e and T_i temperatures at disruption, as recently reported in ALCATOR,[88] and describes very well all the experimentally observed structure of the $T_e(o,t)$ evolution. For observations at radii different from $r =$ 0, a method previously established is used (see Ref. 84). The results obtained for χ_i agree within experimental error with neoclassical transport in the region 3 cm $\leq r \leq$ 4 cm, where χ_i was evaluated. For $r = 0$, however, ion transport appears as low as the classical value for the highest densities attained ($n_0 \cong 10^{15}$). This result is in contradiction with very large values near $r =$ 0 predicted by the standard neoclassical formalism.

3.4.9 High-β Tokamak Modeling Studies

J. T. Hogan

The attainment and maintenance of a high beta ($\beta > 4\%$) plasma by neutral beam injection is an important goal of present tokamak experiments. We discuss work in progress on a number of modeling problems suggested by such experiments: (1) optimization of the configuration by beam deposition and current programming, (2) the role of neutral beam-induced currents in determining the shear profile, (3) possible use of Fisch-Bers lower hybrid current drive for tailoring profiles,[89] and (4) properties of the final stage of FCT evolution.

---

[*] Massachusetts Institute of Technology, Cambridge, Massachusetts

[†] American Science and Engineering, Incorporated

As part of this study, we have modified our 1 1/2-D transport code to

(1) calculate high beta limits self-consistently by using the Bateman-Nelson Ballooning Code[90] within the transport calculation;

(2) calculate lower hybrid power dissipation and current generation using a module developed by D. Ehst (Argonne National Laboratory);[89]

(3) calculate magnetic reconnection of non-monotone current profiles and magnetic island effects due to saturated tearing instabilities, using criteria developed by Waddell, Carreras, and Hicks.

As before, beam deposition is calculated with the Fowler-Rome noncircular version of the FREYA module developed by D. Post (PPPL).

We find that

(1) self-consistent transport-generated "stable" D-shaped plasmas with $\beta > 10\%$ ("stable" = linearly unstable over less than 20% of the plasma volume) and the TOSCA results do not violate the ballooning criterion;

(2) benefits for ballooning stability from force-free currents (from external voltage programming or lower hybrid current drive) may be counterbalanced by tearing-mode-induced enhanced transport;

(3) the Zakharov-Shafranov catastrophe[91] (loss of equilibrium on the post-FCT time scale) should not be accessible in the near future;

(4) neutral-beam-induced currents completely determine the shear profile at low density for coinjected plasmas and thus remove some of the profile tailoring capability. Perpendicular injection restores it, but a study of anisotropic pressure equilibrium and stability is needed for this case.

3.4.10 High Beta Tokamaks[92]

R. A. Dory
D. P. Berger
L. A. Charlton
J. T. Hogan
J. K. Munro, Jr.
D. B. Nelson
Y-K. M. Peng
D. J. Sigmar
D. J. Strickler

MHD equilibrium, stability, and transport calculations are made to study the accessibility and behavior of high beta tokamak plasmas in the range $\beta \approx 5$-15%. For next generation devices, beta values of at least 8% appear to be accessible and stable if there is a conducting surface nearby.

3.4.11 Tokamaks Heated to High Beta[93]

R. A. Dory
D. P. Berger
L. A. Charlton
J. T. Hogan
J. K. Munro, Jr.
D. B. Nelson
Y-K. M. Peng
D. J. Sigmar
D. J. Strickler

Intense plasma heating (neutral beam, wave, alpha, etc.) makes high energy density tokamaks possible. This paper treats the reaction of plasma that is heated to values of beta in the range of 5-10%.

3.5 PLASMA ENGINEERING

S. E. Attenberger
S. K. Borowski
J. N. Davidson
G. A. Emmert
W. A. Houlberg
M. A. Iskra
J. R. McNally, Jr.
A. T. Mense
R. J. Onega
Y-K. M. Peng
J. A. Rome
K. E. Rothe
D. J. Strickler
T. C. Tucker
N. A. Uckan[*]
R. M. Wieland

The Plasma Engineering effort is aimed at developing successful fusion reactors and is, therefore, closely coupled with experiments, theory, and fusion engineering and technology studies. This is accomplished through interpretation of the latest theoretical and experimental results and the application of these understandings to sizing of the advanced devices. This involves the developing, upgrading, and benchmarking of computer codes based on the latest developments in the plasma, MHD, kinetic, and transport modeling theories to suit the specific devices. Also, based on the understanding developed through the engineering and technology research and development efforts, alternate plasma operation scenarios are explored to resolve significant uncertainties and difficulties in building and operating advanced devices.

3.5.1 Plasma Systems Analysis

A. T. Mense
W. A. Houlberg
J. R. McNally, Jr.
S. E. Attenberger
R. M. Wieland
J. N. Davidson
G. A. Emmert
M. A. Iskra

The Plasma Systems activity encompasses several areas of research. This past year the areas were (1) benchmarking of transport code subroutines, e.g., pellet ablation and neutral beam deposition; (2) determination of finite ion temperature and secondary electron emission effects on divertor plasma transport; (3) expanding radius neutral beam heating scenarios for tokamaks; and (4) alpha-particle-driven plasma current.

A Comparison of Beam Deposition for Three Neutral Beam Injection Codes[94]

R. M. Wieland W. A. Houlberg
A. T. Mense

The three neutral beam injection codes BEAM (Houlberg – ORNL), HOFR (Howe – ORNL), and FREYA (Post – PPPL) are compared with respect to the calculation of the fast ion deposition profile $H(r)$. Only plasmas of circular cross section are considered with injection confined to the midplane of the torus. The approximations inherent in each code are pointed out, and a series of comparisons varying several parameters (beam energy and radius, machine size, and injection angle) shows excellent agreement among all the codes. A "cost" comparison (execution time and memory requirements) is made that points out the relative merits of each code within the context of incorporation within a plasma transport simulation code.

PELLET – A Computer Routine for Modeling Pellet Fueling in Tokamak Plasmas[95]

W. A. Houlberg H. C. Howe
M. A. Iskra S. E. Attenberger

Recent experimental results of frozen hydrogenic pellet injection into hot tokamak plasmas and substantial agreement with theoretical predictions have led to a much greater interest in pellets as a means of refueling plasmas. The computer routine PELLET has been developed and used as an aid in assessing pellet ablation models (see Fig. 3.13) and the effects of pellets on plasma behavior. PELLET provides particle source profiles under various options for the ablation model and can be coupled either to a

---

[*] Group Leader

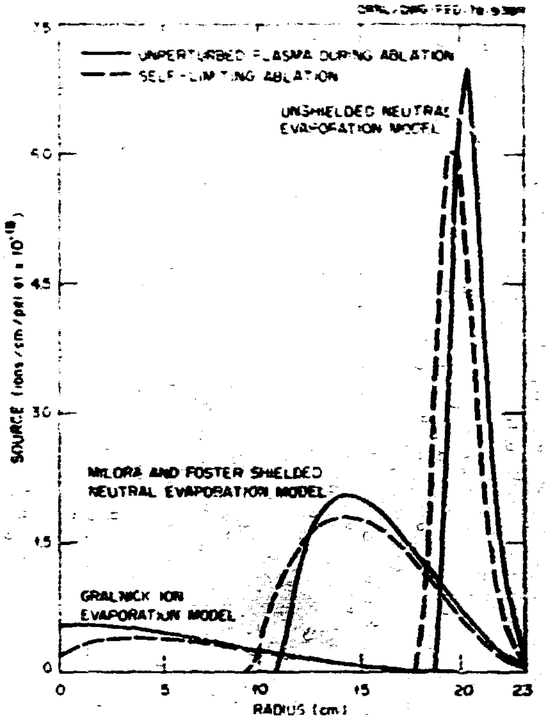

Fig. 3.13. Comparison of the three ablation models in PELLET with and without self-limiting ablation. ISX-A parameters are used [R_0 = 92 cm, a = 23 cm, $n_e(o)$ = 4 x 10^{13} cm^{-3}, $T_e(o)$ = 750 eV].

fluid transport code or to a brief routine that supplies the required input parameters.

Divertor sheath equations

G. A. Emmert A. T. Mense
J. N. Davidson R. M. Wieland

Several fundamental problems occur in trying to assess the energy loss terms along the magnetic field lines in the divertor (or shadow-of-the-limiter) scrape-off zone in a tokamak. The temperature ratio $T_i/T_e > 1$ causes the usual Bohm Sheath Criterion to come into question. The presence of plasma sources along the field lines and cross-field diffusion are also complications.

The formulation of an electric sheath near a plasma-metallic surface interface has been studied for the case in which the ion-to-electron temperature ratio is arbitrary. Most of the earlier work[96-[illegible]] has dealt with plasmas containing cold ions ($T_i < T_e$) with a drift velocity $U_i \sim \sqrt{T_e/M_i}$. However, it is unlikely that this situation will exist in actual divertors. Therefore, it is of interest to consider plasma sheaths with hot ions ($T_i/T_e > 1$) for cases (1) with and without secondary electron emission and (2) with and without volumetric source of plasma. In determining the probability for arcing or high-Z impurity sputtering, one requires the wall and sheath edge potentials. Figure 3.14 shows these potentials as a function of T_i/T_e.

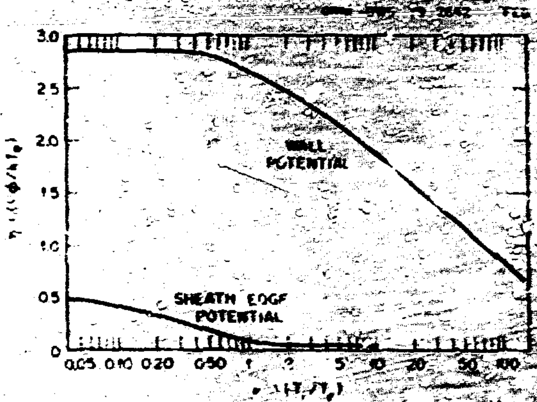

Fig. 3.14. Wall potential as a function of the temperature ratio.

Neutral beam energy and power requirements for expanding radius and full bore startup of tokamak reactors

W. A. Houlberg A. T. Mense
S. E. Attenberger

Neutral beam power and energy requirements are compared for full bore and expanding radius startup scenarios in an elongated TNS (The Next Step) plasma as a function of beam pulse time and plasma density. Because of the similarity of parameters, the results should also be applicable to Engineering Test Facility (ETF) and International Tokamak Reactor (INTOR) studies. A transport model consisting of neoclassical ion conduction and anomalous electron conduction and diffusion based on ALCATOR scaling leads to average densities in the range $\langle n \rangle \sim 0.8\text{-}1.2 \times 10^{14}$ cm^{-3} being sufficient for ignition. Neutral deuterium beam energies in the range 120-150 keV are adequate for penetration with the required power injected into the plasma decreasing with increasing beam energy. The neutral beam power decreases strongly with increasing beam pulse length τ_b until τ_b exceeds a few total energy confinement times, which yields $\tau_b \cong$ 4-6 sec for the TNS plasma. In addition to avoiding skin current effects and possibly allowing for a more impurity-free plasma initiation, the expanding radius scenario has slightly reduced beam energy and/or power requirements. When the expanding radius scenario is extended to even larger power reactors, neutral deuterium beam energy of 150 keV remains sufficient for penetration.

Figure 3.15 shows the neutral beam power requirements for ignition vs the injection time for both full bore and expanding radius scenarios. One can clearly see the gain is in going to beam pulse times approximately a few times the energy confinement time. The total energy expended in igniting with lower power over a longer period of time increases, however.

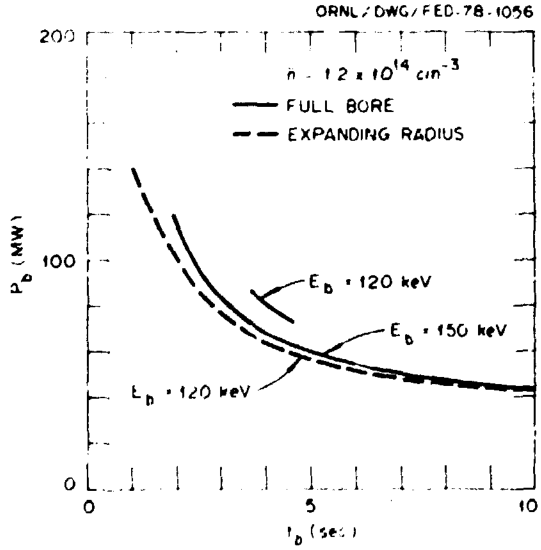

Fig. 3.15. Beam power required for ignition vs injection time t_b.

Alpha-driven steady-state tokamak

J. R. McNally, Jr. K. E. Rothe

A significant net alpha current (~1 MA) is to be expected in high temperature tokamak reactors and may provide the seed current essential to driving a bootstrap current in a tokamak to permit steady-state operation without the need for pulse transformers except during startup.[99] Figure 3.16 illustrates the prompt alpha current resulting in a flat temperature, parabolic-density-profiled,

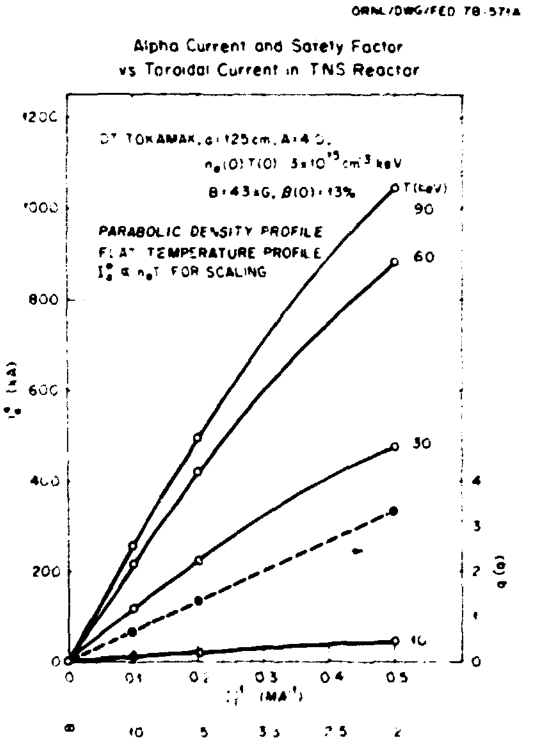

Fig. 3.16. Alpha seed current from prompt and stacking effects as a function of the toroidal current in a TNS-type tokamak. Safety factor q(a) is also shown. The alpha-produced seed current does not completely vanish at r = 0 except at $I_T = \infty$. Scaling for different n_eT involves multiplication of points by $n_eT/3 \times 10^{15}$.

TNS-size tokamak as a function of plasma temperature and toroidal current. At the elevated temperatures possible with temperature excursions of an ignited tokamak, the momentum input to plasma electrons is also grossly reduced, and plasma ions will pick up the bulk of the current (or momentum) from the alphas as they degrade in energy, thus sustaining an ionic seed current component in the plasma. Bootstrap currents due to pressure gradient effects, as well as selective scatter of countercurrent moving alphas into the loss region (banana orbits that intercept the tokamak wall), will enhance the prompt alpha current into the multi-MA range in high temperature plasmas.

3.5.2 Poloidal Field Studies

Y-K. M. Peng T. C. Tucker
D. J. Strickler

Tokamak equilibrium poloidal field studies

D. J. Strickler Y-K. M. Peng
T. C. Tucker

A set of codes has been developed to provide a systematic approach to the study of poloidal fields and free boundary FCT equilibria[100] in both air core and iron core tokamaks.

Pressure P profiles are assumed, and toroidal magnetic flux F functions for high beta are determined by solving the Grad-Shafranov equation

$$r^2 \nabla \cdot \left(\frac{1}{r^2} \nabla\psi\right) = -4\pi r^2 \frac{dP}{d\psi} - F \frac{dF}{d\psi} \qquad (3.15)$$

using the Oak Ridge FCT equilibrium code. The ideal vacuum field (ψ_E) may be extracted from this reference equilibrium by the "virtual casing" principle.[101] A current density distribution on a contour of length L reproducing ψ_E in the plasma region is then found by solving (see Fig. 3.17)

$$\psi_E(r,z) = \int_0^L J(s)G(r,z;s)ds \ ,$$

where G is a known Greens function. This integral equation is inverted numerically by modeling the current density J with a cubic spline function having variable knots and approximating the solution by a least squares method. Poloidal field coil locations based on this current distribution, together with the source functions P and F, may then be used to solve Eq. (3.15) in the free-boundary sense. Figure 3.17 illustrates some of the results.

This approach has been applied in ISX-B, LPTT, and TNS[102] tokamak equilibrium studies.

ORNL DWG 79-2652 FED

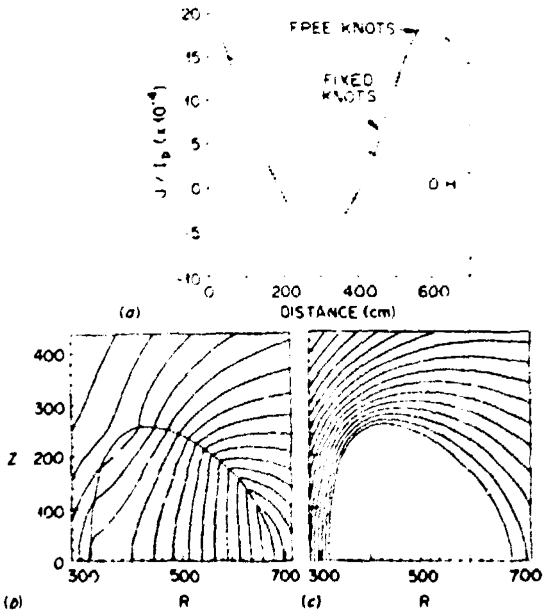

Fig. 3.17. (a) Optimal equilibrium field (EF) current density distributions using fixed and free knot representations and the ohmic heating (OH) current density creating (b) flux lines approximating the ideal vacuum field in the plasma region (dotted) and (c) zero field in the plasma region.

Implementation of GFUN3D magnetostatic computer code on the CDC 7600 at NMFECC

T. C. Tucker   T. A. Cutler*
Y-K. M. Peng   K. W. Fong*

A version of the Rutherford Laboratory's magnetostatic computer code GFUN3D[103] has been implemented on the Control Data 7600 (A machine) at the National Magnetic Fusion Energy Computer Center (NMFECC). The code is now being used for magnetic fusion energy (MFE) work at Livermore, Princeton, M.I.T., and General Atomic, as well as at ORNL.

At ORNL we are applying GFUN3D to studies of ISX and ISX-B. To determine a good GFUN-type model for ISX and to demonstrate the reliability of the code, we are comparing computed and experimentally observed magnetic fields. In the plasma region, the code results are in good agreement with experiment. Near the iron, however, GFUN3D does not always give reliable magnetic fields. The computed fields are strongly dependent upon fine details of the iron model and for some models are definitely wrong. But it does appear possible to define a good model to be used for calculating forces on the tokamak conductors, and we are working towards that end.

3.5.3 Advanced Fuels

J. R. McNally, Jr.   K. E. Rothe

The p(^{6}Li,α) ^{3}He (^{6}Li,p) ^{8}Be chain reaction

J. R. McNally, Jr.   K. E. Rothe

Recently, R. W. Conn has revived[104] the prospect of a charged particle fusion chain reaction involving ^{6}LiH fuel,[105] which might be suitable for use in multipole configurations or other low central magnetic field devices. A completely catalyzed (p + ^{6}Li → α + ^{3}He + 4.0 MeV) + ^{6}Li → α + p + ^{8}Be + 20.9 MeV reaction would promote fast or suprathermal ^{3}He and p ions that would react in propagation chain fashion[106] with ^{6}Li fuel supplemented by chain branching reactions involving p + ^{7}Li, ^{6}Li + ^{6}Li, ^{3}He + ^{6}Li, etc. The two primary mechanisms for propagation chain reaction release of energy give power production (the ^{6}Li^{6}Li reactions involve six exothermic channels)

$$P_{16} = n_1 n_6 \langle \sigma v \rangle_{16} \frac{Q_{16} + p_{36} Q_{36}}{1 - p_{16} p_{36}}$$

and

$$P_{36} = n_3 n_6 \langle \sigma v \rangle_{36} \frac{Q_{36} + p_{16} Q_{16}}{1 - p_{36} p_{16}} ,$$

where 1, 3, and 6 subscripts denote p, ^{3}He, and ^{6}Li; Q_{16} = 4.0 MeV and Q_{36} = 16.9 MeV; and p_{16} and p_{36} are the reaction probabilities of the fast ions with ^{6}Li as they slow down on plasma ions and electrons. Neglecting nuclear elastic collisions (which promote suprathermal ions), the probabilities p_{ij} can be written (provided τ_s ≪ the particle confinement time)

$$p_{i6} = \int_{E_i}^{3/2\ T_i} n_6 (\sigma v)_{i6}\, dt$$

$$= \int_{E_i}^{3/2\ T_i} n_6 (\sigma v)_{i6}\, dE/(dE/dt) ,$$

where

$$\frac{dE}{dt} = - \frac{2(E - 3/2\ T_e)}{\tau_s} - \frac{2(E - 3/2\ T_i)}{\tau_s} \left(\frac{E_c}{E}\right)^{3/2} .$$

---

*Lawrence Livermore Laboratory

Here

$$\tau_s = \frac{1.2 \times 10^{[illegible]} T_e^{3/2}}{n_e} \frac{A_i}{Z_i} ,$$

and

$$E_c = 14.8\, T_e A_i [(\Sigma\, n_{ions} Z_{ions}^2 / A_{ions}) / n_e]^{2/3} .$$

Preliminary synchrotron-free burn calculation results have been obtained and give p_{16} of order 0.06-0.22. No ignition of a closed ($n\tau = \infty$), pulsed burn has been obtained except for pure p^{6}Li plasmas with all the ^{3}He instantly burned with ^{6}Li – a very unlikely prospect.

The effect of nuclear elastic collisions and additional side reactions is expected to enhance the burn prospects, but one needs about a doubling of the charged particle energy release to match the bremsstrahlung power loss alone. Further study of this potentially "clean" advanced fusion fuel seems warranted, although it should be recognized that the use of ^{6}Li as fuel poses the problem of condensation and crud buildup on any cold surfaces in the vacuum chamber.

A simple measure of merit for fusion feasibility

J. R. McNally, Jr.

A simple merit factor for fusion-related experiments is defined in terms of several fusion goals and compared with past and present experimental achievements.[107] The merit factor is taken to be $M = \log 10^{10}k$, where k is the four-factor fusion formula ($fn\epsilon p$) and represents the fusion energy multiplication factor defining ignition for $k \geq 1$ or $M \geq 10$. The value of k can in most present cases be approximated by f, the thermal energy utilization factor, which equals the ratio of the alpha particle fusion power to the thermal power losses from the plasma.[illegible] For upcoming large tokamak experiments, such as TFTR, the fast fusion factor due to beam-plasma reactions may appreciably exceed unity and thus reduce the $Tn\tau_E$ requirements for ignition through f. In the past 20 years, M has increased by six units and k or f by 10^6. Figure 3.18 illustrates progress for several fusion-related experiments. The PLT(I') point includes a correction for $Z_{eff} = 3.5$, which reduces the equivalent $n_e(=n_D + n_T)$ by about a factor of 2.

3.5.4 Plasma Engineering Support of Advanced Systems

Advanced fusion systems design projects (TNS/ETF, EBTR, etc.) and areas of development and technology (controls and instrumentation, neutral beam systems, etc.) receive fusion physics support and guidance from the Plasma Engineering Group.

Oak Ridge TNS Reference Design, 1978: Plasma Engineering Considerations[illegible]

Y-K. M. Peng W. A. Houlberg
J. A. Rome

The 1978 Oak Ridge TNS effort was directed towards preconceptual design of a high duty cycle, ignited tokamak with an emphasis on engineering feasibility. The Plasma Engineering input to this design included the application of our present understanding of fusion plasma physics and the exploration of new approaches to plasma operation that may substantially improve the attractiveness of the tokamak reactor. (For a more detailed discussion of the TNS studies, see Sect. 7).

Plasma current startup. A method of rf (1 MW at 120 GHz) preionization and electron preheating was proposed as a possible scheme to allow an order of magnitude reduction in the startup loop voltage (from 300 V to below 30 V) with minimal resistive loss of flux swing. Engineering studies of the TNS PF system have indicated a significant reduction

ORNL/DWG/FED 78-246R

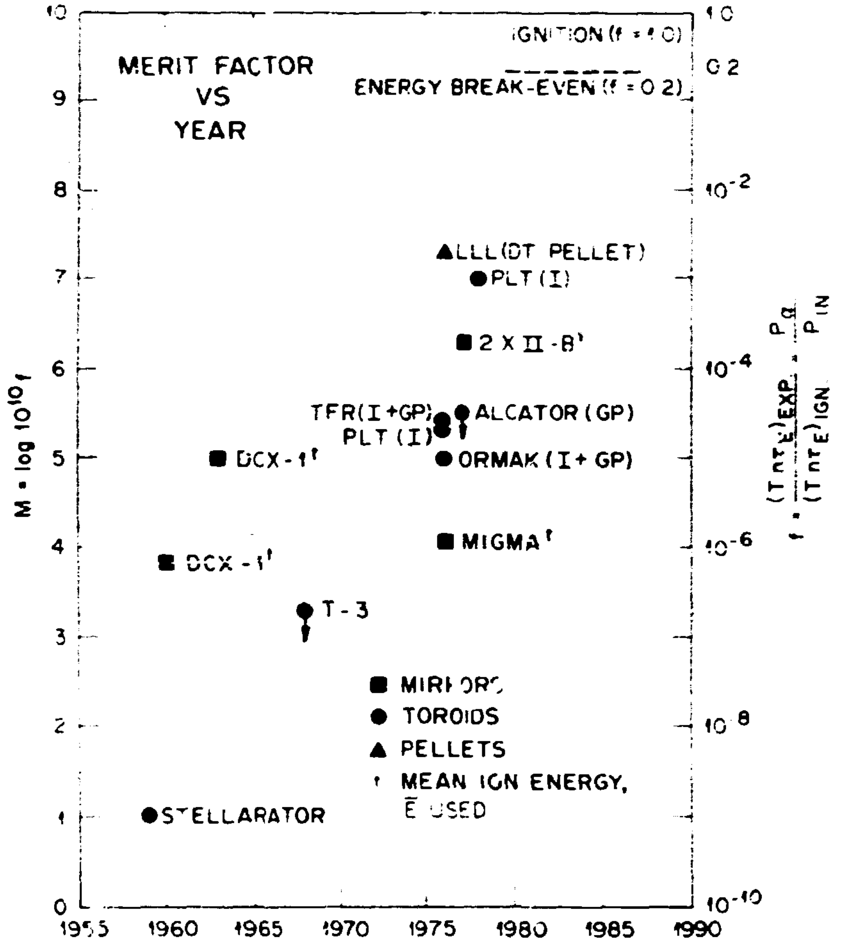

Fig. 3.18. Time dependence of merit factor M suggesting that with comparable improvements in the future, ignition might be achieved in toroidal devices after 1990.

in cost by increasing the current buildup time from 2 to 6 sec. This suggests additional heating during this phase to ensure that the resistive loss is limited to below $0.05\ I_pL_p \simeq 2.5$ Wb, where $I_p = 4$ MA.

Heating to ignition. Nearly perpendicular injection of 50-70 MW neutral deuterium beams at 150 keV is proposed to heat the plasma to ignition in about 6 sec. This result is suggested by detailed 1-D transport calculations of plasma ignition with expanding radius or full bore heating when the density is held constant in time. This result is further supported by 1 1/2-D calculations with simplified transport models in a low density heating scenario account for the effects of noncircular plasma cross section, shift of the magnetic axis as $\bar{\beta}$ increased to 7 , and energy spectrum of the beams.

Beta maintenance. Assuming successful impurity control, refueling, and ash removal, the poloidal flux swing is capable of sustaining the plasma current for 500 sec, which is somewhat less than the magnetic flux diffusion time in the plasma. The hybrid PF coils are analyzed to show that the desired D-shaped cross section can be maintained despite possible large changes in the plasma beta and profiles. Ideal MHD calculations have shown that β values around 7 can be stable with proper shape and profile controls.

Impurity and particle control. Bundle divertors are presently assumed for the Reference Design. Plasma fueling is assumed to be from a combination of neutral beams, pellets, and puffed gas. Further divertor-related physics calculations are needed in this area (e.g., effects on energetic ion confinement).

Shutdown. The effects of plasma shutdown due to major disruption are estimated to be manageable if the disruption time scales like $R^{[illegible]} a^{[illegible]} B_t^{[illegible]} V^{-[illegible]}$ (V = plasma loop voltage) as a result of nonlinear interaction among tearing modes to become roughly 25 msec in the Reference Design.

Tokamak instrumentation and controls

W. A. Houlberg R. J. Onega

The primary input from Plasma Engineering in this study is the definition of the physics transients needed in a complete burn cycle. The impact of potential abnormal operations such as hard shutdown and aborts, as well as the avoidance and amelioration of such impacts, is deemed an area that needs strong attention. The most important consequence of a disruption will be damage to the first wall from thermal and magnetic stress. Severe temperature gradients will cause thermal stress, placing a limit on the number of disruptions that can occur before the integrity of the wall is lost, and eddy currents induced in the wall will interact with the magnetic energy of the plasma and the B_T field to create mechanical forces. Consequences to the ohmic heating (OH) coils, their power supplies, and other coils must also be taken into account.

The two most important parameters for the assessment are the plasma disruption time τ_D and the uniformity of the plasma energy deposition on the wall. Neither of these two parameters can be calculated definitively, but the distribution of energy on the first wall is the more uncertain.

For a TNS-size device, the plasma disruption time is estimated to be τ_D = 24 msec, with 135 MJ of thermal energy and 191 MJ of magnetic energy stored in the plasma. Uniform energy deposition is assumed for this analysis. The temperature rise in the first wall (which is made of type 316 stainless steel) is roughly 400°C from a starting temperature of 104°C, indicating that wall failure due t thermal fatigue will occur after about 45 disruptions.

The ELMO Bumpy Torus Reactor

N. A. Uckan
D. B. Batchelor
E. S. Bettis[*]
R. A. Dandl
C. L. Hedrick, Jr.
E. F. Jaeger
D. G. McAlees
D. B. Nelson
L. W. Owen
R. T. Santoro
D. A. Spong
T. Uckan
M. L. Watts[*]
H. T. Yeh
L. M. Lidsky[#]
J. S. Herring[#]
R. E. Potok[#]

The EBT concept provides a uniquely simple basis for a steady-state modular fusion reactor. Inclusion of recent advances from plasma research has led to a new, smaller design. Critical physics issues are discussed and dimensionless parameter scalings are explored (see Table 3.3).

---

[*] Science Applications, Inc.

EBT group

[‡] Neutron Physics Division

[§] Experimental Confinement Section

Magnetics and Superconductivity Section

[#] Massachusetts Institute of Technology

Table 3.3. Dimensionless parameters for EBT's

		EBT I	EBTR	Critical value
Annulus beta	β_A	0.2-0.4	0.3-0.5	threshold 6-10
Toroidal core beta	β_T	3-5 × 10[illegible]	~25 × 10[illegible]	β_A
Ratio of gyroradii to plasma radius	ρ_e/a	10[illegible]	10[illegible]	
	ρ_i/a	2 × 10[illegible]	4 × 10[illegible]	
Ratio of cold (toroidal) to hot (annulus) electron density	n_c/n_h	3-10	10	
Field errors	$\delta B/B$	10[illegible]	~10[illegible]	$/R_t$
Aspect ratio	A	10	20-60	~10
Ratio of electron to ion temperature	T_e/T_i	~3	~1	
Ratio of electron plasma frequency to cyclotron frequency	ω_{pe}/ω_{ce}	~0.7	0.8	
Ratio of ambipolar potential to temperature	$e\phi/T_j$, j = e or i	~1	~1(?)	
Collisionality	ν_e/ω_e	0.1	0.5	<1
	ν_i/ω_i	0.15	0.015	

Heating Techniques for an EBT Reactor[113]

N. A. Uckan D. B. Batchelor

The heating of an EBT reactor plasma by microwaves (ECH) and neutral beams is discussed. Although past and present EBT experiments use ECH for formation of the hot electron rings (annuli) and for heating of the bulk (toroidal) plasma, an EBT reactor and future proposed experiments may use neutral beams as well as ECH, or a combination of both, for heating of the toroidal plasma. When plasma is heated to ignition in a reactor, the bulk heating is turned off, but the ring heating must be sustained throughout the steady-state operation. For microwave heating in a large, high density reactor plasma, considered are questions of microwave energy penetration and accessibility (to both the ordinary and extraordinary modes). Microwave frequencies required are 120 GHz for the toroidal plasma heating and ~60-70 GHz for the ring formation. These requirements are similar to those frequencies for the proposed EBT-II experiment. Because energetic particles having large pitch angle are well confined in EBT, perpendicular injection of neutral beams appears very attractive. The possibility of perpendicular injection, coupled with the large aspect ratio and relatively small plasma minor radius (~1 m) for an EBT reactor, means that neutral beams of the type being developed for TFTR (~150 keV) will be sufficient.

The ELMO Bumpy Torus (EBT) Reactor[114]

N. A. Uckan D. G. McAlees
R. A. Dandl R. T. Santoro
C. L. Hedrick, Jr. H. L. Watts
E. S. Bettis H. T. Yeh
L. M. Lidsky

The EBT concept has many encouraging and attractive features as a fusion reactor system. These include a high beta, magnetohydrodynamically stable equilibrium; absence of parallel currents; a large aspect ratio; the modular nature of individual sectors; no interlinking coils; ease of maintenance; steady-state operation; and economic potential. The first EBT reactor study was initiated in 1976 and provided the required starting point for continued assessment of the validity of the concept. Major refinements in plasma physics and design engineering have now resulted in a revised system description. A new design based on the present physics, practical design, and present and near-term technologies has been established. This paper discusses the details of key design elements and critical scientific and technological factors that are substantially different from other fusion reactor approaches. The paper also provides a useful summary of where the EBT program is, where it is going, and why these efforts are, in fact, self-consistent, with a motivation towards potential reactor application of EBT's.

3.6 COMPUTING SUPPORT

I. Burnett, III
R. D. Burris
D. N. Clark
J. E. Francis, Jr.
C. E. Hammons*
C. O. Kemper
D. R. Overbey
C. E. Parker
J. W. Reynolds
C. R. Stewart, Jr.
K. A. Stewart
O. C. Yonts

3.6.1 User Service Center

R. D. Burris
I. Burnett, III
D. N. Clark
C. E. Parker

The communications PDP11/45 computer was studied, tuned, and brought to current engineering levels, which has resulted in ~99% uptime for the year. The PDP11/45 was used to off-load some of the operating and plotting chores from the DECsystem-10. Sixteen communications circuits were added to the DN87 communications processor in order to provide better access to the User Service Center (USC) by the Fusion Energy Division staff.

An extremely usable plotting system was installed on the USC's and the Computer Science Division's DEC-10's. With one command, users may direct data in any of four formats to any of eight different types of plotters. Functionality and performance enhancements were added to the generalized Network Command Language, which was developed in FY 1978. The protocol and code for this interconnection of computers have been of interest to several others. This system allows data bases (files) to be transported to other computers so that the data can be processed in the most suitable location. Support for the Diablo (Xerox Corporation) word processor was added to the LASL USC's text editor and distributed to other USC sites. The feasibility and practicality of an array processor were studied. A support processor appears preferable to an array processor due to the associated overhead.

3.6.2 Experimental Data Handling

R. D. Burris
J. E. Francis
C. O. Kemper
D. R. Overbey
C. R. Stewart, Jr.
K. A. Stewart
O. C. Yonts

A PDP11/34-based data acquisition system for the High Energy Test Facility (HETF) was specified, procured, and made operational this year. This system uses CAMAC[115] interfaces for data acquisition. Tektronix 4010 support was added to the METF, and the existing system was converted to DEC's RSX11M.

The data acquisition system for the ISX experiment was augmented by the addition of two PDP11/34's. The effectiveness of existing PDP8's was enhanced by the addition of floppy disks. An RK05 disk was added to the PDP12. Several existing diagnostics were converted to CAMAC interfaces for versatility.

---

*Group Leader

Support programs were added to the PDP11/45 to convert vector data to raster image for subsequent plotting on the PDP11/45. This reduces the plotting/printing load on the USC/DEC-10 considerably.

A new release of the RSX11D operating system was installed on the PDP11/45, and a RSX11M system generation support package was developed. Medium speed communication links and their associated software were installed between the PDP11/45 central system and the PDP11 systems at METF, ISX, and HETF.

The integration of the PDP8A acquisition system for EBT was affected, and the existing data handling and processing codes for EBT data were improved.

REFERENCES

1. R. A. Dandl et al., *The EBT-II Conceptual Design Study*, Oak Ridge National Laboratory Report ORNL/TM-5955, Oak Ridge, Tennessee (1978).
2. L. A. Berry, C. L. Hedrick, and N. Uckan, *ELMO Bumpy Torus*, Oak Ridge National Laboratory Report ORNL/TM-6743, Oak Ridge, Tennessee (1979).
3. D. B. Batchelor and C. L. Hedrick, Nucl. Fusion 19, 235 (1979).
4. D. B. Nelson and C. L. Hedrick, Nucl. Fusion 19, 283 (1979).
5. D. A. Spong, E. G. Harris, and C. L. Hedrick, "Kinetic Transport Properties of a Bumpy Torus with Finite Radial Ambipolar Field," to be published in Nucl. Fusion.
6. E. F. Jaeger and C. L. Hedrick, Nucl. Fusion 19, 443 (1979).
7. B. Carreras, B. V. Waddell, and H. R. Hicks, *Analytic Model for the Nonlinear Interaction of Tearing Modes of Different Pitch in Cylindrical Geometry*, Oak Ridge National Laboratory Report ORNL/TM-6175, Oak Ridge, Tennessee (1978).
8. B. Carreras, B. V. Waddell, and H. R. Hicks, *Poloidal Magnetic Field Fluctuations in Tokamaks*, Oak Ridge National Laboratory Report ORNL/TM-6403, Oak Ridge, Tennessee (1978).
9. B. V. Waddell, M. N. Rosenbluth, D. A. Monticello, R. B. White, and B. Carreras, "Non-Linear Numerical Algorithms for Studying Tearing Modes," p. 79 in *Theoretical and Computational Plasma Physics*, IAEA-SMR-31/27-B, Vienna (1978).
10. B. Carreras, B. V. Waddell, H. R. Hicks, and S. J. Lynch, Phys. Rev. A 18, 2732 (1978).
11. B. V. Waddell, B. Carreras, H. R. Hicks, J. A. Holmes, and D. K. Lee, Phys. Rev. Lett. 41, 1386 (1978).
12. B. V. Waddell, B. Carreras, H. R. Hicks, and J. A. Holmes, "Nonlinear Interaction of Tearing Modes in Highly Resistive Tokamaks," to be published in Phys. Fluids.
13. J. D. Callen et al., "Magnetic 'Islandography' in Tokamaks," paper presented at the 7th Int. Conf. on Plasma Physics and Controlled Nuclear Fusion Research, Innsbruck, Austria, August 23-30, 1978; also Oak Ridge National Laboratory Report ORNL/TM-6564, Oak Ridge, Tennessee (1978).
14. B. Carreras, H. R. Hicks, and B. V. Waddell, *Tearing Mode Activity for Hollow Current Profiles*, Oak Ridge National Laboratory Report ORNL/TM-6570, Oak Ridge, Tennessee (1978); to be published in Nucl. Fusion.
15. J. A. Holmes, B. Carreras, H. R. Hicks, S. J. Lynch, and B. V. Waddell, *Stabilization of Tearing Modes to Suppress Major Disruptions in Tokamaks*, Oak Ridge National Laboratory Report ORNL/TM-6707, Oak Ridge, Tennessee (1979).
16. J. A. Holmes, Y-K. M. Peng, and S. J. Lynch, *Evolution of Flux Conserving Tokamak Equilibria with Preprogrammed Cross Sections*, Oak Ridge National Laboratory Report ORNL/TM-6761, Oak Ridge, Tennessee (1979).
17. D. B. Nelson, "Intense Neutral Beam Heating in the Adiabatic Approximation,"

in *Finite Beta Toroidal Plasmas*, Oak Ridge National Laboratory Report ORNL/TM-6273, Oak Ridge, Tennessee (1978).

18. Y-K. M. Peng, *Continuous Tokamaks*, Oak Ridge National Laboratory Report ORNL/TM-6319, Oak Ridge, Tennessee (1978).

19. Y-K. M. Peng and R. A. Dory, *Very Small Aspect Ratio Tokamaks*, Oak Ridge National Laboratory Report ORNL/TM-6535, Oak Ridge, Tennessee (1978).

20. G. Bateman and D. B. Nelson, Phys. Rev. Lett. 41, 1804 (1978).

21. D. B. Nelson, G. O. Spies, and C. L. Hedrick, Phys. Fluids 21, 1742 (1978).

22. C. H. An and G. Bateman, *Stability of Tokamaks with Elongated Cross Section*, Oak Ridge National Laboratory Report ORNL/TM-6419, Oak Ridge, Tennessee (1978).

23. D. J. Sigmar and H. C. Chan, Nucl. Fusion 18, 1569 (1978).

24. P. J. Catto, Phys. Fluids 21, 147 (1978).

25. K. T. Tsang and J. D. Callen, Phys. Fluids 21, 1172 (1978).

26. P. J. Catto and K. T. Tsang, Phys. Fluids 21, 1381 (1978).

27. P. J. Catto, Plasma Phys. 20, 719 (1978).

28. K. T. Tsang, P. J. Catto, J. C. Whitson, and J. Smith, Phys. Rev. Lett. 40, 327 (1978).

29. K. T. Tsang, J. C. Whitson, J. D. Callen, P. J. Catto, and J. Smith, Phys. Rev. Lett. 41, 557 (1978).

30. K. T. Tsang, Bull. Am. Phys. Soc. 23, 798 (1978).

31. K. T. Tsang, J. C. Whitson, and J. Smith, *Numerical Study of Drift-Alfvén Waves in a Sheared Magnetic Field*, Oak Ridge National Laboratory Report ORNL/TM-6508, Oak Ridge, Tennessee (1978).

32. S. P. Hirshman and K. Molvig, *Turbulent Destabilization and Saturation of the Universal Drift Mode in a Sheared Magnetic Field*, Oak Ridge National Laboratory Report ORNL/TM-6620, Oak Ridge, Tennessee (1978); also Phys. Rev. Lett. 42, 648 (1979).

33. K. Molvig and D. J. Sigmar, "Anomalous Slowing Down of Alpha Particles in Toroidal Plasma," paper E21 presented at the 1978 Annual Controlled Fusion Theory Conference, Gatlinburg, Tennessee, April 26-28, 1978.

34. D. J. Sigmar, S. P. Hirshman, and J. C. Whitson, Bull. Am. Phys. Soc. 23, 785 (1978).

35. K. T. Tsang, J. C. Whitson, J. D. Callen, P. J. Catto, and J. Smith, "Drift-Alfvén Waves in Tokamaks," paper presented at the 1978 Annual Controlled Fusion Theory Conference, Gatlinburg, Tennessee, April 26-28, 1978.

36. M. Rosenbluth and P. Rutherford, Phys. Rev. Lett. 34, 1428 (1975).

37. T. Kaladze and A. Mikhailovskii, Nucl. Fusion 17, 411 (1977).

38. T. Mizoguchi, T. Kammash, and D. J. Sigmar, Phys. Fluids 21, 2086 (1978).

39. D. J. Sigmar and G. Vahala, Phys. Fluids 21, 2280 (1978).

40. D. J. Sigmar, *Proc. Finite Beta Theory Workshop*, published in *Advances in Fusion Science and Engineering*, p. 13, ed. by B. Coppi and W. Sadowski, National Technical Information Service, Virginia, 1978.

41. R. V. Neidigh and D. J. Sigmar, *Hot-Ion Distribution Function in ORMAK, the Oak Ridge Tokamak*, Oak Ridge National Laboratory Report ORNL/TM-6198, Oak Ridge, Tennessee (1978).

42. W. M. Stacey, Jr. and D. J. Sigmar, *Comments on the Effects of Gas Injection upon Radial Particle Fluxes in the ISX-A Flow Reversal Experiment*, Oak Ridge National Laboratory Report ORNL/TM-6339, Oak Ridge, Tennessee (1978).

43. W. M. Stacey, Jr. and D. J. Sigmar, *The Response of a Tokamak Plasma to Particle and Momentum Sources*, Oak Ridge National Laboratory Report ORNL/TM-6575, Oak Ridge, Tennessee (1978).

44. S. P. Hirshman and E. C. Crume, Jr., "Collisionality Dependence of the

Pfirsch-Schlüter Contribution to Neoclassical Diffusion," paper E36 presented at the 1978 Annual Controlled Fusion Theory Conference, Gatlinburg, Tennessee, April 26-28, 1978.

45. A. Samain and F. Werkoff, Nucl. Fusion 17, 53 (1977).
46. R. D. Hazeltine and F. L. Hinton, Phys. Fluids 16, 1883 (1973).
47. J. M. Rawls, M. S. Chu, and F. L. Hinton, Phys. Fluids 18, 1160 (1975).
48. H. K. Meier and D. J. Sigmar, Bull. Am. Phys. Soc. 23, 997 (1978).
49. S. P. Hirshman, "Summary of Collisional Particle Fluxes in a Tokamak Plasma," to be published as Oak Ridge National Laboratory Report ORNL/TM-6481, Oak Ridge, Tennessee.
50. J. A. Rome and Y-K. M. Peng, *The Topology of Tokamak Orbits*, Oak Ridge National Laboratory Report ORNL/TM-6352, Oak Ridge, Tennessee (1978).
51. J. A. Rome, D. G. McAlees, J. D. Callen, and R. H. Fowler, Nucl. Fusion 16, 55 (1976).
52. T. G. Northrop and J. A. Rome, Phys. Fluids 21, 384 (1978).
53. J. A. Rome, W. A. Houlberg, and Y-K. M. Peng, Science 203, 316 (1979).
54. W. D. Metz, Science 202, 370 (1978).
55. A. C. Riviere, Nucl. Fusion 11, 367 (1971); D. R. Sweetman, Nucl. Fusion 13, 157 (1973).
56. J. A. Rome, Y-K. M. Peng, and J. N. Davidson, Trans. Am. Nucl. Soc. 27, 89 (1977); S. C. Scott and J. Sheffield, *Scaling Studies of Beam Heated Tokamaks*, Oak Ridge National Laboratory Report ORNL/TM-6584, Oak Ridge, Tennessee (1978); W. A. Houlberg, A. T. Mense, and S. E. Attenberger, "Neutral Beam Energy and Power Requirements for Expanding Radius and Full Core Startup of Tokamak Reactors," to be published as ORNL report; J. A. Holmes, J. A. Rome, Y-K. M. Peng, S. J. Lynch, "Low Density Ignition Scenarios Using Injection Heating," to be published as ORNL report.
57. P. Raimbault and M. Fumelli, in *Proc. Joint Varenna-Grenoble Int. Symp. on Heating Toroidal Plasmas*, Vol. I, p. 71 (1978).
58. J. A. Rome and Y-K. M. Peng, *Proc. Joint Varenna-Grenoble Int. Symp. on Heating in Toroidal Plasmas*, Vol. I, p. 7 (1979).
59. J. A. Rome and Y-K. M. Peng, "The Topology of Large Banana-Width Tokamak Orbits," paper E17 presented at the 1978 Annual Controlled Fusion Theory Conference, Gatlinburg, Tennessee, April 26-28, 1978.
60. J. F. Lyon, J. A. Rome, and J. T. Hogan, Bull. Am. Phys. Soc. 23, 771 (1978).
61. J. A. Rome, R. H. Fowler, and J. F. Lyon, Bull. Am. Phys. Soc 23, 904 (1978).
62. R. H. Fowler, J. Smith, and J. A. Rome, Abstract of Comput. Phys. Commun. 13, 323 (1978).
63. R. H. Fowler and J. A. Rome, "NFREYA – A Monte Carlo Beam Deposition Code for Non-Circular Tokamak Plasmas," to be published as Oak Ridge National Laboratory Report ORNL/TM-6845, Oak Ridge, Tennessee.
64. R. H. Fowler, D. K. Lee, and P. W. Gaffney, FLCC *Field Line and Orbit Code for the Study of Ripple Beam Injection into Tokamaks*, Oak Ridge National Laboratory Report ORNL/TM-6293, Oak Ridge, Tennessee (1978).
65. H. K. Meier, W. I. van Rij, C. O. Beasley, and J. E. McCune, Plasma Phys. 19, 151 (1977).
66. C. O. Beasley, J. E. McCune, H. K. Meier, and W. I. van Rij, Plasma Phys. 20, 115 (1978).
67. W. I. van Rij, H. K. Meier, C. O. Beasley, and J. E. McCune, "Simulation of Stable Electrostatic Drift Modes in Cylindrical Geometry," paper D30 presented at the 1978 Annual Controlled Fusion Theory Conference, Gatlinburg,

Tennessee, April 26-28, 1978; also presented at the 8th Conf. on Numerical Simulation of Plasmas, Monterey, California, June 28-30, 1978.

68. P. J. Catto, Plasma Phys. 20, 719 (1978).

69. W. I. van Rij, E. C. Crume, Jr., and K. E. Rothe, Bull. Am. Phys. Soc. 23, 760 (1978).

70. F. L. Hinton et al., Rev. Mod. Phys. 48, 239 (1976).

71. C. O. B. sley et al., Plasma Phys. 19, 593 (1977).

72. J. T. Hogan, "MHD/Transport Effects on Tokamak Confinement Scaling," paper C38 presented at the 1978 Annual Controlled Fusion Theory Conference, Gatlinburg, Tennessee, April 26-28, 1978.

73. M. Murakami et al., Phys. Rev. Lett. 42, 655 (1979).

74. M. Murakami et al., "Plasma Confinement and Impurity Flow Reversal Experiments in the ISX-Tokamak," paper IN4 presented at the 7th Int. Conf. on Plasma Physics and Controlled Nuclear Fusion Research, Innsbruck, Austria, August 23 30, 1978.

75. T. Amano and E. C. Crume, Jr., Bull. Am. Phys. Soc. 23, 772 (1978).

76. V. A. Verskhov, T. Amano, E. C. Crume, Jr., S. P. Hirshman, and J. T. Hogan, Bull. Am. Phys. Soc. 23, 771 (1978).

77. S. K. Wong, K. H. Burrell, and T. Amano, Bull. Am. Phys. Soc. 23, 790 (1978).

78. P. H. Edmonds et al., Bull. Am. Phys. Soc. 23, 790 (1978).

79. T. Amano and E. C. Crume, Jr., *Simulation of Multispecies Impurity Transport in Tokamaks*, Oak Ridge National Laboratory Report ORNL/TM-6363, Oak Ridge, Tennessee (1978).

80. R. C. Isler and E. C. Crume, Jr., Phys. Rev. Lett. 41, 1296 (1978).

81. R. C. Isler, E. C. Crume, Jr., and H. C. Howe. *Impurity Behavior during Neutral Beam Injection and Gas Puffing into ORMAK*, Oak Ridge National Laboratory Report ORNL/TM-6366, Oak Ridge, Tennessee (1978); to be published in Nucl. Fusion.

82. J. T. Hogan and A. T. Mense, J. Nucl. Mater. 76 & 77, 508 (1978).

83. J. T. Hogan, B. Carreras, and W. A. Houlberg, "MHD/Transport Interactions in Tokamaks," paper presented at the 8th Conf. on Numerical Simulation of Plasmas, Monterey, California, June 28-30, 1978.

84. M. Soler and J. D. Callen, *On Measuring the Electron Heat Diffusion Coefficient in a Tokamak from Sawtooth Oscillation Observations*, Oak Ridge National Laboratory Report ORNL/TM-616_, Oak Ridge, Tennessee (1978); to be published in Nucl. Fusion.

85. M. Soler and J. D. Callen, "Heat Transport in Tokamaks as Observed from Sawtooth Oscillation Characteristics," paper E 0 presented at the 1978 Annual Controlled Fusion Theory Conference, Gatlinburg, Tennessee, April 26-28, 1978.

86. G. L. Jahns et al., "Internal Disruptions in Tokamaks," to be published in Nucl. Fusion.

87. M. Soler, J. D. Callen, A. P. Navarro, R. Granetz, F. Seguin, and R. Petrasso, Bull. Am. Phys. Soc. 23, 759 (1978).

88. D. Gwinn and R. Granetz, Bull. Am. Phys. Soc. 23, 902 (1978); to be published in Nucl. Fusion.

89. D. Ehst, *Design Constraints for RF-Driven Steady-State Tokamak Reactors*, Argonne National Laboratory Report ANL/FFF/TM-120, Argonne, Illinois (1979).

90. G. Bateman and D. B. Nelson, Phys. Rev. Lett. 41, 1804 (1979).

91. L. E. Zakharov and V. D. Shafranov, Kurchatov Institute Report IAE 3075 (1978); English translation available as ORNL Internal Theory Memo 79/08.

92. R. A. Dory et al., "High Beta Tokamaks," paper K1 presented at the 7th Int. Conf. on Plasma Physics and Controlled Nuclear Fusion Research, Innsbruck, Austria, August 23-30, 1978.

93. R. A. Dory et al., "Tokamaks Heated to High Beta," paper presented at the Joint Varenna-Grenoble Int. Symp. on Heating in Toroidal Plasmas, Centre d'Études Nucléaires de Grenoble, July 3-7, 1978; to be published in Vol. II of proceedings.

94. R. M. Wieland, W. A. Houlberg, and A. T. Mense, *A Comparison of Beam Deposition for Three Neutral Beam Injection Codes*, Oak Ridge National Laboratory Report ORNL/TM-6550, Oak Ridge, Tennessee (1979).

95. W. A. Houlberg, M. A. Iskra, H. C. Howe, and S. E. Attenberger, *PELLET – A Computer Routine for Modeling Pellet Fueling in Tokamak Plasmas*, Oak Ridge National Laboratory Report ORNL/TM-6549, Oak Ridge, Tennessee (1979).

96. S. A. Self, Phys. Fluids 6, 1762 (1963); J. Appl. Phys. 36, 456 (1966).

97. G. D. Hobbs and J. A. Wesson, *Heat Transmission Through a Langmuir Sheath in the Presence of Electron Emission*, Culham Laboratory Report CLM-R61, Culham, England (1966).

98. L. A. Hall and I. Bernstein, *Modification of the Electrostatic Sheath by Secondary Emission of Electrons*, Lawrence Livermore Laboratory Report UCID-17273, Livermore, California (1976).

99. J. R. McNally, Jr., *Alpha-Driven, Steady-State Tokamak*, Oak Ridge National Laboratory Report ORNL/TM-6492, Oak Ridge, Tennessee (1978).

100. Y-K. M. Peng and R. A. Dory, Nucl. Fusion 17, 21 (1977).

101. L. E. Zakharov, Nucl. Fusion 13, 595 (1973).

102. Y-K. M. Peng, D. J. Strickler, and R. A. Dory, *Proc. 7th Symp. on Engineering Problems of Fusion Research*, Vol. I, p. 186 (1977).

103. A. G. Armstrong, C. J. Collie, N. J. Diserens, M. J. Newman, J. Simkin, and C. W. Trowbridge, *GFUN3D User Guide*, Rutherford Laboratory RL-76-029A, Chilton, Didcot, Oxon, England (1976).

104. R. W. Conn (University of Wisconsin), private communication, 1978.

105. J. R. McNally, Jr., Nucl. Fusion 11, 187 (1971).

106. J. R. McNally, Jr., *Encyclopedia of Chemistry*, 3rd ed., p. 481, ed. by C. A. Hampel and G. G. Hawley, Van Nostrand Reinhold Company, New York, 1973.

107. J. R. McNally, Jr., *A Simple Measure of Merit for Fusion Feasibility*, Oak Ridge National Laboratory Report ORNL/TM-6362, Oak Ridge, Tennessee (1978).

108. J. R. McNally, Jr., Nucl. Fusion 17, 1273 (1977); Nucl. Sci. Eng. 6[illegible], 255 (1978).

109. Y-K. M. Peng, W. A. Houlberg, and J. A. Rome, "Oak Ridge TNS Reference Design 1978 – Plasma Engineering Considerations," paper submitted to ANS 1979 Annual Meeting, Atlanta, Georgia.

110. R. J. Onega, W. R. Becraft, and E. S. Bettis, *Major Plasma Disruptions in [illegible]*," Oak Ridge National Laboratory Report ORNL/TM-6616, Oak Ridge, Tennessee (1979).

111. W. R. Becraft, E. S. Bettis, W. A. Houlberg, R. J. Onega, and R. S. Stone, *Tokamak Instrumentation and Controls*, Oak Ridge National Laboratory Report ORNL/TM-6617, Oak Ridge, Tennessee (1979).

112. N. A. Uckan et al., "The ELMO Bumpy Torus Reactor," paper IAEA-CN-37/I-3 presented at the 7th Int. Conf. on Plasma Physics & Controlled Nuclear Fusion Research, Innsbruck, Austria, August 23-30, 1978.

113. N. A. Uckan and D. B. Batchelor, *Heating Techniques for an EBT Reactor*, Oak Ridge National Laboratory Report ORNL/TM-6346, Oak Ridge, Tennessee (1978).

114. N. A. Uckan et al., "The ELMO Bumpy Torus (EBT) Reactor," pp. 369-387 in *Fusion Reactor Design Concepts*, IAEA, Vienna, 1978.

115. Institute of Electrical and Electronics Engineers, Inc., STD No. 583-1975.

4. ATOMIC MOLECULAR, AND NUCLEAR PHYSICS

C. F. Barnett[1]
D. H. Crandall[1]
G. H. Dunn[2]
B. J. Farmer[1]
H. B. Gilbody[3]
D. C. Gregory[2]
B. E. Hasselquist[4]
S. W. Hawthorne[1]
P. Hvelplund[5]
H. J. Kim[1]
M. I. Kirkpatrick[1]
E. W. McDaniel[6]
R. H. McKnight[7]
F. W. Meyer[1]
T. J. Morgan[8]
R. A. Phaneuf[1]
P. H. Stelson[1]
E. W. Thomas[6]

Abstract. A crossed-beams apparatus has been used to obtain the sum of the charge exchange and ionization cross sections of 40-keV H^0 with N^{3+}. These total electron loss cross sections were dominated by the small excited-state population in the H^0 beam that was formed by electron capture collisions of H^+ in H_2O vapor. Electron impact ionization cross sections were extended to the multiply charged ions B^{3+}, C^{3+}, C^{4+}, N^{3+}, N^{4+}, N^{5+}, O^{3+}, O^{4+}, O^{5+}, and Ar^{4+} in the energy range from threshold to 1500 eV. The data indicate that for the lithium-like ions, excitation followed by autoionization contributes significantly to the ionization cross sections. For the ions studied, this contribution increased with the ion charge. Cross-section measurements of electron impact excitation of N^{4+} were in excellent agreement with close-coupling calculations. Measurements of the charge exchange cross sections of various multicharged ions were continued for collision velocities less than 10^8 cm/sec. In general, no scaling relationship with ion charge was found, nor was there a strong velocity dependence of the cross sections. A laser ion source was further developed for the production of multiply charged ions with energies of 1 keV. Operation of the Controlled Fusion Atomic Data Center continued, with emphasis on data compilations of plasma impurity cross sections, sputtering, and particle reflection from surfaces.

4.1 EXCITED-STATE CONTRIBUTION TO THE ELECTRON LOSS COLLISIONS OF A FAST H^0 BEAM ON N^{3+} IONS

Our crossed-beams experiment designed to measure total electron loss cross sections by H^0 in collision with various multiply charged plasma impurity ions utilizes a fast H^0 beam obtained by passing energy-analyzed protons through a neutralizer cell. Because such a neutral beam is known to contain a small, but finite, amount of excited atoms in various excited states n with relative population P_n and because the cross sections σ_n increase rapidly with n, the values of P_n are needed to deduce σ_n from the measured apparent cross section σ_A, which is a sum of products $P_n\sigma_n$ of all contributing states. Figure 4.1 shows the measured σ_A for 40-keV H^0 on N^{3+} as a function

---

1. Physics Division.
2. Participant from the Joint Institute for Laboratory Astrophysics, Boulder, Colorado.
3. Consultant, Queen's University of Belfast, Belfast, Northern Ireland.
4. Summer student, University of Wisconsin, River Falls, Wisconsin.
5. Participant from the University of Aarhus, Aarhus, Denmark.
6. Consultant, Georgia Institute of Technology, Atlanta, Georgia.
7. Consultant, California State Polytechnic University, Pomona, California.
8. Consultant, Wesleyan University, Middletown, Connecticut.

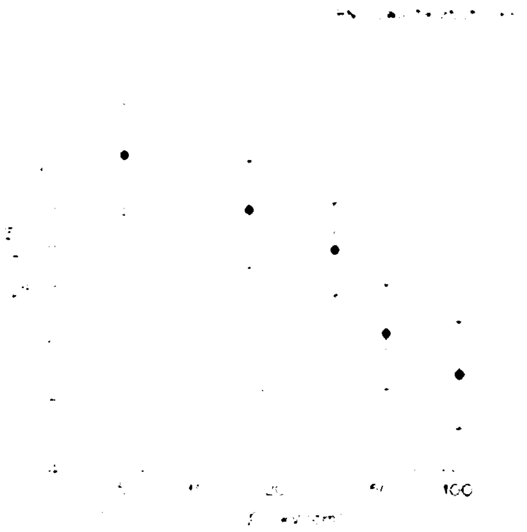

Fig. 4.1. Apparent cross section σ_A vs ionized field strength E.

of a transverse electric field applied to the H^0 beam prior to the interaction region. Because the high H^0 Rydberg states are ionized and attenuated by the electric field, σ_A decreases with increasing field, as illustrated in Fig. 4.1. The populations P_n were determined from auxiliary experiments in which the intensity of the H^0 beam transmitted through the ionizing field was measured for a range of field strengths E. Shown in Fig. 4.2 are the measured transmissions vs $E^{1/2}$ for a 40-keV H^0 beam. The fact that the transmission is linear in $E^{1/2}$ implies that $P_n = a/n^3$, where a is a normalization constant, [illegible] for this particular case. Incorporation of the above relation between P_n and n into the data analysis indicates that the present results are inconsistent with the σ_n [illegible] theoretical prediction but that σ_n varies more nearly as the geometric cross section, which varies as n^4.

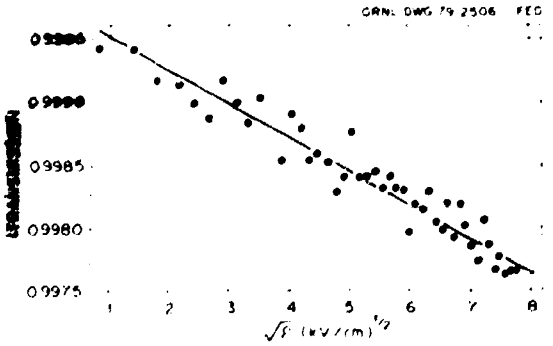

Fig. 4.2. Transmission of 40-keV H^0 high Rydberg states as a function of $E^{1/2}$.

4.2 ELECTRON IMPACT IONIZATION OF MULTICHARGED IONS

Cross sections have been measured for electron impact ionization of a number of multiply charged ions employing a crossed-beams apparatus. After the first reported measurements[3] for C^{3+} and N^{4+}, the apparatus was improved to extend the upper energy limit to 1500 eV and to reduce scattered photons that interfere with the measurement of the ionization signal. Cross sections have now been measured for B^{3+}, $C^{(3,4)+}$, $N^{(3,4,5)+}$, $O^{(3,4,5)+}$, and Ar^{4+}.

For helium-like ions B^{3+}, C^{4+}, and N^{5+}, the semiempirical formula by Lotz[4] and the scaled Coulomb-Born calculations of Golden and Sampson[5] agree with the measurements to within experimental uncertainties (roughly ±10%) at all energies. However, the present measurements for these ions are lower than those computed using a classical binary encounter theory.[6]

The measured cross sections for lithium-like ions C^{3+}, N^{4+}, and O^{5+} do not agree so well with theoretical estimates.[4–8] For the lithium-like ions, the most important feature of the ionization cross sections is the finding that inner-shell excitation followed by autoionization contributed significantly to total ionization.[9] Figure 4.3 shows the results for N^{4+}, where a second peak beginning abruptly at 420 ± 5 eV is attributed to the excitation $e^- + N^{4+}(1s^2 2s) \rightarrow e^- + N^{4+}(1s2s2\ell)$, where ℓ = s or p. The excitations of states $(1s2s^2)\,^2S$ at 413 eV and $(1s2s2p)\,^4P$ at 416 eV and two states $(1s2s2p)\,^2P$ at 423 and 429 eV have recently been

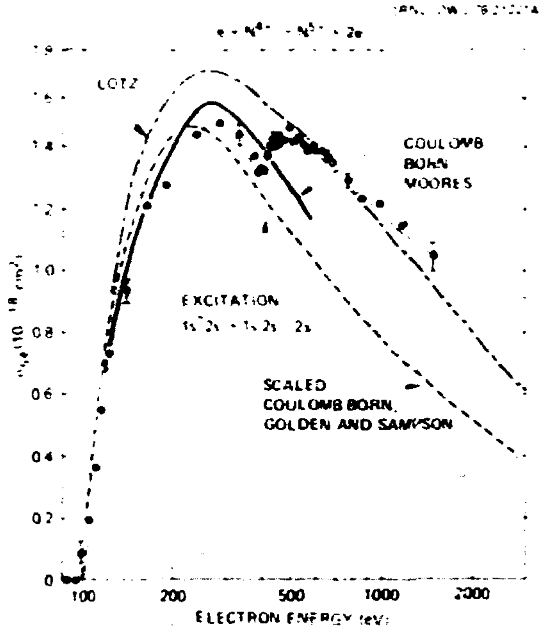

Fig. 4.3. Cross section for electron impact ionization of N^{4+} showing comparison of present experimental results with various theoretical estimates and illustrating the contribution of excitation-autoionization.

calculated by Henry[illegible] in a six-state, close-coupling quantum formalism. The sum of these excitation cross sections predicts a rise in the ionization, which agrees with our measurements to within 25% at 456 eV. For C^{3+}, excitation cross sections recently tabulated by Magee *et al.*[11] for the $1s^22s \rightarrow 1s2s2p$ transitions predict a rise in ionization in even better agreement with our experiment.

An important observation from the data on lithium-like ions is that the relative contribution of excitation-autoionization increases with increasing nuclear charge along the isoelectronic sequence: for O^{5+} the second peak (excitation-autoionization) is larger than the first (direct) peak; for N^{4+} (Fig. 4.3) the two peaks are equal; and for C^{3+} the first (direct) peak is larger. Thus, for higher members of the sequence, the excitation contribution to total ionization may dominate. This process is likely in other isoelectronic sequences as well (such as sodium-like ions[12]), and the effects of excitation-autoionization on the ionization balance of high temperature plasmas need further investigation.

The cross-section measurements for ions of other electronic configurations also exhibit interesting features. Excitation-autoionization peaks are observed for O^{4+} (see Fig. 4.4 at 550 eV) and Ar[illegible]. For beryllium-like ions O^{4+} and N^{3+}, the beam is apparently about 50% ground-state ions $(1s^22s^2)$ ^1S and about 50% metastable ions $(1s^22s2p)$ ^3P, as determined by a detailed measurement of the threshold behavior of ionization, which can occur at energies a few eV lower for the metastable states than for the ground state. Figure 4.4 shows the cross section for ionization of our mixed-state beam of O^{4+} and compares it with scaled Coulomb-Born and Lotz formula calculations for a 50-50 mixture of ground-state and metastable ions. The beryllium-like ions O^{4+} and N^{3+} are interesting because the cross sections are higher than predicted by the best theory (Coulomb-Born) and because there is an unusually large fraction of metastables in the beam. It is expected that metastable states of beryllium-like ions will be highly populated in most plasmas. The role of metastables in plasma processes needs further

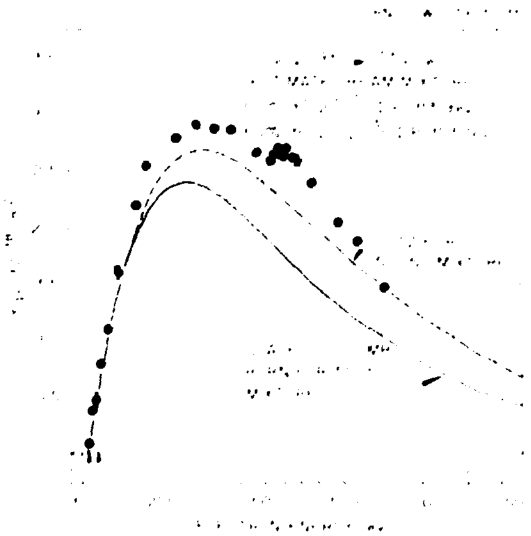

Fig. 4.4. Cross section for electron impact ionization of O^{4+}. For this case the beam contains an unusually high fraction of metastable ions, and the discrepancy with Coulomb-Born predictions is significant.

clarification, and present results can improve the understanding of metastable content and collisional behavior in plasmas.

4.3 ELECTRON IMPACT EXCITATION OF N^{4+}

Measurements of excitation of multicharged ions have continued, employing a crossed-beams apparatus in which a monoenergetic electron beam is crossed by an ion beam obtained from the Penning Multicharged Ion Source (ORNL-PIG) located in the Physics Division. A collaborative effort with the Joint Institute for Laboratory Astrophysics, these measurements are intended to test the developing collisional excitation theories and are directly applicable to understanding photon emissions from high temperature fusion and astrophysical plasmas.

Results for the excitation of C^{3+} ($1s^2 2s \rightarrow 1s^2 2p$) were reported previously[13] and have good agreement with recent theory. As a further test of the theory, the measurements have been extended to the next member of the lithium isoelectronic sequence, N^{4+}. Figure 4.5 compares the N^{4+} results with the close-coupling calculations of Van Wyngaarden and Henry[14] in the most critical near-threshold region. For N^{4+} the agreement of experiment and theory is well within experimental uncertainty, confirming the reliability of theory for predicting excitation cross sections. We now expect that quantum theory can predict the cross sections accurately for resonance lines of lithium-like ions. For other electronic configurations (for example, beryllium-like ions), theoretical computations may not be as reliable; thus, our future measurements will be extended to B^+, C^{2+}, and N^{3+}.

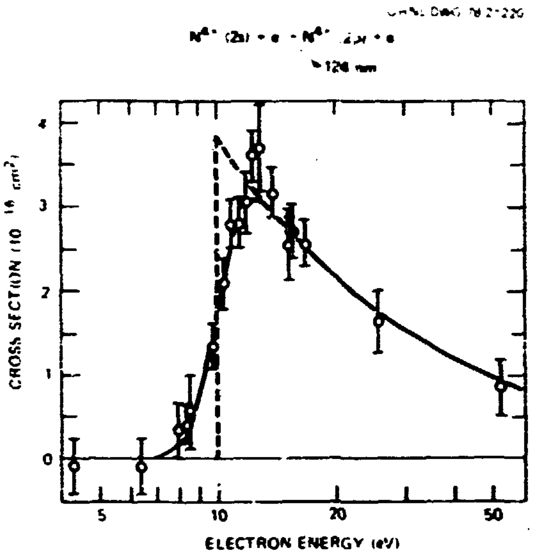

Fig. 4.5. Electron impact excitation of N^{4+}. The dashed line is the theory of Van Wyngaarden and Henry (Ref. 14), and the solid line is the same theory folded with the experimental energy spread. The solid data point is the present absolute measurement, and open data points are measured relative to that. Error bars are 90 confidence level, counting statistics.

4.4 LOW ENERGY MEASUREMENTS OF ELECTRON TRANSFER FROM HYDROGEN ATOMS AND MOLECULES TO MULTICHARGED IONS

Measurements of total cross sections for electron capture by various multicharged ions in atomic and molecular hydrogen at velocities below 10^7 cm/sec have continued, using the ORNL-PIG ion source. Although charge transfer processes at such energies are important in plasma diagnostics and modeling, they have proven difficult to evaluate theoretically because the electrons associated with the interacting ion-atom system have sufficient time to adjust during the collision, thus requiring a quasi-molecular approach to the scattering.

To provide a systematic data basis against which theoretical approaches might be evaluated, we have concentrated our measurements on light ions of the hydrogen, helium, and lithium isoelectronic sequences.[15] From the data some characteristics of the cross-section behavior for such processes have emerged.

(1) For ions of initial charge $q \leq 3$, the cross sections are strongly dependent on the particular ionic species whereas

for q [illegible] 3, the cross sections tend to be large (~10^{-15} cm^2) and relatively species independent.

(2) No uniform scaling laws with q are evident in this velocity range, unlike the situation at higher velocities, where a nearly uniform power-law increase with q is observed.[illegible]

(3) Also, unlike higher velocity behavior, no general or strong velocity dependence of the cross sections is observed.

The magnitudes and velocity dependences of the cross sections are influenced strongly by details of the potential energy curves describing the quasi-molecule that is formed during the collision, especially for q [illegible] 3, where the electron is thought to be captured into already partially filled electron shells.

Measurements are currently being extended to heavier ions such as argon, xenon, and iron and over a wider range of charge states in order to provide further insight into the electron transfer process at even lower collision velocities and higher ion charge states.

4.5 LASER ION SOURCE

After an initial feasibility study,[illegible] work has continued on the development and utilization of the pulsed laser ion source. The transient plasma produced when a pulsed CO_2 laser beam is focused in vacuum onto a solid surface has provided a source of highly ionized ions at relatively low energies (less than a few keV). An ion beam was collimated from the plasma blowoff normal to the target surface. Isolation and identification of ions with different charge-to-mass ratios were accomplished by a combination of time-of-flight and electrostatic analysis. Fully stripped carbon ions at 1 keV have been detected for focused laser power densities of $8 \times 10^{[illegible]}$ W/cm^2 incident on a graphite target.

A CAMAC-based transient data acquisition system was implemented to facilitate development of the ion source and its application to measurements of cross sections for electron capture by fully and highly stripped carbon and iron ions in collisions with gases at energies below 2 keV.

4.6 CONTROLLED FUSION ATOMIC DATA CENTER

The evaluating and editing of our indexed bibliography of atomic and molecular processes for the period 1950-75 have been completed with the addition of new data and the correction of errors in existing data sets. Copies of this bibliography were sent to ten laboratories in the United States and abroad, and magnetic tapes of the file were supplied to the International Atomic Energy Agency (IAEA) for use in publishing a comprehensive bibliography composed of data from several countries. Final editing is in progress for our 1976-77 and 1978 bibliographies, which will receive similar distribution. Searches of 1979 reference data are being received and processed on a current basis.

To facilitate creating and manipulating bibliographical data files, a new computer code was brought on-line January 1978. The new code implements an up-to-date, more universal data format that is compatible with the Oak Ridge Computerized Hierarchical Information System (ORCHIS), developed by the Oak Ridge National Laboratory (ORNL) Computer Sciences Division; this permits convenient and straightforward file management. Data entry is on-line in an interactive environment in which each entry is prompted, checked for certain classes of errors, and expanded in the case of coded responses used for repetitive fields. Hardware for the system includes a Hewlett-Packard 264[illegible]A video display terminal and a DECWRITER III high speed digital printer.

Four indexed bibliographies of primary use to fusion research have been published as ORNL reports. These cover the period 1950-75 and include molecular dissociation, atomic and molecular excitation, electron transfer, and ionization and stripping (ORNL-5500, -5501, -5502, and -5503).

The two-volume *Atomic Data for Controlled Fusion Research* is being updated with the revision of previous data and the addition of new sections on sputtering, particle reflection, and ion trapping. A third volume, in progress, emphasizes those atomic collisions involving impurities found in high temperature plasmas. A computer code using the DISSPLA graphics package has been written to generate production quality plots of the multiply charged ion cross-section data, using plot parameters specified in a data file that can be created under the text-editing program TECO. Data compilation has been completed for charge exchange of plasma impurity ions with H, H_2, and He. Other compilations in this volume include electron excitation and ionization of multicharged ions. For these processes the lack of sufficient experimental data to correlate with theory has created difficulties in presenting the data graphically. In an effort to compensate for this problem, we have prepared a full bibliography of relevant experimental and theoretical work to preface each section of data.

To make our evaluated data more compatible with the needs of plasma modeling, we have devised and implemented a computer program to convert cross sections to reaction rates for Maxwellian-Maxwellian as well as Beam-Maxwellian energy distributions. The new code produces publication quality output of the calculated rate coefficients in both tabular and graphical forms, as well as in the form of Tschebysheff polynomial fits to the calculated rates.

In cooperation with the Atomic Transition Probabilities Data Center of the National Bureau of Standards, we have continued publication of the bulletin *Atomic Data for Fusion*. As a supplement to our bimonthly issues, an author and subject index is produced annually. A recent survey of bulletin recipients indicates that the publication continues to serve as a useful information tool for fusion researchers.

REFERENCES

1. C. F. Barnett, J. A. Ray, and A. Russek, Phys. Rev. A 5, 2110 (1972).
2. I. C. Percival and D. Richards, "The Theory of Collisions Between Charged Particles and Highly Excited Atoms," pp. 1-82 in *Advances in Atomic and Molecular Physics*, Vol. XI, ed. by D. R. Bates and B. Bederson, Academic Press, New York, 1975.
3. D. H. Crandall, R. A. Phaneuf, and P. O. Taylor, Phys. Rev. A 18, 1911 (1978).
4. W. Lotz, Z. Phys. 216, 241 (1968).
5. L. B. Golden and D. H. Sampson, J. Phys. B. 10, 2229 (1977).
6. A. Salop, Phys. Rev. A 14, 2095 (1976).
7. D. L. Moores, J. Phys. B 11, L1 (1978).
8. A. Burgess, H. P. Summers, D. M. Cochrane, and R. W. P. McWhirter, Mon. Not. R. Astron. Soc. 179, 275 (1977).
9. D. H. Crandall, R. A. Phaneuf, B. E. Hasselquist, and D. C. Gregory, "Measured Cross Sections for Ionization of C^{3+}, N^{4+}, and O^{5+} Ions with Contributions due to Excitation-Autoionization," to be published in J. Phys. B.
10. R. J. W. Henry (Physics Department, Louisiana State University), private communication, 1979.
11. N. H. Magee, Jr., J. B. Mann, A. L. Merts, and W. D. Robb, *Electron Impact Excitation of Carbon and Oxygen Ions*, Los Alamos Scientific Laboratory Report LA-6691MS, Los Alamos, New Mexico (1977).
12. O. Bely, J. Phys. B 1, 23 (1968).
13. P. O. Taylor, D. Gregory, G. H. Dunn, R. A. Phaneuf, and D. H. Crandall, Phys. Rev. Lett. 39, 1256 (1977).
14. W. L. Van Wyngaarden and R. J. W. Henry, J. Phys. B 9, 1461 (1976).
15. D. H. Crandall, R. A. Phaneuf, and F. W. Meyer, Phys. Rev. A 19, 504 (1979).

16. F. W. Meyer, R. A. Phaneuf, H. J. Kim, P. Hvelplund, and P. H. Stelson, Phys. Rev. A 19, 515 (1979).
17. *Fusion Energy Division Annual Progress Report for the Period Ending December 31, 1977*, Oak Ridge National Laboratory Report ORNL-5405, pp. 124-125, Oak Ridge, Tennessee (1978).

5. PLASMA HEATING AND FUELING

H. H. Haselton, Section Head

J. E. Akins[1]
R. G. Alsmiller, Jr.[2]
G. C. Barber
W. R. Becraft[3]
C. W. Blue
A. Y. Broverman[4]
E. H. Bryant[4]
C. E. Bush[5]
J. T. Crow[6]
W. K. Dagenhart
R. C. Davis
L. J. Drooks[7]
H. F. Dunlap[4]
R. B. Easter[4]
P. H. Edmonds[5]
W. M. Fletcher[4]
A. T. Forrester[6]
J. W. Forseman[4]
C. A. Foster
T. A. Gabriel[2]
W. L. Gardner
P. Gelpi[4]
H. F. Glavish[8]
D. A. Goebel[6]
D. H. Gray[4]
J. Holdeman[7]
W. A. Houlberg[9]
H. C. Howe[9]
T. J. Huxford[4]
M. Iskra[9]
R. L. Johnson[4]
A. R. Kemp[4]
J. Kim
C. Knight[4]
R. A. Lillie[2]
R. V. Lunsford[4]
E. F. Marguerat[4]
J. A. Mayhall[4]
D. H. McCollough[7]
G. L. McDade[4]
R. W. McGaffey[7]
D. W. McNeill[10]
M. M. Menon
A. T. Mense[9]
R. W. Metzinger[11]
S. L. Milora
R. V. Miskell[4]
J. R. Moore[4]
C. E. Murphy[4]
G. F. Pierce[4]
M. S. Ponte
R. E. Potter
P. M. Ryan
T. L. Ryan[4]
R. T. Santoro[2]
D. E. Schechter
G. L. Schmidt[10]
S. W. Schwenterly
T. Shannon[4]
E. Slaughter[4]
S. J. Sosnowski[4]
D. O. Sparks
R. Stewart[4]
W. L. Stirling
P. A. Tabor[4]
J. B. Talbot[12]
C. E. Thomas[13]
C. C. Tsai
J. E. Warwick[4]
J. W. Watson[12]
J. H. Whealton
J. A. White[4]
P. W. Whitfield[4]
J. Wooten[7]
R. E. Wright

Abstract. The Plasma Technology Section is principally concerned with (1) development of multimegawatt neutral beam lines, including electrical systems and vacuum pumping, for plasma heating and (2) development of techniques to fuel the plasma using high velocity pellets.

In the area of pellet fueling, the pneumatic-type pellet injector was upgraded from a pellet velocity of 350 m/sec to 1000 m/sec with 1-mm-diam pellets. Injection experiments on the upgraded Impurity Study Experiment (ISX-B) showed that for 600-700-eV central plasma temperatures, the pellets can penetrate the entire plasma discharge and impact on the inner wall. When accompanied by neutral beam injection, the plasma remains quiescent and the pellet penetrates 20-30 cm into the discharge. A prototype centrifugal mechanical injector has been operated with 0.8-mm-diam pellets at a feed rate of 150 pellets/sec and has achieved pellet velocities of 290 m/sec.

In the neutral beam development program, two ISX-B injectors similar to those developed for the Princeton Large Torus (PLT) but with

---

1. University of Tennessee, Knoxville, Tennessee.
2. Engineering Physics.
3. General Electric Company.
4. UCC-ND Engineering.
5. Plasma Confinement Section.
6. University of California at Los Angeles, Los Angeles, California.
7. Computer Sciences Division.
8. Stanford University, Stanford, California.
9. Plasma Engineering Section.
10. Princeton Plasma Physics Laboratory, Princeton, New Jersey.
11. Draper Laboratory, Cambridge, Massachusetts.
12. Chemical Technology Division.
13. Student, Massachusetts Institute of Technology, Cambridge, Massachusetts.

BLANK PAGE

shaped extraction apertures were tested on the Medium Energy Test Facility (METF) before being installed on the tokamak. At extraction parameters of 42 kV and 61 A, 900 kW of H^0 was delivered to a 28-cm-diam target 4.1 m from the source; a record high 60% of the I x V extracted power was transmitted, including unneutralized ions. The last of the four PLT beam lines was delivered to Princeton Plasma Physics Laboratory (PPPL); 1 MW of neutral power from three Oak Ridge National Laboratory (ORNL) injectors raised the PLT plasma's ion temperature to 6.5 keV.

A 30-cm-grid-diam Poloidal Divertor Experiment (PDX) ion source has, in preliminary testing, extracted 110-A beams at 41 kV for 100-msec pulses. A lanthanum hexaboride hollow cathode, being developed for long pulse, low noise, high current operation, has been operated in a 30-cm PDX source with 1000-A discharge currents for 150-msec pulses. Novel diagnostics employed during the last year include the scioptlcon, infrared camera and the Fabry-Perot interferometer. The optical properties of a multiaperture, 80-120-kV tetrode source were studied; a total beam power (ions plus neutrals) of 80% of the extracted I x V power was transmitted to a target subtending 2°. Development of high voltage, high current switches, including a floating gradient grid modulator, was instrumental in carrying out this study. Extensive theoretical endeavors, in conjunction with experimental optics and transmission studies, were undertaken, as attested to by the 14 journal publications appearing since the beginning of the report period.

In addition, an energy recovery experiment based on the ORNL concept of transverse magnetic field electron blocking yielded preliminary recovery efficiencies of 60 ± 20%.

A modified 10-cm duoPIGatron has extracted up to 1 A of negative particles by means of H^+-to-H^- conversion on a cesiated surface. A modified calutron ion source, incorporating an efficient electron energy recovery system, has extracted H^- beams with a current density of 60 mA/cm².

Pumping studies were initiated for cryosorption surfaces in an energetic hydrogen environment, and tests were made of the pumping speed of two molecular sieves for a hydrogen/helium mixture. Monte Carlo simulations are now being used to help design vacuum pump chevrons.

5.1 PELLET FUELING

The pellet fueling program continued in the direction established in previous years, with a mix of pellet injector development work and experimental applications on ISX. The pneumatic-type injector[1] used on ISX-A[2] at 350-m/sec pellet velocity was upgraded to 1000 m/sec with 1-mm-diam pellets. The improved performance was obtained by increasing the launch tube length from 3.2 to 17 cm and the propellant working pressure from 10 to 30 atm. The performance scales according to a simple, idealized, unsteady expansion model.

A prototype centrifugal mechanical injector[3] has been operated with 0.8-mm hydrogen and deuterium pellets produced by a continuous high speed extrusion source. A feed rate of 150 pellets/sec was attained at pellet speeds of 290 m/sec. The performance of this device follows closely an idealized, frictionless acceleration process with pellets exiting the rotating arbor at nearly twice tip speed.

Pellet injection experiments are in progress on ISX-B at injection speeds in the range of 800-1000 m/sec with 1-mm hydrogen pellets ($Z = 4 \times 10^{19}$). For central plasma temperatures in the 600-700-eV range, pellets are observed to penetrate the entire plasma discharge and impact the inner vacuum wall. The plasma remains stable to major disruptions, but increased Mirnov oscillations ($m = 2$) are observed during injection. When accompanied by neutral beam injection (>500 kW), the plasma remains quiescent and pellets penetrate only 20-30 cm into the discharge.

5.2 NEUTRAL BEAM DEVELOPMENT

5.2.1 Ion Source Development

PDX prototype source

The neutral beam source for the PDX machine is essentially a scaled-up version of the PLT/ISX source,[4-6] designed to operate at 50-kV, 100-A levels for pulse lengths up to 500 msec (see Fig. 5.1). The anticipated neutral power per injector is 1.5 MW of H^0 to the machine located 4.5 m away subtending a half angle of 2° to the source.

The first type of extractor arrangement (type A) consists of 5-mm-diam cylindrical apertures on a 30-cm-diam grid pattern providing a geometric transparency of ∼50%. The source has been operated at arc currents exceeding 1200 A for the full 500-msec duration. Beam currents up to 110 A (at 41 kV) have been extracted for pulse lengths up to 100 msec. At 40-kV, 75-A level (optimum condition), the pulse length was extended up to 500 msec. The power transmission efficiency, based on measurements made on a ±2° target under optimum conditions, is ∼53%. Extraction grids using shaped apertures are now being investigated.

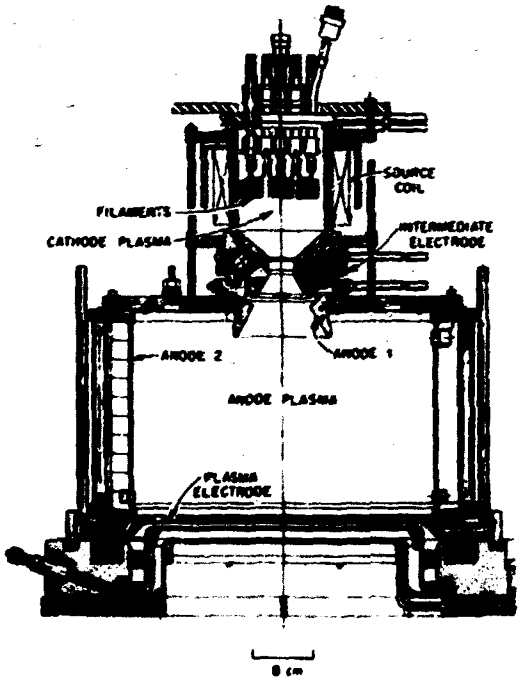

Fig. 5.1. PDX 100-A ion source with a 30-cm-diam extraction grid.

Hollow cathode

A lanthanum hexaboride hollow cathode similar to one operated by Goebel et al. at UCLA[7] was built and operated in several ORNL ion source configurations. This ORNL cathode assembly features an improved heater design that has much less tendency to sag. It has been operated as a direct replacement for the array of borium-oxide-coated filaments in a 30-cm, PDX-type ion source; it has operated satisfactorily up to a discharge current of ∼1000 A for ∼150-msec pulses.

It has also been operated at 300 A for pulses of 10-sec duration on a McKenzie bucket-type source.[8] The lanthanum hexaboride cathode offers the possibility of long life and high current operation for long pulse length ion sources in a variety of configurations for present and future neutral beam systems.

Negative ion sources

The negative ion program concentrated on small scale, proof-of-principle experiments employing the method of in-surface production of negative ions. Two experimental approaches were considered. The first is a modification of the duoPIGatron ion source (10-cm extraction grid diameter) by the addition of a system of cesiated vanes located immediately above the extraction grids on which positive ions from the discharge impinge[9] (see Fig. 5.2). The ions are assumed to be converted to negative ions with a 20-50% probability. Also located in this region is a transverse magnetic field that impedes the flux of electrons to the extraction grids. A summary of results is

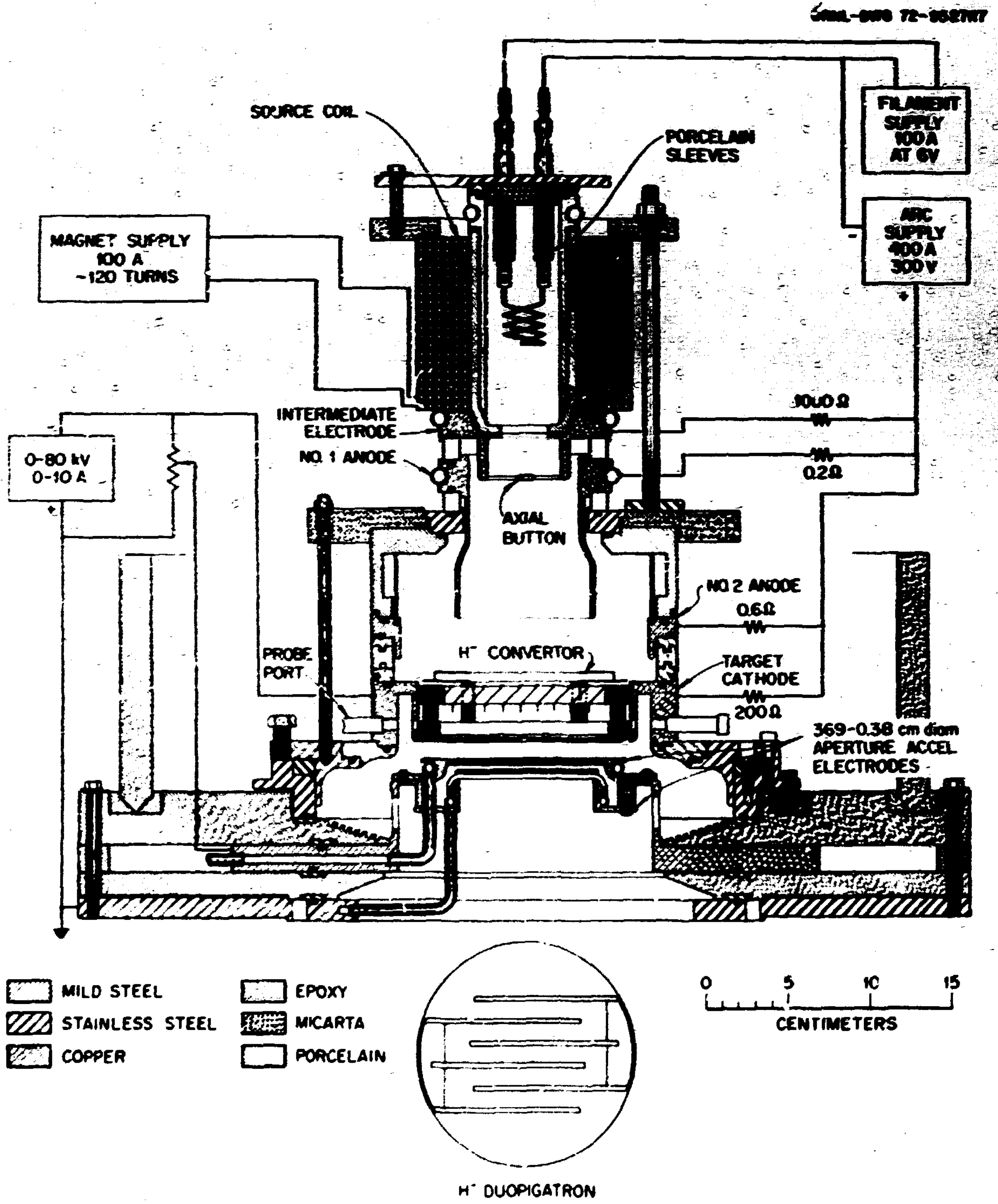
ORNL-DWG 72-
SOURCE COIL
PORCELAIN SLEEVES
FILAMENT SUPPLY 100 A AT 6V
ARC SUPPLY 400 A 300 V
MAGNET SUPPLY 100 A ~120 TURNS
INTERMEDIATE ELECTRODE
NO. 1 ANODE
AXIAL BUTTON
1000 Ω
0.2 Ω
0-80 kV 0-10 A
NO. 2 ANODE
0.6 Ω
PROBE PORT
H⁻ CONVERTOR
TARGET CATHODE
200 Ω
369-0.38 cm diam APERTURE ACCEL ELECTRODES
MILD STEEL
STAINLESS STEEL
COPPER
EPOXY
MICARTA
PORCELAIN
0
5
10
15
CENTIMETERS
H⁻ DUOPIGATRON

Fig. 5.2. Modified duoPIGatron negative ion source, based on H^+-to-H^- conversion on a hot cesiated surface.

shown in Table 5.1. The main effort in this experiment is to analyze the electron and negative ion content of the extracted beam.

The second experiment for producing negative ions is one in which a calutron ion source has been modified[10] as shown in Fig. 5.3. A cesiated molybdenum surface (convertor) has been installed immediately behind the central discharge column. This surface is biased negative with respect to the discharge and, therefore, attracts positive ions and repels [illegible] the resulting negative ions that are produced. In contrast to the duoPIGatron, the ion extraction is transverse to the applied [illegible] extracted from [illegible]

Table 5.1. [illegible] duoPIGatron ion source preliminary performance

Arc discharge	Reliable operation [illegible] positive [illegible]
Duty cycle	Up to 1 pulse/s[illegible]
Pulse length	Up to 300 msec
Oven temperature	Up to ~450°C
Convertor temperature	<330°C
Extraction voltage	Up to 5 kV
Drain current	Up to 1 A
Electron suppression	Promising

[illegible] symmetric, [illegible] as well as a 3-D algorithm.[illegible] We examined single beamlet optics[16-20] and collective beamlet optics[21-25] for a wide variety of situations. The corroboration with experimental data[16-19,26,27] of these and previous[28-31] theoretical studies

ORNL-DWG 78-1107R2 FED

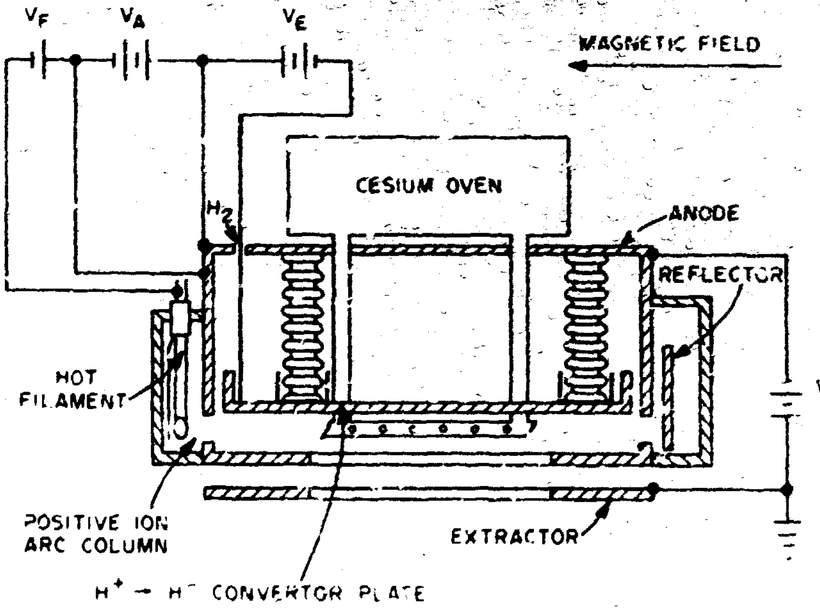

Fig. 5.3. Schematic diagram of the calutron Penning discharge negative ion source.

Table 5.2. Negative ion test facility

	Penning discharge – pulsed	Penning discharge – cw
Arc current	≥10 A	5 A
Arc volts	250 Vdc	200 Vdc
Accel volts	21 kV	21 kV
Accel current	200 mA	80 mA
Analyzed current (H^-)	60 mA/cm^2	30 mA/cm^2
Extraction slit	0.40 cm^2	0.40 cm^2
Pulse length	≥100 msec	>20 sec
Gas efficiency		4%
I_{e^-}/I_{H^-}		4
$\frac{\text{Power } (H^- \text{ ions})}{\text{Power (ions + electrons)}}$		86%
Impurity		≤3%

neatly divides itself into three classes of ascending utility: post mortum, delineation of cause and effect, and a priori prediction. Five predictions have been made. These are that (1) in a PLT source the shape of the beam distribution is dependent on perveance, with large tails mostly at low perveance;[32-34] (2) in a PLT source the rms angle is approximately 2°;[18] (3) tetrode steering is dependent on potential partition;[31] (4) a negative bias on the first electrode will improve beam divergence;[18] and (5) a positive bias on the first electrode will improve beamlet divergence.[20] Four of these predictions have been experimentally verified,[19,26,27] but the fifth one[20] remains untested. A manifestation of these predictions is that a substantial increase in the transmitted power efficiency of the PLT injectors was realized with the addition of a single wire that connected the plasma grid to the negative terminal of the arc supply.

5.2.3 Neutral Beam Line Development

High energy neutral beam sources

Following our two-stage, single beamlet optics studies,[16,19,35] efforts were directed towards understanding the performance of multiaperture, two-stage sources at energies exceeding 100 kV. The first such source, with an 18-cm grid pattern and a total grid column length of 2 cm (inclusive of grid thickness), was operated at voltages up to 80 kV and currents up to 25 A. The performance of the source was studied by varying the parameters, viz., perveance of the extraction gap and the accel gap-to-extraction gap field ratio. The results show (Fig. 5.4) that impressive transmission efficiencies can be achieved at accel-to-extraction field ratios exceeding unity. However, it is also clear that from a practical point of view, the field ratio has to be limited to obtain a compromise between good beam optics and high current density. Experiments using a second source with a 3.2-cm-long grid column at energies up to 120 kV showed that the larger column length gives rise to significantly higher grid loadings (Fig. 5.5) due to increased beam and secondary interception. Minimizing the length of the total grid column is, thus, necessary for high current densities, lower grid loading, and operating flexibility.

Considering the need for operating these sources for pulse lengths of the order of

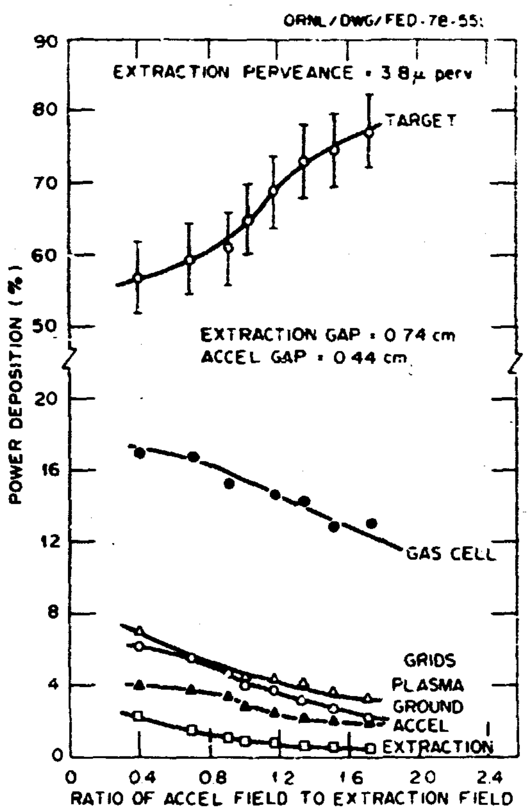

Fig. 5.4. Power deposition as a percentage of the extracted I x V power vs the accel-to-extraction field strengths ratio.

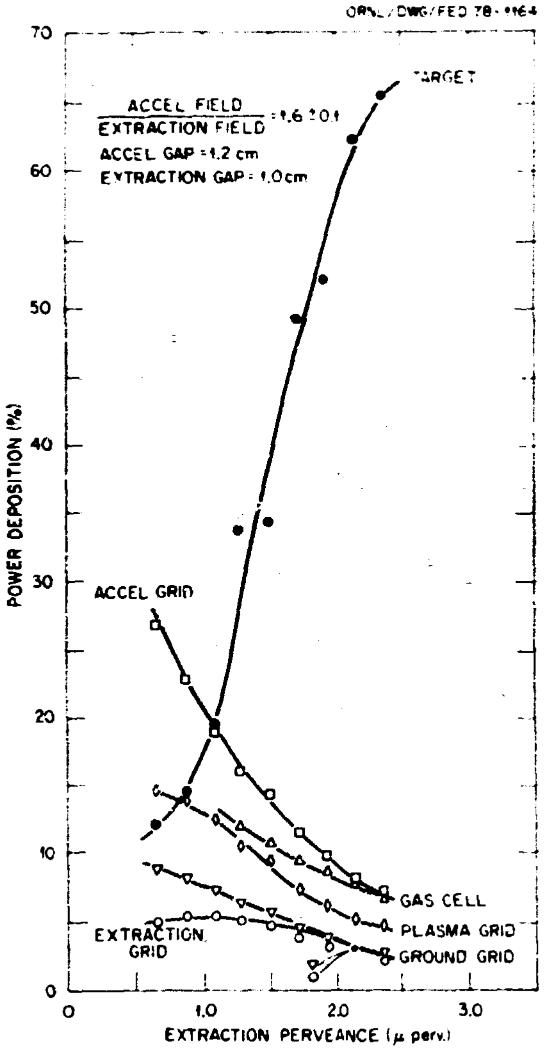

Fig. 5.5. Percentage of extracted I x V power deposited on beam line components as a function of extraction perveance.

seconds, a two-stage, 120-kV, 25-A source with rectangular grids (10 x 25 cm) and circular apertures has been designed. Design exercises involving higher voltages and currents are also being carried out.

5.2.4 Energy Recovery Experiment

An energy recovery experiment has been initiated at the METF using the concept of magnetic blocking of electrons along with grounded recovery electrodes encompassing a large solid angle.[36] The conventional beam line was modified such that the ion source is maintained at a small positive potential above earth ground by an accelerator boost supply while the exit grid and the gas cell are at high negative potential with respect to ground. Also, the gas cell was extended to the pole region of a conventional deflection magnet where electrons escaping the gas cell are allowed to E x B drift onto a biased collector with low energy loss. The fraction of unneutralized ions is deflected by the deflection/blocking magnet while undergoing retardation by the ground potential surroundings. The results are analyzed in terms of calorimetric power deposited on various parts of the beam line.

Following are the preliminary results of the energy recovery experiment.

[illegible]

been observed.

(2) A crude analysis of the calorimetric data indicates a recovery efficiency of [illegible].

(3) This arrangement has reduced the power-handling problem associated with removing the unneutralized beam.

5.2.5 Neutral Beam Systems

Injector development for ISX-B

Two PLT-injector-type duoPIGatron sources with shaped beam-forming apertures have been tested on the METF. The modification of the accelerator column has resulted in a 50% increase in the beam transmission efficiency from that of the straight-bore aperture. Maximum neutral beam powers achieved on a 28-cm-diam target located 4.1 m downstream from the source are 900 kW of H^0 at an accelerator power of 42 kV and 61 A and 1020 kW of D^0 at 43 kV and 55 A. Figure 5.6 provides an example of the distribution of beam power deposition along the beam line. Ion beam optical properties of the injectors were shown to be characterized by an optimum perveance of 6×10^{-6} $AV^{-3/2}$, which is approximately [illegible] of the beam current at a fixed [illegible] voltage of 40 kV. One of the injectors was installed on the West Beam Line of ISX-B and has injected neutrals into the torus.

PDX neutral beam system

The Poloidal Divertor Experiment (PDX) at Princeton Plasma Physics Laboratory (PPPL) is intended to have four operational neutral beam systems of ORNL design attached to it by early 1980. Each 4.5-m-long system will deliver 1.5 MW of neutral power (through a 30- by 34-cm rectangular aperture) to the PDX plasma for 0.5 sec. To achieve this injected neutral power, the Plasma Technology Section at ORNL is developing a scaled-up version of its successful PLT/ISX-B ion source. With an expected proton yield of 80%, this source is being designed to achieve reliable operating parameters of 50 kV and 100 A over a 0.5-sec pulse.

During this report period, a PDX prototype source achieved separately, because of facility limitations, each of the following parameters: 50 kV, 25 A, 0.05 sec; 45 kV, 100 A, 0.1 sec; and 40 kV, 80 A, 0.5 sec. Simultaneous achievement of these parameters awaits the completion of the PDX prototype

ORNL-DWG 79-2025 FED

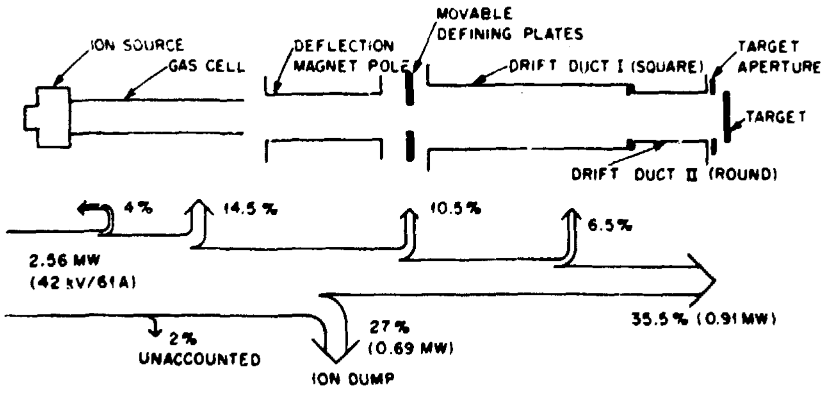

Fig. 5.6. Deposition of beam power along the ISX-B prototype beam line.

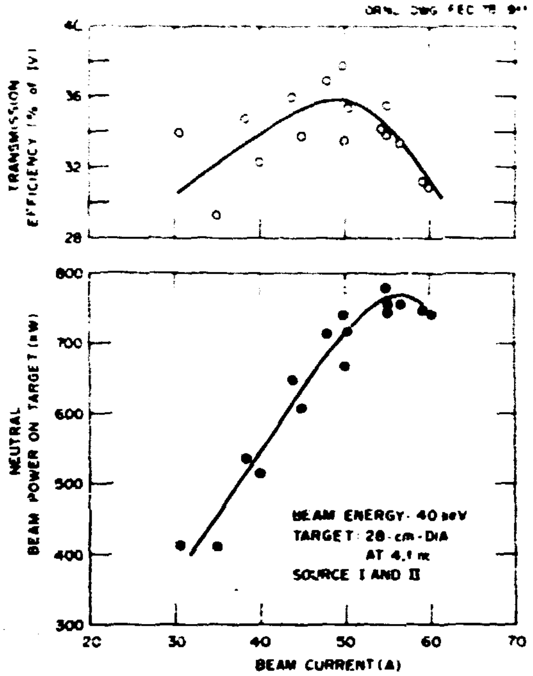

Fig. 5.7. Neutral beam power on target and transmission efficiency as a function of beam current for the ISX-B prototype beam line.

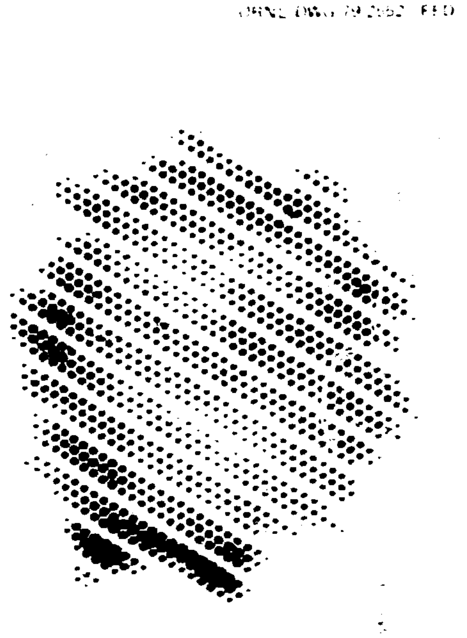

Fig. 5.8. Sciopticon image from a 22-cm PLT source with a 0.49-cm extraction gap. The smaller than normal gap spacing emphasizes the plasma density inhomogeneities resulting from the cusp field magnets.

beam line at the METF. Once reliable prototype source operation is achieved at the stated parameters with 1.5 MW of neutral power to the facility target, the Plasma Technology Section will complete fabrication and qualification of four duplicate sources for the PDX neutral beam systems.

5.2.6 Diagnostics

Sciopticon

The sciopticon, or pinhole camera,[illegible] has been used routinely on the PLT and ISX beam lines to examine the relative contribution of each beamlet to the total beam. The image density on a mylar sheet was seen to be proportional to the total number of incident particles. A typical result for a 22-cm ISX-B source is shown in Fig. 5.8.

Fabry-Perot interferometer

A Fabry-Perot interferometer was used to estimate the ion temperature of duoPIGatron and MacKenzie bucket ion sources by observing the Doppler broadening of H_{α} light emitted by atomic neutrals.[illegible] Both sources had a neutral temperature of ~0.35 eV. The Fabry-Perot interferometer was also used to measure the energy components of a neutral beam by the Doppler shift of the H_{α} emission from the energetic neutrals.[illegible]

Infrared camera[illegible]

The optics of neutral beams was studied with an AGA 680 infrared camera capable of operating in either a color-framing or a line-scanning mode. In the single line-scanning mode, the same line is continuously swept every 625 μsec.

In the first application, a 2-D rectilinear array of small (0.16-cm-diam) apertures was drilled in the beam stop target to allow beamlets of the incident neutral beam to create localized hot spots on a 0.5-mil-thick stainless steel screen located 2-3 cm behind the target. The back of the screen was viewed by the camera and was painted black in order to obtain a spatially uniform, readily determined emissivity whose value approached unity. The full 3-3 array of hot spots was scanned to obtain information about beam power uniformity; however, information from a single row of hot spots coincident with the diameter gave all the necessary time-resolved power and optics information. Figure 5.9 shows normalized comparisons between the temperature profile and a power profile obtained from a water-cooled, movable copper probe. The second application of the infrared camera was to view directly the front and back surfaces of the water-cooled, copper beam-stop target. Single line scanning of the back of the target yielded profiles similar to those in Fig. 5.9, whereas monitoring in the framing mode showed the effects of the cooling lines and their thermal contact with the target.

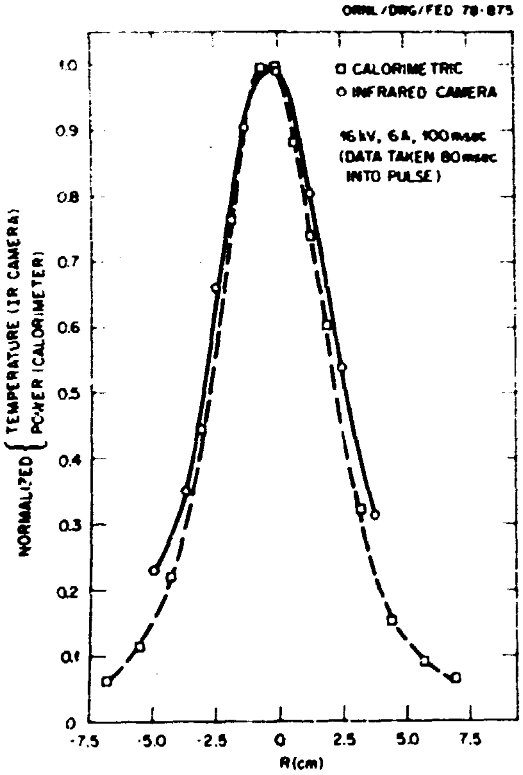

Fig. 5.9. Normalized temperature profile of the single-row target compared with the normalized power profile obtained by scanning the beam with a water-cooled calorimeter probe.

5.2.7 Electrical Technology Development

During 1978 significant increases were made in electrical equipment capability for ion source development.[illegible] These improvements include two new arc supplies capable of continuous operation and a new dual-tube modulator for development of a new generation of ion sources. In addition, a 1975 vintage modulator was modified to enable its output current to be increased by a factor of 2.

For the METF the old 800-A, pulsed duty arc supply was replaced by a new design capable of 1-MVA continuous output. The current rating is 5000 A, with provisions for front panel voltage adjustment from 0 to 200 V with an infinite range of pulse lengths up to continuous duty. Bus bar reconnections permit further flexibility of operation at double voltage, half current.

Concurrently, a dual-tube modulator capable of 80-kV, 100-A output to an ion source accelerating grid was built and installed. This METF upgrade work was done to support neutral beam injector development for the PDX project at PPPL. It also makes possible even higher power future developments at pulse lengths up to 20 sec.

For our High Power Test Facility (HPTF), a new 2500-A, 416-kVA continuous rated arc supply replaced the previous pulse-limited, 800-A unit. The accelerating grid modulator as originally designed consisted of three series-connected tetrodes for high voltage switching at 60 A. Because the preliminary PDX ion source design work required 100-A capability, the modulator was modified to allow reconnection of any two of the three floating decks in parallel. This work not only supports present ion source development up to 120 A, but it also makes possible the extension to pulse lengths of 20 sec. In addition, for future cost savings, the performance of the equipment demonstrates the feasibility of designing modulator decks using series-connected tubes for high voltage that can also be parallel-connected for high current.

5.3 VACUUM COMPONENTS DEVELOPMENT

5.3.1 Beam Line Cryosorption Pump

The 2-m^2 inlet area cryosorption pump,[46] originally ordered from Excalibur Corporation of Waltham, Massachusetts, is now being completed in-house, and Excalibur has been released from its contract obligation. The sorption panels, outer vacuum canister, and cryogen transfer assemblies are finished. An oil-free helium compressor package for the pump cooling system was built up and tested, and the helium supply piping was installed on the METF platform.

5.3.2 Energetic Particle Pumping[47]

In order to test cryosorption pumps with the high energy hydrogen particles encountered in divertor and beam line environments, a small cryosorption pump was borrowed from Los Alamos Scientific Laboratory (LASL). It has two chevrons at 80K and 15K to intercept thermal radiation, precool incoming gas, and trap contaminants. The pump maintains pressures in the mid-10^{-4}-Torr range with ion pulses from a 10-cm source. Ion pulses 100-msec long with energy and current up to 60 eV and 1 A have been injected into the pump at the rate of 5 pulses/min with virtually no observable differences from the pressure pulses obtained with gas alone.

5.3.3 Vacuum Engineering Data Studies

The variable panel and temperature cryostat described previously[46] has been used to obtain hydrogen pumping speeds for two molecular sieves. A comparison of the average pumping speed and temperature for 5-min runs on these two sieves is shown in Fig. 5.10 and is reported elsewhere.[48]

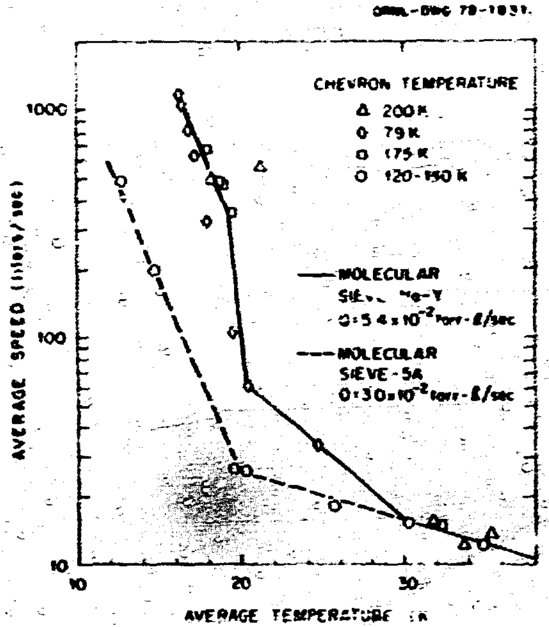

Fig. 5.10. Average pumping speed as a function of average temperature for 5-min runs for MS-5A and MS-Na-Y panels at comparable hydrogen feed rates.

It has previously been shown that cryosorption pumps utilizing a 5-A molecular sieve (MS-5A) at 4.2K cannot pump hydrogen/helium mixtures under conditions expected in plasma recovery systems.[49] Hydrogen condensed on the front of the panel blocks helium sorption. To circumvent this problem, a compound pump concept has been developed in which hydrogen is collected on a cryosorption or cryocondensation panel in front of the helium cryosorption panel. Figure 5.11 shows that admission of 4% hydrogen improves helium pumping performance and that as much as 10% hydrogen does not adversely affect it.

5.3.4 Monte Carlo Simulation of Neutral Particle Transport in a System Containing Cryogenic Pumping Surfaces

Some survey calculations were performed to demonstrate the applicability of a slightly modified version of the MORSE Monte Carlo radiation transport code[50] in simulating neutral particle removal from a system containing cryogenic pumping surfaces. Unlike

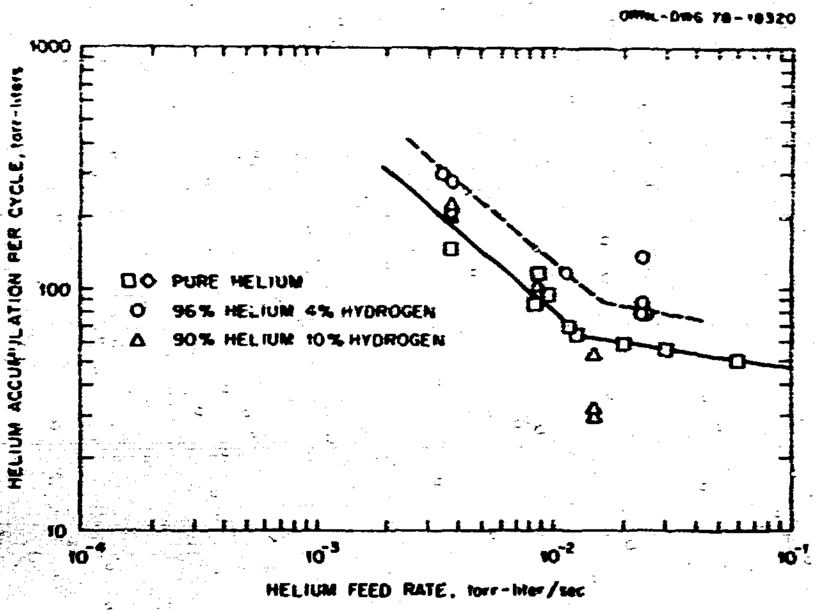

Fig. 5.11. Helium accumulation/cycle as a function of helium feed rate for hydrogen/helium mixtures on the Excalibur CVR 1106 cryosorption vacuum pump.

conventional radiation transport problems, cryogenic pump simulation requires an essentially media-free environment where particle/media interactions occur only at the surfaces of the various components within the cryogenic pump assembly. These interactions were easily treated by incorporating a variety of internal boundary conditions into an existing external boundary condition routine. Neutrals incident on a liquid-nitrogen-cooled component were assumed to reemerge with an outgoing angular direction density function equal to a cosine distribution about the component's surface normal. Those incident on the liquid-helium-cooled pumping panel were removed from the system by assuming a 0.9 sticking probability. The 10% that did stick were assumed to emerge at angles equally distributed within ±10% of 75° from the panel normal. For comparison, calculations were also performed assuming a 1.0 sticking probability on the pumping panel.

The primary components of the geometric model included a rectangular pumping chamber containing a horizontal pumping panel above which liquid-nitrogen-cooled, flat, vertical chevrons were placed to shield the panel from hot neutrals. The flow of neutrals into the chamber was simulated using both isotropic and normal source distributions along a large rectangular opening on one side of the chamber. The sides of the chamber were assumed to be cooled with liquid nitrogen.

A few of the results from the survey calculations are given in Table 5.3. The normal source distribution yields a slightly higher capture rate on the pumping panel and, thus, a higher pumping efficiency than the

Table 5.3. Neutral capture on pumping panel

Source distribution	Neutral captured/entering neutral	
	S.P.[a] = 0.9	S.P. = 1.0
Normal	0.67 (1.6)[b]	0.67 (1.7)
Isotropic	0.54 (1.2)	0.54 (1.4)

[a] Sticking probability on pumping panel.

[b] Numbers in parentheses denote one standard deviation in percent.

isotropic source. The zero change in efficiency associated with the 10 change in the pumping panel sticking probability indicates, at least for the design considered here, that the sticking performance of the pumping panel is not a dominating factor in overall pumping efficiency.

REFERENCES

1. S. L. Milora and C. A. Foster, Rev. Sci. Instrum. 50, 482 (1979).
2. S. L. Milora, C. A. Foster, P. H. Edmonds, and G. L. Schmidt, Phys. Rev. Lett. 42, 97 (1979).
3. C. A. Foster and S. L. Milora, *Proc. Fusion Fueling Workshop*, p. 117, 1978.
4. W. L. Stirling, C. C. Tsai, and P. H. Ryan, Rev. Sci. Instrum. 48, 533 (1977).
5. W. L. Stirling, C. C. Tsai, H. H. Haselton, D. E. Schechter, J. H. Whealton, W. K. Dagenhart, R. C. Davis, W. L. Gardner, J. Kim, M. M. Menon, and P. M. Ryan, "Properties of an Intense 40 kV Neutral Beam Source," to be published in Rev. Sci. Instrum.
6. C. C. Tsai et al., Bull. Am. Phys. Soc. 23, 748 (1978).
7. D. M. Goebel, J. T. Crow, and A. T. Forrester, Rev. Sci. Instrum. 49, 469 (1978).
8. D. E. Schechter et al., Bull. Am. Phys. Soc. 23, 747 (1978).
9. C. C. Tsai, W. L. Stirling, and R. C. Davis, *Proc. Symp. on the Production and Neutralization of Negative Hydrogen Ions and Beams*, p. 340 (1978).
10. W. K. Dagenhart et al., Bull. Am. Phys. Soc. 23, 805 (1978).
11. J. H. Whealton, E. F. Jaeger, and J. C. Whitson, J. Comput. Phys. 27, 333 (1978).
12. J. C. Whitson, J. Smith, and J. H. Whealton, J. Comput. Phys. 28, 408 (1978).
13. J. C. Whitson, J. H. Whealton, E. F. Jaeger, J. Smith, and R. W. McGaffey, *2D Cylindrically Symmetric Convergent Ion Optics Code Including Plasma Electrons*, Oak Ridge National Laboratory Report ORNL/TM-6512, Oak Ridge, Tennessee (1978).
14. L. J. Drooks, J. W. Wooten, R. W. McGaffey, D. H. McCollough, and J. H. Whealton, Bull. Am. Phys. Soc. 23, 846 (1978).
15. L. J. Drooks, D. H. McCollough, R. W. McGaffey, J. H. Whealton, and J. W. Wooten, *QUARTZ: A Numerical Simulation of an Asymmetric Electrostatic Accelerator*, Oak Ridge National Laboratory Report ORNL/TM-6740, Oak Ridge, Tennessee (1979).
16. J. Kim, J. H. Whealton, and G. Schilling, J. Appl. Phys. 49, 517 (1978).
17. J. H. Whealton and C. C. Tsai, Rev. Sci. Instrum. 49, 495 (1978).
18. J. H. Whealton, L. R. Grisham, C. C. Tsai, and W. L. Stirling, J. Appl. Phys. 49, 3091 (1978).
19. W. L. Gardner, J. Kim, M. M. Menon, and J. H. Whealton, Rev. Sci. Instrum. 49, 1214 (1978).
20. J. H. Whealton and J. C. Whitson, "Extraction of Aberrationless High-perveance Ion Beams from a Quiescent Equilibrium Plasma," to be published in J. Appl. Phys.
21. J. H. Whealton, Appl. Phys. Lett. 32, 353 (1978).
22. J. H. Whealton, Rev. Sci. Instrum. 49, 869 (1978).
23. J. H. Whealton, Appl. Phys. Lett. 33, 697 (1978).
24. J. H. Whealton and W. L. Gardner, Bull. Am. Phys. Soc. 23, 747 (1978).
25. J. H. Whealton, *Beam Distributions for Focussed Sources*, Oak Ridge National Laboratory Report ORNL/TM-6421, Oak Ridge, Tennessee (1978).
26. J. H. Whealton, C. C. Tsai, W. K. Dagenhart, W. L. Gardner, H. H. Haselton, J. Kim, M. M. Menon, P. M. Ryan, D. E. Schechter, and W. L. Stirling, Appl. Phys. Lett. 33, 278 (1978).
27. M. M. Menon, W. K. Dagenhart, R. C. Davis, W. L. Stirling, H. H. Haselton, J. Kim,

P. M. Ryan, D. E. Schechter, C. C. Tsai, and J. H. Whealton, "Power Flow Along a 40-kV Multimegawatt Neutral Beam Line," to be published in J. Appl. Phys.

28. J. Kim and J. H. Whealton, Nucl. Instrum. Methods 141, 187 (1977).
29. J. H. Whealton, E. F. Jaeger, and J. C. Whitson, Rev. Sci. Instrum. 48, 829 (1977).
30. L. R. Grisham, C. C. Tsai, J. H. Whealton, and W. L. Stirling, Rev. Sci. Instrum. 48, 1037 (1977).
31. J. H. Whealton, Rev. Sci. Instrum. 48, 1428 (1977).
32. J. H. Whealton, *Proc. Annual Controlled Fusion Theory Conference*, p. I 14 (1977).
33. J. H. Whealton and J. C. Whitson, Bull. Am. Phys. Soc. 23, 151 (1978).
34. J. H. Whealton, "Beam Distribution," paper presented at the IAEA Workshop on Neutral Injectors, Culham, England, June 26-30, 1978.
35. J. Kim, W. L. Gardner, and M. M. Menon, Rev. Sci. Instrum. 50, 201 (1979).
36. W. L. Stirling et al., Bull. Am. Phys. Soc. 23, 747 (1978).
37. J. Kim et al., Bull. Am. Phys. Soc. 23, 746 (1978).
38. P. M. Ryan, R. C. Davis, W. L. Stirling, and C. C. Tsai, Bull. Am. Phys. Soc. 20, 1365 (1975).
39. *Thermonuclear Division Annual Progress Report for the Period Ending December 31, 1975*, Oak Ridge National Laboratory Report ORNL-5154, pp. 121-123, Oak Ridge, Tennessee (1976).
40. W. L. Stirling, P. M. Ryan, C. C. Tsai, and K. N. Leung, Rev. Sci. Instrum. 50, 102 (1979).
41. D. H. McNeill and J. Kim, "High-resolution Spectroscopic Measurements on Neutral Beams and Ion Sources," paper to be presented at the IEEE Int. Conf. on Plasma Science, Montreal, Canada, June 4-6, 1979.
42. P. M. Ryan, C. E. Bush, R. C. Davis, W. L. Stirling, and C. C. Tsai, Bull. Am. Phys. Soc. 23, 904 (1978).
43. G. C. Barber et al., *Proc. 7th Symp. on Engineering Problems of Fusion Research*, p. 1564 (1977).
44. G. C. Barber et al., *Proc. 7th Symp. on Engineering Problems of Fusion Research*, p. 1142 (1977).
45. R. E. Wright, *Proc. 7th Symp. on Engineering Problems of Fusion Research*, p. 1579 (1977).
46. *Fusion Energy Division Annual Progress Report for the Period Ending December 31, 1977*, Oak Ridge National Laboratory Report ORNL-5405, pp. 139-140, Oak Ridge, Tennessee (1978).
47. S. W. Schwenterly, C. C. Tsai, R. C. Davis, and P. M. Ryan, Bull. Am. Phys. Soc. 23, 746 (1978).
48. J. S. Watson and S. D. Clinton (compilers), *Advanced Technology Section Semiannual Progress Report for the Period April 1, 1978 to September 30, 1978, Volume 2: Engineering Sciences Programs*, Oak Ridge National Laboratory Report ORNL/TM-6647/V2, Oak Ridge, Tennessee; to be published.
49. P. W. Fisher and J. S. Watson, "Helium Pumping at 4.2 K by Molecular Sieve 5A," to be published in J. Vac. Sci. Technol.
50. M. B. Emmett, *The MORSE Monte Carlo Radiation Transport System*, Oak Ridge National Laboratory Report ORNL-4972, Oak Ridge, Tennessee (1975).

6. SUPERCONDUCTING MAGNET DEVELOPMENT

P. N. Haubenreich, Manager, Large Coil Program
M. S. Lubell, Head, Magnetics and Superconductivity Section

J. E. Akin[1]
L. Alley, Jr.
J. K. Ballou
R. L. Brown
P. B. Burn[2]
W. D. Cain[3]
L. Dresner
D. S. Easton[4]
J. F. Ellis
W. A. Fietz
C. M. Fitzpatrick
W. M. Fletcher[5]
J. S. Goddard[5]
W. H. Gray
C. G. Hudson[6]
W. J. Kenney
J. P. Kois[3]
M. H. Kunselman[2]
P. S. Litherland[2]
C. J. Long[4]
J. C. Lottin[7]
J. W. Lue
J. N. Luton
T. L. Mann[2]
J. R. May[8]
R. A. Michelotti[2]
J. R. Miller
L. W. Nelms[6]
B. E. Nelson[2]
C. C. Queen[2]
J. P. Rudd
T. L. Ryan[7]
R. E. Schwall[9]
S. S. Shen
R. E. Stamps[2]
R. C. Stewart[6]
W. C. T. Stoddart[3]
P. B. Thompson[2]
W. H. Wagner
P. L. Walstrom
H. T. Yeh

Abstract. Three major U.S. equipment manufacturers, under CPFF (cost plus fixed fee) subcontracts to design and build one test coil each, spent the year in detailed design and in supporting verification tests. Japan and Switzerland joined EURATOM and the U.S. in an international agreement that will culminate in tests of a six-coil toroidal array at Oak Ridge National Laboratory (ORNL). Construction of the Large Coil Test Facility (LCTF) began with preparing the site, pouring the concrete base for the vacuum tank in Building 9204-1, and forming the tank sections, work done by a subcontractor.

The work of the Magnetics and Superconductivity (M&S) Section is divided into four areas: research and development activities (RDAC) in support of the Large Coil Program (LCP), advanced conductor development, the 12-T Coil Program, and magnet design projects. The primary emphasis during the past year has been the RDAC. Most of the facilities constructed have been for verification testing of superconductors in support of LCP subcontractors. Instrumentation, diagnostics, and protection have also made up a large part of the RDAC. Another area of work involving considerable interaction with subcontractors is coil fabrication technology.

The advanced conductor development work has concentrated on (1) bringing conductor force cooled by supercritical helium up to the same level of confidence as conductors cooled by boiling helium and (2) improving high field Nb_3Sn conductor.

The 12-T Coil Program started in FY 1979 as a supplement to the LCP. Its aim is the development of a conductor suitable for tokamak coils in which the maximum field is 12 T. The

---

1. Consultant.
2. Research Engineering Department, UCC-ND Engineering.
3. UCC-ND Engineering.
4. Metals and Ceramics Division.
5. Fusion Energy Electrical and Instrument Engineering Department.
6. ORNL (Y-12) Project Engineering Department, UCC-ND Engineering.
7. On leave from CEN/Saclay, Gif-sur-Yvette, France.
8. Grumman Aerospace Corporation.
9. Present address: Intermagnetics General Corporation, Guilderland, New York.

conductor will be tested in relatively small test coils in a 12-T background field.

We have also participated in a number of design projects, for example, the ELMO Bumpy Torus-II (EBT-II) project and the superconducting cyclotron, principally to carry out a conceptual design of superconducting magnets.

6.1 INTRODUCTION

ORNL has played a leading role in the development of superconducting magnets for toroidal fusion reactors since the initiation of work in this area in 1974. Presently the major effort is on the LCP, which has the objective of proving concepts and providing a data base for design decisions on the toroidal field (TF) coils for a tokamak Engineering Test Facility (EFT) in FY 1983. This entails designing, building, and testing different large 8-T coils in the LCTF at ORNL and performing supporting research and development. In addition to the LCP, ORNL is directing two projects involving industrial subcontractors in the design and development of a large conductor suitable for tokamak TF coils operable at fields to 12 T and in the design and fabrication of a 1-m coil to test the 12-T prototype conductor. ORNL is also advancing magnet technology in areas specific to fusion applications by developing better analysis capabilities and basic design information and by designing, procuring, and evaluating small quantities of conductor embodying advanced design concepts.

6.2 LARGE COIL PROGRAM

The scope and organization of the LCP are indicated by the work breakdown structure shown in Fig. 6.1. Progress was made in 1978 in all areas with the exception of LCTF operation, which is not due to start until 1980. Highlights of 1978 are summarized in Table 6.1.

Table 6.1. Large Coil Program highlights

February	LCTF vacuum vessel contract approved
February	LCTF construction begins
April	Japan signs IEA LCT Agreement
September	Switzerland signs IEA LCT Agreement
December	Contract let for first major component of test stand structure

6.2.1 Program Management

The program schedule in effect during 1978 is shown in Fig. 6.2. At the end of the year a revision of the schedule was under way to reduce FY 1980 costs to meet funding constraints. Major changes include deferring testing with pulsed field until all six coils are installed and stretching out coil and facility schedules by three to six months.

During 1978 the LCP staff, at the request of the Department of Energy (DOE), evaluated alternative ways of providing ETF designers with the option of 12-T TF coils. The recommendation, later implemented, was to supplement the LCP with the development of several types of conductor suitable for 12-T tokamak application (see Sect. 6.4).

The governments of Japan and Switzerland signed the International Energy Agency Agreement on a Program of R&D on Superconducting Magnets for Fusion and Annex I Large Coil Task (LCT) in April and September, respectively. (The U.S. and EURATOM signed in October 1977.) Meetings of the LCT Executive Committee and project technical officers from each participant were held in February and September. Useful exchanges took place on coil cooldown requirements and facility cryogenic system design. Supplemental agreements on the exchange of project information were reached, and progress was made on a definition of compulsory sections of the test

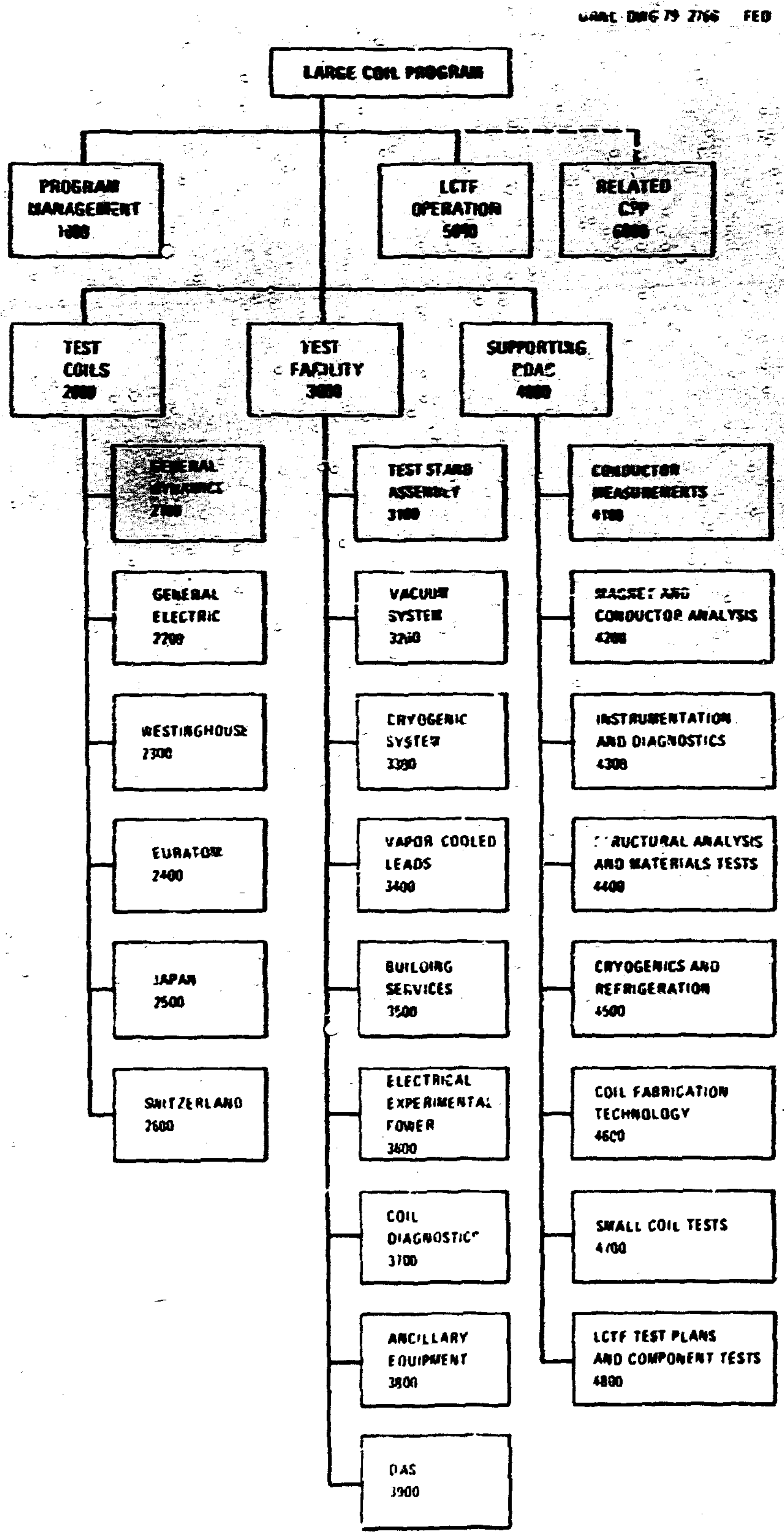
ORNL-DWG 79-2766 FED
LARGE COIL PROGRAM
PROGRAM MANAGEMENT 1000
LCTF OPERATION 5000
RELATED CTP 6000
TEST COILS 2000
TEST FACILITY 3000
SUPPORTING R&D 4000
GENERAL DYNAMICS 2100
GENERAL ELECTRIC 2200
WESTINGHOUSE 2300
EURATOM 2400
JAPAN 2500
SWITZERLAND 2600
TEST STAND ASSEMBLY 3100
VACUUM SYSTEM 3200
CRYOGENIC SYSTEM 3300
VAPOR COOLED LEADS 3400
BUILDING SERVICES 3500
ELECTRICAL EXPERIMENTAL POWER 3600
COIL DIAGNOSTICS 3700
ANCILLARY EQUIPMENT 3800
DAS 3900
CONDUCTOR MEASUREMENTS 4100
MAGNET AND CONDUCTOR ANALYSIS 4200
INSTRUMENTATION AND DIAGNOSTICS 4300
STRUCTURAL ANALYSIS AND MATERIALS TESTS 4400
CRYOGENICS AND REFRIGERATION 4500
COIL FABRICATION TECHNOLOGY 4600
SMALL COIL TESTS 4700
LCTF TEST PLANS AND COMPONENT TESTS 4800

Fig. 6.1. Work breakdown structure for the LCP.

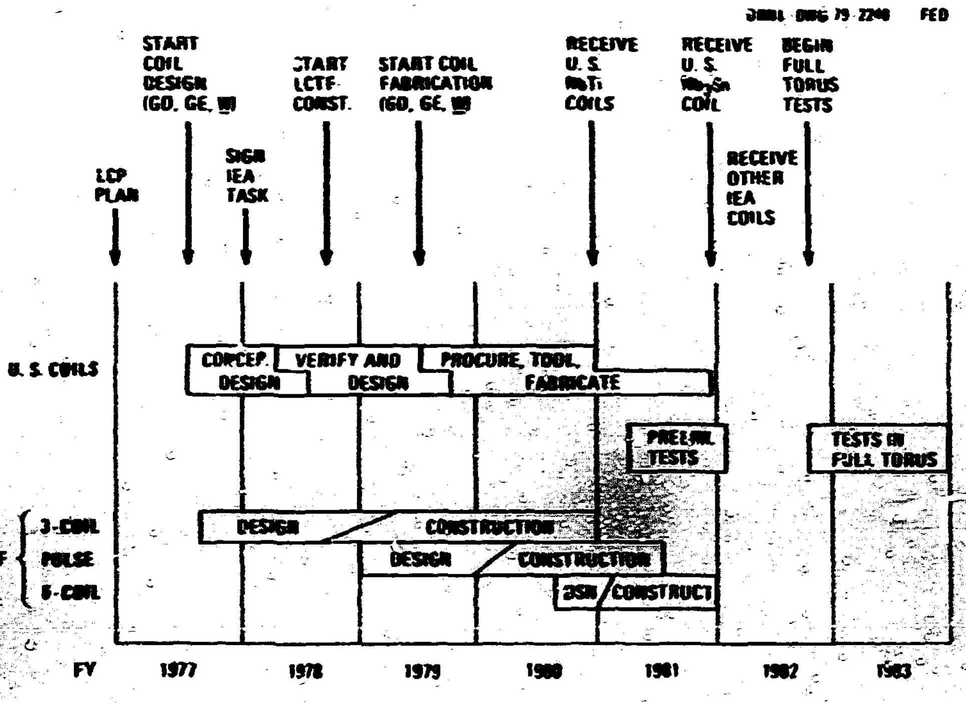

Fig. 6.2. Milestones and reference schedule for the LCP.

coil specifications. The three foreign programs are scheduled to deliver coils to ORNL between December 1981 and April 1982.

6.2.2 Test Coils

At the beginning of 1978, the three U.S. coil design teams [General Dynamics (GD) with Intermagnetics General Corporation (IGC), General Electric (GE) with IGC, and Westinghouse Electric with Airco] had just begun the second phase of their subcontracts: verification testing and detailed design. Substantial progress was made during the year, with most of the major technical questions being resolved. At the end of December, the fractions of Phase II effort completed were approximately as follows: GD, 90%; GE, 80%; and Westinghouse, 60%.

EURATOM supported two preliminary design studies, focusing primarily on coil structural analysis and design, by Siemens AG and Brown Boveri Company. The results, with those of the earlier conceptual design of the superconductor, were used by Kernforschungszentrum Karlsruhe to prepare a request for tenders from European industry for coil design and fabrication. The Japan Atomic Energy Research Institute organized a team involving six major industries and in September initiated an effort to produce a test coil design that would serve as a basis for competitive fixed-price proposals in 1979. The Swiss effort, under the direction of the Swiss Institute of Nuclear Studies and including the Federal Institute for Reactor Development and Brown Boveri Company, moved from preliminary studies into the design phase in the last quarter of 1978.

The principal features of the six test coils are summarized in Table 6.2. Although designed to meet the same performance specifications, the coils are diverse in internal design, reflecting independent approaches to the hitherto unresolved problems of such large coils. Three coils use bath cooling by boiling helium; three are cooled by forced flow of supercritical helium. One uses a Nb_3Sn conductor mounted in a unique bolted aluminum plate structure. The other five are

Table 6.2. LCP test coil features

	GD/Convair	General Electric	Westinghouse	EURATOM	Japan	Switzerland
Core bore (specified)	2.5 x 3.5 m	2.5 x 3.5 m	2.5 x 3.5 m	2.5 x 3.5 m	2.5 x 3.5 m	2.5 x 3.5 m
Peak field (design, specified)	8.0 T	8.0 T	8.0 T	8.0 T	8.0 T	8.0 T
Ampere turns (design)	6.65 x 10^6	6.98 x 10^6	7.36 x 10^6	6.62 x 10^6	6.76 x 10^6	6.6 x 10^6
Conductor current (design)	10,200	10,450	16,000	11,000	10,220	15,000
Conductor material	NbTi	NbTi	Nb_3Sn	NbTi	NbTi	NbTi
Conductor configuration	Flattened cable in extended-surface copper bar	16 subelements spiraled around copper core	Cable (insulated strands) in square conduit	22 subelements spiraled around CrNi core inside rectangular conduit	Flattened cable in rough-surface copper bar	Solder-filled cable surrounded by helium-filled copper cable in square conduit
Helium conditions	Pool boiling (4.2K, 1 atm)	Pool boiling (4.2K, 1 atm)	Supercritical forced flow	Supercritical forced flow	Pool boiling	Supercritical forced flow
Winding configuration	Edge wound in layers (14)	Flat wound in pancakes (7)	Laid in spiral grooves in 26 structural plates	Flat wound in pancakes (7)	Edge wound in pancakes (20)	Pancakes (12)
Structural material	304L stainless steel	316LN stainless steel	2219-T87 plates A286 bolts	Stainless steel similar to 316LN	304L stainless steel	Stainless steel similar to 316LN
Structure configuration	Fully welded case	Welded case with bolted closure	Grooved flat plates, bolted	Welded case with bolted or welded closure	Welded case with bolted side plate closure	Bolted case

similar in using NbTi conductors and a heavy stainless steel case for the structure but differ significantly in conductor and winding configuration. All appear practicable. It appears, therefore, that ETF magnet designers will be able to choose from among different coil designs on the basis of firm data on manufacturing costs and operating performance.

The coil specifications were revised in 1978 to incorporate information obtained during the conceptual design efforts. Principel changes had to do with structural analysis and diagnostic instrumentation of the coils.

Accurate prediction of stresses is essential to reliable operation and safe testing of coils under extended conditions. Specification changes were made to improve the accuracy and efficiency of the process of linking analyses of different parts of the complex structure of test stand and six different coils. ORNL analyzed a mathematical model of the complete array using stiffnesses projected from conceptual designs to generate a set of values for displacements and forces at interfaces under each prescribed test condition. Each coil design team then imposed the specified displacements on their coil model and calculated resulting stresses and forces. As a check on the different proprietary analysis programs being used, each team calculated a benchmark problem. Good agreement was found for the test case.

The test coils will incorporate temperature, voltage, and strain sensors for use in the protection systems and in the determination and analysis of the mechanisms (mechanical, thermal, and electromagnetic) that set practical limits on operability. Analysis of conceptual designs led to specification of sensors at critical points, with levels of redundancy appropriate for safety and data acquisition.

Important accomplishments by the U.S. coil teams during 1978 included verification of adequate heat transfer to boiling helium for the GD and GE conductors in various orientations and of acceptable pressure drop in the Westinghouse conductor. Manufacturing development included a strand insulation process by Westinghouse, a jacketing process by Airco, conductor winding and soldering by IGC, and practice winding by ORNL of a conductor similar to the GD and GE designs. Additional data on structural materials were obtained [from other programs sponsored by the Office of Fusion Energy (OFE)], and progress was made on the difficult structural design problems of the LCP coils.

As the work progressed, information being generated in the LCP by test coil verification testing and design was periodically summarized and disseminated to all participating organizations. There was continual interaction with other U.S. fusion magnet programs and ETF (formerly The Next Step) design teams, with mutually beneficial results.

6.2.3 Large Coil Test Facility

A subcontract with Pittsburgh-Des Moines Steel Company (PDM) for the design and construction of the 11-m-diam vacuum vessel was approved by DOE-ORO (Oak Ridge Operations) on February 28, 1978. Soon thereafter stainless steel plates procured earlier by ORNL were delivered to PDM. During the course of the tank design, UCC-ND revised the specifications to reduce the design pressure from 2.0 to 1.1 atm, simplifying the closure design. The contract was also revised to have the vacuum pumping system required for acceptance testing provided by UCC-ND instead of by PDM. By August design was virtually complete, but a protracted strike in a PDM plant delayed the forming of some of the tank sections; this work had not been completed by the end of the year.

Using drawings produced by UCC-ND, the on-site construction contractor, Rust Engineering, stripped the portion of Building 9204-1 to be occupied by the vacuum vessel, demolished interfering structure, excavated to bedrock, and poured a 5-ft-thick concrete slab to serve as the base for the vacuum vessel. This work was completed in July.

Thermal and structural analysis of the test stand structure was completed by UCC-ND Engineering, with support from subcontractors. The concept of the torque structure was revised to provide a continuous ring at the top and bottom of the coils rather than intercoil beams. This concept, with suitable shims, allowed for differential thermal contraction of the stainless steel and aluminum coils.

In August specifications for the bucking post at the center of the test stand were issued. Two proposals were received for forging and machining the 32-ton post, but one contained unacceptable exceptions. A contract was let in December to Japan Steel Works of America, with delivery scheduled for January 1980. The material is to be type 304N stainless steel, the least expensive material meeting strength requirements.

The desirability of high duty cycle operation led to a decision in March to augment the LCTF helium refrigeration capacity. Because three of the six coils will require forced flow, preliminary steps were also taken towards the development of 150-g/sec helium pumps. This effort was discontinued when it appeared that the NbTi force-cooled coils might require even higher flow rates. Modification of the refrigerator to use the compressors to provide the helium flow would not only be more efficient than the use of pumps but would also substantially reduce facility capital costs.

6.2.4 Research and Development Activities (RDAC)

The RDAC is an integral supporting part of the LCP, containing those RDAC tasks not done by the industrial arm of the LCP but necessary to develop conductors, methods of stress analysis, and fabrication and to conduct materials property and design-specific measurements leading to the design and fabrication of intermediate size 2.5 x 3.5 m bore) coils. Some activity in support of the LCTF has been initiated. Work on instrumentation and diagnostics, coil protection and system safety, and cryogenics and refrigeration has been carried out. In order to disseminate the information widely, a good deal of the RDAC was published or presented at technical meetings. Only abstracts of these activities will be given below.

Conductor measurements

Critical current measurements were conducted on all three grades of sample GD LCP conductors and on two Large Coil Segment (LCS) conductors having the same general configuration and manufacturing process as the GE LCP conductors.

GD conductor. The results of the conductor verification tests for GD were quite encouraging. All three grades of superconducting cable made by IGC for GD were tested in our new high current (20 kA), 8-T split solenoid facility, and the critical currents were found to exceed the guaranteed values. The operating current for the GD coil in the LCP test coil position will be 10.3 kA, at which condition the peak fields in the three grades of conductor will be 8, 6, and 4 T. Cable test results are as follows.

Grade	No. of strands	Design field, T	Field in test, T	Cable critical current, kA	
				Guaranteed at test field	Measured
I	23	8	8.0	13.3	14.4
II	15	6	6.8	13.5	15.2
III	11	4	5.5	13.75	14.3

A check on the above results was made by dividing the critical current for the cable by the number of strands for each grade and comparing it with earlier measurements on single strands supplied by IGC. In all cases the average strand current from the cable measurements fell within the spread of single-strand measurements.

GE conductor. Short sample measurements were also performed on two IGC conductors similar but not identical to the conductor that will be used by GE for their LCP coil. These conductors are made of square, copper subelements twisted about and soldered to a rectangular core. A twisted superconductor cable is soldered into a groove in the subelements. One conductor has the superconductor against the core; the other has it away from the core. These conductors were originally intended for a LCS test where the operating current was 10 kA at 8 T and were procured on competitive bid to ORNL-prepared specifications. The short sample current I_c for both conductors was 15.8 kA at 8 T. (The differences, if any, were within the experimental scatter.) The observed critical current was unexpectedly high in that the specified value was 12.5 kA at 8 T. That I_c was substantially higher than the specified minimum was partially due to an unintentionally large filament diameter.

Westinghouse conductor. Preliminary qualification tests for the Westinghouse conductor consisted of tests on a second NbTi single triplex conductor with an internal heater. The interstices between the superconductor strands in the second sample were filled with solder to exclude helium inside the triplex where the heater is located. Another feature of the present experiment was added tubing and instrumentation that made it possible to measure directly the local pressure rise. Contrary to the hypothesis that expansion of helium trapped in interstices around the heater wire might be responsible for the high stability margin observed at zero bulk flow in our previous insulated triplex sample, the second sample showed an even higher stability margin. In a variation of the present tests, 10-m sections of simulated hydraulic paths were incorporated both upstream and downstream from the 1.25-m-long sample. The simulated hydraulic paths had the same helium cross section as the sample and also contained heater wires. It was found that the added sections affected the pressure relief wave in the sample somewhat but did not significantly reduce the stability margin. It had been hypothesized that a local pressure rise would explain some additional experimental observations on the first triplex. It was observed that the recovery time decreases as the transport current increases. For example, it ranges from 10-15 msec at 300 A and from 45-55 msec at 200 A. Computer analysis also indicated a higher effective heat transfer coefficient at higher transport currents. A possible explanation for these observations is that at higher currents the joule heating is larger when the conductor goes normal and this results in higher transient pressure and therefore higher local flow.

Theoretical work was initiated to obtain a better understanding of the experimental observations of both triplex samples. Dresner succeeded in deriving formulas for the pressure rise and fluid velocity of the thermoacoustic waves induced in stationary supercritical helium by rapid heating. The formulas predict pressure rises ~1 atm and fluid velocities ~1 m/sec as a result of heat transfers to helium of the order of 50-200 mJ/cm^2 in 10-20 msec. It is believed that these high induced fluid velocities are responsible for the good recovery noted in *cable-in-conduit conductors at zero ambient* flow. The present work will be compared with a subsequent series of experiments to be performed on the Westinghouse LCP conductor.

Measurements of Stability of Cabled Superconductors Cooled by Flowing Supercritical Helium.[1] The concept of stability in superconductors cooled by forced flow of supercritical helium is somewhat different from conductors cooled by pool-boiling helium. The crucial point is whether such a conductor can recover from a large deposition of energy before the cryogen is heated to a level that prohibits recovery. In an investigation of the stability of forced-flow conductors, it is usually necessary to use indirect methods of heating the conductor initially, such as by an external pulse coil. However, in using such indirect methods, it is essential to determine accurately the time development and magnitude of the energy deposition. We use ac loss techniques to examine pulse coil heating and compare those results with extensive measurements on a specially constructed sample containing an embedded heater.

Pressure Drop Measurement on Forced Flow Cable Conductors.[2] Forced-flow cable conductors being developed for use in LCP coils and other large superconducting magnets utilize supercritical helium flowing through narrow, uneven channels with large cooling surfaces. Extensive measurements on the pressure drop of a variety of samples were performed. It was found that the data points of friction factor vs Reynolds number are clustered together and behave in a universal way. A friction factor two to three times higher than in the smooth tube value in turbulent helium flow regime can be expected for this type of conductor.

Measurements of Traveling Transition Zone Along A Superconductor.[3] The spatial variation of the temperature in a traveling superconducting normal transition zone can provide valuable information on transient heat transfer in realistic coil conditions. In this paper temperature wave curves are presented for several transport currents corresponding to propagation and recovery in a high magnetic field. The temperature profiles have been constructed in the form $T = T(x + vt)$ by measuring the wave velocity and the temperature at one point as a function of time. The temperature is measured directly with differential thermocouples; simultaneous voltage measurements provide a continuous temperature reference in the current-sharing region. Information is given about thermocouple calibration in the high magnetic field and about the temperature and magnetic field dependence of the thermal conductivity of the sample.

AC loss measurements

In FY 1978 the direction of the pulse coil project was diverted from coil development to conductor ac loss studies. A 2000-A, 300-V bipolar supply was installed, and final acceptance tests were completed. It is now in service for testing pulse coils and ac losses in small samples. This facility (power supply plus ac loss experimental equipment consisting of a 5-T pulse magnet, nonmetallic dewar, and diagnostics plus data acquisition computer) is unique and provides us with an unmatched capability. The fabrication of a 300-kJ pulse coil, which will serve as a facility magnet, was proceeded by the purchase of a low-loss pulsed conductor developed in this project.

Transient Loss Analysis and Measurements on Normal Conductors and Composite Superconductors.[4] An equivalent circuit technique is presented for the calculation and measurement of eddy current losses in conductors under transient external fields. It is demonstrated that such techniques can yield satisfactory results through a much simpler mathematical process than that encountered in the conventional field theory.

Experimental techniques and results of transient loss measurements on both normal conductors and superconducting composites are presented to verify the model and explore its limits.

Interaction of Transport Current and Transient External Field in Composite Conductors.[5] Investigations of transient field losses in superconducting composites carrying transport current are presented. The magnetization and terminal voltage of a variety of composites have been measured as a function of transport current and external field. The losses are analyzed as a sum of magnetization losses and losses due to dynamic resistivity. Results are presented for slowly changing external fields where the magnetization losses are purely hysteretic and for higher rates of change of $\dot{B}$ where coupling losses are important.

Losses in Multifilament Nb_3Sn Superconductors Designed for High $\dot{B}$ Applications. In 1975 IGC began a comprehensive program funded by the Air Force Materials Laboratory to establish the manufacturing technology of multifilamentary Nb_3Sn superconductors to meet a stringent set of design specifications: (1) 200-500-A critical current as wound on a 1-in.-bend diameter at 7 T and 8K, (2) sufficient conductor current density to ensure an overall winding current density of 1×10^4 A/cm^2 at 7 T and 8K, (3) sufficient copper for stable performance under the above conditions, and (4) conductor losses low enough during field ramps at rates as high as 10 T/sec to ensure a less than 1-K rise in winding temperature.

The progression of conductor designs through this program has been guided by an evolving general model for losses in individual cable strands. This paper describes the loss model and five separate loss and magnetization measurements made either to confirm that anticipated losses have been achieved or to provide specific parameters necessary for accurate use of the model.

Theoretical analysis

Stability of Cable-in-Conduit, Force-Cooled Conductors: Elementary Theory.[7] The recovery of cable-in-conduit conductors cooled by supercritical helium has been studied. The initial perturbation is a sudden, uniform deposition of heat. The problem has been solved, and answers have been obtained in the form of simple closed formulas under the simplifying assumption of constant thermophysical properties. Stability-optimized conductors have been identified, and simple formulas for their material properties are given. A rule of design of cable-in-conduit conductors based on the existence of stability-optimized conductors is suggested. Some zero-flow experiments of Miller et al. have been analyzed, and it has been determined that for these experiments the effective heat transfer coefficient promoted by transient flow during the period of recovery is approximately 1000 W m^{-2} K^{-1}.

Distribution of Current Among the Filaments of a Multifilamentary Superconductor Close to the Input Leads. The distribution of current among the filaments of a multifilamentary superconductor is calculated as a function of distance along the conductor from the input lead. Also calculated is the voltage drop per unit length along the surface of the conductor as a function of distance from the input lead. Knowledge of the voltage drop is helpful in determining how close to input leads to place voltage taps, especially in conductors with a large matrix resistivity, e.g., Nb_3Sn in CuSn. The theory is compared to experiment with satisfactory results.

Instrumentation and data acquisition

The data acquisition system designed for the Large-Coil Segment Test Facility (LCSTF) has been delivered and is in operation. The system will be expanded for use in the LCTF by the addition of memory and a reel-to-reel tape drive to the display/storage minicomputer and by the addition of satellite buffer computers for recording fast data from the LCTF coils. Data acquisition software development for the LCTF is being performed by ORNL Engineering according to criteria supplied by Magnet Development Program personnel.

Further testing of strain gages was carried out in 1977. Measurements of the temperature dependence of the magnetoresistance were performed in the range of 4.2-4.9K and showed that the same resistance correction curve can be used over the entire range. Other tests were performed on intrinsic half-bridge-type strain gages and demonstrated that these gages have low temperature-induced zero shifts and magnetoresistance.

A method for fabricating thin-film carbon thermometers was developed, and the thermometers exhibited a millisecond time response and adequate sensitivity.

The double-shielded transformer/carrier amplifier scheme developed for use with strain gages on surfaces at high potential (such as a magnet conductor at high potential) was successfully tested on Impurity Study Experiment (ISX) coils. After removal of the insulating covering at the measurement points, strain gages were cemented directly to the bare copper conductor.

Several cryogenic pressure transducers for low temperature use in the LCTF were purchased and are under test. Several of the devices received have been subjected to thermal cycling and have exhibited no signs of failure after several cycles from room temperature to liquid helium temperature. A more extensive series of tests is planned for these transducers.

A voltage-tap isolation/conditioning unit was fabricated in the shop and tested. The unit meets LCTF requirements.

A one-foot segment of the GD LCP conductor was instrumented with a heater and thermocouples, and transient heat transfer tests were performed on it. Readout of the many transducers was accomplished by a data acquisition system.

Finally, a significant part of the instrumentation effort was dedicated to working with ORNL Engineering in the design of the LCTF instrumentation system and monitoring the instrumentation efforts of the LCP coil contractors.

Moving Coil Linear Variable Differential Transformer. A moving coil linear variable differential transformer is described. The device is essentially interchangeable with a conventional moving coil linear variable differential transformer but is virtually unaffected by ambient magnetic fields up to 5 T. The transducer is connected to a standard, commercially available carrier amplifier for signal conditioning.

Coil protection

Current profiles for coupled superconducting magnets. There are a large number of testing conditions in the LCP. The number of TF coils and their relative location may change. The pulse coils may operate in series, or the pulse coil power supplies may be connected in series to drive only one pulse coil. The current in the TF coils has several different extended operating conditions. The operation may be charging, discharging, partial dump, or complete dump. To ensure the structural and electrical integrity of both the pulse coils and TF coils, the current profile needs to be computed for the various combinations of possible operation conditions.

Several codes were put together for computation of coil inductance (both circular and noncircular coils) and current transients during various quench/dump conditions.

Current profiles for LCP and TNS coils during discharge have been computed and documented. Results are used as input to the LCP design team for loading assessment and comparison for worst case conditions between the LCP and TNS.

Real-time monitoring for magnet variables. TF coils, once charged up, will be operated continuously. Thus, important variables for magnet protection (e.g., pressure, temperature, strain) need to be monitored in real time to give the operator the current status of the magnet. Furthermore, for heating pulse experiments, a pictorial display of temperature/normal-zone profile and time history gives more complete information about the event in progress and alerts the operator of potential troubles. This information is vital for the decision on whether to initiate a dump or allow the magnet to recover completely to the superconducting state.

Two PDP-12 assembly language programs were written for magnet monitoring application. One program (TYPTAB) is used to translate information input, such as magnet variable names, units, and voltages, from teletype to engineering unit conversion tables and from 8-bit ASCII into 24-bit character pattern and store it on magnetic tape.

The second program reads the above data from tape into core then goes into a refresh display/update data sampling loop. During update, analog-to-digital channels are sampled and input data converted into address pointer points at the corresponding engineering unit character pattern of the conversion table. Then the refresh routine outputs these characters on screen.

Eddy current code development. The eddy current code developed last year was further improved in two respects. Instead of perturbation-polynomial expansion, the temporal behavior is now solved by Runge-Kutta method, which is more general and applicable to problems associated with shielding and skin effect. Also, the efficiency of the program has been improved by introducing symmetry options, including the symmetry for TF coil in a tokamak.

Computation of Transient 3-D Eddy Current in Nonmagnetic Conductor.[10] A numerical procedure was developed to solve transient three-dimensional (3-D) eddy current problems for nonmagnetic conductor. Integral equation formulation in terms of vector potential is used to simplify the matching of boundary conditions. The resulting equations and their numerical approximation were shown to be singular and to require special handling. Several types of symmetries were introduced. They not only reduce the number of algebraic equations to be solved, but they also modify the nature of the equations and render them nonsingular. Temporal behavior was obtained with the Runge-Kutta method. The program was tested in several examples of eddy currents for its spatial and temporal profiles, shielding, boundary surface effects, and application of various symmetry options.

Programmable waveform controller (PWC) development. In developing superconducting magnets for future fusion machines, various nonstandard waveforms are needed to simulate different types of heat-releasing events in the conductor. A dedicated PWC was built based on the Intel 8080 family of chips to enable the experimentalists to enter easily the waveform desired from keyboard.

A Programmable Waveform Controller.[11] A PWC was developed for a voltage waveform generator in laboratory. It is based upon the Intel 8080 family of chips. The hardware uses a modular board approach, sharing a common 44-pin bus. The software contains two separate programs. The first program generates a single connected linear ramp waveform. It is capable of bipolar operation, linear interpolation between input data points, extended time range, and cycling capability. The second program generates four independent square waveforms with variable duration and amplitude.

Structural analysis and materials tests

Theoretical work has been completed that extends the previously reported work on the problem of finding bending-free toroidal shell shapes. This new work finds bending-free toroidal shell shapes for nonideal magnetic field distributions. The calculated shapes for the meridian of a bending-free toroidal shell have been shown to be eccentric ellipses for low aspect ratio, becoming more nearly circular with increasing aspect ratio. For aspect ratios greater than 2.5, the meridians are essentially circular. The effect of nonideal magnetic field distribution was found to cause a modest change in the shape of the meridian. The importance of this work is that the D and oval shapes should be modified to more nearly circular shape when realistic out-of-plane structure is included in the minimum-bending calculation.

The Graphics-Oriented Interactive Finite Element Time-Sharing System (GIFTS) has been maintained and supported to respond quickly and efficiently to the wide variety of structural analysis problems that arise during the course of superconducting magnet design. However, there are several classes of problems GIFTS cannot address because of either problem size or lack of capability. These problems have been directed towards the SAP code or some other structural analysis code. An interface has now developed between the Unified Data Base (UDB) of GIFTS and SAP, thereby allowing finite element models to be generated with GIFTS and then analyzed with SAP. This will greatly reduce the man-hour time necessary to generate a finite element model for SAP.

A computer code utilizing the finite element method to solve the reduced magnetostatic potential problem has been written. Clearly, there are advantages to using the finite element method. It is a differential rather than an integral method (such as GFUN3D); therefore, the assembled coefficient matrix is sparse and banded. Further, the reduced scalar formulation requires only one unknown per nodal point instead of three for a fully 3-D vector potential calculation. These facts produce a great computational economy. The results of the application of this code to a two-region iron problem with a known analytical solution are very encouraging.

Theoretical work has been completed on the theory of contouring on isoparametric surfaces. Work is progressing on a general purpose finite element postprocessing computer code using this theory.

Materials efforts during FY 19[illegible] have concentrated on the LCP. The principal effort has been monitoring the industrial contractors' materials efforts, interpreting their problems to LCP management, and discussing management decisions with contractors' material personnel. Existing mechanical testing equipment has been modified to acquire data necessary for the LCP and not available elsewhere; it will be available for other tests as needed. Input to the LCTF design team has also been provided as required.

Bending Free Toroidal Shells for Tokamak Fusion Reactors With Nonideal Magnetic Field Distributions.[12] This paper describes an extension of mathematical solutions to bending-free shapes of toroidal pressure vessels. Previous work on this subject derived a pure tension shape of a toroidal membrane that was subjected to a uniform internal pressure and subjected to a pressure inversely proportional to the square of the toroidal radius. This family of shapes is derived by solving the equilibrium, constitutive and kinematic relationships for a uniform toroidal shell using the linear membrane theory. This paper extends the previous work to the problem of finding bending-free toroidal shell shapes for nonideal magnetic field distributions, i.e., for magnetic fields that do not vary inversely with toroidal radius. Because these bending-free shells provide alternate methods of design for tokamak fusion reactors, serious consideration should be given to them.

Contouring on Isoparametric Surfaces.[13] Contour plotting on 2-D or 3-D isoparametric surfaces is a problem facing many users. Most procedures use some type of linear interpolation to approximate the contour locations. A general nonlinear interpolation procedure is presented for contouring on any isoparametric surface. This procedure uses standard isoparametric interpolation functions.

An Improved Method for Contouring on Isoparametric Surfaces.[14] A general nonlinear interpolation procedure for contouring on any isoparametric surface was presented in a previous article. This method used standard isoparametric interpolation functions and a predictor method for tracing element contour lines. The method presented here extends the previous work by using a predictor-corrector method to trace element contour lines, thereby making the contouring algorithm more accurate.

A User's Guide to the CALVEC Software Library: A Computer Program for Emulation of CALCOMP Graphics on a Versatec Printer/Plotter.[illegible] This document describes a set of FORTRAN subroutines collectively called the CALVEC subprogram library. The purpose of the CALVEC software library is the emulation of CALCOMP pen and ink graphics on a DECsystem 10. A user-level interface with CALVEC software allows standard CALCOMP subprogram calls to produce a VECtor file, SEGMNT.VEC. This vector file may subsequently be postprocessed into an image in a variety of ways.

A System for Vacuum Pouring of Epoxy Tensile and Impact Specimens with a Study of the Behavior of These Specimens at 77K and 293K.[14] The purpose of the investigation described in this report was to establish a suitable technique for vacuum pouring of epoxy test specimens and to study the behavior of these specimens at 77K and 293K. A series of tensile and impact tests was conducted using specimens made from the following resins: Epon 828, Epon 871, and Epon curing agent Z. These materials are of general interest to designers of magnets for cryogenic service. Some of the applications that may be considered are structural support, spacing, electrical insulation, and thermal insulation. The epoxies mentioned above were selected for more extensive testing because they have been used successfully at room temperature in the ELMO Bumpy Torus (EBT) and Oak Ridge Tokamak (ORMAK) Programs in the Fusion Energy Division (FED) at ORNL. Liquid nitrogen was chosen over liquid helium because it is less difficult to handle and less expensive. Also, in most instances the physical properties of epoxies seem to change very little from 77K to 4.2K. The two main features of the vacuum pouring apparatus are that (1) batches can be poured under near-identical conditions and (2) samples can be handled free from air contamination.

Tests of the specimens were carried out at 77K and 293K. The 77-K data indicate that tensile strength increases proportionally with the increase of Epon 871 relative to Epon 828. When the mixture includes more than 90% Epon 871, impact testing at 293K becomes practically impossible because of the rubbery condition of the material. However, when tested at 77K, this same mixture evinces high tensile strength. When optimum data are sought over a wide range of temperatures, 77K to 293K, it appears that a mixture of 70% Epon 871, 30% Epon 828 with 13 pph of curing agent Z or 50% Epon 871, and 50% Epon 828 with 15 pph curing agent Z offers the best compromise in tensile strength, modulus of elasticity, and impact resistance.

Coil fabrication technology

The materials for winding the first Large Coil Segment (LCS) were delivered, and some fabrication had begun before the program was discontinued. The exercise of welding the stainless steel bobbin and performing some practice winding was informative. However, work was stopped before any actual winding was done. Nevertheless, important data were obtained on heat distortion of stainless steel plates, thermal effects on electrical insulation close to welds, and potential pitfalls encountered while winding D shapes. LCP contractors are interested in this type of data. Other practice winding was done to assist LCP contractors in resolving fabrication uncertainties. Information was provided on such things as winding wide conductors on edge, conductor springback, required conductor tension, insulation damage, etc. More practice winding is planned in a continuing effort to reduce these types of fabrication uncertainties.

A concept for fabricating coils using Nb_3Sn superconductors has been proposed. The conductors are flexible until they undergo a furnace reaction at high temperature that creates the desired Nb_3Sn alloy. The Nb_3Sn conductors are then brittle and easily damaged during handling. The proposed method describes a way of winding, then reacting, insulation, and setting the turns in place with little or no tension, thus avoiding possible damage. A coil with a few turns is planned to test this concept.

The spliceless pancake approach to winding coils has been further developed. A 34-pancake, 76-mm-bore, 7.6-T coil has been wound but is as yet untested. It uses two separate superconductors, demonstrating that many different conductors can be used in a coil (grading) without making a joint in each pancake. This permits either a variable current density or the use of a cheaper superconductor in the low field part of the windings.

Equipment has been set up, and some practice winding has been done in preparation for winding a pair of coils for the Coil Winding Test Experiment (CWTX). When finished, this coil will check fabrication methods and will be used as a facility magnet. Materials are on order, and fabrication will take place in the first half of 1979.

6.3 ADVANCED CONDUCTOR DEVELOPMENT

Advanced conductor development involves work on superconducting material, its fabrication into a multicomponent unit, its operating environment, and its performance in a device. The goals are improved performance in terms of current-carrying capacity, stability margin, ac losses, and mechanical strength. The approach is to combine experimental and analytical work on small-scale specimens, to purchase conductors of advanced design from industry, and to evaluate the performance of these conductors in realistic but reduced-scale systems. This approach has involved and will continue to involve a close working relationship with the American conductor manufacturers in order to concentrate the optimum expertise on the problems and to minimize the efforts for technology transfer.

6.3.1 Conductor Development Contracts

Three cost-plus-fixed-fee subcontracts with American manufacturers were brought to or near completion in 1978. The results of these contracts are summarized as follows.

A subcontract with Airco was for the development of forced-flow Nb_3Sn cable-in-conduit conductors. The work statement first called for the manufacture of subsized samples using LCP cable strands but containing only one-third the number of active conductors. Several variations of parameters such as void fraction, shape (round vs square), and core construction were incorporated in the samples prepared for evaluation. These were followed by larger full-LCP-scale samples using values of parameters that appeared most suitable for the LCP. During 1978 all samples were delivered except the full-scale samples that are nearly completed.

A subcontract with IGC was for preliminary evaluation of another Nb_3Sn forced-flow concept. Heat exchangers containing flowing supercritical helium are attached to both sides of a flat cable conductor. The superconductor is cooled by conduction to the heat exchanger, a rectangular tube containing a copper braid sintered to the tube to produce a larger cooling surface with short conduction paths. The work resulted in an analysis of the behavior of the conductor, the production of several short lengths of cooling channel, and some partially processed Nb_3Sn material. The goal of the project, to produce a short length of finished 10,000-A conductor, was not achieved within the funding allocated. The results of this effort are being evaluated to see if further work along these lines is warranted.

A subcontract with Supercon was set up to evaluate forced-flow NbTi cable-in-conduit conductors. A key item in the program was the production of several long lengths of dummy conductor to evaluate the sheathing operation and to try to eliminate some problems encountered earlier. In addition, a number of short evaluation samples were produced with several variations of cable configurations. The earlier problems, which involved a "birdcaging" or loosening of the outer cable layer, appeared to be overcome by using a different cable configuration and by tighter cabling. However, the tooling developed in another DOE program was not successful and has been reworked. No further work on NbTi under this program is contemplated.

6.3.2 Conductor Purchase

A 600-m length of 10,000-A, 8-T conductor was delivered by IGC. The conductor was originally developed for the LCS project, which was cancelled early in 1978. It is the highest current-carrying conductor commercially produced for 8-T application by at least a factor of 2. The final conductor configuration evolved after a number of modifications were introduced because of difficulties encountered during the various manufacturing stages. The GE/IGC conductor design for the LCP will profit greatly from this development work and will utilize a design very similar to the final delivered conductor configuration. The conductor is being used to supply samples for a heat transfer experiment on the GE LCP design, and it will also be used to evaluate various performance aspects of high current cryostable conductors.

Another advanced conductor, not specifically developed for forced flow, was produced in conjunction with IGC. The conductor uses NbTi filaments in a configuration that separates the conductor into segments, thereby reducing eddy current and coupling losses. A small billet was extruded and drawn to fine wire to prove the manufacturability of the complex conductor, and a larger billet was prepared for later extrusion and production of a significant quantity of material. The concept is applicable to either forced-flow or pool-boiling concepts.

6.3.3 Test Facilities

A 30,000-A, 20-V dc current supply has been installed and tested. This is being used in conjunction with an 8-T superconducting magnet and a pair of 20,000-A vapor-cooled leads in a 75-cm-diam dewar as a short sample test facility.

A 2000-A, ±300-V power supply has been installed and tested. This is being used with a small bore, 5-T superconducting magnet for transient loss experiments on TF conductors.

6.3.4 Coil Winding and Test Experiment

The CWTX was conceived as a means of utilizing the conductor obtained for the LCS Program. The conductor will be used to evaluate coil design, winding techniques, and operating characteristics appropriate to large, high field, cryostable superconducting coils. If these tests are successful, the resulting coil, having an 8-T central field, a 40-cm bore, and four 6.6-cm circular radial access ports, will be placed in operation as a facility magnet. The magnet will first be used for the stability experiments of the LCP conductor. Specifications for an insert coil that will produce 12 T in a 20-cm bore have been prepared for bid early next year.

Design work has been completed on the magnetic characteristic and bobbin details Machine shop work has started, and the bobbin is expected to be ready by early 1979.

6.3.5 Analytic Solution for the Propagation Velocity in Superconducting Composites[17]

The propagation velocity of normal zones in composite superconductors has been calculated analytically for the case of constant thermophysical properties, including the effects of current sharing. The solution is compared with that of a more elementary theory in which current sharing is neglected, i.e., in which there is a sharp transition from the superconducting to the normal state. The solution is also compared with experiment. This comparison demonstrates the important influence of transient heat transfer on the propagation velocity.

6.3.6 Transient Heat Transfer to Liquid Helium from Bare Copper Surfaces[18]

Iwasa and Apgar[19] recently published an experimental study of transient heat transfer to liquid helium from bare, vertical copper surfaces in which they found that transient heat transfer exceeded steady-state heat transfer for increasing temperature and was less than steady-state transfer for decreasing temperature. A correction for transient heat transfer that was positive during heating and negative during cooling had already been used in the analysis of normal-zone propagation and contraction velocities.[20] It is shown that the correction for transient heat transfer inferred from the normal-zone velocities is in good agreement with the directly measured correction.

6.3.7 The Toroidal Energy Storage Experiment (TESPE) Project

TESPE is a toroidal array of six D-shaped coils, roughly 50 cm x 60 cm, being built by the Nuclear Research Center in Karlsruhe. The plans call for such high current density and magnetic field that it is impossible to cryostabilize magnets wound with a NbTi Cu-matrix conductor; however, it may be possible to cryostabilize magnets wound with a Nb_3Sn/CuSn Cu-matrix conductor. Early this year it was proposed that the U.S. (Francis Bitter National Magnet Laboratory and ORNL) build for TESPE a cryostable cable-in-conduit Nb_3Sn magnet cooled by supercritical helium.

The principal constraints that challenge the designer in making the coil cryostable are the high current density (7.6 kA cm^{-2} in the winding space; 10-12 kA cm^{-2} over the cable interior), high field (7.5 T maximum at the conductor), and small pump size (12 g sec^{-1} @ 1 atm). In the absence of experimental information on the stability of cable-in-conduit conductors, the design work at ORNL was carried out using theoretical methods previously developed.[21,22] In spite of the stringent constraints, a stable design appeared possible: a jointless, 13-layer, 19-conductor, close-packed layer winding of a 1-cm-OD, 6600-A cable of ~0.3-mm strands. The layers are hydraulically connected in a series-parallel arrangement that provides more flow to the inner layers and less to the outer; the decreased field in the outer layers compensates for the reduced flow there. The total mass flow required with this arrangement is 11 g sec^{-1} @ 0.75 atm within the capabilities of the pump.

Since the early part of the year, when this work was done, a new 12-T program was launched that includes construction of a Nb_3Sn cable-in-conduit solenoidal segment cooled by supercritical helium. The goals of this program supersede those of the U.S. TESPE program; this work has accordingly been stopped.

6.4 12-T COIL DEVELOPMENT PROGRAM

This program was initiated in FY 1979 with the primary goal of developing large, high field, superconducting toroidal coils for the Engineering Test Facility (ETF). This program will supplement the LCP and be carried out concurrently with it but on a much smaller scale. The design and fabrication of the 12-T model test coils, as well as the manufacturing of the Nb_3Sn conductor, will be carried out under subcontracts with industry. ORNL will manage two programs made up of different industrial teams. One team is composed of GD/Convair Division with Airco as the conductor manufacturer, and the second team consists of GE with IGC manufacturing the conductor.

The request for proposal (RFP) to the coil designers consists of two parts. Part I is a scoping study for the development of a high field, 12-T TF coil concept suitable for a tokamak reactor. This includes identification of a viable conductor concept and fabrication scheme. Part II consists of three phases for the design and fabrication of a 12-T model coil. Phase I is the conceptual design of a model coil to test the chosen ETF conductor. Scaling considerations should be considered, especially if constraints prevent the full-size conductor from being tested. Phase II consists of the detailed coil design and component testing. It is expected that most of the testing will be conducted at ORNL. Phase III is the conductor procurement and coil fabrication.

In order to speed up conductor development, contracts are being negotiated directly with the conductor manufacturers. The initial emphasis will be on product improvement of the internal bronze technique at Airco and the external diffusion process at IGC.

6.5 MAGNET DESIGN FOR SPECIFIC MACHINES

The coil design activity encompassed a wide variety of projects, some unrelated to fusion. In each case, however, the project supplied the funding. In addition to the specific design activities discussed below, some consultation service was provided to FED activities such as EBT aspect ratio enhancement (ARE) coils and the Long Pulse Technology Tokamak (LPTT).

6.5.1 Superconducting Magnets for Heavy Ion Cyclotrons

A preconceptual design of a heavy ion cyclotron using superconducting main magnets was begun at the request of the Physics Division at ORNL. This design is similar to an earlier design by Michigan State University but had different physics objectives. The main magnets consist of two coaxial solenoids whose end windings are separated just enough to allow the heavy ion beam to be injected into and extracted from the cyclotron. The field profile in the midplane must be adjusted to suit a particular ion accelerated to a particular energy. The main coils are each divided into two independent circuits that help provide the field shaping.

After a review meeting in Washington, the design was halted and the physics objectives were reevaluated. A new design was initiated that was much larger than the earlier one and used a much larger midplane spacing between the coils. There was some concern that the magnet system was much too difficult or expensive because of the large separation. However, an extensive scoping study of the relevant parameters showed that the magnets were not made too difficult or expensive by their new configuration.

6.5.2 Coal Separation

Some of the pollutants in coal are paramagnetic and lend themselves to magnetic separation. These pollutants include inorganic sulfides and some forms of ash. Magnetic separation is used in industry to remove color impurities in clay used to make pottery. In this process the clay is suspended in a water slurry. It is undesirable to use a water slurry with coal because it will take energy to dry it before it is burned, but it is desirable to use an existing industrial process when possible. In this past year a set of successful experiments was carried out at a magnetic separation manufacturer's plant using air-entrained coal. These experiments were done under a program in the Engineering Technology Division of ORNL with advice from the Magnetics Group in the Fusion Energy Division.

6.5.3 EST-II

The magnet work for EST-II was continued from last year. The effort further refined the mirror and ARE coil designs. The results of the conceptual design study were published, and additional details on EST-II are discussed elsewhere in this annual report.

REFERENCES

1. J. R. Miller, J. W. Lue, S. S. Shen, and J. C. Lottin, *Proc. 1978 Applied Superconductivity Conference*, IEEE Trans. on Magnetics, Vol. MAG-15, No. 1, pp. 351-354 (1979).
2. J. W. Lue, J. R. Miller, and J. C. Lottin, *Proc. 1978 Applied Superconductivity Conference*, IEEE Trans. on Magnetics, Vol. MAG-15, No. 1, pp. 53-55 (1979).
3. J. C. Lottin, J. R. Miller, J. W. Lue, and L. Dresner, *Proc. 1978 Applied Superconductivity Conference*, IEEE Trans. on Magnetics, Vol. MAG-15, No. 1, pp. 363-366 (1979).
4. S. S. Shen and R. E. Schwall, *Proc. 7th Int. Cryogenic Engineering Conference*, Vol. 7, pp. 659-66 (1978).
5. S. S. Shen and R. E. Schwall, *Proc. 1978 Applied Superconductivity Conference*, IEEE Trans. on Magnetics, Vol. MAG-15, No. 1, pp. 232-235 (1979).
6. G. R. Wagner, S. S. Shen, R. E. Schwall, A. Petrovich, and M. S. Walker, *Proc. 1978 Applied Superconductivity Conference*, IEEE Trans. on Magnetics, Vol. MAG-15, No. 1, pp. 228-231 (1979).
7. L. Dresner, *Stability of Cable-in-Conduit, Force-Cooled Conductors: Elementary Theory*, Oak Ridge National Laboratory Report ORNL/TM-6657, Oak Ridge, Tennessee (1979).
8. L. Dresner, Cryogenics 18, 285 (1978).
9. C. F. Ellis and P. L. Walstrom, Rev. Sci. Instrum. 49, 3 (1978).
10. H. T. Yeh, *Proc. 2nd Int. Conf. on the Computation of Magnetic Fields*, Session 5, Paper 7.5 (1978).
11. H. T. Yeh, "A Programmable Waveform Controller," paper presented at the IECI 1979 Conference on Industrial and Control Application of Microprocessors, Philadelphia, Pennsylvania, March 19-21, 1979.
12. W. H. Gray, "Bending Free Toroidal Shells for Tokamak Fusion Reactors with Nonideal Magnetic Field Distributions," paper presented at the ASME Winter Annual Meeting, San Francisco, California, December 10-15, 1978.
13. J. E. Akin and W. H. Gray, *Contouring on Isoparametric Surfaces*, Oak Ridge National Laboratory Report ORNL/TM-5950, Oak Ridge, Tennessee (1977).
14. W. H. Gray and J. E. Akin, Int. J. Numer. Methods Eng. 14, 451-72 (1979); also ORNL/TM-6381.
15. W. H. Gray, *A User's Guide to the CALVEC Software Library: A Computer Program for Emulation of CALCOMP Graphics on a Versatec Printer/Plotter*, Oak Ridge National Laboratory Report ORNL/TM-6477/R1, Oak Ridge, Tennessee (1979).
16. C. M. Fitzpatrick and W. C. T. Stoddart, *A System for Vacuum Pouring of Epoxy Tensile and Impact Specimens With a Study of the Behavior of These Specimens at 77K and 293K*, Oak Ridge National Laboratory Report ORNL/TM-5493/R1, Oak Ridge, Tennessee (1978).
17. L. Dresner, *Proc. 1978 Applied Superconductivity Conference*, IEEE Trans. on Magnetics, Vol. MAG-15, No. 1, pp. 328-330 (1979).
18. L. Dresner, Cryogenics 19, 120-121 (1979).
19. Y. Iwasa and B. A. Apgar, Cryogenics 18, 267 (1978).
20. J. R. Miller, J. W. Lue, and L. Dresner, *Proc. 1976 Applied Superconductivity Conference*, IEEE Trans. on Magnetics, Vol. MAG-13, No. 1, p. 24 (1977).

21. L. Dresner, *Proc. 1976 Applied Superconductivity Conference*, IEEE Trans. on Magnetics, Vol. MAG-13, No. 1, pp. 670-672 (1977).

22. L. Dresner and J. W. Lue, *Proc. 7th Symp. on Engineering Problems of Fusion Research*, Vol. I, pp. 703-709 (1977).

23. D. M. Eissenberg, E. C. Hise, and M. D. Silverman, "ORNL Program for Development of Magnetic Beneficiation of Dry Pulverized Coal," paper presented at the Int. Conf. on Industrial Application of Magnetic Systems, Rindge, New Hampshire, July 30-August 4, 1978.

24. R. A. Dandl et al., *The EBT-II Conceptual Design Study*, Oak Ridge National Laboratory, Report ORNL/TM-5955, Oak Ridge, Tennessee (1978).

7. ADVANCED SYSTEMS

D. Steiner, Manager

W. R. Becraft[1]
E. S. Bettis[2]
T. G. Brown[3]
W. A. Houlberg[4]
T. J. Huxford[2]
A. T. Mense[4]
R. J. Onega[6]
Y-K. M. Peng[4]
R. L. Reid[5]
J. A. Rome[4]
C. Sardella[3]
T. E. Shannon[5]
R. S. Stone[5]
W. M. Wells[5]
G. W. Wiseman[7]

Abstract. The Advanced Systems Program includes six major activities: (1) The Next Step (TNS) Program, (2) the Engineering Test Facility (ETF) Design Center, (3) the Fusion Power Demonstration Study, (4) the Committed Site Evaluation, (5) the Tokamak Instrumentation and Controls (I&C) Study, and (6) the Large Aspect Ratio Tokamak Study (LARTS).

The Next Step (TNS) Program. The TNS studies at Oak Ridge were initiated in FY 1977. During FY 1977 the Oak Ridge effort pursued scoping studies in three broad areas: plasma engineering, systems modeling, and program planning. These activities were carried out in cooperation with the Fusion Power Systems Department of the Westinghouse Electric Corporation. Based upon the findings of the FY 1977 efforts, it was judged that continued activities in the Oak Ridge TNS Program should be directed towards preconceptual design with particular emphasis on engineering feasibility. As a point of departure for the FY 1978 activities, a baseline design was selected, based on the systems modeling effort of FY 1977. The primary objective of our FY 1978 TNS effort has been to evolve the Baseline Design towards a preconceptual design. However, we emphasize that, because of budget constraints, it was not intended that the FY 1978 effort lead to a completed preconceptual design. Therefore, the design resulting from this year's effort is referred to as the Reference Design, rather than as the Preconceptual Design. The FY 1978 activities were carried out in cooperation with the Fusion Energy Department of the Grumman Aerospace Corporation.

The Engineering Test Facility (ETF) Design Center. In September of 1978 the Department of Energy (DOE) introduced a new policy statement for fusion energy. One key element of the strategy outlined in this policy was the decision to have an ETF built to serve as the vehicle by which the fusion program would move from the scientific phase into the engineering test phase. The ETF would provide a testbed for reactor components in a fusion environment. Following the review of recommendations from General Atomic (GA), Oak Ridge National Laboratory (ORNL), and Princeton Plasma Physics Laboratory (PPPL), DOE selected Don Steiner to manage and ORNL to host an ETF Design Center with the responsibility of developing a detailed mission statement for an ETF that could begin operation in the late 1980's, a reference design for a facility with this mission, and recommendations on

---

1. General Electric Company, Schenectady, New York.
2. Present address: Science Applications, Incorporated, Oak Ridge, Tennessee.
3. Grumman Aerospace Corporation, Bethpage, New York.
4. Plasma Theory Section.
5. UCC-ND Engineering.
6. Virginia Polytechnic Institute and State University, Blacksburg, Virginia.
7. Instrumentation and Controls Division.

what [illegible] are necessary, to ensure the technical success of the facility. The ETF design center team has been established with significant supporting responsibility being provided by the major fusion centers of GA, [illegible] and the Massachusetts Institute of Technology (MIT).

The [illegible] Fusion Power Demonstration Study. The ORNL Fusion Power Blanket Study, emerged from FY 1976-77 studies conducted by the Advanced Systems Program. The Blanket Study is being carried out by Westinghouse Electric Corporation under the technical guidance of ORNL personnel. After a review of several existing generic concepts, a tokamak blanket cylindrical module concept was designed, developed, and analyzed. The design is based on use of state-of-the-art structural materials (20% cold-worked type 316 stainless steel), lithium as the breeding material, and pressurized helium as the coolant. The module design consists of nested concentric cylinders and features direct wall cooling by flowing helium between the outer (first wall) cylinder and the inner lithium-containing cylinder. Each cylinder is capable of withstanding full coolant pressure for enhanced reliability. Results show that stainless steel is a viable material for a first wall subjected to a 4-MW/m^2 neutron flux and a 1-MW/m^2 particle heat flux. A lifetime analysis showed that the first wall design meets the goal of operating at 20-min cycles with 95% duty for 10^5 cycles. The design is attractive for further development, and additional work and supporting experiments have been identified to reduce analytical uncertainties and enhance the design reliability.

The Committed Site Evaluation. The Committed Site concept emerged from FY 1976-77 studies conducted by the Advanced Systems Program. The Committed Site study is being conducted by Bechtel National, Incorporated, under the technical guidance of ORNL personnel. The objective of this study is to evaluate the technical and economic merits of a committed fusion development site dedicated to major engineering experiments, not proof-of-principle tests. The dedicated site with shared facilities is being evaluated for the development of a single fusion device, such as the tokamak alone or tandem mirror alone, from ignition through demonstration modes of operations and also for simultaneous development of multiple fusion devices, such as the tokamak, mirror, and ELMO Bumpy Torus (EBT), through all phases of operation. The Committed Site Evaluation is based on reactor requirements submitted by the fusion community for the various fusion concepts under consideration. These reactor concepts include the tokamak, tandem mirror, EBT, torsatron, and reverse field pinch. Major items that have been identified as economically attractive for sharing among reactors during the development phase include pulsed electrical power-handling and conversion systems, cryogenics systems, tritium-processing equipment, heat rejection systems, and buildings. Significant schedule compression appears possible through the use of a single committed site for multiple sequential steps in the development of fusion power as opposed to serial development at several sites.

The Tokamak Instrumentation and Controls (I&C) Study. Instrumentation and controls problems projected for the higher-powered and longer pulse time tokamaks problems accentuated by the increasing research and development (R&D) thrusts towards higher beta and actively shaped plasmas need increasing emphasis. The projected controls problems have been considered (along with integration with ongoing experiments, the hardware-experienced research teams, and the plasma theory and engineering personnel) and the higher priorities selected for early emphasis. The three areas of study emphasis to data are (1) physics implications for controls, (2) computer simulation, and (3) shutdown/aborts. During FY 1978, the first year of these studies, these areas have been addressed. Transient scenario options for the startup of a [illegible] were developed, and the implications for the control system were discussed. A hybrid (analog and digital) computer simulation of the upgraded Impurity Study Experiment (ISX-B) was prepared and is being used for corroborative controls investigations. The simulation will be expanded to represent a TNS/ETF machine. The scoping of the abort potential problem has been initiated, and preliminary results have been presented and show the need for increased emphasis in this area. Areas of study that were relegated to secondary attention in the early work by reason of the limited effort that could be applied include I&C systems description, R&D needs assessment, and development of "road maps" to meet TNS/ETF/DEMO needs.

Large Aspect Ratio Tokamak Study. The Large Aspect Ratio Tokamak Study (LARTS) is investigating the option of mitigating the pulsed mode operation of tokamaks by increasing the plasma burn through enhanced volt-second capability achieved by utilizing high aspect ratios. As a more steady-state mode of tokamak operation is achieved, the cyclic fatigue problem for the blanket first wall is correspondingly reduced. The impact of high aspect ratio on plasma physics parameters (achievable values of beta, plasma current, quality of confinement, required magnetic field, plasma size, etc.) and on the tokamak power level, system cost, and burntime is being addressed in this study.

7.1 THE NEXT STEP PROGRAM

The primary objective of our FY 1978 TNS effort was to evolve the Baseline Design towards a preconceptual design. However, we emphasize that, because of budget constraints, it was not intended that the FY 1978 effort lead to a completed preconceptual design. Therefore, the design resulting from this year's effort is referred to as the Reference Design (Table 7.1 and Fig. 7.1), rather than as the Preconceptual Design. The FY 1978 activities were carried out in cooperation with the Fusion Energy Department of the Grumman Aerospace Corporation.

The major conclusions of the Oak Ridge TNS Program for FY 1978 are summarized below in the context of engineering feasibility, plasma operating characteristics, and project planning.

Engineering feasibility

The activities in the area of engineering feasibility focused on three issues: remote maintenance, the poloidal field (PF) system design, and the divertor design.

Remote maintenance. The remote maintenance features of the Reference Design represent a significant improvement over those of the Baseline Design as a result of three major design changes.

(1) The number of toroidal field (TF) coils was reduced from 20 to 12 in order to allow sufficient room between coils to replace a torus sector. Thus, the TF coils need not be removed for sector replacement.

(2) The TF coil bore was increased by 30 to gain the access necessary to relocate the PF coils inside the TF coils during a sector replacement operation. This eliminated the need for PF coil segmentation in the event of such an operation.

(3) The use of a mechanically assembled torus has eliminated the need for internal cutting and welding to replace a torus sector. The applicability of mechanical torus joints was made feasible through the adoption of an evacuated reactor cell to house the torus.

A 1/40 scale model was constructed to help evaluate the maintenance features of the evolving design.

Poloidal field system. The PF system adopted in the Reference Design represents a

Table 7.1. Reference Design parameters

Plasma major radius, R (m)	5.0
Plasma elongation,	1.6
Plasma minor radius, a (m)	1.2
Plasma volume, V_p (m^3)	230
Plasma current, I_p (MA)	5.0
Neutron wall loading (MW/m^2)	2.4
Total fusion power (MW)	1140
Fusion power density (MW/m^3)	5.0
Number of TF coils	12
TF coil vertical bore (m)	9.9
TF coil horizontal bore (m)	6.2
TF coil conductor	Nb_3Sn
Field at TF coil, B_m (T)	10.9
Field on axis, B_t (T)	5.3
Steady-state burntime(s)	500
Total cycle time(s)	560
Total volt-seconds	83
Neutral beam power (MW)	50
Neutral beam energy	150 keV
Injection time(s)	6.0
Microwave power (MW)	1.0
Microwave frequency	120 GHz
Fueling	Pellet injection
Impurity control	Bundle divertor
Shielding	SS balls & borated water
Vacuum topology	Vacuum building
Vacuum pumping	Cryopumps

significant improvement over that employed in the Baseline Design. The PF system in the Reference Design consists of a superconducting ohmic heating (OH) coil, interior copper equilibrium field (EF) coils (inside the TF coil bore) that carry ~35% of the EF current, and exterior superconducting EF coils (outside the TF bore) that carry 65% of the EF current. The PF system in the Baseline Design consisted of a copper OH coil outside the TF coils and copper EF coils inside the TF coils. The updated PF system design offers a reasonable balance between system cost, coil maintenance, TF coil protection, and power requirements. Moreover, the use of a superconducting central solenoid permits the flux swing for a burntime of ~500 sec without excessive joule heating losses.

Divertor system. A bundle divertor, adopted for impurity control in the Reference Design, contrasts with the compact poloidal divertor adopted in the Baseline Design. The primary reasons for this change in design were to move the divertor system outside the TF coil bore to improve overall access and to provide more space for particle and energy collection. An innovative scheme making use of an array of lithium jets has been proposed as a means of accomplishing the particle and energy collection in the bundle divertor.

ORNL-PHOTO 7328-78

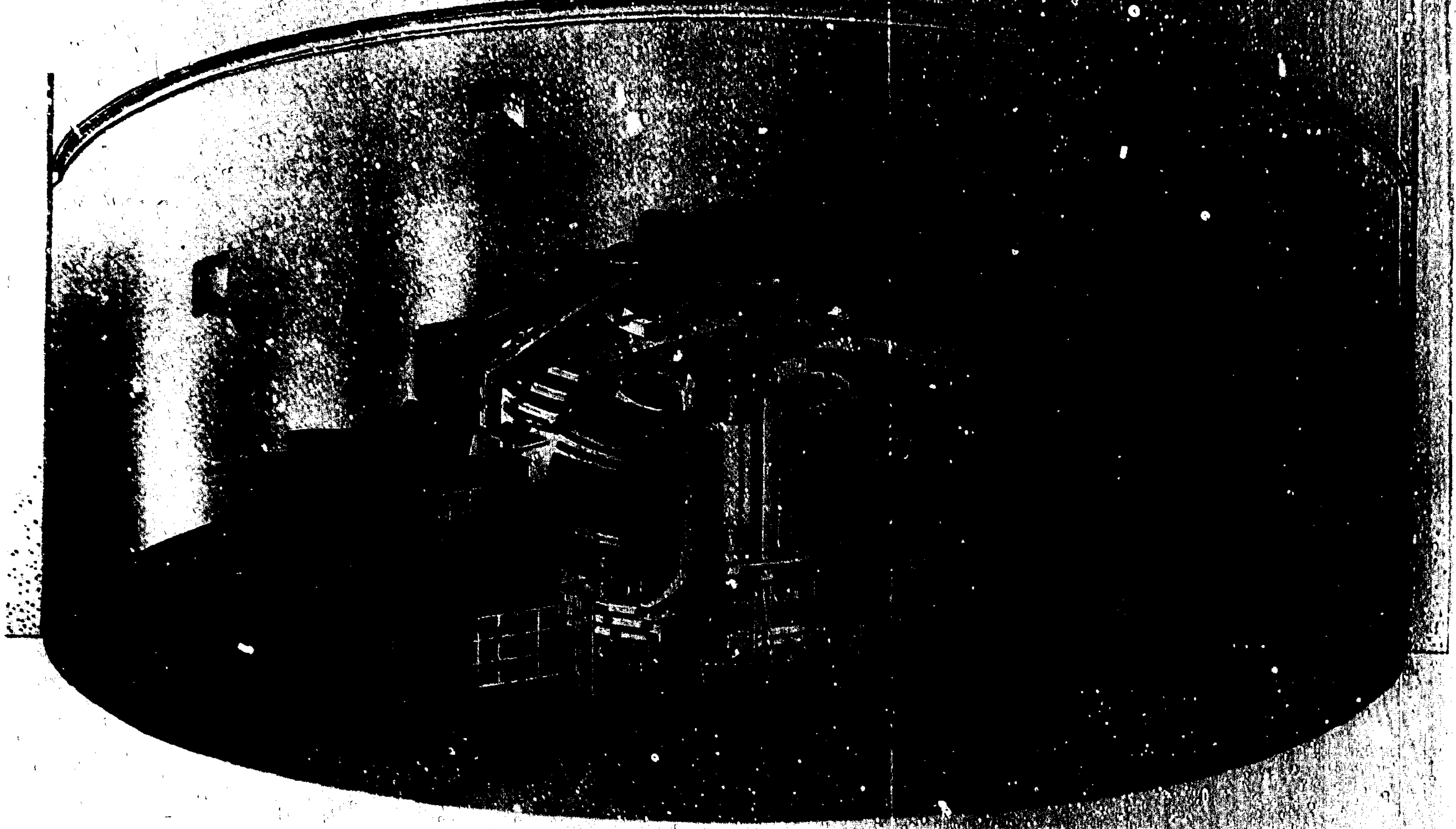

Fig. 7.1. Oak Ridge TNS 1978 Reference Design

Plasma operating characteristics

The activities related to plasma operation focused on the following areas: reducing the technology requirements for startup and heating, maintaining high beta configurations, and identifying the key physics issues requiring investigation in order to achieve a controllable, long pulse, ignited tokamak plasma.

Technology requirements. In order to reduce the power supply requirements during startup, a microwave-assisted startup procedure was proposed and evaluated. It is estimated that the peak voltage requirement might be reduced by roughly an order of magnitude relative to estimates for startup without microwave breakdown and preheating. Additional experimental evidence is required to verify the validity of such an approach. Calculations of neutral beam heating indicate that ignition could be reached with deuterium energies as low as 100 keV without excessive demands on power requirements. These calculations, which must still be confirmed by experiments, suggest that reactor heating requirements could be satisfied with positive ion beam systems employing direct recovery and that negative ion beam systems may not be necessary. Beams of 150 keV were adopted in the Reference Design.

High beta maintenance. The magnetic flux diffusion process in high beta beam and alpha-particle-heated plasmas over long time scales is not well understood. The focus of the studies in FY 1978 has been the maintenance of high beta equilibria during the heating, ignition, and early burn phases. In this context the PF system proposed for the Reference Design will allow the control of the plasma D-shaped cross section despite large changes in the plasma profile and beta during these phases.

Key physics issues. The control and handling of plasma disruptions is identified as a key physics issue relative to the implementation of the TNS. Plasma disruptions would severely limit the useful life of the first wall and would also impose serious design constraints in terms of superconducting magnet protection. The need to characterize, understand, and control disruptions is identified as a major area for further investigation. Overall particle control during the various phases of the plasma operation also represents a key physics area of uncertainty. To date, conceptual solutions based on empirical arguments have been employed to define schemes of particle control, but it is clear that significantly more work needs to be done in this area to define requirements and techniques. A third key physics issue requiring investigation is plasma control during burn, including control of profiles, beta, and impurity content.

Project planning

The project planning activities considered cost and schedule, R&D needs assessment, and operational plan.

Cost and schedule. The cost estimates performed for the TNS indicate that the direct cost of the facility would be ~$500 million and that the total facility cost, excluding escalation and interest during construction, would be ~$1 billion. A cost estimate breakdown on the basis of major functional areas indicates the very large dependence of cost on the TF coil system followed by the electrical power and controls systems. The TNS scheduling exercise suggests a total project time span requirement of about ten years with approximately six years required for device construction.

R&D needs assessments. The R&D needs assessment in the general areas of physics and technology identified two major themes: (1) an expansion of efforts needed to integrate the various physics results in the context of the desired operational cycle of the plasma in order to define more clearly the required R&D needs for a controllable, long pulse, ignition fusion core; and (2) an increased emphasis required in the area of technology and engineering developments to provide reliable, cost-effective components for the TNS on a timely basis.

TNS mission. An operating plan or mission was laid out for the TNS facility. This mission consists of four phases: (1) Phase I – integrated system checkout (0.5 year); (2) Phase II – hydrogen operation (1.5 years); (3) Phase III – ignition test and plasma burn (2.5 years); and (4) Phase IV engineering testing (5.5 years). These mission objectives of the TNS need to be reevaluated relative to their impact on overall device design, facility requirements, and schedule.

7.2 ENGINEERING TEST FACILITY (ETF) DESIGN CENTER

In September of 1978 John Deutch, Director of Energy Research for DOE, articulated the DOE policy for fusion energy. This policy statement encompassed the efforts in both the magnetic confinement and inertial confinement approaches. In order to develop fusion energy as an economically attractive and environmentally acceptable energy option, the DOE policy statement on fusion energy outlined a three-phase strategy. Sequentially these phases focus on scientific feasibility, engineering testing, and reactor demonstration.

It is anticipated that scientific feasibility for both the magnetic confinement approach and the inertial confinement approach will be achieved within the 1980's. Following the achievement of scientific feasibility, each of the two approaches would move from the applied research phase into the engineering testing phase. The vehicle by which the fusion program would move into this phase of development is designated the Engineering Test Facility (ETF). The ETF would provide a testbed for reactor components in a fusion environment. These components would be the essential building blocks of the facilities constructed and operated during the reactor demonstration phase. These facilities are designated the Engineering Prototype Reactor (EPR) and the Commercial Demonstration Reactor (DEMO). It is envisioned that for each confinement approach, a decision will be made to identify which of the competing alternatives will be the basis for the ETF in the 1980's. The current DOE strategy suggests that this decision point would be approximately 1984 for the magnetic confinement approach and approximately 1987 for the inertial confinement approach.

In order to initiate preliminary planning for the 1984 ETF decision in the magnetic confinement approach, the Office of Fusion Energy (OFE) established the ETF Design Center activity in December of 1978. The ETF Design Center has as its objective to define the ETF and to prepare its design, schedule, and cost in appropriate detail to support the initiation of the ETF project. The initial focus of the ETF Design Center will be the tokamak concept; however, as other promising magnetic confinement concepts evolve, they will also be evaluated in the context of the ETF. It is emphasized that many of the technological problems of magnetic confinement fusion concepts are generic in character; thus, the effort directed to the tokamak will be of general value to the magnetic fusion program.

The activities of the ETF Design Center, hosted at ORNL, will be national in focus and will involve representation by the principal tokamak fusion centers (i.e., GA, ORNL, MIT, and PPPL). Moreover, the alternate concept development efforts being carried out at installations such as Lawrence Livermore Laboratory (LLL) and Los Alamos Scientific Laboratory (LASL) will also be integrated into the ETF Design Center deliberations. It is intended that industry play a significant role in the ETF Design Center activity. In its initial phases the ETF Design Center will rely heavily on the work done over the past several years in the area of advanced reactor studies and, in particular, on the work provided for all the TNS activities carried out at GA, ANL, MIT, and PPPL.

7.2.1 ETF Design Center Charter, Goals, and Objectives

The ETF Design Center charter is to coalesce the previous TNS activities into a unified effort to define the ETF and prepare its design in appropriate detail to support the initiation of the project.

The ETF Design Center should have the following key goals and objectives:

- Developing an organizational structure and operational mode that incorporates and represents a national perspective on the ETF.
- Establishing the on-site and off-site capabilities required to support and implement the program.
- Maintaining an effective communication with experimental groups to ensure relevant experimental input to the program.
- Providing recommendations to OFE and the experimental programs concerning additional experiments to strengthen the physics data base for the ETF.
- Maintaining an effective communication with technology development programs including magnetics, plasma heating, tritium handling, materials, etc., to ensure relevant technology input to the program.
- Providing recommendations to OFE and the technology programs concerning new programs and additional emphases to strengthen the technology base for the ETF.
- Maintaining currency in the advancements of plasma theory and plasma engineering to ensure that the program reflects these advancements.
- Providing recommendations to OFE and the theoretical programs concerning method development and computation needs to strengthen the analytical tools for the ETF.
- Preparing and keeping current a program plan for the conceptual design through construction in addition to a ten-year operations plan - for the ETF.
- Providing the opportunity for significant involvement of industries interested in becoming major contributors to the establishment of magnetic fusion as an energy option.
- Serving as the focus for cooperation with international endeavors in advanced magnetic confinement fusion device programs.

7.2.2 ETF Mission Statement

As a point of departure for the ETF Design Center activities, it was deemed essential to establish a well-defined statement on the mission of the ETF in the overall fusion program strategy. In the TNS activities of last year, the various design teams addressed the issue of the mission for the TNS. The Office of Fusion Energy used the mission statement results of last year's TNS activities to develop a preliminary mission statement for the ETF. The essential features of this preliminary mission statement for the ETF lay out a possible testing plan for utilization of the ETF based on the tokamak concept.

The mission statement to result from the planned workshop and the subsequent considerations will represent a point of departure and will be updated and reviewed as the ETF Design Center activities proceed. With the mission statement as a guide, the ETF Design Center will engage in systems analysis and design specifications aimed at developing the most cost-effective facility for achieving the goals and objectives set forth in the mission statement. The design specifications will then be used to lay out an engineering design for the ETF. During this time a comprehensive R&D needs assessment will also be taking place. The R&D needs assessment is being carried out as a fusion community activity and will serve the requirements of both the ETF Design Center and the International Tokamak Reactor (INTOR) activity being conducted under the auspices of the International Atomic Energy Agency (IAEA). The output of the R&D needs assessment will be integrated and evaluated by the ETF Design Center relative to the specific requirements of the ETF. The results of this evaluation and integration, together with the detailed design work, will be used to make recommendations to OFE relative to the ETF program, cost, and schedule. At this point the mission of the ETF will also be reevaluated.

Assuming the above process leads to a favorable result, the ETF Design Center will then focus on a detailed conceptual design of the ETF with a continuing updating of the R&D needs assessment and refining of the ETF mission statement. The ultimate objectives of these activities are to prepare the ETF design in sufficient detail and to perform the associated project engineering and planning functions in sufficient detail to support a decision point for the ETF in 1984.

7.2.3 ETF Design Center Staffing

The leadership of the ETF Design Center team has been established with responsibilities based on a work breakdown structure approach. The major areas of responsibilities are shown in Fig. 7.2. Each area is intended to bring together a grouping of activities that require the application of similar disciplines easily managed as a team.

The plasma system activities are being led by a committee of four physicists, one each from GA, MIT, ORNL, and PPPL, who will receive the necessary support from their colleagues at their home laboratories. The PPPL representative, the senior physicist, chairs the committee and provides the overall guidance in the plasma system area.

Each of the four engineering and technology areas (Fig. 7.3) is being managed by the laboratory selected to be responsible for

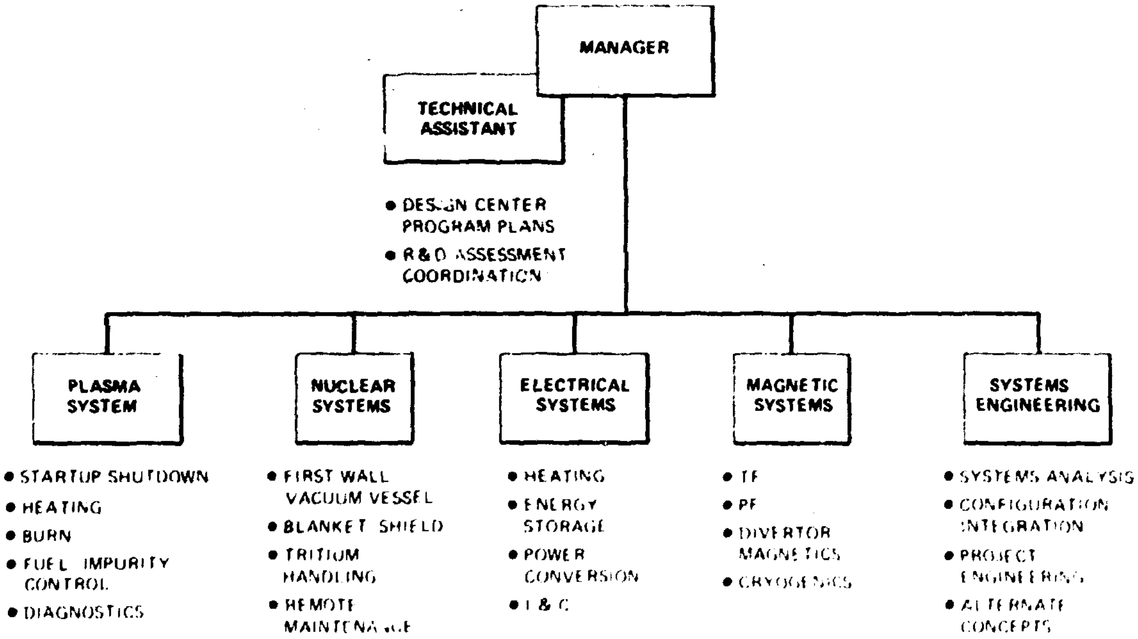
MANAGER
TECHNICAL ASSISTANT
● DESIGN CENTER PROGRAM PLANS
● R&D ASSESSMENT COORDINATION
PLASMA SYSTEM
NUCLEAR SYSTEMS
ELECTRICAL SYSTEMS
MAGNETIC SYSTEMS
SYSTEMS ENGINEERING
● STARTUP SHUTDOWN
● HEATING
● BURN
● FUEL IMPURITY CONTROL
● DIAGNOSTICS
● FIRST WALL VACUUM VESSEL
● BLANKET SHIELD
● TRITIUM HANDLING
● REMOTE MAINTENANCE
● HEATING
● ENERGY STORAGE
● POWER CONVERSION
● I & C
● TF
● PF
● DIVERTOR MAGNETICS
● CRYOGENICS
● SYSTEMS ANALYSIS
● CONFIGURATION INTEGRATION
● PROJECT ENGINEERING
● ALTERNATE CONCEPTS

Fig. 7.2. ETF Design Center organization based on a work breakdown structure approach.

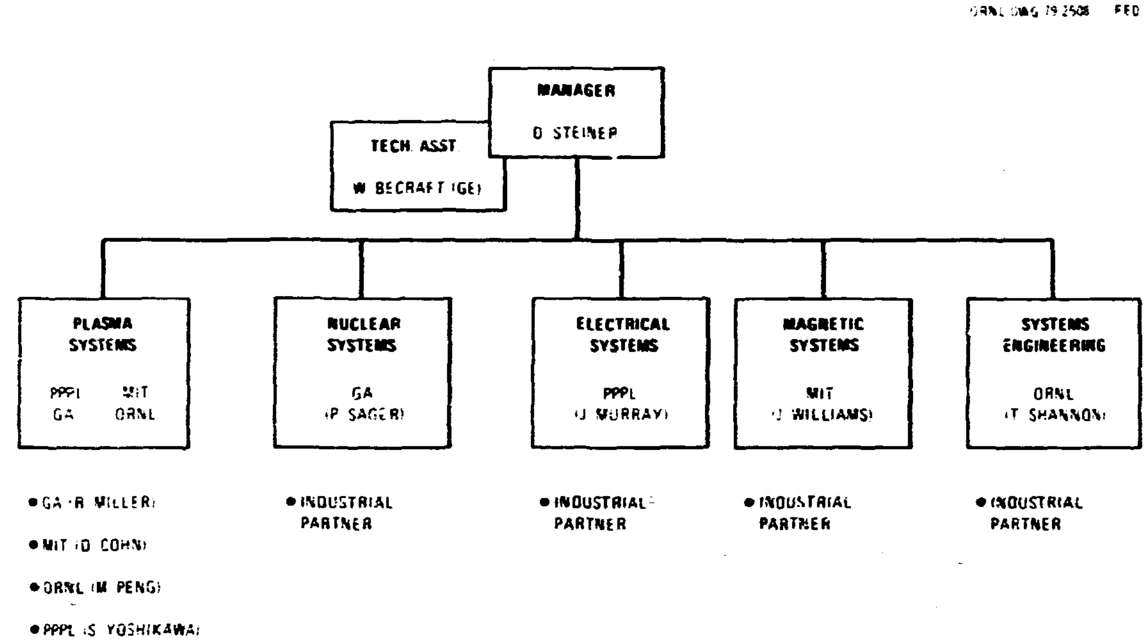
ORNL-DWG 79-2508 FED
MANAGER
D STEINER
TECH ASST
W BECRAFT (GE)
PLASMA SYSTEMS
PPPL MIT
GA ORNL
NUCLEAR SYSTEMS
GA
(P SAGER)
ELECTRICAL SYSTEMS
PPPL
(J MURRAY)
MAGNETIC SYSTEMS
MIT
(J WILLIAMS)
SYSTEMS ENGINEERING
ORNL
(T SHANNON)
●GA (R MILLER)
●MIT (D COHN)
●ORNL (M PENG)
●PPPL (S YOSHIKAWA)
●INDUSTRIAL PARTNER
●INDUSTRIAL PARTNER
●INDUSTRIAL PARTNER
●INDUSTRIAL PARTNER

Fig. 7.3. The ETF Design Center team will represent a laboratory/industry partnership.

that portion of the ETF program. Figure 7.3 shows the laboratories and individuals responsible. An industrial partner will be chosen to work under the direction of each area manager to provide a significant portion of the design and development required for that part of the program. Additional expertise and consultation to address particular problems may be obtained by the responsible laboratory.

7.3 ORNL FUSION POWER DEMONSTRATION STUDY

The development of practical blanket systems that would allow the adaptation of fusion to produce electric power in a utilities application has been identified as an important area of study in the Advanced Systems Program.

During FY 1978 the Westinghouse Electric Corporation, under subcontract to ORNL, completed a design study for the blanket system of a tokamak concept reactor. The scope of this study was limited to generic blanket designs incorporating a combination of stainless steel structure, lithium moderator, and helium coolant. The decision to focus our conceptual engineering effort was based on favorable conclusions of previous work that indicated the feasibility of such a generic system. Our objective in this current study was to focus the conceptual design effort so that a more in-depth assessment of the reliability and performance capabilities of this generic blanket system could be obtained. A summary of the nominal operating conditions and characteristics of the reactor around which the blanket study was based is given in Table 7.2.

7.3.1 The Emphasis on Reliability in Design Approach

In the initial phase of this study, an effort was made to select a promising candidate from generic designs that had been conceptualized previously. It was thought that the upgrading of an existing concept would lead to a design that was defensible with respect to function and reliability potential.

A critical review of previous designs indicated that no individual concept could

Table 7.2. Design parameters relevant to ORNL/Westinghouse Demonstration Reactor Blanket Study

Reactor	
Geometry	"D" cross-section torus
Minor radius	1.5 m
Elongation	1.6
Aspect ratio (torus)	4
Neutron wall loading	2-4 MW/m²
First wall particle heat flux	0.5-1.0 MW/m² (no divertor)
Blanket	
Breeding medium	Lithium
Structural material	Type 316 austenitic stainless steel
Coolant	Pressurized helium Inlet pressure 54 atm Inlet temperature 200°C Outlet temperature 435°C
Structural concept	Modular
Vacuum enclosure	External to blanket
Reactor material temperatures	First wall (radiation damage zone) [illegible]°C Low radiation zone 500°C Maximum (nonstructural) 550°C
Pumping power $\left(\frac{\text{Pump work}}{\text{Thermal output}}\right)$	[illegible]
Tritium-breeding ratio	1.2
Duty cycle	20-min cycle, 95% duty
Operating mode	Pulsed to $10^{[illegible]}$ cycles

stand up to the most fundamental considerations involving reliability and tolerance for failure. Basic considerations of reliability and tolerance for failure have led to two fundamental design requirements for this generic type of blanket.

(1) It is essential that all critical blanket structure be actively cooled. This requirement arises because of the particular character of the heat deposition throughout all portions of the blanket and the uncertainty in surface contact between the stagnant lithium and the structural material.

(2) Because of the potential for a leak in the high pressure coolant circuit, it is essential that all enclosed regions of the lithium container be capable of sustaining the full coolant pressure without rupture or other catastrophic failure.

7.3.2 Development of a New Design

In the process of developing a design around basic reliability requirements, a cylindrical module concept was evolved. The new module concept that was developed in detail for this study is shown in Fig. 7.4. This concept consists of an outer cylinder (with a spherical nose first wall) surrounding an inner lithium-containing cylinder with helium flowing between these concentric cylinders to achieve adequate cooling of both

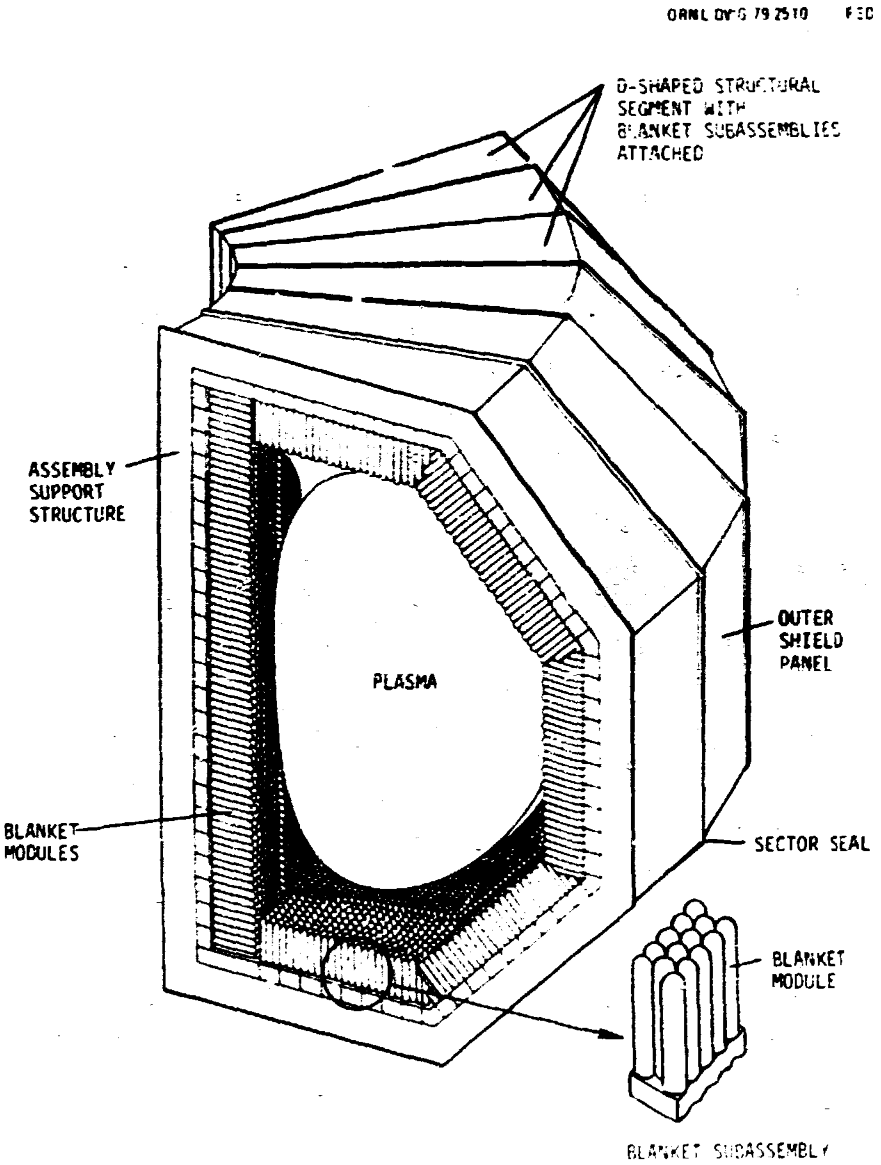
ORNL DWG 79 2510 FED
D-SHAPED STRUCTURAL SEGMENT WITH BLANKET SUBASSEMBLIES ATTACHED
ASSEMBLY SUPPORT STRUCTURE
OUTER SHIELD PANEL
PLASMA
BLANKET MODULES
SECTOR SEAL
BLANKET MODULE
BLANKET SUBASSEMBLY

Fig. 7.4. Cylindrical blanket module.

the lithium and the outer first wall. The schematic illustration of the assemblage of modules as they would be placed in the reactor is shown in Fig. 7.5.

7.3.3 Conclusions of Study

Based on analysis performed in support of the new module concept developed in this study, a viable blanket concept was developed that warrants further development and design refinement. This work will be continued under Westinghouse subcontract in FY 1979. This cylindrical module concept meets the goals of the study to produce a blanket concept that operates under a reasonable set of reactor conditions. In addition, this study has advanced the state of the art in blanket component development by considering reliability, thermal performance, structural lifetime, helium generation, and tritium

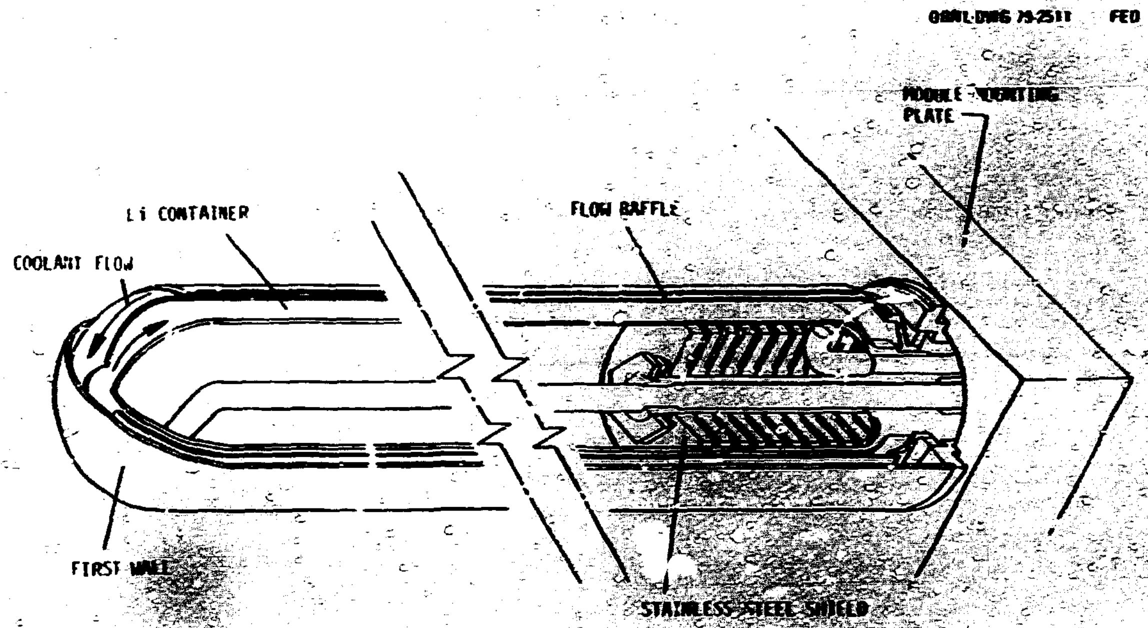

Fig. 7.5. Blanket sector assembly.

breeding. The following is a list of specific conclusions resulting from the study.

- Based on the current understanding of radiation materials data, stainless steel module design is adequate for neutron wall loading up to 4 MW/m^2. Under these conditions the design meets the goal of 10^5 cycles of 20 min with 95% duty, based on considerations of crack growth and brittle fracture at 450°C operating temperatures.
- The concept can reliably withstand full coolant pressure; thus, it satisfactorily addresses a basic reliability requirement of preventing breach of the lithium container in the event of failure of high pressure coolant circuits.
- The method of first wall cooling is not sensitive to the accumulation of helium generated within the lithium that compromised cooling in earlier designs.
- The concept is structurally efficient, amenable to analysis, and simple in shape, can be readily fabricated and evaluated by testing, and is adaptable to mass production.
- Structural support of the modules as replaceable subassemblies is judged a reasonable approach to assembly and maintenance and is compatible with remote handling techniques.
- A first wall temperature of ~450° can be achieved with a 200°C inlet temperature at ~2% pumping power with reasonable helium exit temperatures (~450°C) compatible with acceptable power conversion.
- The main support structure is designed to operate at helium inlet conditions, thereby minimizing thermal growth of the structure and relative motions between the blanket assembly and the interfacing piping.
- Mechanical sealing between the plasma and the outer vacuum boundary can be achieved.
- Scoping analysis indicates that a tritium-breeding ratio of ~1.2 can be obtained.

7.4 COMMITTED SITE EVALUATION

Bechtel National, Inc. (BNI), under guidance from ORNL and with input from the fusion community, evaluated the merits of a committed site with shared facilities for the development of fusion devices. The committed site was evaluated for the following: (1) the development of a single device alone, i.e., tokamak, tandem mirror, or EBT; (2) the development of two devices at the committed site, i.e., tokamak plus tandem mirror and tokamak plus EBT; and (3) the development of all three devices at one site, i.e., tokamak plus tandem mirror plus EBT. A typical scenario for the development of a candidate device consists of three phases: ignition demonstration, power technology demonstration, and commercial prototype demonstration. The scenario for a tokamak is depicted schematically in Figs. 7.6-8. The following sections discuss the results and conclusions drawn at the completion of the one-year study.

7.4.1 Economic Impact

The major cost advantage of the committed site lies in its implementation in the development of a single fusion device as opposed to the development of multiple fusion devices on the same site. The cost saving in site preparation, structures, and reactor support equipment for tokamak development on a committed site is $610 million (TNS/EPR/DEMO), and the cost saving for EBT on a committed site is $576 million. These savings represent a reduction in cost of ~50% compared to the cost of three separate sites for tokamak and three separate sites for EBT. However, combining the development of the tokamak and EBT on a single site results in much less cost advantage (~$80 million) compared to the combined cost of the development of the tokamak on a separate dedicated site and the development of EBT on a separate dedicated site. Grouping the tokamak with the tandem mirror reactor leads to the same conclusion.

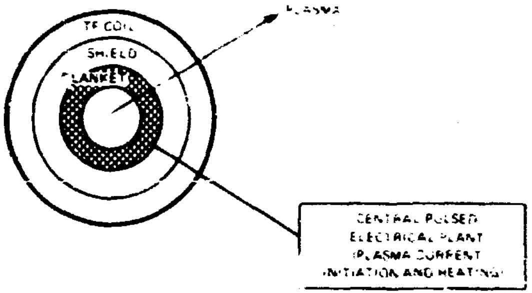
PLASMA
TF COIL
SHIELD
BLANKET
CENTRAL PULSED ELECTRICAL PLANT (PLASMA CURRENT INITIATION AND HEATING)

Fig. 7.6. The ignition phase establishes the basic facility and fusion energy source.

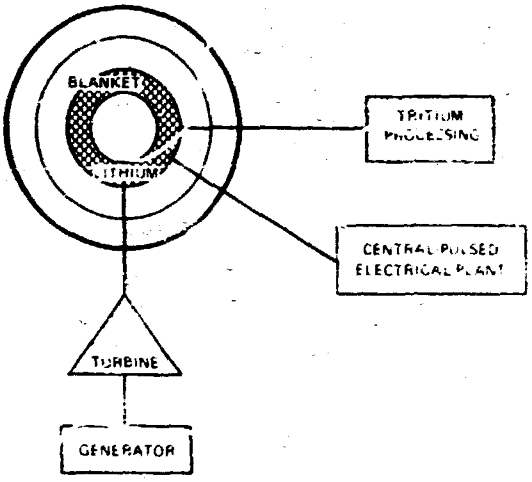

Fig. 7.7. The power generation phase integrates systems external to the fusion energy source.

The cost advantage of the committed site for single fusion concept development over that for multiple concept development results because not much equipment can be shared among upgrades of the different fusion reactor plants. The tokamak needs large quantities of pulsed electrical power for current initiation and heating. Power supplies that are needed on a tokamak TNS can be used on the EPR upgrade and shared between multiple tokamak units in a demonstration phase. However, EBT and tandem mirror reactors are steady-state machines and do not need the large banks of pulsed electrical energy.

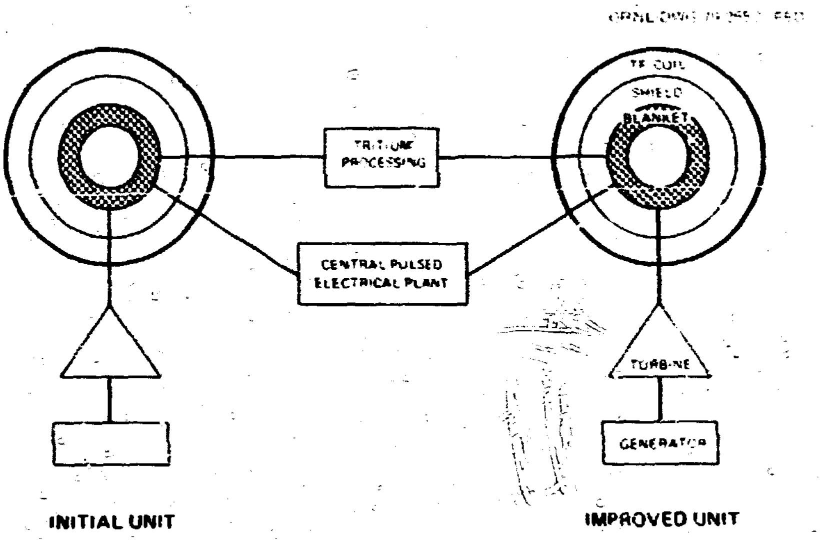

Fig. 7.8. The prototype operation phase involves adding an improved reactor unit to the existing facility.

required for pulsed operation. The mirror needs large amounts of high energy neutral beams to drive the reactor, but this power is drawn off the utility grid in a continuous fashion. The primary cost elements that can be shared among different fusion concepts at a committed site are the costs associated with site selection and development and the cost advantage of higher capacity process equipment, such as heat rejection systems, tritium-handling systems, etc., sized to meet the combined needs of the candidate fusion reactors.

7.4.2 Schedule Impact

It takes approximately five years, as shown in Table 7.3, to select a site, certify it, and make site improvements. At a committed site this is done only once, and the time required for development of a fusion concept is compressed compared to the time required for serial development of multiple sites for each phase of operation.

7.5 TOKAMAK INSTRUMENTATION AND CONTROLS

To date, the controls approaches in fusion have been largely preprogrammed and open loop, but they have sufficed for the low power, short pulse experiments. The successful extrapolation of such approaches to high power, long pulse machines appears improbable where serious constraints such as the avoidance of high energy wall loading must be satisfied throughout the operation. The need for active, closed loop control systems has been underscored further by the emphasis on the high beta and plasma shapes that require active establishment and maintenance, the need for burn control and refueling, and the possible need for feedback control of the plasma-heating energy.

The instrumentation systems used on magnetic confinement fusion experiments include many innovative approaches that have successfully provided the information required from the tests. For the most part these diagnostics are laboratory-type equipment and may require extensive modification if used in a reactor environment of the TNS or ETF device. The data handling approaches to be used on experiments such as the Tokamak Fusion Test Reactor (TFTR) will provide an excellent base for supporting the definition of instrumentation and diagnostic needs for the TNS/ETF, although the long pulse times

Table 7.3. Schedule for site selection/certification and site improvements (5 years – $25 million)

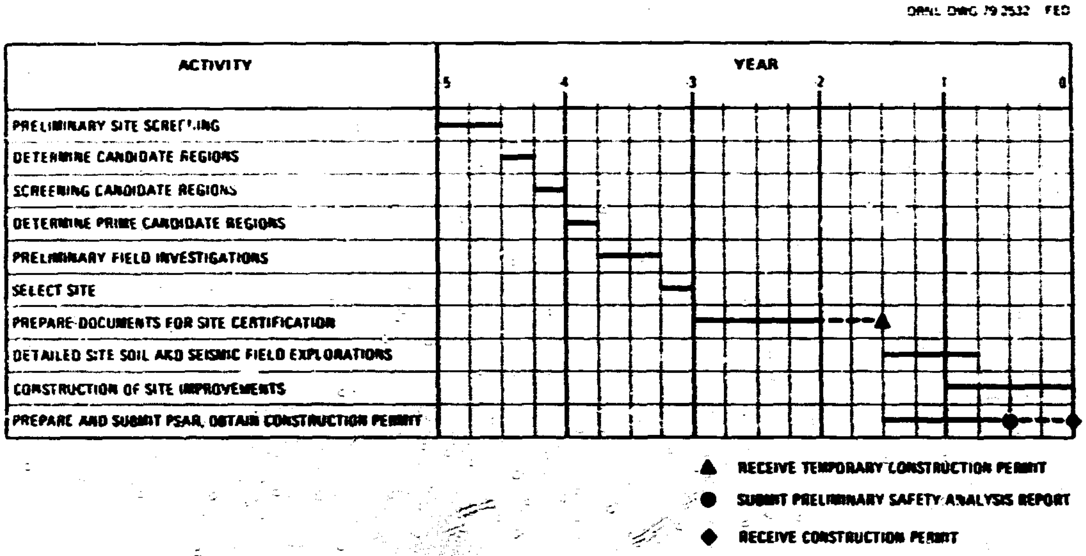

and the ignition operation may place significant demands on the equipment's real-time and archival capabilities. It is expected that the TNS/ETF will impose the most stringent requirements on the I&C equipment, and it is towards this device that these studies are focused.

The emphasis of prime importance in this study program is the definition of the physics transients needed in a complete burn cycle. Thus, the largest portion of the past year's investigation was so applied. The impact of potential abnormal operations such as hard shutdown and aborts, as well as the avoidance and amelioration of such impacts, was given strong attention. The simulation of a tokamak and its control system is a valuable development tool for testing design concepts, especially when the experiment is being operated in the same facility as the I&C study. The verification of the simulation that can be achieved with actual tokamak operation, as well as the potential for getting real transient data to test some particular control hypotheses, provides an excellent corroborative climate for development of the model and expanding it towards the TNS/ETF needs. The initial simulation development was accomplished in FY 1978.

The summary highlights of the FY 1978[2] work that is building a valuable foundation for I&C R&D leading to meeting tokamak reactor needs include the following.

(1) Pertinent physics has been coalesced for studies of control implications.
(2) Transient characteristics in startup phases have been scoped with evolving codes.
(3) Simplified ISX-B control equations have been run on analog and some of the stability concerns identified.
(4) A full set of uniform torus, ISX-B horizontal control equations has been programmed for analog machine.
(5) Preliminary studies[3] showed plasma disruptions as an area needing increased study emphasis.
(6) Plasma disruption effects have been identified (e.g., temperature distribution, eddy currents, thermal stress, number of disruptions tolerable).
(7) R&D needs assessment has been initiated.
(8) Future study plans have been recast based on work to date.

7.6 LARGE ASPECT RATIO TOKAMAK STUDY

The Large Aspect Ratio Tokamak Study (LARTS) is an investigation of the potential for producing a viable long burn tokamak reactor through the enhanced volt-second capability of the OH transformer by employing high aspect ratio designs. The long burn is desirable in order to ameliorate the effect of the pulsed operation of the tokamak on the cyclic fatigue problem for the blanket first wall. Current reactor design studies generally assume 10^4-10^5 pulses/year. However, concern has been expressed that such pulse rates could limit the lifetime of a stainless steel first wall to ∿1-2 years. If the burntime could be extended by an order of magnitude relative to current assumptions, first wall lifetime of at least ten years could be projected.

As a follow-up to the ORNL Fusion Power Demonstration Study, the potential of increasing the volt-second capability by going to high aspect ratio devices was investigated. Preliminary results from this study are shown in Fig. 7.9 for an aspect ratio of 8. This figure plots unit cost [\$/kW(e)], burntime (hours), and plasma current (MA) vs power output [MW(e)]. Plasma radius (meters) and maximum field at the conductor (tesla) are also given. The quantity L_p is the neutron loading at the plasma surface. These results were obtained with the ORNL Systems Code[1] and are normalized to the ORNL DEMO Reactor parameters given in Table 7.4.

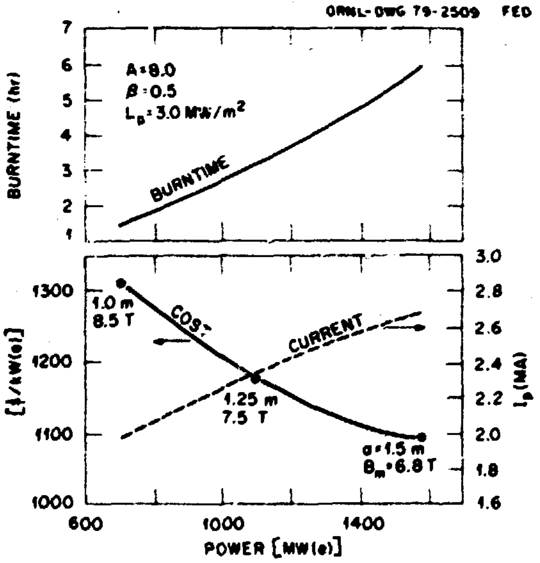

Fig. 7.9. Variation in tokamak burntime, cost, and current as a function of plasma parameters for constant values of beta, aspect ratio, and neutron wall loading.

Table 7.4. ORNL DEMO Reactor parameters

Aspect ratio, A	4
Average beta, β	10%
Plasma radius, a	1.5 m
Maximum field, B_m	8 T
Unit cost	\$1200/kW(e)
Output power	825 MW(e)
Plasma current, I_p	4 MA
Burntime	20 min
Pulse rate	∿2 x 10^4 cycles/year

The high aspect ratio devices are expected to yield a lower beta limit than the moderate aspect ratio devices. Figure 7.9 shows calculations for an average beta of 5% for the A = 8 device based on the 10% value for the A = 4 device shown in Table 7.4. Figure 7.9 indicates burntime capabilities of ∿2-5 hr and associated pulse rates of ∿1.3 x 10^3-3.3 x 10^3 cycles/year, a factor of 6-15 less than in the DEMO Reactor. Moreover, the cost and power output of the high aspect ratio device need not be dramatically different from that of the DEMO Reactor, ∿\$1200-1400/kW(e) and ∿1000 MW(e). Confinement of the alpha depends to first order on the product of current and aspect ratio. Alpha confinement at the higher aspect ratio and lower current devices should be comparable to that in the DEMO Reactor.

On the basis of these preliminary results, it appears that the high aspect ratio tokamak offers potential for extended burn. However, a more detailed study, currently in progress, is necessary to make an in-depth evaluation of the impact of high aspect ratio on the plasma physics issues of magnetohydrodynamic (MHD) stability, quality of confinement, particle control, and burntime.

REFERENCES

1. D. Steiner et al., *ORNL Fusion Power Demonstration Study: Interim Report*, Oak Ridge National Laboratory Report ORNL/TM-5813, Oak Ridge, Tennessee (1977).
2. W. R. Becraft et al., *Tokamak Instrumentation and Controls*, Oak Ridge National Laboratory Report ORNL/TM-6617, Oak Ridge, Tennessee (1979).
3. R. J. Onega et al., *Major Plasma Disruptions in TNS*, Oak Ridge National Laboratory Report ORNL/TM-6616, Oak Ridge, Tennessee (1979).

8. MATERIALS

J. Bentley[1]
B. L. Bishop[2]
E. E. Bloom[1]
C. R. Brinkman[*,1]
R. R. Coltman, Jr.[*,3]
B. L. Cox[2]
J. H. DeVan[*,1]
H. L. Dodds, Jr.[*,4]
K. Farrell[*,1]
T. A. Gabriel[5]
M. L. Grossbeck[1]
T. J. Hoffman[5]
J. R. Keiser[*,1]
R. H. Kernohan[3]
C. E. Klabunde[*,3]
R. A. Lillie[5]
C. T. Liu[*,1]
K. C. Liu[1]
C. J. Long[*,1]
P. J. Maziasz[1]
M. T. Robinson[3]
T. K. Roche[1]
J. L. Scott[1]
J. E. Selle[*,1]
J. O. Stiegler[*,1]
J. B. Talbot[6]
K. R. Thoms[*,7]
P. F. Tortorelli[1]
F. W. Wiffen[1]
J. W. Woods[1]

Abstract. The materials work described in this report falls into three areas: (1) alloy development for irradiation performance, (2) damage analysis and fundamental studies, and (3) radiation effects on organic insulators for superconducting magnets. Alloy development activities, which constitute the major portion of the effort, are directed at four systems: (1) austenitic stainless steels; (2) higher strength Fe-Ni-Cr alloys; (3) reactive and refractory metals; and (4) innovative concepts, especially long-range-ordered (LRO) alloys. With austenitic stainless steels and higher strength Fe-Ni-Cr alloys, emphasis is placed on the irradiation behavior in mixed spectrum fission reactors, where both high atomic displacement rates and high helium production rates occur.

Because reactive metals e.g., titanium alloys and refractory metals, especially molybdenum, niobium, and vanadium alloys are not at the same stage of advancement, emphasis is on unirradiated properties and irradiation tests to high displacement levels only. The corrosion rates of important alloys in liquid lithium and molten salts are also being assessed.

In the area of damage analysis, application of numerical transport theory to particle range distribution in solids has begun with the example of 100-keV ^{197}Au recoils in Au. Comparisons of the binary collision approximation (BCA) code MARLOWE and the dynamical code COMENT have been made with respect to their treatments of linear collision sequences.

Irradiation tests on organic insulators for superconducting magnets showed that no significant changes occurred in specimens irradiated to 4.9K to a dose of $2 \times 10^{[illegible]}$ rads. In a second experiment in which samples were exposed to $2 \times 10^{[illegible]}$ rads, significant changes were observed in the mechanical properties of some samples while other samples remained relatively unaffected. Sample preparation is now complete for a test to an irradiation dose of $1 \times 10^{[illegible]}$ rads.

8.1 ALLOY DEVELOPMENT FOR IRRADIATION PERFORMANCE

8.1.1 The Behavior of Type 316 Stainless Steel under Simulated Fusion Reactor Irradiation[1]

F. W. Wiffen F. E. Bloom
P. J. Maziasz J. C. Stiegler
M. L. Grossbeck

Fusion reactor irradiation response in alloys containing nickel can be simulated in

---

[*] Part-time.

1. Metals and Ceramics Division.
2. Computer Sciences Division.
3. Solid State Division.
4. University of Tennessee, Knoxville, Tennessee.
5. Engineering Physics Division.
6. Chemical Technology Division.
7. Engineering Technology Division.

thermal spectrum fission reactors, where displacement damage is produced by the high energy neutrons and helium is produced by the capture of two thermal neutrons in the reactions: $^{58}Ni + n \rightarrow {}^{59}Ni + \gamma$, $^{59}Ni + n \rightarrow {}^{56}Fe + \alpha$. Examination of type 316 stainless steel specimens irradiated in the High Flux Isotope Reactor (HFIR) has shown that both swelling due to cavity formation and degradation of mechanical properties are more severe than can be predicted from fast reactor irradiations where the helium contents produced are far too low to simulate fusion reactor service. Swelling values are greater and the temperature dependence of swelling is different from those in the fast reactor case. The property change most restrictive for fusion reactor performance is the low values of ductility that result from irradiation. These results imply limitations on the operating conditions and useful lifetimes of stainless steel first wall and high flux region structural components of fusion reactors.

8.1.2 Tensile Properties of Type 316 Stainless Steel Irradiated in a Simulated Fusion Reactor Environment[2]

M. L. Grossbeck P. J. Maziasz

In a fusion reactor the first wall will be subject to intense neutron radiation, resulting in displacement damage as well as the formation of helium and hydrogen from transmutation reactions. Because type 316 stainless steel is a candidate first wall material, an investigation of the strength and ductility of this alloy and of a titanium-modified variation was conducted. Simulation of the fusion reactor environment was accomplished in HFIR, which has an appropriate spectrum to produce both displacement damage and helium through a two-step thermal neutron reaction with nickel contained in the stainless steel.

Miniature tensile specimens were irradiated at temperatures from 350-600°C and subsequently tested in tension; the results were compared with the literature data of type 316 stainless steel irradiated in the Experimental Breeder Reactor II (EBR-II).

For irradiation and test temperatures of 350°C, the yield strength of annealed (1 hr at 1050°C) and 20% cold-worked 316 and 316 TiM material increases very rapidly compared with EBR-II-irradiated material; a slight decrease in strength follows. The peak in yield strength occurs at a fluence of ~1.0 × 10^{26} neutrons/m^2 ($E > 0.1$ MeV). At 450 and 575°C, the yield strength of 20% cold-worked material decreases monotonically with an indication of saturation above ~1.6 × 10^{26} neutrons/m^2 ($E > 0.1$ MeV). Whereas at the lower temperature, type 316 and 316 TiM had nearly the same yield strength, at the higher temperatures the titanium-modified alloy exhibited ~40-50% greater strength, depending upon fluence and temperature. In the annealed condition the two alloys behaved similarly, both exhibiting a peak in yield strength at 350 and 450°C but increasing to a saturation value at 575°C.

The ductility of both alloys in the cold-worked condition decreased monotonically, tending to approach saturation. The exception was 20% cold-worked 316 TiM at 450°C, which appeared to have a constant elongation of ~8% to a fluence of 2 × 10^{26} neutrons/m^2 ($E > 0.1$ MeV), the highest fluence attained. In the annealed condition both alloys exhibited a ductility minimum with increasing fluence. This behavior differs from EBR-II-irradiated 20% cold-worked 316 stainless steel, which displays a ductility maximum at low fluence.

The rapid hardening and rapid initial drop in ductility are attributed to the generation of helium and the coalescence into clusters and bubbles which impede dislocation motion. Nonetheless, based on this low fluence data, at 350 and 450°C total elongation appears to saturate at a value above 6%. The ductility appears adequate for the early life of a structural material in a fusion reactor.

8.1.3 Precipitation Response of Austenitic Stainless Steel to Simulated Fusion Irradiation[3]

P. J. Maziasz

The precipitation response of annealed type 316 stainless steel irradiated in HFIR was studied and compared to previously observed thermal aging and fast reactor irradiation responses. Irradiation in HFIR simultaneously produces high levels of helium and displacement damage and partially simulates a fusion environment. Samples have been irradiated at temperatures from 550-600°C to fluences producing up to 3300 appm helium and 47 dpa. If the precipitation response after HFIR irradiation is compared to that after thermal aging on a time-temperature-precipitation diagram, HFIR irradiation is seen to result in phase combinations similar to those after thermal aging; but the precipitation response shifts to lower temperatures and shorter times relative to thermal aging. The shifts range from 70-200°C and are different for different phase combinations. However, the phase regions resulting from fast reactor irradiation require little or no shift in temperature or time relative to thermal aging. Therefore, HFIR irradiation also results in shifting the phase regions to shorter times and lower temperatures relative to fast reactor irradiation. The addition of simultaneous helium production to the irradiation environment is coincident with the absence of the unidentified rod-shaped precipitate and the presence of M_6C (since determined to be eta phase precipitate) and Laves phases for HFIR relative to fast reactor irradiation at similar temperatures and fluences. Most voids produced by irradiation in a fast reactor are heterogeneously nucleated on the rod-shaped precipitates or $M_{23}C_6$, and after HFIR irradiation, only a fraction of the cavities is attached to precipitates, with Laves being the most preferred and $M_{23}C_6$ the least preferred. Helium has been shown to change the swelling, mechanical properties, and cavity response of annealed type 316 stainless steel relative to fast reactor irradiation. Helium has also been shown to change the precipitate response as well and is important in understanding and anticipating fusion environment materials response.

8.1.4 Estimates of Time-Dependent Fatigue Behavior of Type 316 Stainless Steel Subject to Irradiation Damage in Fast Breeder and Fusion Power Reactor Systems[4]

C. R. Brinkman K. C. Liu
M. L. Grossbeck

[illegible] lives obtained from strain-controlled fatigue tests at 593°C from specimens irradiated in EBR-II to a fluence of 1-2.63 x 10^{26} neutrons/m^2 (E > 0.1 MeV) were compared to predictions based on the method of strain range partitioning. It was demonstrated that when appropriate tensile and creep-rupture ductilities are employed, reasonably good estimates of the influence of hold periods and irradiation damage on the fully reversed fatigue life of type 316 stainless steel can be made. Having demonstrated the applicability of this method, ductility values for 20% cold-worked type 316 stainless steel specimens irradiated in a mixed spectrum fission reactor were used to estimate fusion reactor first wall lifetime. The ductility values used were from irradiations that simulate the environment of the first wall of a fusion reactor. Neutron wall loadings ranging from 2-5 MW/m^2 were used. Results, although conjectural because of the many assumptions, tended to show that 20% cold-worked type 316 stainless steel can be used as a first wall material with a 7.5-8.5 MWyr/m^2 lifetime goal provided the neutron wall loading does not exceed more than ~2 MW/m^2. These results were obtained for an air environment, and it is expected that the actual vacuum environment will extend lifetime beyond 10 MWyr/m^2.

8.1.5 The Response of Inconel 600 to Simulated Fusion Reactor Irradiation[5]

F. W. Wiffen

Inconel 600 was irradiated in HFIR to provide a partial simulation of fusion reactor service. Samples were irradiated at 55-700°C to investigate swelling and postirradiation tensile properties as a function of irradiation and test temperatures under conditions of concurrent displacement damage and helium production. Helium contents from 500-1800 appm and displacement levels of 4-9 dpa were achieved, and the results were used to estimate performance in a fusion reactor environment. Between 300 and 600°C, the swelling [illegible] dependent on temperature, with swelling ranging from 0 to ~1%. However, above 600°C swelling increased rapidly. The swelling values were much larger than expected from fast reactor and ion bombardment results. Furthermore, cold work was not effective in suppressing the swelling of Inconel 600. Tensile property measurements and fractography on the same samples showed that strength values increased for irradiation at 55-400°C but decreased below unirradiated values for irradiations at 600 and 700°C. Elongation values were lowest at the temperature extremes. Total elongations below 1% were found only for irradiation and test temperatures of 600 and 700°C. The fractures were completely transgranular for samples irradiated and tested at 300 and 400°C, of mixed mode but predominately intergranular at 500°C, and fully intergranular at 600 and 700°C. The results suggest that Inconel 600 does not offer any advantages over type 316 stainless steel and does not warrant further development for fusion reactor application.

8.1.6 Plastic Instability in Neutron Irradiated Niobium[6]

F. W. Wiffen

Niobium alloys irradiated and tested over a wide range of conditions show ductile behavior in almost all available data. Tensile tests show irradiation-produced increases in strength properties and decreases in total elongation. However, an important restriction on the use of these alloys for service in irradiation environments involves the plastic instability exhibited in a number of cases. This behavior is characterized by zero uniform elongation, even though the total tensile elongation may be high. The plastic instability does not relate to a critical value of irradiation strengthening, nor is it accompanied by any change in the fracture mode. In these two respects, it is different from the embrittlement produced by cleavage fractures and a shift in the ductile-to-brittle transition temperature (DBTT), the classical embrittlement mechanism in irradiated ferritic steels and in molybdenum. The plastic instability ductility limitation in niobium alloys results from the channeling deformation mode observed in samples irradiated to produce a microstructure in which a high concentration of small dislocation loops dominates. Dislocations moving in channels eliminate the loops, thereby softening the matrix for further deformation at a decreasing total load. Plastic instability is suppressed if the irradiation-produced microstructure contains a large population of voids. The voids are not removed by moving dislocations and are believed to act as pinning sites, allowing the material to work harden and exhibit greater-than-zero uniform elongation.

8.1.7 The Ductility in Bending of Molybdenum Alloys Irradiated between 425 and 1000°C[7]

B. L. Cox F. W. Wiffen

Molybdenum alloys are potential candidate materials for fusion reactor applications, either in structural or protective components. These alloys offer the potential of operation at higher temperatures than alternative materials, but they also present new materials limitations. One of the identified problems that could limit the application of molybdenum alloys is the shift in the DBTT into the range of operating temperatures as a result of irradiation.

Samples of Mo, Mo-0.5 Ti, and Mo-0.5 Ti-0.09 Zr (TZM), initially fully recrystallized, were irradiated in the EBR-II to fluences of 2.5 × [illegible] neutrons/m² (>0.1 MeV). Four irradiation temperatures spanned the range 425-1000°C. Only small segments of these materials were available, in the form of rectangular coupons 3 x 2.8 x 0.4 mm. These specimens were electropolished and then tested in vacuum in slow three-point bending at temperatures from 22-650°C. The DBTT was bracketed by establishing the shift from failure in bending to full 45° bend under load. These results will be supplemented by scanning electron microscope (SEM) examination of the fracture surfaces.

All three alloys showed qualitatively similar behavior. The most severe degradation was produced by irradiation at 585°C. These samples failed in all tests from 22-650°C, indicating a DBTT above the irradiation temperature. Both higher and lower irradiation temperatures had less effect on the ductility, with indicated DBTT between 100 and 200°C for 425°C irradiation and above 200 but below 300°C for both 790 and 1000°C irradiation temperatures. These results are qualitatively consistent with the microstructural features reported for the same specimens. Void concentrations were higher at 585°C than for the other three irradiation temperatures.

8.1.8 Neutron Irradiation Damage in Molybdenum at High Temperatures

J. Bentley F. W. Wiffen

Commercial purity molybdenum (~30 wppm carbon) has been irradiated in EBR-II to a fluence of ~6 x [illegible] neutrons/m² (E > 0.1 MeV), which corresponds to ~2 dpa. Irradiations at nominal temperatures in the range 600-1500°C (~0.3[illegible] 0.6[illegible] of the absolute melting temperature) were accomplished in individual holders in a sealed capsule containing a static argon gas atmosphere. Specimens cut from the 2.5-mm-diam irradiated rods were examined by transmission electron microscopy (TEM). The damage structure consists of two components: voids and dislocations. At the lowest irradiation temperature, the high concentration of small voids is imperfectly ordered on a body-centered cubic (bcc) superlattice. At higher irradiation temperatures, the void size increases and concentration decreases markedly. At the highest irradiation temperatures, rod-shaped or "super" voids are observed. Dislocation densities are low, with dislocations in the form of a network at all temperatures except the lowest, where some small loops are also present. Quantitative microstructural data was studied, with particular reference to the special features of the present irradiations: the high irradiation temperatures and intermediate fluences.

8.1.9 The Tensile Properties of High Oxide SAP Containing Helium and Tritium

P. J. Maziasz K. Farrell

Sintered aluminum product (SAP), an alloy of aluminum and aluminum oxide particles, has been suggested as a potential material for the first wall of a fusion reactor with minimum radioactivity inventory that would operate at ~400°C, where SAP retains more strength than any other aluminum alloy. Because this temperature is ~0.7 of the absolute melting temperature, neutron displacement damage is not likely to be troublesome. However, swelling and embrittlement by the gases helium and hydrogen from (n,α) and (n,p) reactors and by tritium picked up from the plasma and the breeder blanket may be a problem.

To investigate the effects of gases in SAP, alloys containing ^{6}Li isotope were made and were neutron irradiated in a thermal reactor to produce helium and tritium from burnup of the ^{6}Li. The irradiated alloys were then annealed for 1000 hr at temperatures in the range 300-500°C and were tensile tested to failure at the postirradiation annealing temperature. The alloys contained 17-24 wt % Al_2O_3 and gas levels between 0 and 1700 appm each of helium and tritium.

Immersion density measurements indicated no discernible swelling from the gases, some of which were shown to be trapped in tiny bubbles at the Al_2O_3/Al interfaces. Only materials with the higher gas levels showed a measurable loss in ductility, but even without gas, the ductility was low, <1% elongation. However, there was no marked reduction in ultimate tensile strength (UTS) or fracture stress, implying that embrittlement from gases was not severe. These data suggest that incorporation of stable, inert particles in first wall alloys might provide a means of ameliorating potential problems of gas swelling and embrittlement.

8.1.10 Recovery of Tritium from Solid Lithium-Sintered Aluminum Product (SAP) and Lithium-Aluminum Alloys[13]

J. B. Talbot F. W. Wiffen

The tritium release rates of irradiated samples of lithium-containing aluminum (Li-Al) and lithium-containing sintered aluminum product (Li-SAP) were investigated to evaluate the potential application of both materials in fusion reactors. The observed release rates followed the pattern expected for bulk diffusion of tritium in a solid. Therefore, diffusion coefficients were determined for tritium in Li-SAP over a temperature range of 383-500°C and for tritium in Li-Al at 450°C. At 450°C the diffusion coefficients of tritium in Li-SAP and Li-Al are 2.988×10^{-10} cm^2 sec^{-1} and 1.462×10^{-6} cm^2 sec^{-1}, respectively.

8.1.11 Current Irradiation Experiments in the MFE Materials Program

M. L. Grossbeck J. W. Woods

Magnetic fusion energy (MFE) irradiation experiments at Oak Ridge National Laboratory (ORNL) are all neutron irradiations in fission reactors. EBR-II, HFIR, and the Oak Ridge Research Reactor (ORR) are the reactors now being used. HFIR and ORR are mixed spectrum reactors used because of their ability to form helium through thermal neutron absorption in nickel. HFIR is used primarily to study the effects of high helium concentrations; ORR is used for instrumented irradiation under conditions more closely simulating the fusion reactor environment. An experiment now being planned will have the neutron spectrum tailored in order to match the helium/damage ratio of a fusion reactor. EBR-II is being used (1) to achieve high damage levels with little helium production and (2) in conjunction with cyclotron helium injection and tritium decay to correlate such helium-doping techniques with continuous helium production in a mixed spectrum reactor.

Specimen types include tensile specimens, pressurized tube irradiation creep specimens, electron microscope specimens, fatigue specimens, and auger fracture specimens. Table 8.1 gives summary information on recent reactor experiments.

8.1.12 Future MFE Materials Irradiation Experiments

M. L. Grossbeck K. R. Thoms

Experiments are now in the design and fabrication stages for both HFIR and ORR for the irradiation of Paths A and B candidate first wall materials.

The spectrum-tailored ORR experiment will consist of an instrumented cylindrical capsule contained in a removable core piece that will be changed periodically during the irradiation in order to achieve the appropriate neutron spectrum to duplicate the helium/damage ratio experienced by a fusion reactor first wall. The experiment will be irradiated for five years with specimen discharges at one, two, three, and five years (Fig. 8.1). For the first cycle only Path A

Table 8.1. ORNL-ADIP[a] irradiation experiments of fusion reactor materials currently being examined or irradiated

Fission reactor	Experiment	Type of material[b]	Type of specimen	Number of specimens	Date removed from reactor
ORR	MFE-1	Paths A,B,C,D	Tensile; fatigue; TEM[c]	500	June 1978
ORR	MFE-2	Paths A,B,C,D	Tensile; fatigue; pressure tube; TEM	442	In reactor
EBR-II	X-264	Paths A,C	Tensile; TEM	100	January 1977
EBR-II	X-287	Paths A,B,C	Tensile; pressure tubes; welds; TEM	984	January 1979
HFIR	CTR-4,-7, -8	Path B	Tensile	33	August 1977
HFIR	CTR-9 to-13	Path A	Tensile	55	April 1977
HFIR	CTR-14,-15, -20 to -22	Path A	Fatigue	50	Various, 1978
HFIR	CTR-16	Paths A,B	Tensile	42	July 1977
HFIR	CTR-17,-19	Path A	Tensile; welds	22	December 1977
HFIR	CTR-18	Paths A,B	Tensile	11	October 1978
HFIR	CTR-23	Path B	Fatigue	10	February 1979
HFIR	CTR-24	Path A	Tensile; temperature monitors	11	January 1979

[a] ADIP = Committee on Alloy Development for Irradiation Performance.

[b] Specimen materials are designated as in the ADIP Program Plan, DOE/ET-0032/1 (July 1978).

[c] TEM = disks for transmission electron microscopy.

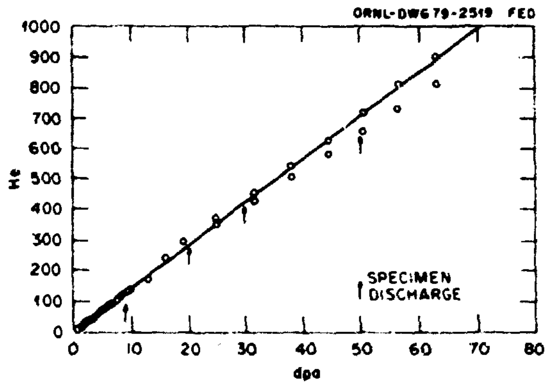

Fig. 8.1. Helium content as a function of dpa for type 316 stainless steel. The solid line represents irradiation at a fusion reactor first wall; the symbols represent irradiation in ORR with neutron energy spectral tailoring.

alloys will be irradiated, but following this, the spectrum will permit Path B alloys to be irradiated with the proper helium/damage ratio.

The experiment will consist of two subassemblies, each with two specimen chambers, each operating at one of the following actively controlled temperatures: 300, 400, 500, and 600°C. Temperature will be controlled by providing a mixture of argon, helium, and/or neon in an envelope surrounding the specimen chambers. Control of the gas mixture produces control of thermal conductivity and, therefore, heat transfer from the specimens and specimen temperature. Neutron flux will also be monitored by flux wires that may be removed and replaced during irradiation. Irradiation for the first subassembly is expected to begin by January 1980.

Six experiments are planned for HFIR. Four experiments will contain tensile specimens of the MFE reference heat of 20% cold-worked type 316 stainless steel. The remaining two will contain mostly TEM disk specimens to be used for swelling, microstructural examination, and mechanical tests of ductility. The specimens will include the Path A prime candidate alloy and Path B base research alloys. Both compositional and microstructural variations will be included.

8.1.13 Design of Materials Irradiation Experiments Utilizing Spectral Tailoring

T. A. Gabriel R. A. Lillie
B. L. Bishop

The helium production-to-displacement per atom (He/dpa) ratio expected at the first wall of a fusion reactor for stainless steel alloys can be, within reasonable limits, reproduced in real time in fission reactors such as ORR because of the helium production characteristics of nickel ($^{58}Ni + n_{th} \rightarrow {}^{59}Ni$, $^{59}Ni + n_{th} \rightarrow {}^{56}Fe + \alpha$). The reproduction of the He/dpa ratio can be accomplished by intermittent modification of the thermal-to-fast neutron flux ratio because the helium production will be dominated by the thermal fluence and the fast fluence will determine the dpa. This report summarizes some of the neutronic calculations that are being carried out to determine the amount of change as a function of time necessary in the thermal-to-fast ratio and the design of the experimental capsules that will produce the needed changes.

The results of the preliminary calculations, shown in Fig. 8.2, are for one heat of stainless steel (i.e., a fixed nickel content) and indicate the level of change required in the thermal flux and dpa rate. There is nothing unique about the data; other modifications of the thermal flux and dpa rate can yield the same desired end points. The solid straight line represents the He/dpa expected at the first wall of a fusion reactor. Approximately 10 dpa and 140 appm helium/year will be obtained for this composition of stainless steel in a fusion reactor at 1-MW/m² wall loading. To obtain this level of damage in ORR will require ~1.3 years of irradiation. The x's, △'s, O's, and *'s represent the calculated data obtained using a representative ORR neutron spectrum, but with variations of the thermal flux and dpa rates. (These data have been extended out to ~30 dpa.) Initially the thermal flux is increased by 20%, and the dpa rate is decreased by 20%. Following this initial period, the remainder of the time of irradiation requires various reductions in the thermal flux and various increases in the dpa rates (fast neutron flux).

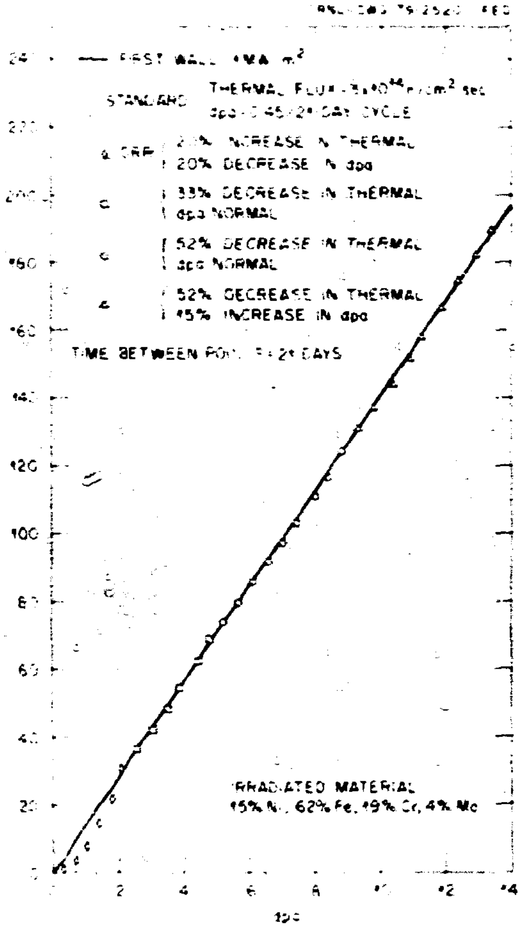

Fig. 8.2. Helium vs the dpa expected on a fusion reactor first wall and what can be obtained in ORR by spectral tailoring.

Consideration has also been given to utilizing EBR-II to increase the dpa level without helium production if the helium buildup becomes excessive. This reactor has essentially no thermal flux and would produce helium only by direct interactions that occur at a much slower rate.

The data in Fig. 8.2 indicate only the level of change required in the thermal flux and dpa rates. Methods to yield the desired changes were obtained from three-dimensional (3-D) neutron diffusion calculations using the VENTURE[11] computer code with the ORR core configuration shown in Fig. 8.3. The experiment, which for these calculations has been assumed to be 40% stainless steel and 60% void, will be located in the center of the C-3 core piece. The calculations were carried out for various Al plus H_2O compositions that constitute the core piece. The variation of the thermal neutron flux and dpa rate is shown in Fig. 8.4. These data have been used to specify preliminarily the design of the core piece for the first two periods of irradiation. During the first period of irradiation, the core piece will, as presently planned, be composed of ~37% Al and ~63% H_2O because this composition yields the changes suggested by the data given in Fig. 8.2. During the second period, the core piece will be composed of [illegible]. The changes in the thermal [illegible] and the dpa rate resulting from [illegible] fuel 20 g to B-3, 20 g to [illegible] around the C-3 core piece [illegible] left side of Fig. 8.4. [illegible] done for a 100% Al [illegible] the experimental capsule. [illegible] that the thermal flux can be [illegible] the dpa rate can [illegible]

Additional [illegible] are planned for larger fuel [illegible] different core piece materials such as [illegible] or tungsten because

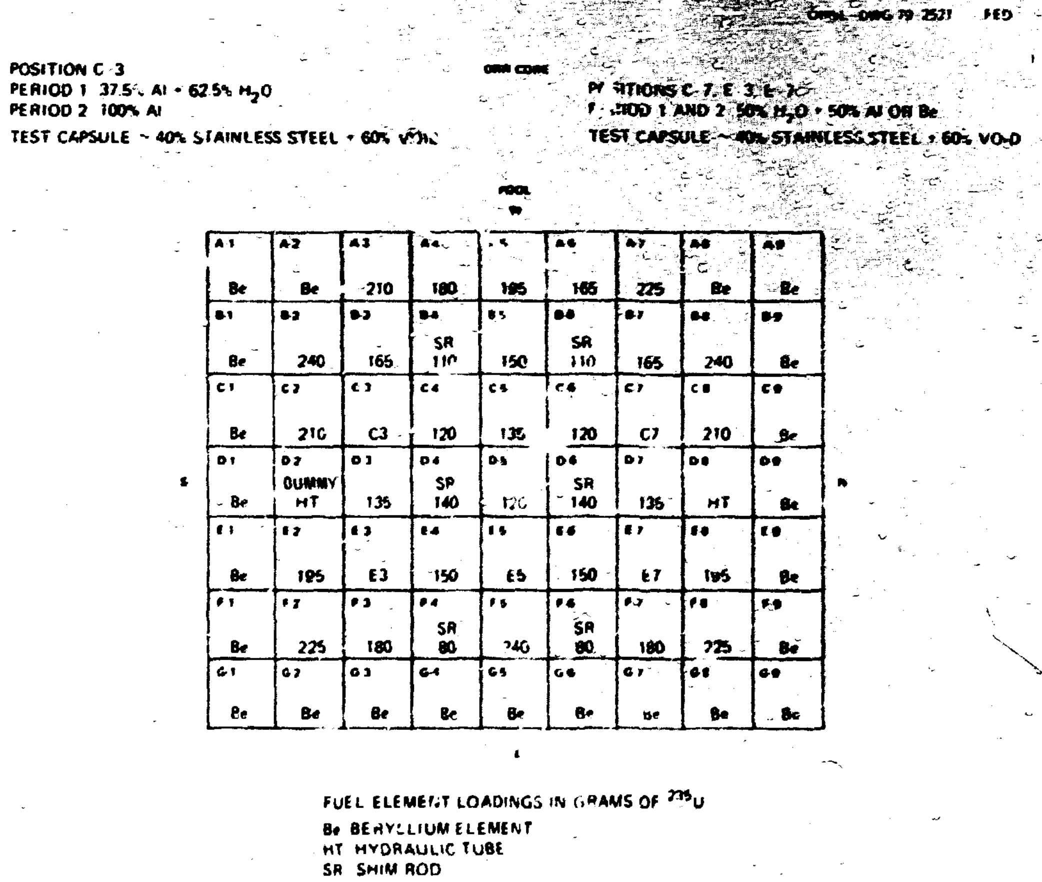
ORNL-DWG 79-2521 FED
POSITION C-3
PERIOD 1 37.5% Al + 62.5% H_2O
PERIOD 2 100% Al
TEST CAPSULE ~ 40% STAINLESS STEEL + 60% VOID
ORR CORE
POSITIONS C-7, E-3, E-7
PERIOD 1 AND 2 50% H_2O + 50% Al OR Be
TEST CAPSULE ~ 40% STAINLESS STEEL + 60% VOID
POOL
W
S
N
E

A1 Be	A2 Be	A3 210	A4 180	A5 195	A6 165	A7 225	A8 Be	A9 Be
B1 Be	B2 240	B3 165	B4 SR 110	B5 150	B6 SR 110	B7 165	B8 240	B9 Be
C1 Be	C2 210	C3 C3	C4 120	C5 135	C6 120	C7 C7	C8 210	C9 Be
D1 Be	D2 DUMMY HT	D3 135	D4 SR 140	D5 120	D6 SR 140	D7 135	D8 HT	D9 Be
E1 Be	E2 195	E3 E3	E4 150	E5 E5	E6 150	E7 E7	E8 195	E9 Be
F1 Be	F2 225	F3 180	F4 SR 80	F5 240	F6 SR 80	F7 180	F8 225	F9 Be
G1 Be	G2 Be	G3 Be	G4 Be	G5 Be	G6 Be	G7 Be	G8 Be	G9 Be

FUEL ELEMENT LOADINGS IN GRAMS OF ^{235}U
Be BERYLLIUM ELEMENT
HT HYDRAULIC TUBE
SR SHIM ROD

Fig. 8.3. ORR core loading for neutronics calculations.

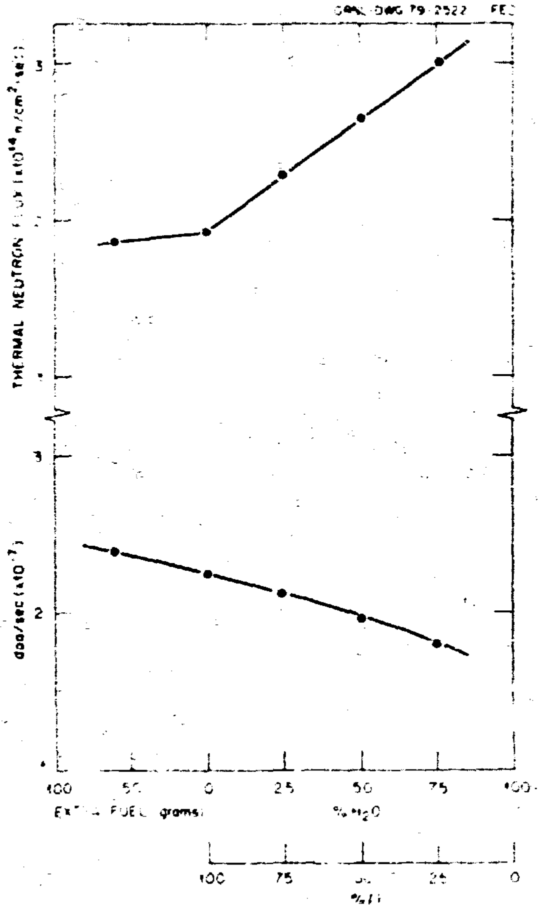

Fig. 8.4. Variation in the dpa and thermal neutron flux in the C-3 position in ORR as a function of core piece composition and fuel loading around C-3.

the preliminary calculations for large dpa levels require a 15% increase in the dpa rate and up to a 75% decrease in the thermal flux.

8.1.14 Thermal-Gradient Mass Transfer in Lithium-Stainless Steel Systems[12]

P. F. Tortorelli J. H. DeVan

The possible uses of lithium as a coolant and/or breeding fluid in fusion reactors have renewed interest in the compatibility of molten lithium with engineering materials. Both loss of material due to corrosion and development of flow restrictions by mass transfer of the dissolved elements to the cooler parts of the system are areas of concern.

The corrosion of type 316 stainless steel by flowing lithium (108 m/hr) was studied as a function of time in thermal convection loops. After a transient period, the corrosion rates were observed to be constant with time with values ranging from 10-20 mg/m^2 hr. Preliminary analysis indicated that the corrosion rate is controlled by the diffusion of iron through the liquid-lithium boundary layer. The deposition processes, which led to flow restrictions in several loops, involved the formation of crystals of nearly pure chromium in the coldest parts of the systems.

8.1.15 Effects of Nitrogen and Nitrogen Getters in Static Lithium on the Corrosion of Type 316 Stainless Steel[13]

P. F. Tortorelli J. H. DeVan
J. E. Selle

Because nitrogen is a principal impurity in lithium, its effect on the corrosion of type 316 stainless steel was investigated by purposely adding nitrogen to lithium and subsequently conducting tests under static conditions. This corrosion was studied as a function of exposure time and temperature. It was found that the corrosion of type 316 stainless steel in nitrogen-contaminated lithium between 500 and 700°C was severe, but in a closed system, the corrosion rate decreased rapidly with time. The corrosion resulted in a uniform, porous surface layer at 500°C, and the attack was intergranular at 600 and 700°C. The grain boundary penetration was described by an empirical equation modified by a time-dependent nitrogen concentration of the lithium.

In an attempt to offset the deleterious effect of nitrogen on the compatibility of stainless steel with lithium, calcium, zirconium, titanium, and yttrium were used as gettering agents. When added to nitrogen-contaminated lithium at 500°C, calcium, zirconium, and titanium reduced the extent of corrosion of type 316 stainless steel, but their effectiveness was not great at 600 and 700°C. Yttrium was ineffective at all three temperatures.

8.1.16 Corrosion Tests of Austenitic Stainless Steels in Static Lithium

P. F. Tortorelli J. H. DeVan
J. E. Selle

The compatibility of type 316 stainless steel with liquid lithium that contained either oxygen, carbon, hydrogen, aluminum, titanium, zirconium, silicon, or lead was studied. The addition of aluminum and silicon resulted in continuous and potentially inhibiting reaction layers on the stainless steel surfaces. Zirconium and titanium additives produced no significant effects compared with baseline tests, but lead in lithium resulted in slightly greater corrosion. The presence of oxygen or hydrogen in the liquid lithium had very little influence on the corrosion of type 316 stainless steel under static conditions. On the other hand, the addition of carbon altered the near-surface microstructure and resulted in corresponding weight gains. The comparative corrosion resistance of a variety of 300-series stainless steels was determined in purified lithium. Only small differences in corrosion response occurred among the steels tested. Types 310 and 321 stainless steel exhibited the largest and smallest weight losses and surface degradations, respectively.

8.1.17 Corrosion of Long-Range-Ordered (Co-V-Fe) Alloy in Static Lithium

P. F. Tortorelli C. T. Liu
J. H. DeVan

Coupons of the long-range-ordered (LRO-1) alloy (60 wt % Co, 25 wt % V, 15 wt % Fe) were exposed to pure, static lithium in order to determine qualitatively their corrosion resistance relative to other materials. Tensile specimens were placed in LRO-1 alloy cups containing lithium and were subsequently sealed inside type 316 stainless steel capsules. Experiments were performed for 2000 hr at 600 and 850°C with resulting average weight changes of -0.2 g/m^2 and +2.1 g/m^2, respectively. In comparison, type 316 stainless steel that was exposed to lithium for 2000 hr at 600°C experienced an average weight loss of 0.1 g/m^2. The lithium-exposed specimens were then tensile tested at room temperature to determine their mechanical properties. Lithium exposure at 600°C caused a decrease in ductility at room temperature. However, the ductility is unaffected after exposure at 800°C. The reduction in ductility after 600°C exposure is not well understood at the present time but may be related to contamination by interstitials that come from the lithium or the stainless steel capsules.

8.1.18 Compatibility of Molten Salts with Type 316 Stainless Steel[14]

J. R. Keiser J. H. DeVan

Molten salts may have several applications in tokamak deuterium-tritium-type fusion reactors. Lithium-bearing molten salts are being considered for use as the breeding material, low melting point salts are candidates for the coolant, and other selected salts may be used for electrochemical extraction of tritium from lithium. Thermal convection loops have been used to study the compatibility of type 316 stainless steel with $LiF-BeF_2$, $KNO_3-NaNO_2-NaNO_3$, and LiF-LiCl-LiBr. Results of weight change measurements indicate that the corrosion rate of type 316 stainless steel in $LiF-BeF_2$ drops from 15 μm/year to <2 μm/year when a beryllium reductant is added to the salt. The corrosion rate of the same steel in $KNO_3-NaNO_2-NaNO_3$ was found to be a function of maximum temperature and ranged from 7 μm/year at 430°C to >74 μm/year at 550°C. In the LiF-LiCl-LiBr salt mixture, the measured corrosion rate of

316 stainless steel was 2 μm/year. During the experiments, controlled potential voltametry was used successfully to monitor changes in the oxidation potential of the salts.

8.1.19 Procurement of Materials for the MFE Alloy Development for Irradiation Performance in Fusion Reactor Programs

T. K. Roche

Four classes of materials will be evaluated simultaneously in support of the program for alloy development for irradiation performance in fusion reactors. These are

(1) Path A – austenitic stainless steels,
(2) Path B – higher strength Fe-Ni-Cr alloys,
(3) Path C – reactive and refractory metal alloy, and
(4) Path D – innovative concepts.

Procurement of Paths A, B, and C alloys has been initiated and is now partially completed.

A 3000-lb double vacuum-melted heat of Path A prime candidate alloy (composition shown in Table 8.2) was produced by Teledyne Allvac and converted to plate and bar products. During 1979 these products will be the subject of additional mechanical working and heat treating experiments for determining microstructural response and its effect upon irradiation performance.

Two 300-lb double-vacuum-melted heats of each of the five Path B base research alloys (compositions shown in Table 8.2) have also been made by Teledyne Allvac and converted to bar product. A small quantity of each alloy was subsequently processed to a 0.024-in.-thick sheet at ORNL by extrusion and rolling procedures. The sheet stock was provided to Hanford Engineering Development Laboratory, which will perform microstructural studies on these alloys prior to investigating irradiation performance.

A contract was negotiated with Westinghouse Electric Corporation for the production of

Table 8.2. Composition of alloys for irradiation performance evaluation (wt)

Path A austenitic stainless steels
    MFE reference heat of 316 stainless steel, reference condition 20 cold worked
    Prime candidate alloy:
        Fe-16 Ni-14 Cr-2 Mo-0.25 Ti-2 Mn-0.5 Si-0.05C

Path B higher strength Fe-Ni-Cr alloys
    Base research alloys:
        B-1/Fe-25 Ni-10 Cr-1 Mo-3 Ti-1.5 Al-1 Mn-0.03C
        B-2/Fe-40 Ni-12 Cr-3 Mo-1.5 Ti-1.5 Al-0.2 Mn-0.03C
        B-3/Fe-30 Ni-12 Cr-2 Nb-2 Ti-0.5 Al-1 Mn-0.03C
        B-4/Fe-40 Ni-12 Cr-3 Nb-1.8 Ti-0.3 Al-0.2 Mn-0.03C
        B-6/Fe-75 Ni-15 Cr-1 Nb-2.5 Ti-1.5 Al-0.2 Mn-0.03C

Path C reactive and refractory metal alloys
    Scoping alloys:
        V-20 Ti
        V-15 Cr-5 Ti
        V-9 Cr-3.3 Fe-1.3 Zr-0.05C (Vanstar 7)
        Nb-1 Zr
        Nb-5 Mo-1 Zr

three vanadium- and two niobium-base Path C alloys (compositions shown in Table 8.2). Sheet and rod products of these alloys are expected during 1979.

8.2 DAMAGE ANALYSIS

8.2.1 Range Calculations Using Multigroup Transport Methods

T. J. Hoffman M. T. Robinson
H. L. Dodds, Jr.

The application of the discrete ordinates transport theory code ANISN to calculations of light-ion sputtering yields was discussed in a previous report.[15] We have now applied similar methods to the calculation of particle range distributions. These techniques are illustrated by analysis of ^{197}Au atoms recoiling from (n,2n) reactions in Au. The results of these calculations agree well with range calculations performed with the atomistic code MARLOWE. Although some detail of the atomistic model is lost in the multigroup transport calculations, the improved computational speed may prove useful in the solution of fusion material design problems. The work will be described in a forthcoming report in the *Journal of Nuclear Materials*.

8.2.2 Study of the Low Energy Responses of the BCA Code MARLOWE

M. T. Robinson

Because dynamical methods require too great an investment in computational resources, an efficient methodology for displacement cascade simulation requires the use of codes based on the binary collision approximation (BCA) at high energies. At sufficiently low energies the BCA is no longer an adequate representation of the motion of the recoiling atoms mainly because individual collisions become difficult to identify. In order to determine a reasonable (lower) energy limit for BCA calculations, comparisons of the BCA code MARLOWE[16] with the dynamical code COMENT[17] and the quasi-dynamical code ADDES[18] are being made. Some contributions to the BCA part of this comparison are described here.

A potentially important parameter in MARLOWE is p_m, the maximum impact parameter allowed in any collision. This quantity establishes the effective sizes of the atoms in the crystal. If face-centered cubic (fcc) crystals are described by first and second neighbors only, $(1/6)^{1/2} < p_m/a < (5/8)^{1/2}$, where a is the cubic unit cell edge, is required to obtain correct generation of crystal by the program. As a first study of this parameter, a series of recoil range calculations was made for copper primaries slowing down in copper, using 1000 primaries in each group. No simple dependence of the range on p_m is observed, the differences being attributable to statistical effects alone. Thus, for range calculations, which are determined mainly by energies near the initial primary energy, the results are insensitive to the impact parameter cutoff. This reflects the very small amount of energy lost in the large impact parameter encounters.

Schiffgens and Schwartz[18] reported a series of comparisons of linear collision sequences (LCS's) evaluated by COMENT and ADDES. These same LCS's have also been examined with MARLOWE, using the same Molière potential and screening length. Each atom was bound to its lattice site by an amount E_b. Other work has shown that perfectly focused <011> LCS's in this potential require $E_b \approx 0.5$ eV for MARLOWE to give agreement with dynamical results. Preliminary studies of LCS's with Version 11 of MARLOWE suggested several modifications of the program, particularly with respect to improving the procedure for avoiding unphysical repetitive cycles of collisions with small sets of targets. In general, MARLOWE <011> sequences are shorter than those in COMENT. In contrast to <011> LCS behavior, the <001> and <111> sequences generated by MARLOWE are longer than those in COMENT, and these lengths are less sensitive to the choice of parameters. Both aspects accord with expectations based on the approximations used in MARLOWE.

8.3 RADIATION EFFECTS ON ORGANIC INSULATORS FOR SUPERCONDUCTING MAGNETS[19,20]

R. H. Kernohan R. R. Coltman, Jr.
C. J. Long C. E. Klabunde

The impetus for a program to study the effects of irradiation at liquid helium temperature on the properties of organic insulators is derived from the need to understand the irradiation behavior of materials that may be used in the construction of large superconducting coils that provide magnetic containment for the plasma in a fusion reactor.

During this reporting period an experiment assembly was irradiated near 4.9K in the ORNL Low Temperature Irradiation Facility (LTIF), which receives a highly thermalized neutron flux originating in the ORNL Bulk Shielding Reactor (BSR). Neutron capture gamma rays produced in a cadmium shield surrounding the assembly added to the ambient gamma level to provide an intense gamma ray flux that was by far the principal damaging radiation received by the samples within. The specimens were arranged in two groups, one for the in situ measurement of resistance changes during the irradiation and annealing program and the other for postirradiation measurement of mechanical and electrical properties after warmup to room temperature. Measurements after warmup are considered appropriate because periodic annealing is expected during the operating life of a fusion reactor magnet. The measurements and observations included lap shear, three-point flexure and compression strength, resistance and voltage breakdown, weight loss, and changes in color and surface features. The materials tested were Stycast 2850 Blue and Epon 828 epoxies, EF-527 B-stage glass cloth-epoxy composite, NEMA G-10 and FR-5 glass-epoxy laminates, Nomex paper, Kapton film, Formvar varnish on copper wire, and aluminized Mylar.

In this experiment the dose was increased to 2 x 10^9 rads, a factor of 10 greater than for our first test.[21] The in situ resistivity specimens showed decreases to as little as one-third the starting value, but all values remained in the usable range. The apparent resistance of the in situ resistivity specimens dropped by a factor of 2-50 on warmup above 200K after irradiation. The original resistance was restored, however, by purging the sample chamber with clean helium gas. This result could be explained by electrical leakage due to contamination of the chamber atmosphere by a species that is immobile at 4K. Its identity and source are presently unknown.

In contrast to the first experiment, the higher dose in the second experiment produced significant changes in some mechanical properties. One example shown in Table 8.3 is the three-point flexure strength tested at 77K after irradiation at 4.7K and warmup to 300K. This property is particularly important in magnet design. Upon removal from the experiment assembly, aluminized Mylar specimens fractured into several pieces, suggesting limited use of this material as reflective insulation for superconducting coils.

The electrical properties of all materials, while changed by the irradiation, remained suitable for their intended use, but some degradation in mechanical properties appeared after a dose of 2 x 10^9 rads.

Sample preparation is now complete for future tests that will examine the influence

Table 8.3. Three-point flexure strength (MPa)[a]

	Control	2 x 10^9 rads
Stycast 2850	254	143
Epon 828	225	283
G-10	862	191

[a] Each value is the average for three tests.

of fast neutrons combined with gamma rays on property changes and extend the irradiation dose to 1 x 10[illegible] rads.

REFERENCES

1. F. W. Wiffen, P. J. Maziasz, E. E. Bloom, J. O. Stiegler, and M. L. Grossbeck, "The Behavior of Type 316 Stainless Steel Under Simulated Fusion Reactor Irradiation," paper presented at the AIME Symp. on the Metal Physics of Stainless Steels, Denver, Colorado, March 2, 1978; to be published in proceedings.
2. M. L. Grossbeck and P. J. Maziasz, "Tensile Properties of Type 316 Stainless Steel Irradiated in a Simulated Fusion Reactor Environment," paper presented at the 1st Topical Meeting on Fusion Reactor Materials, Miami Beach, Florida, January 29-31, 1979; proceedings to be published in J. Nucl. Mater.
3. P. J. Maziasz, "Precipitation Response of Austenitic Stainless Steel to Simulated Fusion Irradiation," paper presented at the AIME Symp. on the Metal Physics of Stainless Steels, Denver, Colorado, March 2, 1978; to be published in proceedings.
4. C. R. Brinkman, K. C. Liu, and M. L. Grossbeck, "Estimates of Time-Dependent Fatigue Behavior of Type 3[illegible] Stainless Steel Subject to Irradiation Damage in Fast Breeder and Fusion Power Reactor Systems," paper presented at the 9th ASTM Int. Symp. on Effects of Radiation on Structural Materials, Richland, Washington, July 10, 1978; to be published in proceedings.
5. F. W. Wiffen, "The Response of Inconel 600 to Simulated Fusion Reactor Irradiation," paper presented at the 9th ASTM Int. Symp. on Effects of Radiation on Structural Materials, Richland, Washington, July 10, 1978; to be published in proceedings.
6. F. W. Wiffen, "Plastic Instability in Neutron Irradiated Niobium," paper presented at the 107th AIME Annual Meeting, Denver, Colorado, February 26-March 2, 1978.
7. B. L. Cox and F. W. Wiffen, "The Ductility in Bending of Molybdenum Alloys Irradiated between 425 and 1000°C," paper presented at the 1st Topical Meeting on Fusion Reactor Materials, Miami Beach, Florida, January 29-31, 1979; proceedings to be published in J. Nucl. Mater.
8. J. Bentley and F. W. Wiffen, "Neutron Irradiation Damage in Molybdenum at High Temperatures," paper presented at the 107th AIME Annual Meeting, Denver, Colorado, February 26-March 2, 1978.
9. P. J. Maziasz and K. Farrell, "The Tensile Properties of High Oxide SAP Containing Helium and Tritium," paper presented at the 1st Topical Meeting on Fusion Reactor Materials, Miami Beach, Florida, January 29-31, 1979; proceedings to be published in J. Nucl. Mater.
10. J. B. Talbot and F. W. Wiffen, "Recovery of Tritium from Solid Lithium-Sintered Aluminum Product (SAP) and Lithium-Aluminum Alloys," to be published in J. Inorg. Nucl. Chem.
11. D. R. Vondy, T. B. Fowler, and G. W. Cunningham, *VENTURE, A Code Block for Solving Multigroup Neutron Problems Applying Finite-Diffusion-Theory Approximations to Neutron Transport*, Oak Ridge National Laboratory Report ORNL-5062, Oak Ridge, Tennessee (1975).
12. P. F. Tortorelli and J. H. DeVan, "Thermal-Gradient Mass Transfer in Lithium-Stainless Steel Systems," paper presented at the 1st Topical Meeting on Fusion Reactor Materials, Miami Beach, Florida, January 29-31, 1979; proceedings to be published in J. Nucl. Mater.
13. P. F. Tortorelli, J. H. DeVan, and J. E. Selle, "Effects of Nitrogen and Nitrogen Getters in Static Lithium on the Corrosion of Type 316 Stainless Steel," paper presented at Corrosion/79, Atlanta, Georgia, March 12-16, 1979.

14. J. R. Keiser and J. H. DeVan, "Compatibility of Molten Salts with Type 316 Stainless Steel," paper presented at the 1st Topical Meeting on Fusion Reactor Materials, Miami Beach, Florida, January 29-31, 1979; proceedings to be published in J. Nucl. Mater.

15. *Fusion Energy Division Annual Progress Report for the Period Ending December 31, 1977*, Oak Ridge National Laboratory Report ORNL-5405, pp. 208-209, Oak Ridge, Tennessee (1978).

16. I. M. Torrens and M. T. Robinson, Phys. Rev. B 9, 5008 (1974).

17. J. O. Schiffgens and R. D. Bourquin, J. Nucl. Mater. 69/70, 790 (1978).

18. J. O. Schiffgens and D. M. Schwartz, *Damage Analysis and Fundamental Studies Quarterly Progress Report*, January-March 1978, DOE/ET-0065/1, pp. 88-111 (1978).

19. R. H. Kernohan, R. R. Coltman, Jr., and C. J. Long, *Radiation Effects on Organic Insulators for Superconducting Magnets: Annual Progress Report for Period Ending September 30, 1978*, Oak Ridge National Laboratory Report ORNL/TM-6708, Oak Ridge, Tennessee (1979).

20. R. H. Kernohan, C. J. Long, and R. R. Coltman, Jr., "Cryogenic Radiation Effects on Electric Insulators," paper presented at the 1st Topical Meeting on Fusion Reactor Materials, Miami Beach, Florida, January 29-31, 1979; proceedings to be published in J. Nucl. Mater.

21. C. J. Long, R. H. Kernohan, and R. R. Coltman, Jr., Proc. ICMC Symp. *Nonmetallic Materials and Composites at Low Temperatures*, pp. 141-153 (1979).

9. NEUTRON TRANSPORT

R. G. Alsmiller, Jr.
J. Barish
J. M. Barnes
B. L. Bishop
G. T. Chapman
T. A. Gabriel
R. A. Lillie
J. L. Lucius
B. F. Maskewitz
J. T. Mihalczo[1]
G. L. Morgan
E. M. Oblow
M. M. H. Ragheb
R. W. Roussin
M. J. Saltmarsh
R. T. Santoro
Y. Seki
D. K. Trubey[1]

Abstract. The neutron transport program includes both experimental and analytic phases. The experimental program is designed to provide data necessary for verifying the analytic methods and cross-section data that are used at Oak Ridge National Laboratory (ORNL) and throughout the United States for fusion reactor neutronics design calculations. Experiments are being carried out to determine the neutron transport in typical fusion reactor shield materials and configurations and to determine the effects of penetrations in these shields. The analytic program is directed at providing support for the design of the integral experiments and comparing the calculated data with those obtained experimentally. Neutronics calculations have also been carried out in support of the design of the Tokamak Fusion Test Reactor (TFTR) being built at Princeton University and of fusion-fission hybrid reactor studies at ORNL. The Radiation Shielding Information Center (RSIC) has continued to supply a broad range of services to the fusion energy research community.

9.1 ANALYSIS OF MAGNETIC FUSION ENERGY INTEGRAL EXPERIMENTS

R. G. Alsmiller, Jr.
J. M. Barnes
G. T. Chapman
G. L. Morgan
E. M. Oblow
R. T. Santoro
Y. Seki

An integral experiment and analysis program supported by the Office of Fusion Energy (OFE) has been under way at ORNL for approximately two years. The purpose of this program is to design and carry out integral experiments that will provide data necessary to verify the nuclear data and radiation transport methods that will be used in the design of the blanket and shield assemblies of fusion reactors and to provide this verification through extensive comparisons between calculated and experimental data.

The experiments for measuring neutron and gamma ray spectra at several detector locations behind laminated slab shields have been completed. The neutrons are produced via deuterium-tritium (D-T) reactions and are used to measure the 14-MeV neutron transport through materials that would be found in the inner toroidal shield of a large tokamak reactor. The slabs of shield material are 152-cm square and are supported on all sides

---

1. Engineering Physics Division.
2. Computer Sciences Division.
3. Instrumentation and Controls Division.
4. Present address: Los Alamos Scientific Laboratory, Los Alamos, New Mexico.
5. Present address: Fusion Technology Program, University of Wisconsin, Madison, Wisconsin.
6. Present address: Thermonuclear Fusion Research Division, Japan Atomic Energy Research Institute, Tokai Research Establishment, Japan.

in a concrete structure having a minimum thickness of 152 cm. Studied were six experimental configurations ranging from no shield around the D-T source to a 61-cm-thick shield consisting of layers of stainless steel and borated concrete. The full shield consisted of 30.5 cm of stainless steel followed by 30.5 cm of alternating 5-cm-thick layers of stainless steel and borated polyethylene. The neutron and gamma ray spectra behind these shields were measured using an NE-213 liquid scintillator.

Calculations of these spectra are being performed, and preliminary comparisons of the neutron spectra are available. The calculations are carried out using the two-dimensional (2-D) discrete ordinates code DOT.[1] In order to facilitate the calculations, a reduced geometry is used to describe the experimental facility. The deuteron drift tube, the iron source can, and the concrete support structure are fully modeled. The walls and ceiling of the experimental hall are, however, replaced by albedo surfaces chosen so that the scalar flux profiles are the same as those obtained with the full experimental geometry. The experimental configuration is described using 42 radial and 62 axial mesh intervals. The radiation transport is performed using a 42-neutron group cross-section library obtained by collapsing the 171-neutron group VITAMIN C library.[2] A P_3 expansion of the cross sections and an S_{12} angular quadrature are used in the calculations.

Shown in Fig. 9.1 is a comparison of the calculated and experimental neutron flux spectra behind 30.5 cm of stainless steel shielding at one of the detector locations. The solid lines, showing the experimental results, indicate the unfolded statistical uncertainty in the experimental results, and the dots are the calculated results. The calculated data were obtained by smoothing the flux per unit energy in each multigroup energy interval with an energy-dependent Gaussian distribution that characterizes the neutron detector response. The agreement among the data is encouraging. However, the D-T neutron source representation that was used in the analysis was approximate.

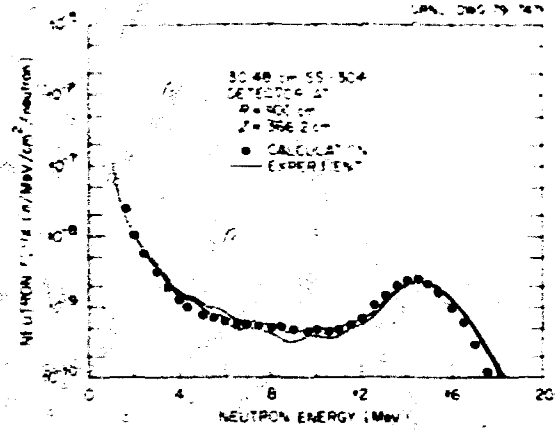

Fig. 9.1. Comparison of calculated and experimental neutron spectra behind 30.48 cm of SS-304.

The calculations are now being performed with a more accurate representation of the neutron source that takes into account the angle-energy relationship of the D-T neutron source. Also, a cross-section library that includes 21 gamma ray energy groups will be incorporated to allow for comparison of the experimental and calculated photon spectra.

Experiments to determine the neutron streaming through a typical shield penetration are also in progress.

9.2 MACROSCOPIC CROSS SECTION SENSITIVITY STUDY FOR FUSION REACTOR SHIELDING EXPERIMENTS[3]

Y. Seki E. M. Oblow
R. T. Santoro J. L. Lucius

Sensitivities of the calculated neutron and gamma ray responses of an NE-213 detector to the macroscopic cross sections for neutron interactions in materials used in an integral experiment for fusion reactor shielding studies are presented. Sensitivities for the interactions in the 14-MeV and 1- to 2-MeV energy ranges are found to be large enough to ensure the derivation of a significant amount of information from the experiment.

9.3 COMPARISON OF ONE- AND TWO-DIMENSIONAL CROSS SECTION SENSITIVITY CALCULATIONS FOR A FUSION REACTOR SHIELDING EXPERIMENT[4]

Y. Seki E. M. Oblow
R. T. Santoro J. L. Lucius

Cross-section sensitivities calculated with 1- and 2-D models of a fusion reactor shielding experiment are compared. The effectiveness of the 2-D calculation in accurately modeling the experiment and detector configurations is demonstrated. At the same time, the validity of a 1-D sensitivity study is also demonstrated.

9.4 CROSS SECTION SENSITIVITY ANALYSIS OF A PROPOSED NEUTRON STREAMING EXPERIMENT WITH A TWO-DIMENSIONAL MODEL[5]

Y. Seki E. M. Oblow
R. T. Santoro J. M. Barnes
J. L. Lucius

Cross-section sensitivity analysis of a proposed streaming experiment for a typical penetration in a fusion reactor shield has been performed using a 2-D sensitivity method. The neutron streaming was shown to be determined mostly by the 4.5-cm-thick duct liner made of iron and by the concrete structure immediately surrounding the liner. The neutrons scattered near the surface of the liner were found to be very important. A recommendation is made to move the proposed detector position to improve spatial resolution in the measurements without changing the sensitivity of the measurement to the nuclear characteristics of the duct materials.

9.5 TWO- AND THREE-DIMENSIONAL NEUTRONICS CALCULATIONS FOR THE TFTR NEUTRAL BEAM INJECTORS[6]

R. T. Santoro R. G. Alsmiller, Jr.
R. A. Lillie J. M. Barnes

Two- and three-dimensional radiation transport methods have been employed to estimate the nuclear performance of the neutral beam injectors being designed for the TFTR. The nuclear heating rates and neutron and gamma ray energy spectra have been calculated at various locations in a detailed calculational model of the injector using Monte Carlo methods. Calculations have also been carried out using discrete ordinates methods to obtain estimates of these data in a 2-D model of the injector. The 2-D calculational procedure was developed as an analytic tool for more cost-efficient scoping and parametric studies of the effects of design changes on the injector performance due to the streaming of 14-MeV neutrons. The nuclear responses and spectra obtained using the 2-D calculational model agree with the more definitive data obtained using the 3-D model within approximately a factor of 5.

9.6 SHIELDING CALCULATIONS FOR THE TFTR NEUTRAL BEAM INJECTORS[7]

R. T. Santoro R. A. Lillie
R. G. Alsmiller, Jr. J. M. Barnes

Two-dimensional neutronics calculations have been carried out to determine the shielding requirements for the neutral beam injectors to be used with the TFTR. Neutral deuterium was injected into the tritium plasma through a duct that passes through a concrete pillbox-shaped shield (igloo) that surrounds the reactor. The reactor and igloo are housed in a large concrete building (test cell). The concrete in the igloo and in the roof and walls of the test cell is sufficiently thick to reduce the biological dose rate from neutrons and secondary gamma rays outside the test cell to an acceptable limit of 0.5 mrem/D-T pulse.[7] However, some of the neutrons produced in the D-T pulse stream through the injection duct resulted in an increase in the dose rate on the roof and outside the test cell wall. The purpose of this study was to determine the location and thickness of additional concrete shielding around the neutral beam injector necessary for maintaining the dose rate outside the test cell at the acceptable limit.

Two series of calculations were performed. In the first, only the igloo and test cell were included in the calculational model to determine the biological dose rate outside the test cell with no injectors present. In the second, the injector and the test cell were modeled to determine the dose rate outside the test cell from radiation streaming through the injection duct. Because the details of many of the calculational procedures may be found in Ref. 6, they are only briefly summarized here.

The D-T neutron source distribution was taken to be that at strong postcompression of the plasma[8] and was transported using the 2-D discrete ordinates code DOT[1] with the TFTR, igloo, and test cell modeled in r-z geometry with toroidal symmetry about the z axis. The flux distributions from this calculation were folded with neutron[9] and gamma ray[10] flux-to-dose conversion factors to obtain the biological dose rates on the test cell outer surfaces.

The contributions to the dose rate from neutrons streaming through the injection duct and from the radiation leaking through the igloo wall and interacting in the injector were obtained in a second calculation. The neutral beam injector and the test cell were modeled in r-z geometry with symmetry about the axis of injection. The source for this analysis was obtained by processing the outward-directed angular flux at the surface of the igloo obtained in the calculation using the toroidal geometry with the interface code DOMINO.[11] The normalized probability distribution functions in energy, space, and angle generated by DOMINO were sampled using the MORSE code[12] to obtain the radiation current through a 200-cm-radius disk located in front of the injector. These data were then processed with the code GRTUNCL[13] to obtain the first-collision and uncollided flux distributions of the radiation leaking through the igloo that interacted in the injector. The neutrons from the plasma streaming directly through the duct were also calculated using GRTUNCL to obtain the uncollided flux and first-collision source in the injector and test cell wall that are in line of sight with the plasma. The direct streaming and leakage distributions were appropriately combined and used as the source term in DOT for completing the radiation transport through the injector.

All of the calculations were carried out using a 35-n, 21-γ energy group, P_3-expanded transport cross-section library obtained by collapsing the 171-n, 36-γ VITAMIN C data set.[14] An S_8 angular quadrature was used in all of the DOT calculations. The dose rates were normalized to a source strength of 3.5 x 10^{18} neutrons/D-T pulse.

The dose equivalent per pulse as a function of distance along the test cell roof (from the roof center to the outer edge) and along the wall (from the injector centerline to the roof) is shown in Figs. 9.2 and 9.3, respectively. In both figures the curve labeled "without injector" was obtained from the calculation including only the reactor, igloo, and test cell and represents the dose rate outside the test cell with no injector present. The curves labeled "unshielded injector" and "shielded injector" were obtained from the calculation including only the injector and test cell, and these represent

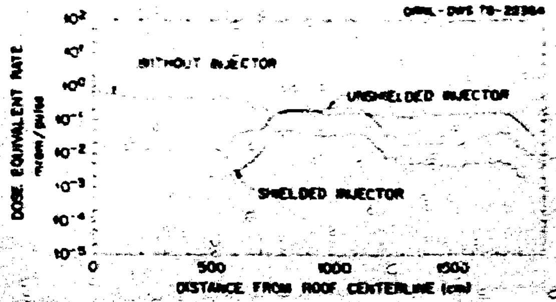

Fig. 9.2. Dose equivalent rate as a function of distance along the test cell roof.

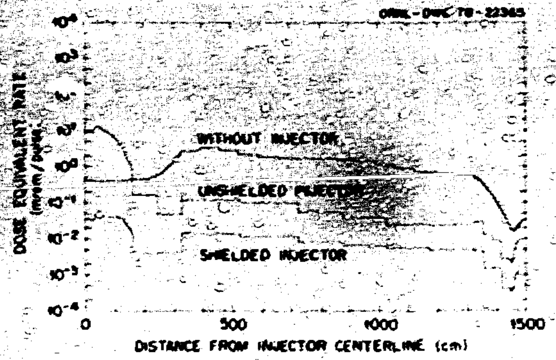

Fig. 9.3. Dose equivalent rate as a function of distance along the test cell wall.

the additional dose outside the test cell due to the presence of the injector. For the shielded injector, 30 cm of concrete lines the lateral surface of the injector, and 60 cm of concrete is used to attenuate the neutrons streaming out of the back of the injector. The total dose is obtained by adding the curve without the injector and either of the two remaining curves.

The TFTR is designed to operate with several neutral beam injectors. Therefore, the curves obtained when the injector is present must be multiplied by the number of injectors and then added to the curve obtained without the injector. This may result in a slight overestimate of the dose because all of the injectors are not at the same distance from a given point on the roof. It appears, then, that some shielding of the lateral surfaces of the injector may be required to maintain the dose rate on the roof at the acceptable level. The amount and location of the shielding will depend on the orientation of the injectors about the reactor. It is, however, necessary to include the 60-cm-thick shield behind the injectors to reduce the contribution to the dose outside the wall from neutrons streaming directly through the injection duct.

9.7 DOSE RATES FROM INDUCED ACTIVITY IN THE TFTR TEST CELL[14]

R. G. Alsmiller, Jr.	R. A. Lillie
J. Barish	J. M. Barnes
R. T. Santoro	M. M. H. Ragheb

The TFTR, which will operate on a D-T cycle, is being constructed at Princeton University. In this paper calculated results of the induced activity in the TFTR test cell are presented. Calculated results similar to those presented here have previously been presented by R. A. Friedenberg.[15] In the work of Friedenberg, the effects of a neutral beam injector and the large penetrations through the primary shield needed to accommodate neutral beam injection were neglected; here they are taken into account. Furthermore, the calculational procedure used to obtain the results presented here differs from that of Friedenberg in that the photon transport calculations are carried out by Monte Carlo methods rather than by discrete ordinates methods. The use of Monte Carlo methods allows all of the time-dependent calculations to be carried out after the photon transport calculations[16] and greatly facilitates the consideration of a large number of D-T pulse sequences and times after machine shutdown.

In Fig. 9.4 a very schematic diagram of the TFTR test cell is shown. The scalar neutron fluxes used here are those obtained previously by R. T. Santoro et al.[7] for the same geometry as that considered here. Although the compilation of D. W. Muir[17] was

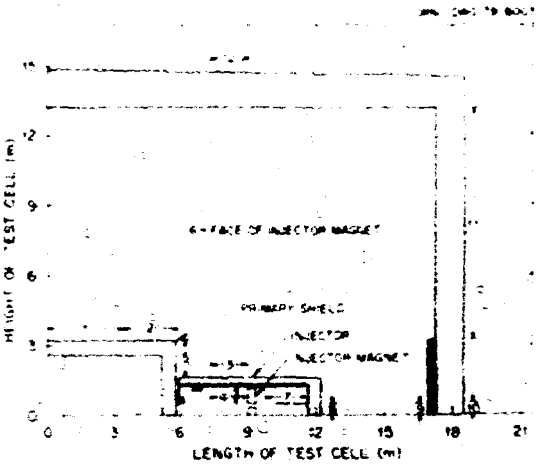

Fig. 9.4. Schematic diagram of the TFTR test cell with a neutral beam injector.

the primary source of activation cross-section data, a few reaction cross sections from ENDF/B-IV[16] were used.

The photon spectra from each radioactive residual nucleus considered in the calculation were obtained from the Evaluated Nuclear Structure Data Files that are available from the Nuclear Data Project at ORNL.[17] Calculations of photon transport were performed with the Monte Carlo code MOPSE[18] using cross-section data taken from Ref. 20. The photon fluxes were converted to dose equivalent rate using the flux-to-dose equivalent rate conversion factors of Claiborne and Trubey.[19]

In Fig. 9.4 the numbers between the arrows indicate that approximate positions where the activation dose equivalent rates will be presented, and the arrows indicate the spatial intervals over which the dose rates have been averaged. In Table 9.1 the total activation dose equivalent rates, i.e., the dose rates from all residual nuclei considered, are presented for the case of 1000 D-T pulses applied at the rate of 100 D-T pulses/day for each of ten consecutive days. The duration of a D-T pulse is 0.5 sec, and the time between pulses is 5 min. In the table the dose rates are given for one hour, one day, and one week after the last pulse. The error on each entry in the table is the statistical error, one standard deviation, expressed in percent. Results are presented separately for the case of the test cell with no injector present and for the contribution from an injector. The geometries are such that the two contributions are additive, but it must be understood that when the two contributions are additive, only an upper limit on the dose rate is obtained; in the photon transport calculation without injector, the injector structure is not present to attenuate the photons. When there is no injector present, the calculated results are comparable to those obtained by Friedenberg[15] but are not exactly the same because the concrete compositions used here are not exactly the same as those used in the calculations of Friedenberg.

Calculated results similar to those given in Table 9.1 for a variety of different pulse repetition sequences, times after the last pulse, and other positions in the test cell have also been obtained and will be presented. Furthermore, for each total dose equivalent rate obtained, the contribution to this dose equivalent rate from each residual nucleus considered is available, and some of this information will also be presented.

9.8 DESIGN CALCULATIONS FOR A 14-MeV NEUTRON COLLIMATOR[21]

R. A. Lillie R. G. Alsmiller, Jr.
J. T. Mihalczo

A number of SS-316 right circular cylindrical shells of varying lengths have been analyzed using 2-D discrete ordinates transport methods together with first and last flight particle estimators to aid in the design of neutron collimators for the TFTR. In the TFTR the 14-MeV neutron source has a very large spatial extent, and the collimators must be designed to allow spectral measurements that refer to only a small spatial region of

Table 9.1. Dose equivalent rate vs time after last pulse[a]

	1 hour after last pulse		1 day after last pulse		1 week after last pulse	
Position[b]	Test cell without injector	Injector contribution	Test cell without injector	Injector contribution	Test cell without injector	Injector contribution
1	1.9 x 10[illegible] ± 11[c]	[illegible] x 10[illegible] ± 19	4.7 x 10[illegible] ± 14	3.9 x 10[illegible] ± [illegible]	[illegible] ± 11	2.1 x 10[illegible] ± 19
2	6.6 x 10[illegible] ± 11	9.0 x 10[illegible] ± 38	1.7 x 10[illegible] ± 13	1.3 x 10[illegible] ± [illegible]	[illegible] ± 9	3.7 x 10[illegible] ± [illegible]
3	6.5 x 10[illegible] ± 15	1.6 x 10[illegible] ± 17	1.6 x 10[illegible] ± 15	[illegible]	[illegible]	9.2 x 10[illegible] ± [illegible]
4	6.5 x 10[illegible] ± 17	2.0 x 10[illegible] ± 5	1.5 x 10[illegible] ± 22	[illegible]	[illegible]	1.9 x 10[illegible] ± [illegible]
5	9.9 x 10[illegible] ± 11	[illegible].5 x 10[illegible] ± 17	2.4 x 10[illegible] ± 14	4.2 x 10[illegible]	[illegible]	[illegible] ± 10
6	5.6 x 10[illegible] ± 17	1.8 x 10[illegible] ± 9	3.4 x 10[illegible] ± 22	[illegible]	[illegible]	[illegible]
7	3.1 x 10[illegible] ± 17	4.7 x 10[illegible] ± 8	9.5 x 10[illegible] ± 16	[illegible]	[illegible]	[illegible]
8	3.6 x 10[illegible] ± 26	5.9 x 10[illegible] ± 9	1.1 x 10[illegible] ± 28	[illegible]	[illegible]	[illegible]
9	2.0 x 10[illegible] ± 13	2.0 x 10[illegible] ± 88	5.6 x 10[illegible] ± 15	[illegible]	[illegible]	[illegible]
10	5.3 x 10[illegible] ± 31	[illegible] x 10[illegible] ± 17	3.8 x 10[illegible] ± 32	[illegible] ± 17	[illegible]	7.6 x 10[illegible] ± 16
11	8.2 x 10[illegible] ± 13	1.2 x 10^{-3} ± 21	2.6 x 10[illegible] ± 13	4.2 x 10[illegible] ± 21	6.4 x 10[illegible] ± 20	2.0 x 10[illegible] ± 13
12	1.2 x 10[illegible] ± 23	3.6 x 10[illegible] ± 14	3.9 x 10[illegible] ± 28	1.2 x 10[illegible] ± 15	[illegible] x 10[illegible] ± 26	1.9 x 10[illegible] ± 42

[a] 100 pulses: 100 pulses on each of ten consecutive days; pulse length = 0.5 s; time between pulses = 5 min; dose equivalent rate mrem/hr.

[b] See Fig. 9.4.

[c] Statistical error, one standard deviation, expressed in percent.

this extended source. The analysis identifies the 14-MeV neutrons from scattering in the SS-316 immediately adjacent to the collimator opening as the dominant contributor to detector background. Collimator lengths greater than 0.[illegible] m were found to be sufficient to attenuate uncollided background neutrons for reasonable source-detector distances. The lower energy (<13.8 MeV) neutron background and gamma background were not found to be significant.

9.9 NUCLEAR PERFORMANCE OF MOLTEN SALT FUSION-FISSION SYMBIOTIC SYSTEMS FOR CATALYZED DD AND DT REACTORS[22]

M. M. H. Ragheb   J. M. Barnes
R. T. Santoro   M. J. Saltmarsh

The nuclear performance of a fusion-fission hybrid reactor having a molten salt composed of Na-Th-F-Be as the blanket fertile material and operating with a catalyzed D-D plasma is compared to a similar system utilizing a Li-Th-F-Be salt and operating with a D-T plasma. The production of fissile fuel via the ^{232}Th-^{233}U fuel cycle was considered on the basis of its potential nonproliferation aspects. The calculations were performed using 1-D discrete ordinates methods to compare neutron balances, fuel production rates, energy deposition rates, and the radiation damage in the reactor structure. The results indicate that the Na salt in conjunction with the catalyzed D-D plasma represents a viable alternative to the Li salt and D-T plasma. In a reactor consisting of a 42-cm-thick salt compartment followed by a 40-cm-thick graphite reflector, the Na salt-catalyzed D-D system exhibits a higher fissile nuclide production potential via ^{232}Th(n,γ) reactions (0.880 reactions/source neutron) than the Li salt D-T system (0.737 reactions/source neutron) without the additional complication of tritium production in the blanket. A 1000-MW(e) D-D hybrid reactor is estimated to be able to support 14 fission reactors of the same power operating in the once-through cycle; a D-T hybrid reactor can support about 8 fission reactors.

9.10 RADIATION SHIELDING INFORMATION CENTER

B. F. Maskewitz R. W. Roussin
D. K. Trubey

The RSIC, established in 1962, serves its user community by collecting, organizing, processing, evaluating, packaging, and disseminating information related mainly to reactor and weapons radiation. The scope includes the physics of interaction of radiation with matter, radiation production and transport, radiation detectors and measurements, engineering design techniques, shielding materials properties, computer codes useful in research and design, and nuclear data compilations. Originally established to support research related to fission, RSIC now supports fusion reactor technology. The major activities include (1) operating a computer-based information system and answering inquiries; (2) collecting, testing, packaging, and distributing computer codes; and (3) evaluating and processing nuclear data libraries.

All RSIC activities contribute to the fusion technology program. During the current reporting period, special emphasis has been placed on providing a general purpose fine-group library for use by the fusion neutronics community. A 61-material version of this library, DLC-41B/VITAMIN C, was released during FY 1978, and its use was demonstrated in a seminar-workshop on multigroup cross sections.[23,24] Plans have been proposed to produce an updated new version based on evaluated data from ENDF/B-V.[25]

A second seminar-workshop included a presentation of sensitivity and uncertainty analysis[26] applied to fusion reactor systems.

During the year the RSIC data base increased in each subtask:

(1) literature · 8500 citations[27] may be accessed on DOE-RECON, 42 RSIC reports issued with several volumes in series;
(2) codes collection there are 340 complex shielding code packages[28] and 140 auxiliary data processing packages;[29]
(3) data collection · 62 data library packages[30] and additional working cross-section libraries are maintained for DOE-OFE and Defense Nuclear Agency (DNA) sponsors.

The RSIC newsletter distribution is ~1550.

RSIC latest user statistics (FY 1978) indicate that 2900 separate letters and telephone calls (~12/workday) were processed during the year and 113 visitors were received. The fusion research community accounted for ~20% of the total number of requests.

REFERENCES

1. W. A. Rhoades and F. R. Mynatt, *The DOT-II Two-Dimensional Discrete Ordinates Code*, Oak Ridge National Laboratory Report ORNL/TM-4280, Oak Ridge, Tennessee (1973).
2. *The CTR Processed Multigroup Cross-Section Library for Neutronic Studies*, DLC-41/VITAMIN C, Radiation Shielding Information Center, Oak Ridge National Laboratory, Oak Ridge, Tennessee (1978).
3. Y. Seki, R. T. Santoro, E. M. Oblow, and J. L. Lucius, *Macroscopic Cross Section Sensitivity Study for Fusion Reactor Shielding Experiments*, Oak Ridge National Laboratory Report ORNL-5467, Oak Ridge, Tennessee (1978).
4. Y. Seki, R. T. Santoro, E. M. Oblow, and J. L. Lucius, *Comparison of One- and Two-Dimensional Cross Section Sensitivity Calculations for a Fusion Reactor Shielding Experiment*, Oak Ridge National Laboratory Report ORNL/TM-6667, Oak Ridge, Tennessee (1979); to be published in Nucl. Sci. Eng.
5. Y. Seki, R. T. Santoro, E. M. Oblow, J. M. Barnes, and J. L. Lucius, *Cross Section Sensitivity Analysis of a Proposed Neutron Streaming Experiment with a Two-Dimensional Model*, Oak Ridge National Laboratory Report ORNL/TM-6588, Oak Ridge, Tennessee (1979); submitted to Nucl. Sci. Eng.

6. R. T. Santoro, R. A. Lillie, R. G. Alsmiller, Jr., and J. M. Barnes, *Two- and Three-Dimensional Neutronics Calculations for the TFTR Neutral Beam Injectors*, Oak Ridge National Laboratory Report ORNL/TM-6354, Oak Ridge, Tennessee (1979); to be published in Nucl. Sci. Eng.
7. R. T. Santoro, R. A. Lillie, R. G. Alsmiller, Jr., and J. M. Barnes, "Shielding Calculations for the TFTR Neutral Beam Injectors," paper to be presented at the 1979 Annual Meeting of the American Nuclear Society, Atlanta, Georgia, June 3-8, 1979.
8. B. Pritchard (Princeton Plasma Physics Laboratory), private communication, 1978.
9. *Protection Against Neutron Radiation*, NRCP Report No. 38, National Council on Radiation Protection and Measurements (1971).
10. H. C. Claiborne and D. K. Trubey, Nucl. Technol. 8, 450 (1970).
11. M. B. Emmett, C. E. Burgart, and T. J. Hoffman, *DOMINO, A General Purpose Code for Coupling Discrete Ordinates and Monte Carlo Radiation Transport Calculations*, Oak Ridge National Laboratory Report ORNL-4835, Oak Ridge, Tennessee (1973).
12. M. B. Emmett, *The MORSE Monte Carlo Radiation Transport System*, Oak Ridge National Laboratory Report ORNL-4972, Oak Ridge, Tennessee (1975).
13. R. L. Childs (Oak Ridge National Laboratory), private communication, 1978.
14. R. G. Alsmiller, Jr., J. Barish, R. T. Santoro, R. A. Lillie, J. M. Barnes, and M. M. H. Ragheb, "Dose Rates From Induced Activity in the TFTR Test Cell," paper to be presented at the 1979 Annual Meeting of the American Nuclear Society, Atlanta, Georgia, June 3-8, 1979.
15. R. A. Friedenberg, Trans. Am. Nucl. Soc. 28, 657 (1978).
16. R. G. Alsmiller, Jr., T. A. Gabriel, and J. Barish, Nucl. Instrum. Methods 155, 399 (1978).
17. D. W. Muir, *DLC-33 Data Library MONTAGE*, Radiation Shielding Information Center, Oak Ridge National Laboratory, Oak Ridge, Tennessee (1975).
18. D. J. Garber and C. Brewster, *ENDF/B Cross Sections*, Brookhaven National Laboratory Report BNL-17100 (ENDF-200), 2nd ed., Upton, New York (1975).
19. W. B. Ewbank, "Evaluated Nuclear Structure Data Files (ENSDF) for Basic and Applied Research," paper presented at the 5th CODATA Conf., June 28-July 1, 1976; D. C. Kocher, W. B. Ewbank, and M. J. Martin, "Standardized Radioactivity Decay Data Sets for Use in Radioactivity Dosimetry," paper presented at the IAEA Symp. on National and International Standardization of Radiation Dosimetry, Atlanta, Georgia, December 5-9, 1977.
20. D. M. Plaster, R. T. Santoro, and W. E. Ford, III, *Coupled 100-Group Neutron and 21-Group Gamma-Ray Cross Sections for EPR Calculations*, Oak Ridge National Laboratory Report ORNL/TM-4872, Oak Ridge, Tennessee (1975).
21. R. A. Lillie, R. G. Alsmiller, Jr., and J. T. Mihalczo, *Design Calculations for a 14-MeV Neutron Collimator*, Oak Ridge National Laboratory Report ORNL/TM-6487, Oak Ridge, Tennessee (1979); to be published in Nucl. Technol.
22. M. M. H. Ragheb, R. T. Santoro, J. M. Barnes, and M. J. Saltmarsh, *Nuclear Performance of Molten Salt Fusion-Fission Symbiotic Systems for Catalyzed DD and DT Reactors*, Oak Ridge National Laboratory Report ORNL/TM-6560, Oak Ridge, Tennessee (1979); submitted to Nucl. Technol.
23. R. W. Roussin, C. R. Weisbin, J. E. White, R. Q. Wright, N. M. Greene, W. E. Ford, III, J. B. Wright, and B. R. Diggs, "Experience in Developing and Using the VITAMIN-C 171-Neutron, 36-Gamma-Ray Group Cross Section Library," *Proc. Seminar-Workshop on Multigroup Nuclear Cross-Section Processing*, pp. 107-120 (1978).

24. D. K. Trubey and H. R. Hendrickson, compilers, *A Review of Multigroup Nuclear Cross Section Processing-Proceedings of a Seminar-Workshop*, Oak Ridge National Laboratory Report ORNL/RSIC-41, Oak Ridge, Tennessee (1978).

25. C. R. Weisbin, R. W. Roussin, J. J. Wagschal, J. E. White, and R. Q. Wright, *VITAMIN-E: An ENDF/B-V Multigroup Cross-Section Library for LMFBR Core and Shield, LWR Shield, Dosimetry and Fusion Blanket Technology*, Oak Ridge National Laboratory Report ORNL-5505 (ENDF-274), Oak Ridge, Tennessee (1979).

26. C. R. Weisbin, R. W. Roussin, and H. R. Hendrickson, *A Review of the Theory and Application of Sensitivity and Uncertainty Analysis*, Oak Ridge National Laboratory Report ORNL/RSIC-42, Oak Ridge, Tennessee (1979).

27. D. K. Trubey, R. W. Roussin, J. Gurney, and A. B. Gustin, *Bibliography, Subject Index, and Author Index of the Radiation Shielding Information Center (Reactor and Weapons Radiation Shielding)*, Oak Ridge National Laboratory Report ORNL/RSIC-5, Vols. I-V, Oak Ridge, Tennessee (1978).

28. B. McGill, B. F. Maskewitz, C. M. Anthony, H. E. Comolander, and H. R. Hendrickson, *Abstracts of Digital Computer Code Packages Assembled by the Radiation Shielding Information Center*, Oak Ridge National Laboratory Report ORNL/RSIC-13, Vols. I-IV, Oak Ridge, Tennessee (1976, updated 1978).

29. B. F. Maskewitz, *Abstracts of Peripheral Shielding Code Packages Assembled by the Radiation Shielding Information Center*, Oak Ridge National Laboratory Report ORNL/RSIC-31, Vol. I, Oak Ridge, Tennessee (updated 1978).

30. R. W. Roussin, *Abstracts of the Data Library Packages Assembled by the Radiation Shielding Information Center*, Oak Ridge National Laboratory Report ORNL/RSIC-30, Vol. I, Oak Ridge, Tennessee (1972).

10. MANAGEMENT SERVICES

R. H. Dilworth, Section Head

S. K. Adkins
D. R. Alford
A. B. Barnette
P. G. Beasley
S. S. Bell[1]
D. P. Brooks
J. L. Burke
E. L. Cagle[1]
C. J. Chamberlain
M. B. Clark
C. H. Cox
J. D. Craven[2]
K. M. Dobbs[1]
M. V. Dunn
R. S. Edwards
J. C. Ezell
H. W. Jernigan
J. R. Jernigan*
R. P. Jernigan
B. L. Johnson[1]
C. H. Johnson[1]
J. Y. Johnson[1]
M. N. Johnson*
R. B. Johnston[1]
J. A. Kelman[1]
M. G. Kincaid[1]
J. K. Lovin
J. B. Martin*,[1]
B. J. McClure[1]
J. C. Neeley[1]
M. C. Rhea*
E. T. Rogers*,[1]
E. M. Ruckart
W. K. Russell
R. C. Satterfield
S. R. Schwartz[1]
C. M. Sekula[1]
D. G. Sharp
J. G. Sharp[1]
B. L. Straine
C. K. Thomas
E. L. Watkin[1]
E. E. Webster[1]
F. R. Wells
T. G. Yow[1]

Abstract. The Management Services Section provides coordinated professional administrative services to the Fusion Energy Division (FED), allowing the work of technical professionals to be more fully concentrated in their areas of specialty. Services are provided in general administration, personnel, financial management, communications (including text and graphics generation), management information, library, safety, quality assurance, and nonprogrammatic engineering services. Highlights of the past year included adoption of the Procurement Module in the FED Management Information System (MIS) for use by the entire Laboratory, completion of the Personnel Module of the MIS, greatly increased personnel recruiting activity, and increased industrial subcontracting activity.

10.1 INTRODUCTION

The Management Services Section has now completed two years of operation in essentially the same organizational form as originated. The value of centralizing management functions within a section has been clearly demonstrated, and the general methodology of the functioning of the section within the Division has been established. Thus, more attention is now turning to improvements in relationships with external organizations and to procedural improvements. In the following sections of this report, highlights of specific accomplishments are presented. The organization chart for the Division is shown in Fig. 10.1.

10.2 FINANCE OFFICE

The funding trend for the Fusion Energy Division and Program continues to exhibit substantial growth, as illustrated in Table 10.1 and Fig. 10.2. This trend creates a related need for growth and improvement in specific areas of financial control. In order to meet the research objectives of the Program, increased emphasis must be placed on financial analysis, variance reporting, and accurate cost projections.

During the past year the Finance Office continued to provide monthly cost reports for the various work breakdowns, to work with

---

*Part-time.

1. Information Division.
2. Finance and Materials Division.

ORNL–DWG 79–2184 FED

FUSION ENERGY DIVISION

MARCH 1979

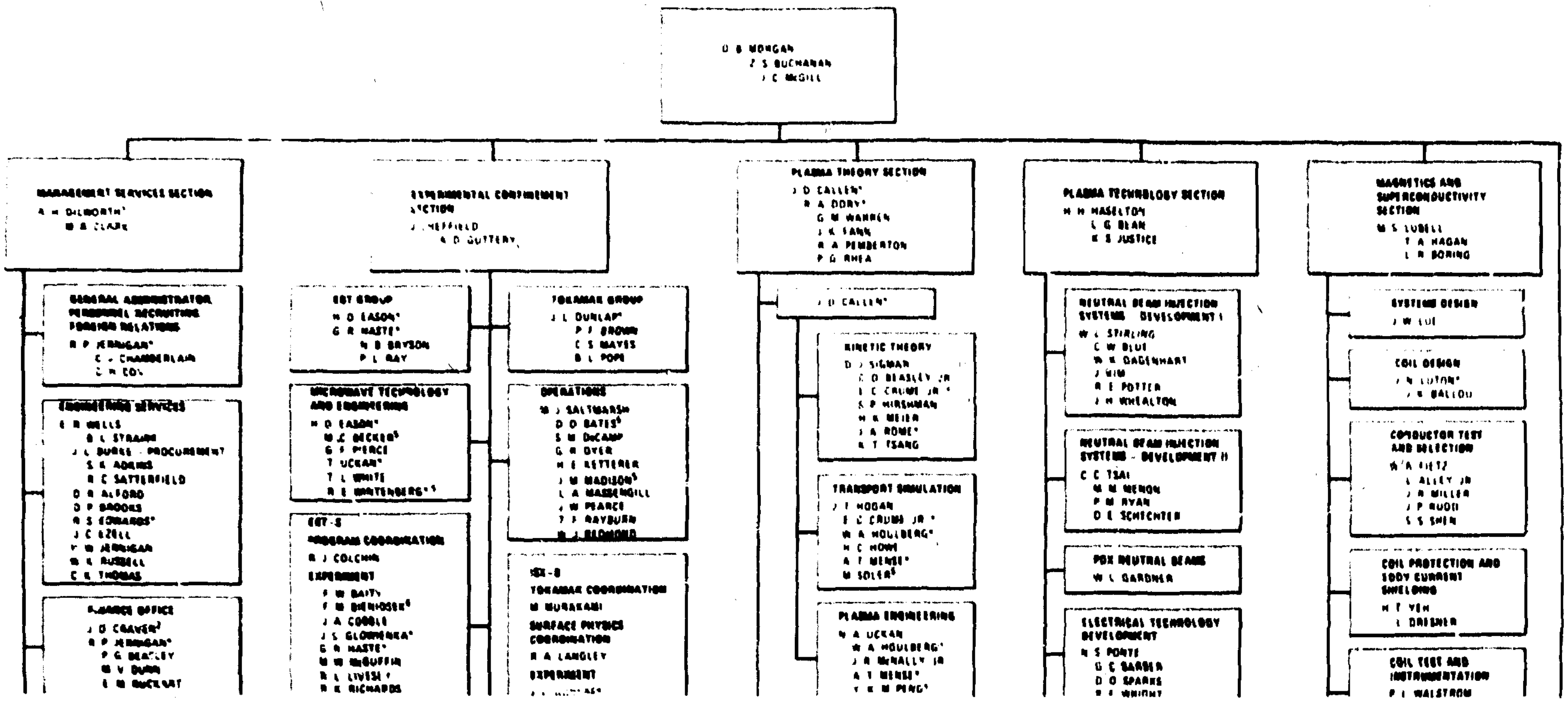
O B MORGAN
Z S BUCHANAN
J C McGILL
MANAGEMENT SERVICES SECTION
A H DILWORTH*
W B CLARK
GENERAL ADMINISTRATION PERSONNEL RECRUITING FOREIGN RELATIONS
R P JERNIGAN*
C J CHAMBERLAIN
C H COX
ENGINEERING SERVICES
E R WELLS
B L STRAHM
J L BURKE - PROCUREMENT
S K ADKINS
R C SATTERFIELD
D R ALFORD
D P BROOKS
R S EDWARDS*
J C EZELL
F W JERNIGAN
W K RUSSELL
C E THOMAS
FINANCE OFFICE
J D CRAVER[2]
R P JERNIGAN*
P G BEATLEY
W V DUNN
E M BUCKHART
EXPERIMENTAL CONFINEMENT SECTION
J SHEFFIELD
R D GUTTERY
EBT GROUP
H O EASON*
G R HASTE*
W B BRYSON
P L RAY
MICROWAVE TECHNOLOGY AND ENGINEERING
H O EASON*
W J DECKER[5]
G F PIERCE
T UCKAN*
T L WHITE
R E WINTENBERG*[5]
EBT-S
PROGRAM COORDINATION
R J COLCHIN
EXPERIMENT
F W BAITY
F M BIENIOSEK[6]
J A COBBLE
J S GLOWIENKA*
G R HASTE*
W W McGUFFIN
R L LIVESEY
R K RICHARDS
TOKAMAK GROUP
J L DUNLAP*
P J BROWN
C S MAYES
B L POPE
OPERATIONS
W J SALTMARSH
D D BATES[5]
S M DeCAMP
G R DYER
H E KETTERER
J M MADISON[5]
L A MASSENGILL
J W PEARCE
T F RAYBURN
W J REDMOND
ISX-B
TOKAMAK COORDINATION
M MURAKAMI
SURFACE PHYSICS COORDINATION
R A LANGLEY
EXPERIMENT
PLASMA THEORY SECTION
J D CALLEN*
R A DORY*
G M WARREN
J K FANN
R A PEMBERTON
P G RHEA
J D CALLEN*
KINETIC THEORY
D J SIGMAR
C O BEASLEY JR
E C CRUME JR*
S P HIRSHMAN
H K MEIER
J A ROME*
K T TSANG
TRANSPORT SIMULATION
J T HOGAN
E C CRUME JR*
W A HOULBERG*
H C HOWE
A T MENSE*
M SOLER[6]
PLASMA ENGINEERING
N A UCKAN
W A HOULBERG*
J R McNALLY JR
A T MENSE*
Y K M PENG*
PLASMA TECHNOLOGY SECTION
H H HASELTON
L G BEAN
K S JUSTICE
NEUTRAL BEAM INJECTION SYSTEMS – DEVELOPMENT I
W L STIRLING
C W BLUE
W K DAGENHART
J KIM
R E POTTER
J H WHEALTON
NEUTRAL BEAM INJECTION SYSTEMS – DEVELOPMENT II
C C TSAI
M M MENON
P M RYAN
D E SCHECHTER
PDX NEUTRAL BEAMS
W L GARDNER
ELECTRICAL TECHNOLOGY DEVELOPMENT
H S PONTE
G C BARBER
D O SPARKS
R E WRIGHT
MAGNETICS AND SUPERCONDUCTIVITY SECTION
M S LUBELL
T A HAGAN
L R BORING
SYSTEMS DESIGN
J W LUE
COIL DESIGN
J N LUTON*
J K BALLOU
CONDUCTOR TEST AND SELECTION
W A FIETZ
L ALLEY JR
J R MILLER
J P RUDD
S S SHEN
COIL PROTECTION AND EDDY CURRENT SHIELDING
H T YEH
L DRESNER
COIL TEST AND INSTRUMENTATION
P L WALSTROM

BLANK PAGE

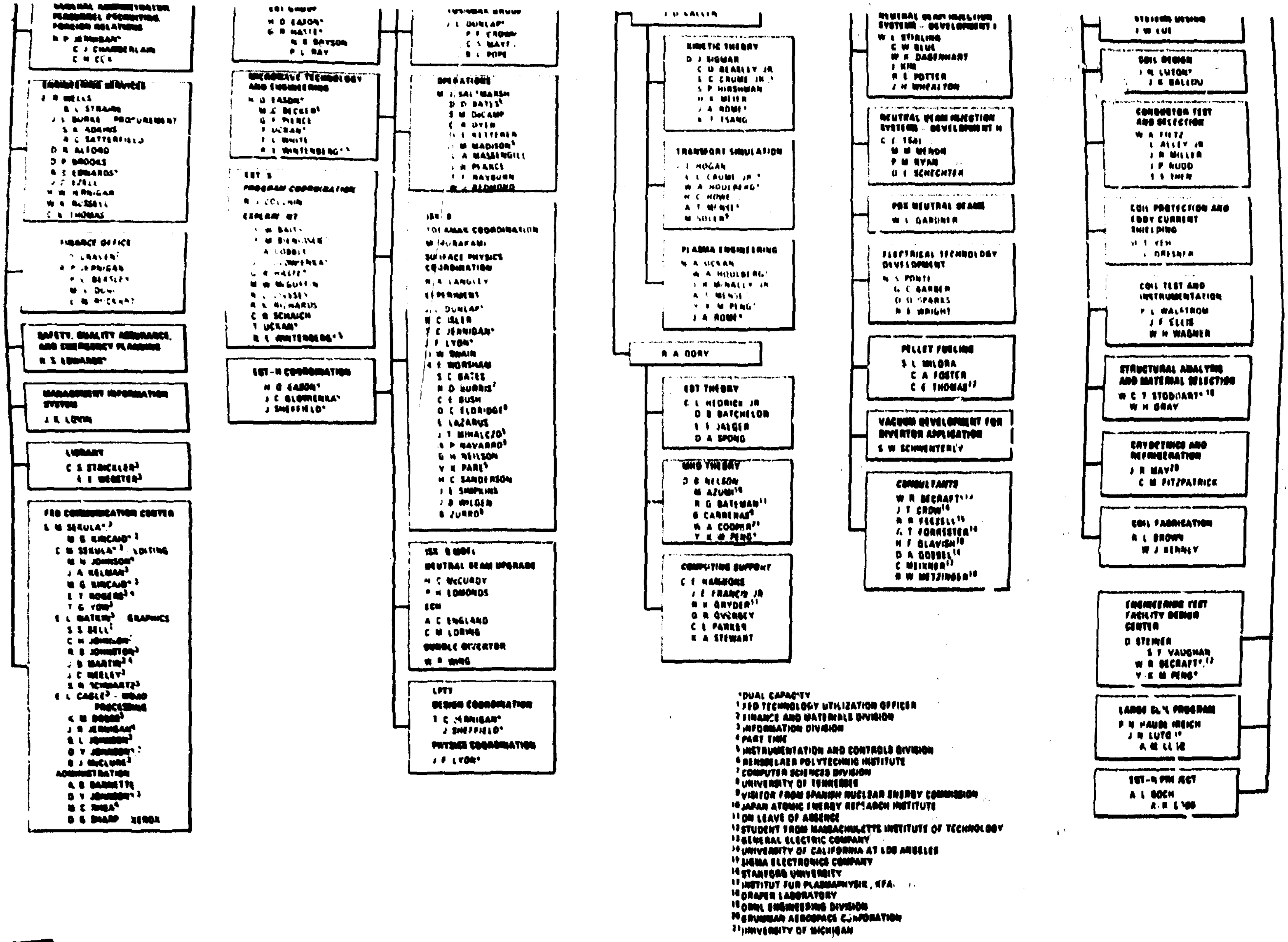

ENGINEERING SERVICES
FINANCE OFFICE
SAFETY, QUALITY ASSURANCE, AND EMERGENCY PLANNING
MANAGEMENT INFORMATION SYSTEM
LIBRARY
FED COMMUNICATION CENTER
MICROWAVE TECHNOLOGY AND ENGINEERING
EBT-S PROGRAM COORDINATION
EBT-P COORDINATION
OPERATIONS
TOKAMAK COORDINATION
SURFACE PHYSICS COORDINATION
NEUTRAL BEAM UPGRADE
BUNDLE DIVERTOR
DESIGN COORDINATION
PHYSICS COORDINATION
KINETIC THEORY
TRANSPORT SIMULATION
PLASMA ENGINEERING
EBT THEORY
MHD THEORY
COMPUTING SUPPORT
NEUTRAL BEAM INJECTION SYSTEMS - DEVELOPMENT I
NEUTRAL BEAM INJECTION SYSTEMS - DEVELOPMENT II
PDX NEUTRAL BEAMS
ELECTRICAL TECHNOLOGY DEVELOPMENT
PELLET FUELING
VACUUM DEVELOPMENT FOR DIVERTOR APPLICATION
CONSULTANTS
COIL DESIGN
CONDUCTOR TEST AND SELECTION
COIL PROTECTION AND EDDY CURRENT SHIELDING
COIL TEST AND INSTRUMENTATION
STRUCTURAL ANALYSIS AND MATERIAL SELECTION
CRYOGENICS AND REFRIGERATION
COIL FABRICATION
ENGINEERING TEST FACILITY DESIGN CENTER
LARGE COIL PROGRAM
EBT-P PROJECT
*DUAL CAPACITY
1 FED TECHNOLOGY UTILIZATION OFFICER
2 FINANCE AND MATERIALS DIVISION
3 INFORMATION DIVISION
4 PART TIME
5 INSTRUMENTATION AND CONTROLS DIVISION
6 RENSSELAER POLYTECHNIC INSTITUTE
7 COMPUTER SCIENCES DIVISION
8 UNIVERSITY OF TENNESSEE
9 VISITOR FROM SPANISH NUCLEAR ENERGY COMMISSION
10 JAPAN ATOMIC ENERGY RESEARCH INSTITUTE
11 ON LEAVE OF ABSENCE
12 STUDENT FROM MASSACHUSETTS INSTITUTE OF TECHNOLOGY
13 GENERAL ELECTRIC COMPANY
14 UNIVERSITY OF CALIFORNIA AT LOS ANGELES
15 SIGMA ELECTRONICS COMPANY
16 STANFORD UNIVERSITY
17 INSTITUT FUR PLASMAPHYSIK, KFA
18 DRAPER LABORATORY
19 ORNL ENGINEERING DIVISION
20 GRUMMAN AEROSPACE CORPORATION
21 UNIVERSITY OF MICHIGAN

Fig. 10.1. Fusion Energy Division organization chart.

Table 10.1. Fusion Energy Program expense funding

Activity	FY 76 actual cost	FY 77 actual cost	FY 78 actual cost	FY 79 funding as of March 79	FY 80 budget submission	FY 81 budget submission
	Dollars in thousands					
Confinement systems – tokamak systems – research operations	$ 3,846	$ 6,811	$ 5,973	$ 6,900	$ 8,100	$ 9,175
Confinement systems – tokamak systems – major device fabrication	2,534	4,574	4,709	5,290	2,880	2,451
Confinement systems – magnetic mirror systems – research operations	1,080	1,969	2,295	2,900	5,282	6,585
Confinement systems – magnetic mirror systems – major device fabrication (EBT-II)	0	178	205	2,000	8,400	20,600
Total confinement systems	$ 7,4[illegible]	$13,532	$13,182	$17,090	$25,662	$38,811
Development and technology – magnetic systems	$ 3,367	$ 5,691	$ 7,593	$10,910	$14,925	$13,514
Development and technology – plasma engineering	4,998	6,063	5,442	5,560	3,425	9,700
Development and technology – fusion reactor materials	1,016	1,645	2,796	2,945	3,460	3,708
Development and technology – fusion systems engineering	1,230	2,535	1,954	1,855	5,000	6,620
Development and technology – environment and safety	0	0	55	260	100	100
Total development and technology	$10,611	$15,934	$17,840	$21,530	$31,910	$33,642
Applied plasma physics – fusion plasma theory	$ 1,804	$ 2,063	$ 2,196	$ 2,250	$ 2,950	$ 3,400
Applied plasma physics – experimental plasma research	580	843	898	895	963	1,198
Applied plasma physics – national MFE computer network	0	271	169	290	350	450
Total applied plasma physics	$ 2,384	$ 3,177	$ 3,283	$ 3,435	$ 4,263	$ 5,048
Reactor projects – TFTR	0	321	0	0	0	0
Total reactor projects	0	321	0	0	0	0
Total ORNL funding	$20,455	$32,964	$34,305	$42,055	$61,835	$77,501

research personnel in properly planning expenditures within budget constraints, to operate the coordinated work order control system, and to perform many other functions associated with Division financial/accounting transactions.

10.3 OFFICE OF THE ADMINISTRATOR

This office is responsible for most of the general administrative functions of the Division.

10.3.1 Visitors

Arrangements were made during the past year for 1186 visitors to the Division, including 123 noncitizens.

10.3.2 Personnel Functions

During the past year arrengements were made for interviews with 38 prospective employees, 7 of whom accepted employment. In addition, 6 new employees transferred from

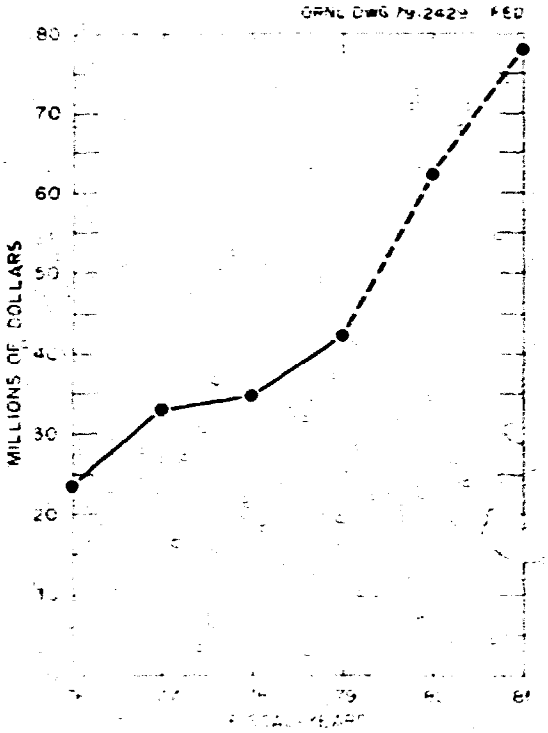

Fig. 10.2. Funding projection.

other ORNL organizations. Twenty-eight guest assignments were processed, by which nonemployees participate in Division programs.

10.3.3 Subcontracts

In 1978 industrial involvement through subcontracts exceeded $6 million. Major contracts were for the [illegible] Program (LCP) prototype fusion reactor coils and microwave power tube development for the ELMO Bumpy Torus (EBT) and Impurity Study Experiment (ISX) programs.

10.3.4 FED Communications Center

The name of the FED Communications Center accurately reflects the broad range of services provided by this group. The center provides a complete documentation service that includes editing, typing, drafting, photographic art, and copying services. In 1978, 118 numbered reports, 81 journal articles, 71 meeting papers, and 6 special projects were published; 212 abstracts were processed. The graphics group prepared approximately 1500 drawings, 5000 prints, 3000 viewgraphs, 150 posters and embossograph signs, and 200 diazo signs. In addition, plans were made for the installation of a 9400 Xerox copier with simultaneous front and back printing.

Growth of this group has continued in order to keep pace with the increasing publication output of the Division; furthermore, while the volume of work has increased, the average processing time has decreased. Our records continue to verify the productivity and cost-effectiveness of this group.

10.4 MANAGEMENT INFORMATION SYSTEM

The purpose of the FED Management Information System (MIS) is to provide the Division's management staff with timely and relevant information required to maintain control of costs and schedules. As described in the remainder of this section, progress was made in several areas during 1978. However, the accomplishments were limited by the lack of available programming support personnel, a problem that is being solved by utilizing subcontracts.

Several tasks were completed on the Labor Information Module, which will provide weekly data on nondivision labor charges. The software that processes the cost data is running, and work is in progress to extract data from the accounting system. This will greatly reduce the manual data input. The Labor Information Module will become operational for cost information during the current year.

In addition, the Personnel Information Module, used to generate personnel-related reports, is operational. This module is also being used as a test bed in the development of new techniques for interacting with users who do not have a computer background and managers who do not have the time necessary to learn a complex set of instructions. These techniques are then utilized in other parts of the M.S.

A new module is also being used to provide information relative to equipment being held in the Division's storage area. The problem was analyzed and a system designed and put into operation within a few weeks. This was accomplished by using an existing module in the MIS and making the changes necessary to perform the new task. This ability to respond quickly to Management's changing needs is the real test of a MIS.

Further, an interactive program for project scheduling is now operational at FED. PERT6 (Program Evaluation and Review Techniques) is a system that was leased from a software vendor. Attempts are under way to provide a graphics capability for use with this system.

Also, the FED Procurement Module has been installed for use by the entire Laboratory. The basic design of the software was such that only minor changes were required to make the transition to laboratory-wide use. Several new capabilities, which are more of a concern at the Laboratory level, were added to the system. Some of these capabilities will also be incorporated into the FED system.

10.5 ENGINEERING SERVICES, QUALITY ASSURANCE, SAFETY AND EMERGENCY PLANNING, AND PROCUREMENT EXPEDITING

10.5.1 Engineering Services

The Engineering Services Group provides all of the nonprogrammatic engineering work and coordination for the Division. This includes coordination of machine shop work, maintenance craft work, inventory and storage of equipment and materials, telecommunications coordination, and the coordination of Division requests for general plant projects (GPP), general plant equipment, and line item facility improvements. The group is also responsible for maintaining buildings, facilities, and equipment and for planning future facilities. Some of the highlights of this activity in the past year include the following:

(1) completion of 15 expense and 4 equipment projects;
(2) initiation of 3 GPP, 12 expense, and 6 equipment projects; and
(3) coordination of 18 man-years of machine shop work in X-10 shops and 37 man-years in Y-12 shops, including 64 jobs at X-10 and 216 jobs at Y-12 with a total value well in excess of $2 million.

Also, construction was started on the office and laboratory space addition to Building 9201-2, the demineralized water system in Building 9204-1, and the electrical power upgrade of Building 9204-1.

10.5.2 Procurement Expediting

The Procurement Expediting Group is functioning well in the Engineering Services Group. During 1974 this group processed 2152 requisitions for materials, equipment, and services representing a volume of over $10.5 million. Efforts to improve delivery of ordered items are continuing and are showing success on certain commodities. One person was added to the group for this specific purpose.

10.5.3 Safety and Emergency Planning

The Division Safety Program includes monthly safety inspections by individual sections, fire inspections by professional fire inspectors, and six formal safety training sessions per year for all Division personnel. A formal training program in cardiopulmonary resuscitation (CPR) was instituted. Forty people completed this course.

10.5.4 Quality Assurance

The Quality Assurance (QA) Program for FED continues to function well. Also, the interface with Engineering QA made significant progress during the year. The program continues to be effective in ensuring reliable and cost-effective experimental equipment, both fabricated and purchased.

A complete revision of the Division QA Manual was started in order to bring the Division QA Program into compliance with ORO IMD 02xx and UCC-ND SPP 2-16 standards.

10.6 FED LIBRARY

The Fusion Energy Division Library provides library and information services to FED, ORNL, UCC-ND, and DOE. A specialized collection of books, technical reports, and scientific journals in the areas of plasma physics and fusion energy technology is maintained.

Also available are computerized information retrieval services using DOE RECON and other commercial bibliographic systems.

LIST OF ABBREVIATIONS

ADIP	Committee on Alloy Development for Irradiation Performance
AEDC	Arnold Engineering Development Center
AES	Auger electron microscopy
appm	atomic parts per million
APS	American Physical Society
ARE	aspect ratio enhancement
ATC	Adiabatic Toroidal Compressor
BCA	binary collision approximation
bcc	body-centered cubic
BSR	Bulk Shielding Reactor
COM	constants-of-motion
CPFF	cost plus fixed fee
CPM	Collisional Plasma Model
CPR	cardiopulmonary resuscitation
cw	continuous wave
CWTX	Coil Winding Test Experiment
DBTT	ductile-to-brittle transition temperature
D-D	deuterium-deuterium
DEMO	Commercial Demonstration Reactor
DNA	Defence Nuclear Agency
DOE	Department of Energy
dpa	displacement per atom
D-T	deuterium-tritium
EBT	ELMO Bumpy Torus
EBTR	ELMO Bumpy Torus Reactor
EBT-S	ELMO Bumpy Torus Scale Experiment
ECH	electron cyclotron heating
ECR	electron cyclotron resonance
EF	equilibrium field
EPR	Experimental Power Reactor
ETF	Engineering Test Facility
EURATOM	European Atomic Energy Community
fcc	face-centered cubic
FCT	flux-conserving tokamak
FED	Fusion Energy Division
FIFPC	Fast Ion Fokker-Planck Code
FLR	finite Larmor radius
GA	General Atomic
GD	General Dynamics
GE	General Electric
GIFTS	Graphics-Oriented Interactive Finite Element Time-Sharing System
GPP	general plant projects
HFIR	High Flux Isotope Reactor
HPTF	High Power Test Facility
IAEA	International Atomic Energy Agency
I&C	instrumentation and controls
IGC	Intermagnetics General Corporation
INTOR	International Tokamak Reactor
ISX	Impurity Study Experiment
LARTS	Large Aspect Ratio Tokamak Study
LASL	Los Alamos Scientific Laboratory
LCP	Large Coil Program
LCS	Large Coil Segment
LCS's	linear collision sequences
LCSTF	Large Coil Segment Test Facility
LCT	Large Coil Task
LCTF	Large Coil Test Facility
LLL	Lawrence Livermore Laboratory
LPTT	Long Pulse Technology Tokamak
LRO	long-range-ordered
LTIF	Low Temperature Irradiation Facility

M&S	Magnetics and Superconductivity
METF	Medium Energy Test Facility
MFE	magnetic fusion energy
MHD	magnetohydrodynamic
MIS	Management Information System
MIT	Massachusetts Institute of Technology
NMFECC	National Magnetic Fusion Energy Computer Center
OFE	Office of Fusion Energy
OH	ohmic heating
ORCHIS	Oak Ridge Computerized Hierarchical Information System
ORMAK	Oak Ridge Tokamak
ORNL	Oak Ridge National Laboratory
ORNL-PIG	Penning Multicharged Ion Source
ORO	Oak Ridge Operations
ORR	Oak Ridge Research Reactor
PDM	Pittsburgh-Des Moines Steel Company
PDX	Poloidal Divertor Experiment
PERT6	Program Evaluation and Review Techniques
PF	poloidal field
PLT	Princeton Large Torus
PPPL	Princeton Plasma Physics Laboratory
PS	Pfirsch-Schlüter
PWC	programmable waveform controller
QA	Quality Assurance
R&D	research and development
RDAC	research and development activities
RENTOR	Rensselaer Torus
rf	radio frequency
RFP	request for proposal
RGA	residual gas analysis
rms	root mean square
RSIC	Radiation Shielding Information Center
SAP	sintered aluminum product
SEM	scanning electron microscope
TEDI	Time Evolution of Drift Instabilities
TEM	transmission electron microscopy
TESPE	Toroidal Energy Storage Experiment Project
TF	toroidal field
TFTR	Tokamak Fusion Test Reactor
TNS	The Next Step
TZM	Mo-0.5% Ti-0.09% Zr
UCC-ND	Union Carbide Corporation-Nuclear Division
UDB	Unified Data Base
USC	User Service Center
UTRC	United Technologies Research Center
UTS	ultimate tensile strength
UVC	Universal Voltronics Corporation
vuv	vacuum ultraviolet
wppm	weight parts per million
0-D	zero-dimensional
1-D	one-dimensional
2-D	two-dimensional
3-D	three-dimensional

PUBLICATIONS, PAPERS, AND REPORTS

BOOKS AND JOURNAL ARTICLES

R. G. Bateman and H. R. Hicks, "Magnetic Fluctuations in Tokamaks," in *AIP Pamphlet*, September 1978.

C. O. Beasley, Jr., J. E. McCune, H. K. Meier, and W. I. van Rij, "Calculation of a Self-Consistent, Low Frequency Electrostatic Field in the Drift-Kinetic Approximation," Plasma Phys. 20, 116-26 (1978).

B. Carreras, B. V. Waddell, H. R. Hicks, and S. J. Lynch, "Comments on 'Simulation of Large Magnetic Islands: A Possible Mechanism for a Major Tokamak Disruption,'" by R. B. White, D. A. Monticello, and M. N. Rosenbluth, Phys. Rev. Lett. 39, 1818 (1977) in Phys. Rev. A 18, 2732 (1978).

P. J. Catto, "Adiabatic Modifications to Plasma Turbulence Theories," Phys. Fluids 21, 147-8 (1978).

P. J. Catto and K. T. Tsang, "Trapped Electron Instability in Tokamaks: Analytic Solution of the Two-Dimensional Eigenvalue Problem," Phys. Fluids 21, 1381-8 (1978).

R. J. Colchin, C. E. Bush, P. H. Edmonds, A. C. England, K. W. Hill, R. C. Isler, T. C. Jernigan, P. W. King, R. A. Langley, D. H. McNeill, M. Murakami, R. V. Neidigh, G. H. Neilson, J. E. Simpkins, J. Wilgen, J. C. DeBoo, K. H. Burrell, and E. S. Ensberg, "Plasma Wall Impurity Experiments in ISX-A," J. Nucl. Mater. 76 & 77, 405 (1978).

P. L. Colestock, K. A. Connor, R. L. Hickok, and R. A. Dandl, "Direct Measurement of Plasma Space Potential on EBT," Phys. Rev. Lett. 40, 1717-20 (1978).

L. Dresner, "Distribution of Current Among the Filaments of a Multifilamentary Superconductor Close to the Input Leads," Cryogenics 18, 285-8 (1978).

P. H. Edmonds and A. C. England, "Energy Loss to the Wall and Limiter in Normal ORMAK Discharges," Nucl. Fusion 18, 23-7 (1978).

J. F. Ellis and P. L. Walstrom, "Moving Coil Linear Variable Differential Transformer," Rev. Sci. Instrum. 49, 398-400 (1978).

W. L. Gardner, J. Kim, M. M. Menon, and J. H. Whealton, "Ion Beamlet Steering by Aperture Displacement for a Tetrode Accelerating Structure," Rev. Sci. Instrum. 49, 1214-5 (1978).

H. H. Haselton, "Positive Ion Systems – State of the Art and Ultimate Potential," in *Proc. Meeting of the Division of Magnetic Fusion Energy Workshop on Plasma Heating Development Requirements*, pp. 164-7, Washington, D.C., 1978.

W. A. Houlberg, Y-K. M. Peng, A. T. Mense, and S. E. Attenberger, "Startup Scenarios in Tokamak Reactors," Trans. Am. Nucl. Soc. 28, 42 (1978).

R. C. Isler and E. C. Crume, Jr., "Charge-Transfer Excitation of Impurity Ions in Tokamaks," Phys. Rev. Lett. 41, 1296 (1978).

E. F. Jaeger, D. A. Spong, and C. L. Hedrick, "Neoclassical Transport in the ELMO Bumpy Torus," Phys. Rev. Lett. 40, 866-9 (1978).

G. L. Jahns, M. Soler, B. V. Waddell, J. D. Callen, and H. R. Hicks, "Internal Disruptions in Tokamaks," Nucl. Fusion 18, 609-28 (1978).

R. H. Kernohan, H. M. Long, M. M. Menon, and S. W. Schwenterly, "The Use of Field Plotting Paper for Resistance Thermometry at Low Temperatures," Cryogenics 17, 247-8 (1977).

J. Kim, J. H. Whealton, and G. Schilling, "A Study of Two-Stage Ion-Beam Optics," J. Appl. Phys. 49(2), 517-24 (1978).

J. W. Lue, J. R. Miller, and L. Dresner, "Vapor Locking as a Limitation to the Stability of Composite Conductors Cooled by Boiling Helium," Adv. Cryog. Eng. 23, 226-33 (1978).

J. R. McNally, Jr., "Fusion-Fission Analogy and Tn-Tau Criterion for Fusion Plasmas," Nucl. Sci. Eng. 67, 255-7 (1978).

J. R. McNally, Jr., "Lean Deuterium – Rich Helium-3 as a 'Clean' Fusion Reactor," Nucl. Fusion 18, 133-6 (1978).

M. M. Menon, S. W. Schwenterly, R. H. Kernohan, and H. M. Long, "Dielectric Strength of Liquid Helium Impregnated Plastic Tapes," pp. 277-86 in *Electrical Insulation and Dielectric Phenomena*, National Academy of Science, Washington, D.C., 1978.

T. G. Northrup and J. A. Rome, "Extensions of Guiding Center Motion to Higher Order," Phys. Fluids 21, 384-9 (1978).

J. W. Pearce, "Optically Coupled High-Voltage Isolation Amplifier," Rev. Sci. Instrum. 49, 1562-4 (1978).

Y-K. M. Peng, S. K. Borowski, and T. Kammash, "Microwave Start-Up of Tokamak Plasmas Near Electron Cyclotron and Upper Hybrid Resonances," Nucl. Fusion 18, 1489-98 (1978).

Y-K. M. Peng, R. A. Dory, D. B. Nelson, and R. O. Sayer, "Magnetohydrodynamic Equilibria and Local Stability of Axisymmetric Tokamak Plasmas," Phys. Fluids 21, 467-75 (1978).

J. A. Rome, "Beam Penetration – Theory and Predictions," in *Proc. Workshop Fusion Fueling*, pp. 23-6, Princeton, New Jersey, 1978.

D. J. Sigmar, "Fundamental Timescales for Flux Conserving Tokamak Heating, and Certain Global FCT-Equilibrium Properties," in *Advances in Fusion Science and Engineering* by the Division of Magnetic Fusion Energy.

D. J. Sigmar and H. C. Chan, "Anomalous Alpha-Particle Transport in Thermonuclear Tokamak Plasma," Nucl. Fusion 18, 1569-81 (1978).

D. J. Sigmar and G. Vahala, "Analytic, High β Flux Conserving Equilibria for Cylindrical Tokamaks," Phys. Fluids 21, 2280-6 (1978).

P. T. Spampinato, C. Sardella, and T. E. Shannon, "Design Improvements Simplify Remote Maintenance of Tokamaks," Trans. Am. Nucl. Soc. 30, 800-1 (1978).

D. Steiner and J. F. Clarke, "The Tokamak: Model T Fusion Reactor," Science 199, 1395-403 (1978).

D. Steiner and C. E. Easterly, "Fusion as an Energy Option: Preliminary Observations on Environmental and Economic Implications," in *Global Energy – Its Effect on Man and Health* by the National Environmental Health Association.

K. T. Tsang, J. D. Callen, and G. Vahala, "Turbulence Theory for the Dissipative Trapped Electron Instability," Phys. Fluids 21, 1172-80 (1978).

K. T. Tsang, P. J. Catto, J. C. Whitson, and J. Smith, "Absolute Universal Instability' is not Universal," Phys. Rev. Lett. 40, 327-31 (1978).

K. T. Tsang, J. C. Whitson, J. D. Callen, P. J. Catto, and J. Smith, "Drift Alfvén Waves in Tokamaks," Phys. Rev. Lett. 41, 557-61 (1978).

B. V. Waddell, B. Carreras, H. R. Hicks, J. A. Holmes, and D. K. Lee, "A Mechanism for Major Disruptions in Tokamaks," Phys. Rev. Lett. 41, 1386 (1978).

B. V. Waddell, G. L. Jahns, J. D. Callen, and H. R. Hicks, "Interpretation of Tokamak Sawtooth Oscillations," Nucl. Fusion 18, 735-9 (1978).

B. V. Waddell, M. N. Rosenbluth, D. A. Monticello, R. B. White, and B. Carreras, "Non-Linear Numerical Algorithms for Studying Tearing Modes," pp. 79-91 in *Theoretical Computational Plasma Physics*, IAEA, Vienna, 1978.

J. H. Whealton, "Effect of Beamlet-Beamlet Interaction on Ion Optics of Multiaperture Sources," Appl. Phys. Lett. 32, 353-5 (1978).

J. H. Whealton, "Effect of Electrode Shielding of Beamlet-Beamlet Interaction in Multiaperture Sources," Appl. Phys. Lett. 33, 697-8 (1978).

J. H. Whealton, "Mitigation of Residual Space Charge Ion Optics Effects in Gas Cell by Adjustment of Beam Perveance," Rev. Sci. Instrum. 49, 869-70 (1978).

J. H. Whealton, L. R. Grisham, C. C. Tsai, and W. L. Stirling, "Effect of Preacceleration Voltage Upon Ion-Beam Divergence," J. Appl. Phys. 49, 3091-3101 (1978).

J. H. Whealton, E. F. Jaeger, and J. C. Whitson, "Optics of Ion Beams of Arbitrary Perveance Extracted from a Plasma," J. Comput. Phys. 27, 32-41 (1978).

J. H. Whealton, G. G. Kelley, O. B. Morgan, and G. Schilling, "Steady-State Space Charge Blowup and Recovery of Intense Ion Beams," Nucl. Instrum. Methods 154, 441-4 (1978).

J. H. Whealton and C. C. Tsai, "Influence of Chromatic Aberrations on Space Charge Ion Optics," Rev. Sci. Instrum. 49, 495-8 (1978).

J. H. Whealton, C. C. Tsai, W. K. Dagenhart, W. L. Gardner, H. H. Haselton, J. Kim, M. M. Menon, P. M. Ryan, D. E. Schechter, and W. L. Stirling, "Effect of Preacceleration on Intense Ion Beam Transmission Efficiency," Appl. Phys. Lett. 33, 278-9 (1978).

J. H. Whealton and J. C. Whitson, "Solution of the Collisionless Plasma Sheath Equation for Ion Extraction Through an Aperture," in *Proc. 30th Gaseous Electronic Conference*, published in Bull. Am. Phys. Soc. 23, 151 (1978).

J. C. Whitson, J. Smith, and J. H. Whealton, "Calculation Evolving Ion Beam Source," J. Comput. Phys. 28, 408 (1978).

N. A. Uckan, "The ELMO Bumpy Torus – An Alternate Fusion Reactor Concept," p. 2439 in *Alternate Energy Sources: An International Compendium*, Vol. 5, ed. N. Veziroglu, Hemisphere Publishing Corporation, 1978.

N. A. Uckan, R. A. Dandl, C. L. Hedrick, E. S. Bettis, L. M. Lidsky, D. G. McAlees, R. T. Santoro, H. L. Watts, and H. T. Yeh, "The ELMO Bumpy Torus (EBT) Reactor," p. 369 in *Fusion Reactor Design Concepts*, IAEA, Vienna, 1978.

PRESENTATIONS AT MEETINGS AND CONFERENCES

Meeting of the Division of Magnetic Fusion Energy Workshop, Washington, D.C., December 1977 (proceedings published in 1978)

W. L. Stirling, "The ORNL Negative Ion Program."

Office of Fusion Energy Workshop on Development of Superconductors for Fusion Power, Washington, D.C., January 26, 1978

W. A. Fietz, "ORNL Superconductor Development Program."

IAEA Workshop on Neutral Injectors, Culham, England, January 26-30, 1978

J. H. Whealton et al., "Beam Distribution."

J. H. Whealton et al., "Theoretical Study of Ion Optics and Extraction."

1st Topical Meeting on Fusion Reactor Materials, Miami, Florida, January 29-31, 1978

R. J. Colchin, "Materials Experience with Tokamak Plasmas."

Department of Energy/Sandia Laboratories First Wall Coating Workshop, Sandia Laboratories, Albuquerque, New Mexico, January 31-February 2, 1978

R. A. Langley, "ISX-A Plasma Wall Interaction Studies."

Junior Science and Humanities Symposium, February 24, 1978

M. Roberts, "We Believe Fusion Can Be A Real Energy Alternative in the Early Part of the 21st Century."

2nd Workshop on the Use of VUV and X-Ray Radiometry in Plasma Diagnostics, Santa Fe, New Mexico, February 28, 1978

R. C. Isler, "Monochromator Calibration Techniques from 460-3000 Å."

Superconducting Cyclotron Presentation to the Subcommittee of the Nuclear Science Advisory Committee (NUSAC), Oak Ridge National Laboratory, March 1, 1978

J. K. Ballou and J. N. Luton, Jr., "Holifield Heavy Ion Accelerator Facility, Phase II."

2nd American Physical Society Topical Conference on High-Temperature Plasma Diagnostics, Santa Fe, New Mexico, March 1-3, 1978 (proceedings published February 2, 1978, Conf. LA-7160-C)

C. E. Bush, "Detectors and Techniques for Energy Flux Measurements on ISX," p. 91.

E. C. Crume, Jr., R. C. Isler, and T. Amano, "Interpretation of ORMAK Impurity Radiation Data Using Simulation Models," p. 82.

K. W. Hill, S. von Goeler, B. Frankel, R. Horton, R. D. Cowan, and J. Hovey, "Fe Charge-State Distributions in PLT from Bragg X-Ray Spectroscopy," p. 89.

J. T. Mihalczo, G. H. Neilson, J. F. Lyon, and R. E. Worsham, "Perpendicular Charge Exchange Diagnostic for ISX-B," p. 105.

A. P. Navarro, V. K. Paré, and J. L. Dunlap, "Determination of Spatial Distribution of Volume Soft X-Ray Emission from Plasmas," p. 86.

G. H. Neilson, "Mass-Energy Neutral Analyzer for ISX," p. 106.

3rd International Conference on Plasma Surface Interactions in Controlled Fusion Devices, Culham, England, April 3-7, 1978 (proceedings published in J. Nucl. Mater. 76 & 77)

J. A. Borders, R. A. Langley, and K. L. Wilson, "Low Energy Hydrogen and Deuterium Sputtering Measurements of Stainless Steel, Graphite, and Beryllium Oxide," p. 168.

M. A. Janocko, R. D. Blaugher, and P. W. Eckels, "Flow Characteristics of Forced-Flow Nb_3Sn Conductors for Toroidal-Field Coils."

R. A. Langley, R. S. Blewer, and P. S. Peercy, "Surface Preparation Effects on Blister Formation and Stress Buildup in Polycrystalline Vanadium," p. 261.

R. A. Langley, R. S. Blewer, and J. Roth, "Behavior of Implanted D and He in Pyrolytic Graphite," p. 313.

Symposium on Fusion Energy, Montreal, Quebec, Canada, April 11-12, 1978

D. Steiner, "The Technological Implications of Fusion Power: Requirements and Status."

[illegible] Divertors, Culham, England, April [illegible]

[illegible] and R. A. [illegible], "The [illegible] Bundle Divertor for Tokamaks."

Annual Controlled Fusion Theory Conference, [illegible], Tennessee, April [illegible], 1978

T. Amano, "Numerical Simulation of Impurity Transport in ISX."

R. A. Appleton, R. [illegible] Clausing, R. J. Colchin, L. C. Emerson, Y. Gomay, L. Heatherly, J. E. Simpkins, S. P. Withrow, and R. A. Zuhr, "Surface Impurity Problems in the ISX-A Tokamak.

G. Bateman and C. H. An, "Ballooning Modes in Highly Elongated Tokamaks."

J. D. Callen and C. L. Hedrick, "Direct Particle Losses in the ELMO Bumpy Torus (EBT)."

B. Carreras, H. R. Hicks, J. A. Holmes, D. K. Lee, S. J. Lynch, and B. V. Waddell, "Status of Nonlinear Resistive MHD Research at Oak Ridge National Laboratory."

A. Cooper, G. Bateman, D. B. Nelson, and T. Kammash, "Effect of Tensor Pressure on Tokamak Equilibrium and Stability."

C. L. Hedrick, D. A. Spong, and E. F. Jaeger, "Banana Transport in EBT."

H. R. Hicks, B. Carreras, J. A. Holmes, D. K. Lee, S. J. Lynch, and B. V. Waddell, "Major Disruptions in Tokamaks: T-4 and PLT.

J. T. Hogan, "MHD/Transport Effects on Tokamak Confinement Scaling."

J. T. Hogan and D. B. Nelson, "Axisymmetric Transport in Tokamaks."

W. A. Houlberg, S. L. Milora, C. A. Foster, H. C. Howe, and M. A. Iskra, "Pellet Injection Model and Comparison with ISX.

H. C. Howe and [illegible] Arrhenius, "Two Species Neutral Transport Model."

E. F. Jaeger, D. A. Spong, and C. L. Hedrick, "Neoclassical Transport in the ELMO Bumpy Torus."

S. J. Lynch, B. Carreras, H. R. Hicks, J. A. Holmes, D. K. Lee, and B. V. Waddell, "Generation of Large Magnetic Islands in the Single Pitch Approximation."

[illegible] and [illegible], "Anomalous Slowing Down of Alpha Particles in Toroidal Plasma."

L. W. Owen, R. A. Dandl, and C. L. Hedrick, "Calculated Effects of Aspect Ratio Enhancement on Particle Confinement in EBT.

Y-K. M. Peng, "Continuous Tokamaks.

J. A. Rome and Y-K. M. Peng, "The Topology of Tokamak Orbits."

M. Soler and J. D. Callen, "Heat Transport in Tokamaks as Observed from Sawtooth Oscillation Characteristics."

K. T. Tsang, J. C. Whitson, J. D. Callen, P. J. Catto, and J. Smith, "Drift-Alfvén Waves in Tokamaks."

W. I. van Rij, H. K. Meier, C. O. Beasley, Jr., and J. E. McCune, "Numerical Study of Drift Mode Behavior Using a Self-Consistent Drift-Kinetic Expansion."

B. V. Waddell, B. Carreras, and H. R. Hicks, "Poloidal Magnetic Field Fluctuations in Tokamaks."

3rd American Nuclear Society Topical Meeting on the Technology of Controlled Nuclear Fusion, Santa Fe, New Mexico, May 9-11, 1978 (proceedings published in 1978, Conf.-780508)

W. R. Becraft for the ORNL TNS Team, "Neutral Beam Injection Status and R&D Needs for TNS," p. 1101.

W. K. Dagenhart, H. H. Haselton, W. L. Stirling, C. C. Tsai, D. E. Schechter, R. C. Davis, M. M. Menon, J. Kim, W. L. Gardner, and J. H. Whealton, "The ORNL/PLT Neutral Beam Lines," p. 1216.

P. N. Haubenreich, "Superconducting Magnets for Fusion Reactors," p. 620.

A. T. Mense, W. A. Houlberg, S. E. Attenberger, and S. L. Milora, "Start-Up Scenarios for Tokamak Reactors," p. 833.

R. L. Reid and D. Steiner, "Economic Trends of Tokamak Power Plants Independent of Physics Scaling Models," p. 529.

M. Roberts, "Oak Ridge TNS Program: A Status Report," p. 1243.

P. T. Spampinato and T. E. Shannon, "The Oak Ridge TNS/PEPR Program Is Considering Modified Physics and Engineering Criteria to Ease Remote Maintenance Problems," p. 1026.

D. Steiner, "Tokamak Reactor Design Studies: Progress and Prognosis," p. 440.

N. A. Uckan, T. S. Bettis, R. A. Dandl, C. L. Hedrick, R. T. Santoro, H. L. Watts, and H. T. Yeh, "The ELMO Bumpy Torus (EBT) Reactor A Status Report," p. 74.

1978 IEEE Meeting on Plasma Science, Monterey, California, May 17-19, 1978 (proceedings published by IEEE, 78CH1357-3NPS)

W. R. Becraft for the ORNL TNS Team, "An Assessment of Neutral Injection for TNS," p. 299.

W. R. Becraft, W. A. Houlberg, and W. M. Stacey, Jr., "Controls and Instrumentation for Tokamak Reactors," p. 246.

J. A. Cobble and J. C. Glowienka, "A Barium I$^+$ Beam for Spatially Resolved Magnetic Field and Density Measurements on ELMO Bumpy Torus," p. 43.

R. J. Colchin, C. E. Bush, R. E. Clausing, P. H. Edmonds, L. C. Emerson, Y. Gomay, K. W. Hill, R. C. Isler, R. V. Neidigh, M. Murakami, and J. E. Simpkins, "Conditions During Low Z_{eff} Operation of ISX-A," p. 88.

W. K. Dagenhart, C. W. Blue, H. H. Haselton, M. M. Menon, S. W. Schwenterly, W. L. Stirling, C. C. Tsai, and J. H. Whealton, "Beam Blocking Experiments Performed on the ORNL/PLT Beam Lines at ORNL," p. 10.

P. H. Edmonds, M. Murakami, C. E. Bush, R. J. Colchin, J. L. Dunlap, R. C. Isler, and G. H. Neilson, "Plasma Confinement Results from ISX-A," p. 178.

J. Kim, W. K. Dagenhart, H. H. Haselton, M. M. Menon, J. T. Mihalczo, W. L. Stirling, and C. C. Tsai, "D-D Neutron Yields From the ORNL 40 keV/60 A Neutral Beam Injector," p. 12.

S. P. Kuo, K. A. Connor, and B. H. Quon, "Pump Depletion and Anomalous Absorption in Parametric Decay Instabilities," p. 141.

M. M. Menon, G. C. Barber, W. R. Becraft, C. W. Blue, W. K. Dagenhart, R. C. Davis, C. A. Foster, W. L. Gardner, H. H. Haselton, J. Kim, C. M. Loring, S. L. Milora, P. M. Ryan, D. E. Schechter, S. W. Schwenterly, W. L. Stirling, C. C. Tsai, J. H. Whealton, and R. E. Wright, "Power Flow Along the ORNL/PLT Neutral Beam Line," p. 9.

A. T. Mense, S. E. Attenberger, W. A. Houlberg, and S. L. Milora, "Pellet Fueling in Tokamak Reactors," p. 254.

D. A. Spong, J. B. Batchelor, L. Deleanu, R. L. Goldfinger, C. L. Hedrick, E. F. Jaeger, L. W. Owen, and J. S. Tolliver, "Theoretical Studies for the ELMO Bumpy Torus (EBT) Device," p. 131.

C. C. Tsai, W. L. Stirling, H. H. Haselton, W. K. Dagenhart, R. C. Davis, W. L. Gardner, J. Kim, M. M. Menon, P. M. Ryan, D. E. Schechter, and J. H. Whealton, "Positive or Negative Ions from a DuoPIGatron Ion Source for Neutral Beam Injectors," p. 17.

J. H. Whealton, C. C. Tsai, W. K. Dagenhart, W. L. Gardner, H. H. Haselton, J. Kim, M. M. Menon, P. M. Ryan, D. E. Schechter, and W. L. Stirling, "Effect of Preacceleration on Intense Ion Beam Transmission Efficiency," p. 14.

Neutral Beam Development Program Review, Washington, D.C., May 22-24, 1978

H. H. Haselton and W. L. Stirling, "ORNL/Plasma Technology Section Status Report."

Seminar presented at Westinghouse Electric Corporation, Pittsburgh, Pennsylvania, May 24, 1978

R. L. Brown, "Minimizing Risks in Nb_3Sn Superconducting Coils by Winding Before Reacting."

1978 Annual Meeting of the American Nuclear Society, San Diego, California, June 18-23, 1978 (proceedings published in Trans. Am. Nucl. Soc. 28, 1978)

W. A. Houlberg, Y-K. M. Peng, A. T. Mense, and S. E. Attenberger, "Startup Scenarios in Tokamak Reactors," p. 42.

Seminar presented at the Department of Energy, Germantown, Maryland, June 22, 1978

M. S. Lubell, "Magnet Facilities."

Ion Source Workshop, Culham, England, June 28-30, 1978

C. C. Tsai, G. C. Barber, W. R. Becraft, C. W. Blue, W. K. Dagenhart, R. C. Davis, W. L. Gardner, H. H. Haselton, J. Kim, M. M. Menon, N. S. Ponte, P. M. Ryan, D. E. Schechter, W. L. Stirling, J. H. Whealton, and R. E. Wright, "ORNL Positive Ion Source."

J. H. Whealton, H. H. Haselton, G. C. Barber, C. W. Blue, W. K. Dagenhart, R. C. Davis, W. L. Gardner, J. Kim, M. M. Menon, N. S. Ponte, P. M. Ryan, D. E. Schechter, S. W. Schwenterly, W. L. Stirling, C. C. Tsai, and R. E. Wright, "ORNL Positive Ion Neutral Beam Program."

8th Conference on Numerical Simulation of Plasmas, Monterey, California, June 28-30, 1978

T. Amano and E. C. Crume, Jr., "Simulation of Multi-Species Impurity Transport in Tokamaks."

H. R. Hicks, B. Carreras, J. A. Holmes, D. K. Lee, S. J. Lynch, and B. V. Waddell, "Fourier Transform vs Finite Difference Techniques in Nonlinear Resistive MHD Codes."

J. T. Hogan, B. Carreras, and W. A. Houlberg, "MHD/Transport Interactions in Tokamaks."

J. A. Holmes, Y-K. M. Peng, and R. A. Dory, "1-1/2 Dimensional Transport: Time Dependent Evolution of Fixed Boundary Equilibria in a Toroidal D-Shaped Flux Conserving D-T Reactor."

W. I. van Rij and H. K. Meier, "The Numerical Calculation of Low-Frequency Electrostatic Fields in the Drift-Kinetic Approximation."

International Symposium on Heating in Toroidal Plasmas, Grenoble, France, July 3-7, 1978 (proceedings published in 1979)

D. B. Batchelor, A. H. Kritz, and R. C. Goldfinger, "A Theoretical Study of Microwave Heating in ELMO Bumpy Torus," p. 191.

O. C. Eldridge, W. Namkung, and A. C. England, "Wave Heating of Toroidal Plasmas at Electron Cyclotron Harmonics," p. 203.

H. H. Haselton, G. C. Barber, W. R. Becraft, C. W. Blue, W. K. Dagenhart, R. C. Davis, P. H. Edmonds, C. A. Foster, W. L. Gardner, J. Kim, C. M. Loring, M. M. Menon, H. C. McCurdy, S. L. Milora, P. M. Ryan, D. E. Schechter, S. W. Schwenterly, W. L. Stirling, D. W. Swain, C. C. Tsai, J. H. Whealton, and R. E. Wright, "PLT and ISX Neutral Beam Injectors," p. 67.

G. H. Neilson, J. F. Lyon, and M. Murakami, "Injection-Dominated Tokamak Experiments at ORNL," p. 49.

J. A. Rome and Y-K. M. Peng, "The Topology of Tokamak Orbits," p. 7.

7th International Cryogenic Engineering Conference, Imperial College, South Kensington, London, July 4-7, 1978

W. A. Fietz, J. W. Lue, and J. R. Miller, "Development and Testing of Toroidal Field Superconductors for Fusion Devices."

M. Hoenig and L. Dresner, "Design and Development of the US-TESPE Toroidal Coil."

S. Shen and R. E. Schwall, "Transient Loss Analysis and Measurements on Normal Conductors and Composite Superconductors."

Fusion Power Coordinating Committee Meeting, Oak Ridge National Laboratory, August 2-3, 1978

J. D. Callen, "Plasma Theory Program at ORNL."

IAEA *7th International Conference on Plasma Physics and Controlled Nuclear Fusion Research, Innsbruck, Austria, August 23-30, 1978*

J. D. Callen, "Tokamak Discharge Modeling Through Magnetic Perturbation Effects: Rapporteuring of Papers F-1-1, F-1-2, and F-1-3."

J. D. Callen, P. J. Catto, J. Smith, K. T. Tsang, and J. C. Whitson, "Anomalous Transport in Tokamaks Caused by Magnetic Effects of Drift Waves."

J. D. Callen, B. V. Waddell, H. R. Hicks, J. A. Holmes, D. K. Lee, S. J. Lynch, K. T. Tsang, J. C. Whitson, B. Carreras, M. Soler, H. Azumi, and P. J. Catto, "Magnetic 'Islandography' in Tokamaks."

R. A. Dandl, F. W. Baity, Jr., K. H. Carpenter, J. A. Cobble, H. O. Eason, J. C. Glowienka, G. R. Haste, W. Hiroe, N. H. Lazar, T. Uckan, B. H. Quon, T. L. White, C. L. Hedrick, D. B. Batchelor, L. Deleanu, R. C. Goldfinger, E. F. Jaeger, L. W. Owen, D. A. Spong, J. S. Tolliver, M. E. Hesse, J. B. McBride, N. A. Krall, and A. L. Sulton, Jr., "Experimental and Theoretical Studies of the ELMO Bumpy Torus (EBT)."

EBT Experimental Group, EBT Theory Group, UV Spectroscopy Group, and Heavy Ion Beam Group, "Experimental and Theoretical Studies of the ELMO Bumpy Torus (EBT)."

R. A. Dory, R. G. Bateman, D. P. Berger, L. A. Charlton, J. T. Hogan, J. Munro, D. B. Nelson, Y-K. M. Peng, D. J. Sigmar, and D. Strickler, "High Beta Tokamaks."

H. H. Haselton, G. C. Barber, W. R. Becraft, C. W. Blue, W. K. Dagenhart, R. C. Davis, C. A. Foster, W. L. Gardner, J. Kim, C. M. Loring, M. M. Menon, S. L. Milora, P. M. Ryan, D. E. Schechter, S. W. Schwenterly, W. L. Stirling, C. C. Tsai, J. H. Whealton, and R. E. Wright, "Neutral Beam Injectors for Application on PLT, ISX, and PDX Tokamaks."

C. L. Hedrick, D. B. Batchelor, L. Deleanu, R. C. Goldfinger, E. F. Jaeger, L. W. Owen, D. A. Spong, and J. S. Tolliver, "EBT Theoretical Studies Focusing on Transport."

M. Murakami, K. H. Burrell, T. C. Jernigan, T. Amano, S. C. Bates, C. E. Bush, R. E. Clausing, R. J. Colchin, E. C. Crume, Jr., J. C. DeBoo, J. L. Dunlap, G. R. Dyer, P. H. Edmonds, L. C. Emerson, A. C. England, E. S. Ensberg, C. A. Foster, Y. Gomay, K. W. Hill, H. C. Howe, R. C. Isler, H. E. Ketterer, P. W. King, R. A. Langley, J. F. Lyon, D. H. McNeill, J. T. Mihalczo, S. L. Milora, W. Namkung, A. P. Navarro, R. V. Neidigh, G. H. Neilson, V. K. Paré, R. Prater, H. J. Saltmarsh, M. J. Schaffer, J. E. Simpkins, D. W. Swain, J. B. Wilgen, W. R. Wing, S. K. Wong, and B. Zurro, "Plasma Confinement and Impurity Flow Reversal Experiments in the ISX-A Tokamak."

R. A. Phaneuf, J. T. Hogan, H. J. Kim, P. W. Meyer, P. H. Stelson, P. Hvelplund, and [illegible] Barnett, "The Opacity of Tokamak Plasmas to Neutral Beams."

P. Sager and M. Roberts, "Tokamak TNS Studies."

M. Roberts, Oak Ridge TNS Team, "Oak Ridge TNS Program: A Status Report."

N. A. Uckan, D. B. Batchelor, E. S. Bettis, R. A. Dandl, C. L. Hedrick, E. F. Jaeger, D. G. McAlees, D. B. Nelson, L. J. Owen, R. T. Santoro, D. A. Spong, T. Uckan, H. L. Watts, H. T. Yeh, L. M. Lidsky, J. S. Herring, and R. E. Potok, "The ELMO Bumpy Torus (EBT) Reactor."

Seminar presented at the Department of Energy, Germantown, Maryland, August 30, 1978

M. S. Lubell, "Advanced Conductor Development."

IAEA Technical Committee Meeting on Engineering of Large Tokamak Experiments, Paris, France, September 1-6, 1978

T. C. Jernigan, "The Long Pulse Technology Tokamak."

COMPUMAG Conference on the Computation of Magnetic Fields, Grenoble, France, September 4-6, 1978

H. T. Yeh, "Computation of Transient 3-D Eddy Current in Nonmagnetic Conductor."

International Conference on Ion Beam Modification of Materials, Budapest, Hungary, September 4-8, 1978

R. Behrisch, R. S. Blewer, J. Borders, R. A. Langley, J. Roth, and B. M. U. Scherzer, "Trapping and Release of Deuterium in Beryllium Oxide."

Society of Industrial and Applied Mathematics 1978 Fall Meeting, Knoxville, Tennessee, October 1978

H. R. Hicks, D. K. Lee, B. Carreras, and B. V. Waddell, "Nonlinear Resistive MHD Studies of Tokamak Plasmas."

1978 Applied Superconductivity Conference, Pittsburgh, Pennsylvania, September 25-28, 1978

J. W. H. Chi, "Conceptual Design of a Hollow Cable Conductor for the Large Coil Program."

J. W. H. Chi, "Effect of Subchannel Flow Velocities on the Stability of Hollow Cable Conductors."

F. W. Domelson, D. T. Hackworth, and L. R. Stuebinger, "Structure Design of the Westinghouse Superconducting Magnet for the Large Coil Program."

L. Dresner, "Analytic Solution for the Propagation Velocity in Superconducting Composites."

W. A. Fietz, "Nb_3Sn in 1978: State of the Art."

P. N. Haubenreich, J. N. Luton, and P. B. Thompson, "The Role of the Large Coil Program in the Development of Superconducting Magnets for Fusion Reactors."

J. C. Lottin, J. R. Miller, J. W. Lue, and L. Dresner, "Measurements of Traveling Transition Zone Along a Superconductor."

J. W. Lue, J. R. Miller, and J. C. Lottin, "Pressure Drop Measurements on Forced Flow Cable Conductors."

J. R. Miller, J. W. Lue, S. S. Shen, and J. C. Lottin, "Measurements of Stability of Cabled Superconductors Cooled by Flowing Supercritical Helium."

S. S. Shen and R. E. Schwall, "Interaction of Transport Current and Transient External Field in Composite Conductors."

G. R. Wagner, S. S. Shen, A. Petrovich, R. E. Schwall, and M. S. Walker, "Losses in Multifilament Nb_3Sn Conductors Designed for High B Applications."

American Chemical Society Meeting, Oak Ridge High School, Oak Ridge, Tennessee, October 3, 1978

D. B. Batchelor, "Fusion Energy and the Research Program Which Will Produce It."

D. B. Batchelor and C. L. Hedrick, "Investigation of Trapped-Particle Instabilities in EBT."

Alternate Concepts Development Program Meeting, Office of Fusion Energy, Germantown, Maryland, October 16-18, 1978

L. A. Berry, J. D. Callen, R. A. Dandl, R. A. Dory, C. L. Hedrick, and N. A. Uckan, "ELMO Bumpy Torus."

National Bureau of Standards Department of Energy Workshop, October 24-26, 1978

P. N. Mazandarany, "Materials Utilization in the General Electric Coil for the Large Coil Program."

Southeastern Section of the American Physical Society Annual Meeting, Blacksburg, Virginia, October 26-28, 1978

D. Steiner, "The Tokamak Concept: A Promising Approach to Fusion Power Demonstration."

Meeting of the American Physical Society, Colorado Springs, Colorado, October 30-November 3, 1978 [proceedings published in Bull. Am. Phys. Soc. 23(7), 1978]

T. Amano and E. C. Crume, Jr., "Numerical Simulation of ISX-A Tungsten Injection Experiment," p. 772.

C. H. An and R. G. Bateman, "Analytic Study of Ballooning Instabilities with High Toroidal Mode Number in Circular and Elongated Tokamaks," p. 779.

S. E. Attenberger, W. A. Houlberg, and A. T. Mense, "Startup Scenarios for Tokamak Reactors," p. 866.

M. Azumi and J. D. Callen, "Transport Equations in a Helical Coordinate System Including Magnetic Island Effects," p. 885.

F. W. Baity, J. C. Glowienka, B. H. Quon, S. Hiroe, and S. P. Kuo, "Experimental Study of Energy Confinement in EBT-I," p. 910.

D. B. Batchelor, "A Simple Power Balance Model for Microwave Heating in EBT," p. 877.

R. G. Bateman, "Resistive Ballooning Modes," p. 778.

S. C. Bates, ISX-B Group, "Experimental Program for ISX-B," p. 791.

C. O. Beasley, Jr., J. E. McCune, H. K. Meier, and W. I. van Rij, "Study of Nonlinear Effects for Drift Waves in a Cylindrical Plasma Using the CPM," p. 794.

S. K. Borowski, Y-K. M. Peng, W. A. Houlberg, and T. Kammash, "Plasma Confinement in a Tokamak Without Toroidal Current," p. 772.

C. E. Bush, R. C. Isler, and E. C. Crume, Jr., "Time and Spatially Resolved Measurements of Plasma Power Losses in ISX-A," p. 790.

J. D. Callen and M. Azumi, "Heat Transport in the Presence of a Low Order Magnetic Island," p. 885.

K. H. Carpenter and N. H. Lazar, "Modified Multiplicative Algebraic Reconstruction Technique Applied to VUV Studies in EBT," p. 803.

B. Carreras, H. R. Hicks, and B. V. Waddell, "Tearing Mode Activity for Hollow Current Profiles," p. 831.

L. A. Charlton, R. A. Dory, Y-K. M. Peng, and D. J. Strickler, "Possible Scaling Laws Found with a Numerical Stability Study," p. 897.

J. A. Cobbie, R. A. Dandl, and M. Hesse, "Thomson Scattering on EBT-S," p. 877.

R. J. Colchin, C. E. Bush, R. C. Isler, M. Murakami, and J. E. Simpkins, "Correlations Between Plasma Impurities and Vacuum Conditions and ISX," p. 855.

A. Cooper, G. Bateman, D. B. Nelson, and T. Kammash, "Ballooning Modes in Tokamaks with Tensor Pressure," p. 778.

W. K. Dagenhart, W. L. Stirling, and C. C. Tsai, "Development of a Long Pulse Penning Type Negative Ion Source," p. 805.

R. C. Davis, H. H. Haselton, D. E. Schechter, W. L. Stirling, C. C. Tsai, G. C. Barber, W. K. Dagenhart, W. L. Gardner, J. Kim, M. M. Menon, N. S. Ponte, P. M. Ryan, S. W. Schwenterly, J. H. Whealton, and R. E. Wright, "High Energy DC Ion Source for Future Neutral Beam Injectors," p. 805.

R. Dory, L. A. Charlton, Y-K. M. Peng, and D. J. Strickler, "Stability Study of High β FCT Equilibrium," p. 897.

L. J. Drooks, J. W. Wooten, R. W. McGaffey, D. H. McCollough, and J. H. Whealton, "A Computer Code for Modeling the Asymmetric Neutral Beam Injector," p. 846.

J. L. Dunlap, A. Navarro, E. C. Crume, Jr., and V. K. Paré, "Soft X-Ray Enhancement Factors in the ISX-A Tokamak," p. 790.

G. R. Dyer, G. H. Neilson, and G. G. Kelley, "Calculated Effects of Pulse Pileup on Soft X-Ray Energy Spectra," p. 807.

P. H. Edmonds, C. A. Foster, S. L. Milora, H. C. Howe, C. E. Bush, M. Murakami, and J. B. Wilgen, "Pellet Injection Gas Puff Experiment and a Numerical Simulation of Pellet Injection on ISX-A," p. 790.

O. C. Eldridge, A. C. England, and W. Namkung, "The Interaction of Microwave Radiation at Electron Cyclotron Frequency with Runaway Electron Populations in Tokamaks," p. 878.

G. A. Emmert, J. N. Davidson, and A. T. Mense, "Divertor Sheath Revisited," p. 896.

A. C. England, J. L. Dunlap, W. Namkung, and R. V. Neidigh, "MHD Instability Activity in the Surface Plasma of ISX-A," p. 791.

C. A. Foster and S. L. Milora, "Hydrogen Pellet Injection Apparatuses," p. 790.

R. H. Fowler and J. A. Rome, "Beam Deposition Profiles for Non-Circular Tokamak Plasmas Calculated Using Monte Carlo Techniques and Bounce Averages," p. 865.

W. L. Gardner, W. L. Stirling, C. C. Tsai, R. C. Davis, H. H. Haselton, J. H. Whealton, M. M. Menon, W. K. Dagenhart, N. S. Ponte, G. C. Barber, and R. E. Wright, "An Ion Beam Direct Energy Recovery Experiment at ORNL," p. 747.

R. C. Goldfinger, D. B. Batchelor, and A. H. Kritz, "Analysis and Computations of Microwave Heating in the ELMO Bumpy Torus," p. 877.

C. L. Hedrick, D. A. Spong, and L. W. Owen, "Analytic Expressions for EBT Particle Orbits," p. 876.

H. R. Hicks, B. Carreras, B. V. Waddell, and D. K. Lee, "Effects on the Nonlinear Interaction of Tearing Modes Due to Temperature Evolution and Profile Tailoring," p. 831.

S. P. Hirshman, "Steady State Classical Diffusion in the Presence of Heat Transport," p. 760.

J. A. Holmes, Y-K. M. Peng, and D. J. Strickler, "High Beta Equilibria Through Large Toroidal Compression," p. 896.

W. A. Houlberg and J. T. Hogan, "Simulation of MHD Effects on Transport: Sawtooth and Skin Currents," p. 760.

H. C. Howe, M. Murakami, G. H. Neilson, and R. M. Wieland, "Interpretation of Confinement Measurements on ISX-A," p. 854.

R. C. Isler, C. E. Bush, and E. C. Crume, Jr., "Radiative Losses from the ISX-A Tokamak," p. 855.

E. F. Jaeger and C. L. Hedrick, "Collisionless Transport in the ELMO Bumpy Torus (EBT)," p. 876.

T. C. Jernigan, ISX Group, "Summary of ISX-A Results," p. 854.

H. E. Ketterer, J. T. Mihalczo, and A. C. England, "Neutron Measurements on ISX-A," p. 790.

J. Kim, G. C. Barber, S. C. Bates, C. W. Blue, W. K. Dagenhart, C. C. Tsai, W. L. Stirling, R. C. Davis, H. H. Haselton, M. M. Menon, P. M. Ryan, D. E. Schechter, and J. H. Whealton, "Neutral Beam Injector Experiments on ISX-B Prototype Beam Line," p. 746.

P. W. King, T. Amano, C. E. Bush, J. C. DeBoo, M. Murakami, and B. Zurro, "Simulation of Heavy Metal Impurities in a Tokamak by Tungsten Injection," p. 855.

G. Knorr, "Time Evolution of the Linear Drift Wave Instability as an Integral Equation," p. 826.

R. A. Langley, R. E. Clausing, R. J. Colchin, L. C. Emerson, L. Heatherly, J. E. Simpkins, R. A. Zuhr, and Y. Gomay, "Summary of Surface Studies in ISX-A," p. 855.

J. F. Lyon, J. A. Rome, and J. T. Hogan, "The Role of Beam Induced Currents in High-β_T Experiments," p. 771.

J. R. McNally, Jr., "Alpha Sustained, Steady-State Tokamak," p. 8[illegible]

H. K. Meier and D. J. Sigmar, "Analytical High Beta Tokamak Equilibria," p. 897.

M. M. Menon, C. C. Tsai, D. E. Schechter, G. C. Barber, P. M. Ryan, R. C. Davis, W. L. Gardner, J. Kim, and H. H. Haselton, "Beam Optics of a Two Stage Multiaperture Intense Neutral Beam Source," p. 746.

J. T. Mihalczo, R. E. Worsham, and J. F. Lyon, "Velocity Filter Electrostatic Analyzer for Charge Exchange Diagnostics on ISX-B," p. 904.

S. L. Milora, C. A. Foster, P. H. Edmonds, C. E. Bush, J. B. Wilgen, H. C. Howe, and G. L. Schmidt, "Hydrogen Pellet Fueling Experiments on ISX-A," p. 855.

M. Murakami, "Review of Confinement Studies in Tokamaks," p. 745.

M. Murakami, R. D. Burris, B. Carreras, J. L. Dunlap, H. R. Hicks, A. P. Navarro, V. K. Paré, and B. V. Waddell, "Tearing Mode Analyses of MHD Activity in ISX-A," p. 791.

W. Namkung, A. C. England, and O. C. Eldridge, "Langmuir Probe Measurements of the Scrape-Off Plasma in ISX-A," p. 791.

A. P. Navarro, V. K. Paré, and J. L. Dunlap, "Plasma Shape from Analysis of Soft X-Ray Signals," p. 772.

R. V. Neidigh and J. F. Lyon, "Neutral-Beam Induced Toroidal Rotation in ORMAK," p. 771.

G. H. Neilson, C. E. Bush, P. H. Edmonds, R. C. Isler, T. C. Jernigan, P. W. King, D. H. McNeill, and M. Murakami, "Plasma Confinement Experiments in ISX-A," p. 854.

B. E. Nelson, LPTT Group, "Design Studies of Long Pulse Technology Tokamaks at ORNL," p. 772.

D. B. Nelson, "Self-Consistent Collisional Tokamak Transport," p. 761.

L. W. Owen, C. L. Hedrick, and D. A. Spong, "Numerical Evaluation of Transport Coefficients for EBT," p. 876.

V. K. Paré, J. L. Dunlap, A. P. Navarro, R. D. Burris, and M. Murakami, "MHD Activity in ISX-A," p. 790.

Y-K. M. Peng, R. A. Dory, L. A. Charlton, D. J. Strickler, D. K. Lee, and J. K. Munro, "Very Small Aspect Ratio Tokamak Equilibria and Stability," p. 896.

B. H. Quon and R. A. Dandl, "Stability of EBT Equilibrium to Global Magnetic Perturbations," p. 910.

J. A. Rome, R. H. Fowler, and J. F. Lyon, "Effects of Finite Orbit Size on Interpretation of Charge-Exchange Flux in Non-Circular Tokamaks with Toroidal Field Ripple," p. 904.

P. M. Ryan, C. E. Bush, R. C. Davis, W. L. Stirling, and C. C. Tsai, "Neutral Beam Studies Utilizing an Infrared Camera," p. 904.

D. E. Schechter, D. Goebel, J. Kim, W. L. Stirling, W. K. Dagenhart, C. C Tsai, H. H. Haselton, R. C. Davis, A. T. Forrester, and J. T. Crow, "Hollow LaB$_6$ Cathode, Magnetic Cusp Ion Source," p. 747.

S. W. Schwenterly, C. C. Tsai, R. C. Davis, and P. M. Ryan. "Cryosorption Pumping of an Energetic Hydrogen Ion Beam," p. 896.

J. Sheffield, "Long Pulse Technology Tokamaks," p. 909.

D. J. Sigmar, S. P. Hirshman, and J. C. Whitson, "Shear Alfvén Wave Destabilized by Alpha Particles in a Tokamak Reactor," p. 785.

J. E. Simpkins, R. J. Colchin, R. C. Isler, R. A. Langley, M. Murakami, J. L. Cecchi, V. L. Corso, H. F. Dylla, R. A. Ellis, and M. Nishi, "Effects of Graphite Limiters in ISX-A," p. 791.

J. Smith, K. T. Tsang, and J. C. Whitson, "Pitch Angle Scattering Model in Electromagnetic Drift Wave Calculation," p. 826.

M. Soler, J. D. Callen, A. P. Navarro, R. Granetz, F. Seguin, and R. Petrasso, "Analysis of Heat Transport in Alcator From Sawtooth Observations," p. 759.

D. A. Spong, C. L. Hedrick, and L. W. Owen, "Formalism for EBT Transport Coefficients Including Noncircular Orbit Effects," p. 876.

W. M. Stacey, Jr. and D. J. Sigmar, "Effect of Momentum Source on Plasma Rotation, Flows, Equilibrium and Transport in a Tokamak," p. 908.

L. Stirling, H. H. Haselton, J. Kim, R. C. Davis, W. K. Dagenhart, W. L. Gardner, C. C. Tsai, J. H. Whealton, G. C. Barber, and R. E. Wright, "Positive Ion Beam Energy Recovery Employing Crossed Magnetic Field Electron Blocking," p. 747.

D. J. Strickler, Y-K. M. Peng, J. A. Holmes, T. Tucker, and R. A. Dory, "Applications of Free Boundary FCT Equilibrium Calculations," p. 896.

D. W. Swain, ISX-B Group, "Initial Experiments on the ISX-B Tokamak," p. 855.

C. C. Tsai, W. L. Stirling, H. H. Haselton, W. L. Gardner, D. E. Schechter, G. C. Barber, W. K. Dagenhart, R. C. Davis, J. Kim, M. M. Menon, N. S. Ponte, P. M. Ryan, S. W. Schwenterly, J. H. Whealton, and P. E. Wright, "100 A Source for PDX(ISX) Injector," p. 748.

K. T. Tsang, "Numerical Studies of Electromagnetic Drift Wave Stability in a Sheared Magnetic Field," p. 793.

K. T. Tsang and P. J. Catto, "Resistive Drift-Alfvén Waves in a Sheared Magnetic Field," p. 825.

N. A. Uckan, D. B. Batchelor, C. L. Hedrick, E. F. Jaeger, and D. A. Spong, "On the Dimensionless Parameter Scaling of EBT," p. 877.

T. Uckan, "Wave Propagation in EBT Plasmas," p. 877.

G. Vahala, S. P. Hirshman, J. C. Jardin, and W. I. van Rij, "Steady State Profiles for MHD Variables $p(r)$, $B_z(r)$," p. 885.

L. Vahala and G. Vahala, "MHD Turbulence in Cylindrical and Spherical Geometries," p. 757.

W. I. van Rij, E. C. Crume, Jr., and K. E. Rothe, "Precision Calculation of Neoclassical Electron Transport Coefficients Using the CPM," p. 760.

V. A. Vershkov, T. Amano, E. C. Crume, Jr., S. P. Hirshman, and J. T. Hogan, "T4 Argon Injection Experiment Compared with Neoclassical Impurity Diffusion Theory," p. 771.

B. V. Waddell, J. A. Holmes, B. Carreras, and H. R. Hicks, "Stabilization of the m/n = 2 Tearing Mode in Tokamaks," p. 831.

J. H. Whealton and W. L. Gardner, "Neutralizer Gas Evolution Due to Beam Interaction," p. 747.

R. M. Wieland, W. A. Houlberg, and A. T. Mense, "Neutral Beam Injection Code Benchmark Calculations," p. 865.

J. B. Wilgen, J. T. Mihalczo, and G. H. Neilson, "Details of Confinement Experiments in ISX-A: Charge-Exchange," p. 769.

J. C. Whitson, K. T. Tsang, and J. Smith, "Numerical Study of Kinetic Tearing Modes," p. 826.

B. Zurro, P. W. King, M. Murakami, D. H. McNeill, R. M. Wieland, and J. B. Wilgen, "Details of Energy Confinement Studies in the ISX-A Tokamak," p. 789.

5th Conference on Application of Small Accelerators, Denton, Texas, November 6-8, 1978

J. Kim, G. C. Barber, W. R. Becraft, C. W. Blue, W. K. Dagenhart, R. C. Davis, W. L. Gardner, H. H. Haselton, M. M. Menon, N. S. Ponte, P. M. Ryan, D. E. Schechter, S. W. Schwenterly, W. L. Stirling, C. C. Tsai, J. H. Whealton, and R. E. Wright, "Neutral Beams for Fusion Research: Development and Application."

American Nuclear Society 1978 Winter Meeting, Washington, D.C., November 12-16, 1978 (proceedings published in Trans. Am. Nucl. Soc. 30, 1978)

W. R. Becraft, E. S. Bettis, and R. J. Onega, "Tokamak Power Reactor Shutdown — A Go or No-Go Situation," p. 814.

P. T. Spampinato, C. Sardella, and T. E. Shannon, "Design Improvements Simplify Remote Maintenance of Tokamaks," p. 800.

1978 Fall Digital Equipment Corporation User's Society, U.S. Symposium, San Francisco, California, November 27-30, 1978

R. D. Burris and W. H. Gray, "A Generalized Plotting Facility."

R. D. Burris, C. E. Hammons, and C. O. Kemper, "NET — A Powerful File-Transfer Facility."

25th National Vacuum Symposium, American Vacuum Society, San Francisco, California, November 27-December 1, 1978

J. E. Simpkins, R. J. Colchin, and D. R. Overbey, "Residual Gas Analysis in ISX-A."

IEEE *International Electron Devices Meeting, Washington, D.C., December 4-6, 1978* (proceedings published by IEEE, 78 CH1324-3 ED)

T. L. White, N. J. Taylor, and S. J. Evans, "Gyrotron Output Transmission Circuit," p. 396.

FPCC *Committee Meeting at Lawrence Livermore Laboratory, Livermore, California, December 4-6, 1978*

J. Sheffield, LPTT Group, "Long Pulse Technology Tokamak — Status Report, November 1978."

ASME *Winter Annual Meeting, San Francisco, California, December 10-15, 1978*

J. E. Akin and W. H. Gray, eds, "Computer Technology in Fusion Energy Research," by the Computer Technology Committee, the Pressure Vessel and Piping Division, ASME.

ORNL REPORTS

Author(s)	Title	Number
C. M. Fitzpatrick and W. C. T. Stoddart	A System for Vacuum Pouring of Epoxy Tensile and Impact Specimens with a Study of the Behavior of These Specimens at 77K and 293K	ORNL/TM-5493
J. K. Lovin and S. A. Clark	Procurement Module for a MIS: User's Manual	ORNL/TM-5854
R. A. Dandl, F. W. Baity, Jr., J. K. Ballou, D. B. Batchelor, E. S. Bettis, D. B. Campbell, G. L. Campen, K. H. Carpenter, J. A. Cobble, J. S. Culver, H. O. Eason, D. A. Everitt, W. M. Fletcher, J. C. Glowienka, W. R. Hamilton, G. R. Haste, C. L. Hedrick, S. Hiroe, H. Ikegami, E. F. Jaeger, K. L. Kilby, S. P. Kuo, N. H. Lazar, J. N. Luton, J. A. Mayhall, J. R. Moore, D. B. Nelson, L. W. Owen, G. F. Pierce, B. H. Quon, D. A. Spong, N. A. Uckan, H. L. Watts, T. L. White, R. A. Wright, W. L. Wright, and J. W. Yarbrough	*The EBT-II Conceptual Design Study*	ORNL/TM-5955
A. P. Fraas and A. S. Thompson	ORNL Fusion Power Demonstration Study: Fluid Flow, Heat Transfer, and Stress Analysis Considerations in the Design of Blankets for Full-Scale Fusion Reactors	ORNL/TM-5960
W. E. Wood	Draft Program Plan for TNS - The Next Step After the Tokamak Fusion Test Reactor Part IV - Program Planning	ORNL/TM-5984
W. F. Gauster	A Note on the Cryostatic Stability of Superconducting Composites	ORNL/TM-5989
A. T. Mense, W. A. Houlberg, S. E. Attenberger, and S. L. Milora	Effects of Fueling Profiles on Plasma Transport	ORNL/TM-6026
D. J. Sigmar and H. C. Chan	Anomalous Alpha Particle Transport in Thermonuclear Tokamak Plasma	ORNL/TM-6027
L. W. Nelms, P. B. Thompson, and T. L. Mann	Large Coil Test Facility Conceptual Design Report	ORNL/TM-6032
D. J. Sigmar and G. Vahala	Analytic, High β Flux Conserving Equilibria for Cylindrical Tokamaks	ORNL/TM-6040
J. T. Hogan	The Accessibility of High β Tokamak States	ORNL/TM-6049
G. L. Campen, R. D. Easter, and L. E. Nickels	*ORMAK Upgrade Ohmic Heating Coil Generator Protection*	ORNL/TM-6079
M. Soler and J. D. Callen	On Measuring the Electron Heat Diffusion Coefficient in a Tokamak from Sawtooth Oscillation Observations	ORNL/TM-6165
B. Carreras, B. V. Waddell, and H. R. Hicks	Analytic Model for the Nonlinear Interaction of Tearing Modes of Different Pitch in Cylindrical Geometry	ORNL/TM-6175
J. Kim	Health Physics Aspects of Nuclear Radiations from Deuterium Beam Injectors	ORNL/TM-6149
P. L. Litherland	Conceptual Design of the LCP Coil Support Structure	ORNL/TM-6195

B. E. Nelson	Evaluation of Pulse Coil Alternatives for the Large Coil Program	ORNL/TM-6197
R. V. Neidigh and D. J. Sigmar	Hot-Ion Distribution Function in ORMAK, the Oak Ridge Tokamak	ORNL/TM-6198
D. Steiner, T. G. Brown, Y-K. M. Peng, R. L. Reid, M. Roberts, T. E. Shannon, and P. T. Spampinato	Oak Ridge TNS Program: Context, Scope, and Baseline Design of the FY 1978 Activities	ORNL/TM-6201
J. W. Pearce	An Optically Coupled High Voltage Isolation Amplifier	ORNL/TM-6202
W. B. Wood, M. Roberts, T. E. Shannon, and D. Steiner	ORNL Fusion Power Demonstration Study: An Illustrative Example of Planning for the Demonstration of the Commercial Feasibility of Tokamak Fusion Power in This Century (A Demonstration Study)	ORNL/TM-6212
B. V. Waddell, B. Carreras, H. R. Hicks, J. A. Holmes, and D. K. Lee	A Mechanism for Major Disruptions in Tokamaks	ORNL/TM-6213
W. M. Wells	ORNL Fusion Power Demonstration Study: Lithium as a Blanket Coolant	ORNL/TM-6214
D. A. Spong, E. G. Harris, and C. L. Hedrick	Kinetic Transport Properties of a Bumpy Torus with Finite Radial Ambipolar Field	ORNL/TM-6215
S. J. Zweben, B. V. Waddell, D. W. Swain, and H. H. Fleischman	High Energy Runaway Orbits in the Presence of m = 2 Magnetic Islands	ORNL/TM-6216
D. Berger, L. C. Bernard, R. Gruber, and F. Troyon	Wall Stabilization Action on MHD Instabilities	ORNL/TM-6219
J. Sheffield and R. A. Dory	The Ripple Bundle Divertor for Tokamaks	ORNL/TM-6220
R. G. Bateman	Inductive Effects in Flux Conserving Tokamaks	ORNL/TM-6271
R. G. Bateman, D. B. Nelson, D. J. Sigmar, and N. A. Uckan	Finite Beta Toroidal Plasma	ORNL/TM-6273
A. T. Mense and G. A. Emmert	Simulation of Poloidal Divertors in One-Dimensional Tokamak Transport Codes	ORNL/TM-6279
R. G. Bateman	High Pressure Tokamaks	ORNL/TM-6289
R. H. Fowler, D. K. Lee, P. W. Gaffney, and J. A. Rome	FLOC Field Line and Orbit Code for the Study of Ripple Beam Injection into Tokamaks	ORNL/TM-6293
W. A. Houlberg and R. W. Conn	Space-Dependent Thermal Stability of Reacting Tokamak Plasmas	ORNL/TM-6297
E. F. Jaeger, C. L. Hedrick, and J. S. Tolliver	A Kinetic Transport Model for the ELMO Bumpy Torus	ORNL/TM-6313
D. B. Batchelor and C. L. Hedrick	A Preliminary Investigation of Trapped Particle Instabilities in EBT	ORNL/TM-6318
Y-K. M. Peng	Continuous Tokamaks	ORNL/TM-6319
D. B. Batchelor	Status of the Theoretical Study of Microwave Heating in EBT	ORNL/TM-6320
W. M. Stacey, Jr. and D. J. Sigmar	Comments on the Effects of Gas Injection Upon Radial Particle Fluxes in the ISX-A Flow Reversal Experiment	ORNL/TM-6339
N. A. Uckan and D. B. Batchelor	Heating Techniques for an EBT Reactor	ORNL/TM-6346
J. A. Rome and Y-K. M. Peng	The Topology of Tokamak Orbits	ORNL/TM-6352

C. C. Tsai, W. L. Stirling, H. H. Haselton, D. E. Schechter, G. C. Barber, W. K. Dagenhart, R. C. Davis, W. L. Gardner, M. M. Menon, N. S. Ponte, P. M. Ryan, J. H. Whealton, and R. E. Wright	Performance of a Modified DuoPIGatron Ion Source for PLT Neutral Beam Injectors	ORNL/TM-63[illegible]
J. R. McNally, Jr.	A Simple Measure of Merit for Fusion Feasibility	ORNL/TM-6362
T. Amano and E. C. Crume, Jr.	Simulation of Multispecies Impurity Transport in Tokamaks	ORNL/TM-6363
R. C. Isler, E. C. Crume, Jr., and H. C. Howe	Impurity Behavior During Neutral Beam Injection and Gas Puffing into ORMAK	ORNL/TM-6366
W. K. Dagenhart, C. W. Blue, H. H. Haselton, M. M. Menon, S. W. Schwenterly, W. L. Stirling, C. C. Tsai, and J. H. Whealton	Drift Tube Beam Blocking Experiments Performed on the ORNL/PLT Neutral Beam Line at the ORNL Medium Energy Test Facility	ORNL/TM-6374
W. H. Gray and J. E. Akin	An Improved Method for Contouring on Isoparametric Surfaces	ORNL/TM-6381
C. R. Stewart, Jr., J. E. Francis, C. E. Hammons, and W. K. Dagenhart	Data Acquisition System for Medium Power Neutral Beam Test Facility	ORNL/TM-6394
B. Carreras, B. V. Waddell, and H. R. Hicks	Poloidal Magnetic Field Fluctuations in Tokamaks	ORNL/TM-6403
C. H. An and R. G. Bateman	Stability of Tokamaks with Elongated Cross Section	ORNL/TM-6419
R. A. Dory, D. P. Berger, L. A. Charlton, J. T. Hogan, J. K. Munro, D. B. Nelson, Y-K. M. Peng, D. J. Sigmar, and D. J. Strickler	Tokamaks Heated to High Beta	ORNL/TM-6434
R. J. Colchin, C. E. Bush, P. H. Edmonds, A. C. England, K. W. Hill, R. C. Isler, T. C. Jernigan, P. W. King, R. A. Langley, D. H. McNeill, M. Murakami, R. V. Neidigh, G. H. Neilson, J. E. Simpkins, J. B. Wilgen, J. C. DeBoo, K. H. Burrell, and E. S. Ensberg	Plasma-Wall Impurity Experiments in ISX-A	ORNL/TM-6446
R. A. Dandl, F. W. Baity, Jr., M. C. Becker, K. H. Carpenter, J. A. Cobble, H. O. Eason, M. Fujiwara, J. C. Glowienka, G. R. Haste, M. E. Hesse, S. Hiroe, H. Ikegami, H. W. Moos, J. M. Tyson, E. S. Warden, N. H. Lazar, R. L. Livesey, M. W. McGuffin, D. H. McNeill, B. H. Quon, J. W. Reynolds, F. M. Bieniosek, F. J. Bresnock, P. L. Colestock, K. A. Conner, R. L. Hickok, S. S. Kuo, W. J. Schill, T. Uckan, T. L. White, and R. E. Wintenberg	Summary of EBT-I Experimental Results	ORNL/TM-6457

H. Weitzner and D. B. Batchelor	Conversion Between Cold Plasma Modes in an Inhomogeneous Plasma	ORNL/TM-6462
W. H. Gray	A User's Guide to the CALVEC Software Library: A Computer Program for Emulation of CALCOMP Graphics on a Versatec Printer/Plotter	ORNL/TM-6477
J. R. McNally, Jr.	Alpha-Driven, Steady-State Tokamak	ORNL/TM-6492
S. L. Milora, C. A. Foster, P. H. Edmonds, and G. L. Schmidt	Hydrogen Pellet Fueling Experiment on the ISX-A Tokamak	ORNL/TM-6496
K. H. Carpenter and N. H. Lazar	NCMART: Algorithms and Computer Codes for a Modified Algebraic Spatial Reconstruction of Spectroscopic Emissivities for ELMO Bumpy Torus	ORNL/TM-6500
G. H. Neilson, J. F. Lyon, and M. Murakami	Injection-Dominated Tokamak Experiments at ORNL	ORNL/TM-6506
K. T. Tsang, J. C. Whitson, and J. Smith	Numerical Study of Drift-Alfvén Waves in a Sheared Magnetic Field	ORNL/TM-6508
J. C. Whitson, J. H. Whealton, E. F. Jaeger, J. Smith, and R. W. McGaffey	Two-Dimensional Cylindrically Symmetric Convergent Ion Optics Code Including Plasma Electrons	ORNL/TM-6512
N. A. Uckan, D. B. Batchelor, E. S. Bettis, R. A. Dandl, C. L. Hedrick, E. F. Jaeger, D. G. McAlees, D. B. Nelson, L. W. Owen, R. T. Santoro, D. A. Spong, T. Uckan, H. L. Watts, H. T. Yeh, L. M. Lidsky, J. S. Herring, and R. E. Potok	The ELMO Bumpy Torus (EBT) Reactor	ORNL/TM-6532
Y-K. M. Peng and R. A. Dory	Very Small Aspect Ratio Tokamaks	ORNL/TM-6535
G. R. Dyer, G. H. Neilson, and G. G. Kelley	Pulse Pileup Effects on Plasma Electron Temperature Measurements by Soft X-Ray Energy Analysis	ORNL/TM-6541
C. R. Stewart, Jr., W. D. Joubert, D. R. Overbey, and K. A. Stewart	TEK11 Graphics User's Guide	ORNL/TM-6546
J. D. Callen, B. V. Waddell, H. R. Hicks, J. A. Holmes, D. K. Lee, S. J. Lynch, K. T. Tsang, J. C. Whitson, B. Carreras, M. Soler, and M. Azumi	Magnetic "Islandography" in Tokamaks	ORNL/TM-6564
B. Carreras, H. R. Hicks, and B. V. Waddell	Tearing Mode Activity for Hollow Current Profiles	ORNL/TM-6570
M. Murakami, K. H. Burrell, T. C. Jernigan, T. Amano, S. C. Bates, C. E. Bush, R. E. Clausing, R. J. Colchin, E. C. Crume, Jr., J. C. DeBoo, J. L. Dunlap, G. R. Dyer, P. H. Edmonds, L. C. Emerson, A. C. England, E. S. Ensberg, C. A. Foster, Y. Gomay, K. W. Hill, H. C. Howe, R. C. Isler, H. E. Ketterer, P. W. King, R. A. Langley, J. F. Lyon, D. H. McNeill, J. T. Mihalczo, S. L. Milora, W. Namkung, A. P. Navarro, R. V. Neidigh, G. H. Neilson, V. K. Paré, R. Prater, M. J. Saltmarsh, M. J. Schaffer, J. E. Simpkins, D. W. Swain, J. B. Wilgen, W. R. Wing, S. K. Wong, and B. Zurro	Plasma Confinement and Impurity Flow Reversal Experiments in the ISX-A Tokamak	ORNL/TM-6583

S. C. Scott and J. Sheffield	Scaling Studies of Beam-Heated Tokamak	ORNL/TM-65[illegible]
S. L. Milora and C. A. Foster	Pneumatic Hydrogen Pellet Injection System for the ISX Tokamak	ORNL/TM-65[illegible]
S. P. Hirshman and K. Molvig	Turbulent Destabilization and Saturation of the Universal Drift Mode in a Sheared Magnetic Field	ORNL/TM-662[illegible]
W. Namkung, A. C. England, and O. C. Eldridge	Langmuir Probe Measurements of the Scrape-Off Plasma in ISX-A	ORNL/TM-66[illegible]1
R. G. Bateman and D. B. Nelson	Resistive Ballooning Mode Equation	ORNL/TM-6629
D. D. Bates, H. E. Ketterer, and S. J. Sosnowski	The ISX-B Tokamak Experiment Safety Analysis Report	ORNL/CF-78/207
H. E. Ketterer, C. M. Loring, and S. J. Sosnowski	Safety Analysis Report for the ISX-B Neutral Beam Injection Systems	ORNL/CF-78/244
A. B. Mikhailovskii, D. J. Sigmar, and L. Kobylenski (translator)	Review of Instability Theory for High Pressure Tokamak Plasma	ORNL/tr-4610
Fusion Energy Division Staff	Fusion Energy Division Annual Progress Report for Period Ending December 31, 1977	ORNL-5405
Fusion Energy Division Staff	Fusion Research at ORNL	